

Fischer-Tropsch Based Biomass to Liquid
Fuel Plants in the New Zealand Wood
Processing Industry Based on
Microchannel Reactor Technology

Chris Penniall

A thesis presented for the degree of

Doctor of Philosophy

in

Chemical and Process Engineering

at the

University of Canterbury

Christchurch, New Zealand

2013

Abstract

This research forms part of a programme of work at the University of Canterbury investigating the production of liquid fuels from biomass. The drivers for this research are the plentiful supply of woody biomass in New Zealand as well as the necessity for a reduction in the use of fossil fuels.

Fischer-Tropsch synthesis has been chosen as the base conversion method for syngas to liquid fuels. While Fischer-Tropsch plants are traditionally very large, the low geographical density of the biomass feedstock necessitates a shift from a traditional economies of scale approach. In this research a sawmill integrated polygeneration scenario is proposed that recognises the synergy between the heat and electrical requirements of a mill and the Fischer-Tropsch process that can supply both as well as liquid fuels. Techno-economic modelling of variations to this polygeneration arrangement were performed using a traditional Fischer-Tropsch slurry reactor as the basis. The breakeven price of syncrude produced in the process based on a 30 year plant life and 10% discount factor was as low as \$US 167 per barrel.

This arrangement is coupled with development of and experimentation with a microchannel reactor in a further attempt to overcome economies of scale disadvantages. The lab scale microchannel reactor consisted of a shim with 50 channels of 37mm length with 0.2mm height and 0.3mm width. The microchannel reactor was tested with shorter run periods to compare different catalyst washcoats consisting of neat cobalt, cobalt on titania and a combustion synthesis method over a temperature range of 210-240°C at 20 bar. Comparison was also made to a lab scale fixed bed reactor with a powdered cobalt on titania catalyst. The neat cobalt washcoat proved to have the best performance per unit mass of catalyst of the three washcoats. The performance of the microchannel reactor was 32-40 times better per unit catalyst mass than the fixed bed reactor.

From data based on the shorter runs the neat cobalt washcoat and the cobalt on titania washcoat were selected for further analysis over longer runs at a range of pressures from 2-20 bar and temperatures from 210-240°C. These runs were each approximately 70 hours long and provided a better analysis of the narrowed catalyst choice. The productivity results of the catalysts were fitted to established kinetic equations from literature with an excellent correlation. More accurate Anderson-Schultz-Flory selectivity values were also obtained ranging between 0.72 to 0.82. This is certainly an area that would warrant further attention as a higher selectivity has a very positive affect on plant economics.

Establishment of the kinetic equations for the catalyst performance allowed modelling of reactors with greater volume along with investigation of mass transfer limitations to assist in scale up of the technology. It was found that under 4-5mm hydraulic diameter channel dimensions the mass transfer limitation from the bulk gas phase to the catalyst interface is negligible.

A scaled up microchannel reactor concept design is proposed utilising stainless steel mesh folded into 2mm channels to increase catalyst surface area compared to straight shim. A costing correlation was produced per unit of reactor volume to allow a full scale cost of the microchannel reactor to be estimated for inclusion into the techno-economic model. The revised techno-economic model was optimised through pressure variation to give a breakeven syncrude value of \$US118 per barrel at Fischer-Tropsch reaction conditions of 10 bar and 240°C. This brings the value well within historical crude price trends.

Acknowledgments

Thanks must first go to Professor Shusheng Pang, who provided the scholarship that has enabled my research and whose research group I consider a privilege to be part of. Dr Chris Williamson, my supervisor certainly warrants mention. His sage advice at the right times has helped with the direction of this research and prevented wasteful tangents. The technical staff in the Chemical and Process Engineering Department have demonstrated great capability and can't be thanked enough for their work and advice.

To my wife Katie, whom I married during the course of this research, your love and support is treasured. Also to my family, particularly Mum, who has always been supportive during both the ups and downs.

Lastly but certainly not least, I am thankful to my Father in heaven who has created this world in an amazing and ordered way. It is a joy to be able to study it further and try to do my small part in being a better steward of His creation.

Table of Contents

1. Introduction	1
2. Literature Review	3
2.1. Project Justification.....	3
2.2. Biomass Availability	3
2.3. Cost of Residues.....	7
2.4. Offsetting New Zealands Fossil Fuel Usage	8
2.5. Fischer Tropsch Background	12
2.6. Process Configuration	13
2.7. Techno-economic aspects.....	15
2.8. The Reaction and Kinetics	17
2.9. Selectivity	21
2.10. Catalysts	22
2.11. Water Effects in FT Synthesis.....	27
2.12. Effect of Different Precursors and Solvents.....	29
2.13. Effect of Promoters	30
2.14. Cobalt Particle Size.....	31
2.15. Catalyst Deactivation	31
2.16. Summarising the Catalyst Review	37
2.17. Fischer-Tropsch Reactors	37
2.18. Microchannel Reactors	45
2.19. Product Upgrading/Refining	49
3. Techno-Economic Study of Small Scale Fischer-Tropsch in the New Zealand Wood Processing Industry.....	50
3.1. Introduction	50
3.2. Methodology.....	51

3.3.	Modelling	57
3.4.	Results and Discussion	60
3.5.	Conclusion.....	69
4.	Microchannel Experiments.....	70
4.1.	Laboratory Microchannel Reactor Design and Construction.....	70
4.2.	Microchannel Reactor Experimental Methods.....	82
5.	Microchannel Experimentation Results and Discussion	97
5.1.	Ex-situ Analysis.....	97
5.2.	Ease and Repeatability of Washcoating.....	98
5.3.	SEM Analysis	99
5.4.	Online Performance	107
5.5.	Longer Time Frame Comparison.....	115
5.6.	Washcoat Comparison	127
5.7.	Deactivation	131
5.8.	Conclusions and Recommendations of Experimental Work.....	132
6.	Modelling of the CAPE Microchannel Reactor	134
6.1.	Introduction	134
6.2.	Theory and Modelling.....	135
6.3.	Results and Discussion	140
6.4.	Conclusion.....	146
7.	Scale Up Design of the Microchannel Reactor for Small Scale Biomass to Liquid Fischer Tropsch Plants	147
7.1.	Reactor Scale Up	147
7.2.	Current Similar Technology Comparisons.....	154
7.3.	Concept Design for Scaled Up Reactor	163
8.	Techno-economic Evaluation and Optimisation of Plant Incorporating the Microchannel Reactor.....	173
8.1.	Introduction	173

8.2.	Optimising for Small Scale – Pressure Effects.....	174
8.3.	Incorporation of the Microchannel Reactor into Plant Economics	175
8.4.	Sensitivity Analysis	179
9.	Conclusions, Recommendations and Perspective	184
9.1.	Conclusions of current work	184
9.2.	Recommendations	187
9.3.	Final Perspective	188
10.	References.....	189
Appendix A	Unisim Model	
Appendix B	Techno-economic Study Results	
Appendix C	Rig Safety and Risk Considerations	
Appendix D	XRD results	
Appendix E	Fitting Kinetic Equations to Experimental Data	
Appendix F	Batch Slurry Reactor Fischer Tropsch Catalyst Development	

Nomenclature

a	stoichiometric constant
A	effective mass transfer area (m ²)
C _g	concentration in bulk gas phase (mol/m ³)
C _i	concentration at gas-catalyst interface (mol/m ³)
d	channel diameter or hydraulic diameter (m)
D	diffusivity (m ² /s)
Fin _i	flow of component i into experimental reactor (cc/min)
Fin _{tot}	total flow into experimental reactor (cc/min)
Fout _i	flow of component i out of the experimental reactor (cc/min)
Fout _{tot}	total gaseous flow out of the experimental reactor (cc/min)
Fout _{meas}	total measured gaseous flow out of the experimental reactor (cc/min)
F _x	molar flowrate of component x (mol/s)
F _T	total molar flowrate (mol/s)
k	mass transfer coefficient (m/s)
y	mole fraction
M	molar mass (g/mol)
m	stoichiometric constant
n	stoichiometric constant
\dot{n}_A	mass transfer rate (mol/s)
P _x	partial pressure component x (MPa)
P _{atm}	pressure (atm)
P _T	total pressure (MPa)
R	ideal gas constant 8.314 J/mol/K
-R _{CO}	rate of consumption of CO (mmol/min/g catalyst unreduced basis)
r _x	reaction rate of component x (mol/s/m ³ reactor volume)
T	temperature (K)
V	reactor volume (m ³)
V _m	molar volume (cc/gmol)
Xin _i	molar fraction of component i into the experimental reactor
Xout _i	molar fraction of gaseous component i leaving the experimental reactor

z	linear distance down channel (m)
c	critical point
α	temperature dependent constant
α	selectivity in Anderson Shultz Flory distribution
β	temperature dependent constant
ρ	density (kg/m^3)
ρ_b	catalyst bulk density (g/m^3)
μ	viscosity
v	velocity (m/s)
Sh	Sherwood number
Gz	Graetz number

List of Figures

Figure 1: Regional distribution of forest and annual harvest volume (thousands of green tonnes (SCION, et al., 2007)	4
Figure 2: Wood processing residues available for use 2005 (thousands of green tonnes) (SCION, et al., 2007)	4
Figure 3: Distribution of all woody biomass resources for New Zealand 2007 (tonnes/year) (SCION, et al., 2007)	5
Figure 4: Forecast of annual wood supply with RAD being Pinus Radiata, FIR being Douglas Fir and OTH being other species (million m ³ /year). (SCION, et al., 2007)	6
Figure 5: CO ₂ emissions from fuel combustion per capita for OECD countries in 2005. (Ministry of Economic Development, 2008b).....	9
Figure 6: Percentage change in total CO ₂ emissions from fuel combustion for OECD countries in 2005 relative to 1990. (Ministry of Economic Development, 2008b)	10
Figure 7: Percentage reduction in greenhouse gas emissions compared to petrol or diesel for various processes. (SCION, Hall, & Jack, 2008).....	10
Figure 8: Weekly average Dubai crude incorporating New Zealand exchange rate (Ministry of Economic Development, 2009).....	11
Figure 9: Balance between production cost and plant size for a biomass based energy plant (Searcy & Flynn, 2009).....	16
Figure 10: Product composition as a product of chain growth ($p_g = \alpha$) (A. Steynberg & Dry, 2004)	21
Figure 11: Diagram showing water effects for a Co catalyst for FTS (Dalai & Davis, 2008).....	27
Figure 12: A - no water addition, B - 10 mmol water vapour, C - 10 mmol water as liquid (X. Liu, et al., 2011a)	28
Figure 13: Rates of formation and hydrogenation of carbon (N) vs. inverse temperature (Bartholomew, 2001)	35
Figure 14: Multitubular fixed bed FT reactor (Mark E. Dry, 2002)	39
Figure 15: Sasol circulating fluidised bed reactor (Burtron H. Davis, 2005)	40
Figure 16: Fixed fluidised bed reactor (Mark E. Dry, 2002)	42
Figure 17: Slurry bed FT reactor (Tijmensen, et al., 2002).....	43
Figure 18: Influence of catalyst loading (C_s) and the superficial gas velocity (U_{Go}) on the flow characteristics in the slurry reactor (Burtron H. Davis, 2005)	43
Figure 19: Block diagram of the Fischer-Tropsch process	51

Figure 20: Simple schematic of twin fluidised bed gasifier operation (J. P. Rutherford & Williamson, 2006)	53
Figure 21: Schematic of combined heat, power and liquid fuels process	57
Figure 22: Flow diagram of the economic modelling of the process.....	57
Figure 23: Simplified layout and flows for scenario 1.....	61
Figure 24: Simplified layout and flows for scenario 2.....	62
Figure 25: Simplified layout and flows for scenario 3.....	62
Figure 26: Sensitivity analysis for on peak scenario (Scenario 1)	66
Figure 27: Sensitivity analysis for off peak scenario (Scenario 2)	66
Figure 28: Sensitivity analysis for scenario where no power is generated (Scenario 3).....	67
Figure 29: Stacking arrangement of feed and reactor shims, along with cross-flow cooling/heating shims	71
Figure 30: Visual explanation of photolithography process	72
Figure 31: Example of mask filmwork.....	73
Figure 32: Schematic of etch tank arrangement.....	74
Figure 33: Close-up of channels revealing EDM start holes	76
Figure 34: Arrangement of shims sandwiched between gauge plate for wire cutting with the feed shim on the left and reactor shim on the right.....	76
Figure 35: View of feed and reactor shims demonstrating smallest sealing faces.....	77
Figure 36: First reactor created using 316 stainless steel.....	78
Figure 37: Second reactor model constructed from Stavax on left, in comparison to stainless steel model on right.....	79
Figure 38: Demonstration of the use of 4.9mm drill bits as 'dowel pins' for accurate alignment of plates.....	80
Figure 39: Schematic of lab scale Fischer Tropsch Rig.....	83
Figure 40: Picture showing the manifolding system to allow only one gas to flow at a time (N ₂ top left valve, H ₂ top right, syngas from bottom of lower valve) as well as the mass flowmeter, pressure indication and pressure relief valve.....	84
Figure 41: Arrangement of reactor showing outlet to collection pot. Note the line is separated and capped between runs to eliminate air oxidising the catalyst	85
Figure 42: From the collection pot the outlet flows through the manual flow control valve before entering the three way valve where the valve can be turned to obtain a manual sample. Otherwise the line going vertical to the left of the picture is the vent, which has a take-off point for the micro-GC.....	85

Figure 43: The glass vial inside the collection pot. The tube to the left is the inlet directly into the vial, the outlet of the vial is to the larger collection pot	86
Figure 44: Fixed bed reactor plate. Photo shows the inlet and outlet ducts to the horizontal reactor space	89
Figure 45: Schematic of TPR rig arrangement	93
Figure 46: Physical arrangement of TPR system	94
Figure 47: Example image provided by webcam every 30 seconds	96
Figure 48: TPR profiles for freeze dried titania, precipitated titania and alumina based cobalt FT catalysts	98
Figure 49: SEM micrograph showing the gasket material with a straight cobalt washcoat. Note the damaged layer is due to separating the reactor post run	100
Figure 50: View of an individual channel of the straight cobalt washcoat showing the different formations on the wall to the centre of the channel.....	101
Figure 51: Close up of the centre channel of the straight cobalt washcoat	101
Figure 52: SEM micrograph showing the boundary between the centre and outside edges of the channel for the straight cobalt washcoat. Note the microfibril structures can just be seen in the left side of the image.....	102
Figure 53: Closer view of the structure of the cobalt washcoat near the edges of the channel.....	102
Figure 54: Further magnification of the straight cobalt washcoat near the channel edges showing the high surface area structure	103
Figure 55: SEM micrograph of cobalt on titania washcoat.....	104
Figure 56: Closer view of cobalt on titania washcoat showing the differing structure to that of the straight cobalt washcoat.....	104
Figure 57: This image was of a channel with the stainless steel shim still in place with the focus being on the cobalt on titania washcoat on the vertical wall	105
Figure 58: Higher magnification of the wall structure of the cobalt on titania washcoat showing a significantly different structure to that of the straight cobalt washcoat on the gasket surfaces	105
Figure 59: SEM micrograph of the channel centre in the combustion synthesis washcoat showing identical structure to the straight cobalt washcoat.....	106
Figure 60: Image of a wire separator between the channels. The rough surface to the left is the wire cut surface, while the surface to the right is the polished mill finish of the stainless steel shim	107
Figure 61: Visual comparison of relative catalyst activities	110
Figure 62: Graphical comparison of selectivities for different catalysts and varying temperature ...	112
Figure 63: Product fractional yield vs. temperature for the neat cobalt washcoat	113

Figure 64: Product fractional yield vs. temperature for the cobalt on titania washcoat	113
Figure 65: Product fractional yield vs. temperature for the combustion synthesis method	114
Figure 66: Product yield vs. temperature for the fixed bed reactor.....	114
Figure 67: Example of fit of experimental liquids analysis to ASF distribution. Run 26/04/2012 20 bar 240°C neat cobalt washcoat with an α value of 0.78	119
Figure 68: Example of methodology of fitting an α value to experimental data. Run 26/04/2012 20 bar 240°C neat cobalt washcoat with an α value of 0.78	119
Figure 69: Plot of linearised equation 23.....	120
Figure 70: Productivity vs reactor pressure with the theoretical kinetic equation fit to the data along with comparative data from Yates and Satterfield (1991). Note the units of volume in the productivity refer to the reactor volume in this case	121
Figure 71: Reaction rate and selectivity as a function of temperature for the neat cobalt washcoat	122
Figure 72: Reaction rate and selectivity as a function of reaction pressure for the neat cobalt washcoat.....	122
Figure 73: Raw data of reaction rate as a function of reaction pressure for the cobalt on titania washcoat.....	123
Figure 74: Best linearised fit of cobalt on titania data ignoring 10 bar outlier.....	123
Figure 75: Theoretical equation comparison to raw data and Yates and Satterfield data for reaction rate as a function of reaction pressure.....	124
Figure 76: Graph to enable visualisation of ASF distribution with experimental results fitted to an α of 0.78 and comparison made to an α of 0.87.....	126
Figure 77: Reaction rate and selectivity as a function of reaction temperature for the cobalt on titania washcoat.....	127
Figure 78: Reaction rate and selectivity as a function of reaction pressure for the cobalt on titania washcoat.....	127
Figure 79: Comparison of the two washcoats in terms of conversion per unit volume of the reactor as a function of reaction pressure.....	128
Figure 80: Comparison of reaction rate in terms of C_{2+} products per gram of catalyst per hour as a function of reaction pressure	129
Figure 81: Comparison of reaction rate in terms of C_{2+} products per gram of catalyst per hour as a function of reaction temperature.....	129
Figure 82: Comparison of reaction rate in terms of C_{2+} products produced per gram of cobalt per hour as a function of reaction pressure.....	130

Figure 83: Comparison of reaction rate in terms of C ₂₊ products produced per gram of cobalt per hour as a function of reaction temperature	130
Figure 84: Intraparticle temperature gradient vs. catalyst particle size (Cao, et al., 2009)	135
Figure 85: Reaction rate in terms of reactor volume as a function of reaction pressure showing the experimental data in red, with the fitted kinetic model in blue, while the green is the comparison with Yates and Satterfield's work	140
Figure 86: Estimated conversion of CO over the reactor volume at various total pressures. 240°C, 25cc/min feed	141
Figure 87: Comparison of CO estimated conversion over the length of the reactor at various pressures based on a reactor ten times the volume of the experimental reactor. 240°C, 25cc/min feed	142
Figure 88: CO estimated conversion vs. reactor pressure based on a reactor ten times the volume of the experimental reactor. 240°C, 25cc/min feed	142
Figure 89: Analysis of estimated conversion over a longer reactor with varying multiplications of the reaction rate per unit volume	143
Figure 90: Graph showing the estimated difference in bulk phase to surface partial pressure of CO over the length of the reactor at 240°C, 20 bar, 25cc/min feed	144
Figure 91: Estimated fractional difference in partial pressure between bulk gas phase and catalyst interface as a function of channel hydraulic diameter. Based on kinetic data at 240°C and 10 bar.	145
Figure 92: Affect on catalyst activity and methane selectivity with increasing washcoat thickness (Kapteijn, et al., 2005).....	146
Figure 93: Schematic of gas fired heating of the scaled up microchannel reactor	149
Figure 94: Design basis for wire cutting cost estimation	152
Figure 95: Velocys reactor showing reacting channels (Velocys, 2012b)	154
Figure 96: View of reactor showing cooling channels (Velocys, 2012b).....	155
Figure 97: Core reactor block to produce 30 bbl/day estimated at 600mm in all dimensions (Velocys, 2012b)	155
Figure 98: Reactor housing for microchannel core (Velocys, 2012b)	156
Figure 99: Close-up of Heatric etched channels bonded together (Southall, Le Pierres, & Dewson, 2008)	157
Figure 100: Example of formed channels for Heatric heat exchangers (Southall, et al., 2008)	157
Figure 101: Example of zig-zag etched pattern for Heatric heat exchangers (Southall, et al., 2008)	157
Figure 102: Heatric H2X heat exchanger. It is estimated the folded channels are in the order of 2mm (Southall, et al., 2008).....	158

Figure 103: Expanded view of Danfoss MPHE (Danfoss, 2012)	159
Figure 104: Example of Alfa Laval fusion bonded heat exchanger (Alfa Laval, 2012)	160
Figure 105: GEA welded plate heat exchanger exploded view (GEA, 2012)	161
Figure 106: Example of woven stainless steel wire mesh formed into channels	163
Figure 107: Assembled concept reactor design showing mesh channels and cooling channels in a crossflow pattern. Please note this is not to scale, rather this model was constructed at a size to allow easy visualisation.....	164
Figure 108: Solidworks drawing showing manifold and reactor core arrangement	165
Figure 109: Exploded view of reactor concept showing the individual components.....	166
Figure 110: Example of roller style for forming corrugations in the stainless steel mesh (Shree Krishna Engineering Works, 2012).....	169
Figure 111: Costing relationship of reactor to reacting volume	171
Figure 112: Comparison of the parameters in the techno-economic model at varying reaction pressure. Note the units are ratioed to allow comparison.....	178
Figure 113: Sensitivity analysis for the 10 bar scenario.....	179
Figure 114: Sensitivity analysis for capital cost for differing pressure cases.....	180
Figure 115: Sensitivity analysis for electricity price for differing pressure cases	180
Figure 116: Sensitivity analysis for wood cost	181
Figure 117: Sensitivity analysis for selectivity for the 10 bar scenario.....	181

List of Tables

Table 1: Delivered cost of forest residues to a user ($\$/m^3$, 2007) (SCION, et al., 2007).....	7
Table 2: Fischer-Tropsch synthesis plants either in operation or under construction (Guettel, Kunz, & Turek, 2008).....	13
Table 3: Typical HTFT product composition (A. P. Steynberg, Espinoza, Jager, & Vosloo, 1999).....	14
Table 4: Typical distillation range for LTFT syncrude fractions (A. Steynberg & Dry, 2004).....	14
Table 5: Summary of Kinetic Studies extracted from Yates & Satterfield (1991).....	19
Table 6: Summary of kinetic studies extracted from Atashi et al. (2010).....	20
Table 7: Summary of deactivation mechanisms retrieved from Tsakoumis et al. (2010).....	33
Table 8: Contaminant concentrations and their maximum values for FT synthesis (Tijmensen, et al., 2002).....	54
Table 9: Economic breakdown for modelled scenarios.....	63
Table 10: Operating cost and profit breakdown example for scenario 1.....	65
Table 11: GC oven temperature parameters.....	92
Table 12: Product conversion (gC_{2+} product/g catalyst/hr) over temperature range for various washcoats established in this experimental research.....	109
Table 13: Values of α and % of converted CO converted to methane over temperature range.....	112
Table 14: Product distribution (mass %) for various catalysts over temperature range calculated from α	112
Table 15: Summary of pertinent data from longer runs.....	116
Table 16: Velocity and Reynolds numbers within microchannel reactor with varying activities per volume and reactor length while maintaining consistent residence time.....	148
Table 17: Cost of base reactor and support unit operations for 100 bpd scenario.....	170
Table 18: Changes in production, capital cost and breakeven crude price for a slurry reactor plant as a function of reaction pressure.....	175
Table 19: Parameters of the techno-economic analysis based on differing reaction pressures at 240°C.....	177
Table 20: Parameters of the techno-economic analysis based on a 10 bar, 225°C, $\alpha = 0.89$ scenario.....	183

1. Introduction

One barely needs an introduction to the issue of global warming due to greenhouse gas emissions as the topic has moved well beyond discussion within the scientific community and has become a generally known and accepted reality. Solutions for the reduction in greenhouse gas emissions have rightly garnered significant attention for a number of years now. This driver, coupled with the increasing threat of diminishing oil reserves as well as potential biomass feedstock from significant forestry resource within New Zealand creates a multifaceted justification for renewable, carbon neutral energy technology in this country.

There are numerous methods that allow the production of electricity from renewable resources, many of which are already in significant use in New Zealand such as hydro and wind power. However, the methods available for producing renewable liquid fuels are considerably narrower.

This thesis has focussed on the Fischer-Tropsch (FT) process for producing liquid fuels from syngas as part of the overall goal of developing biomass to liquid fuels technology at the University of Canterbury. This goal is being fulfilled by the Biomass to Syngas and Liquids (BTSL) group. This team lead by Professor Shusheng Pang and comprising of academics, post-doctoral fellows and postgraduate students is collectively working to develop interconnected processes or unit operations to allow production of liquid fuels from biomass.

It was very much the intention of this thesis to develop new and novel concepts while remaining practical and applicable to the context the technology is being developed for, which is the New Zealand wood processing industry. Simpler solutions that are effective at a smaller scale were called for and have been adhered to in the design and experiments as much as practicable. Therefore, this focus has led to microchannel reactor technology being employed along with a polygeneration FT plant arrangement as the basis for research and development.

The first section of the thesis is a literature review which begins with data based arguments and justification for the biomass based FT to liquid fuels process. This is complemented by examination of the FT process including worldwide FT liquid production. Reactor and catalyst technology are investigated, both historical/traditional and developing. The literature review is completed by

examining the developing technology of microchannel reactors as this was elected to be the focus technology of the thesis.

Following the literature review a techno-economic study was performed. While there are many justifications for pursuing biomass to FT liquids the technology still requires an element of economic viability to create investment interest. The techno-economic study employed a polygeneration scenario configured within a sawmill to provide heat and power to the attached mill, as well as FT product. This allows excellent synergy with the parent sawmill and is a novel means of improving the viability of an FT process at a smaller scale.

The process for the techno-economic study was, however, based on traditional reactor technology, whereas the benefits of microchannel reactors, particularly at smaller scale are being promoted in literature. Therefore this was determined to be a potentially fruitful area of study, both for the potential advantages of such a reactor type in the scenario in question, as well as the ability to add to the knowledge base of this emerging technology. Therefore, description of the design and construction of a lab scale microchannel reactor is reported as well as the methodology for experimental work. This experimental work is completed, based on manipulation of variables to gain an adequate understanding of the reactors performance to assist with scale up design of the technology.

The microchannel experimental work is complemented by experiments in a batch slurry reactor carried out at the University of Kansas. This provides a comparison to the work performed at the University of Canterbury as well as presenting a means for rapid catalyst investigation.

Kinetic data obtained from experiments allows modelling of the mass transfer and general performance in the reactor. This provides a means to predicting scale up which leads to the next section in the thesis which is conceptual design of a scaled up reactor. The performance and cost of this reactor is estimated.

From experimental work and scaled up reactor design a further techno-economic study can be completed with adjusted parameters and a microchannel reactor. This allows comparison to the first techno-economic study to examine the improvements. One could consider this section the culmination of the thesis as all the previous chapters from research, design, experimentation and modelling were performed to feed into this section of work.

2. Literature Review

A key focus in the literature review is to understand why this project should be pursued in the first instance. Hence justification for the project is discussed. Following this the background for the FT process is discussed which in turn explains why FT is the process selected for biomass conversion. This leads to review and discussion of microchannel reactors selected for use in this study, why such a reactor would be selected and where related research has progressed.

2.1. Project Justification

Justification for this research can be found at both ends of the process. At the input there is the availability of biomass within New Zealand. At the output a renewable fuel is being produced offsetting fossil fuel usage within New Zealand, as well as generating local production rather than importation. These aspects will be explored further.

2.2. Biomass Availability

2.2.1. The potential biomass resource

New Zealand's wood harvest is currently 20 million m³ of round wood per year (Cox, 2008). Around 20%, or 4-5 million m³ per year, ends up as wood residues (sawdust, bark or chips) during processing. Wood residue use currently accounts for around 25 Petajoules (PJ) of New Zealand's 700 PJ of primary energy supply. However, only about two thirds of the wood processing residue is used for energy and much of the remainder is sent to landfill. Forest logging generates a further 4 million m³ of residues per year (SCION, Hall, & Gifford, 2007) and, unlike wood processing residue, little of this is utilised. Considering these two sources of wood waste there is more than 5 million m³ (50 PJ) available per year for additional use.

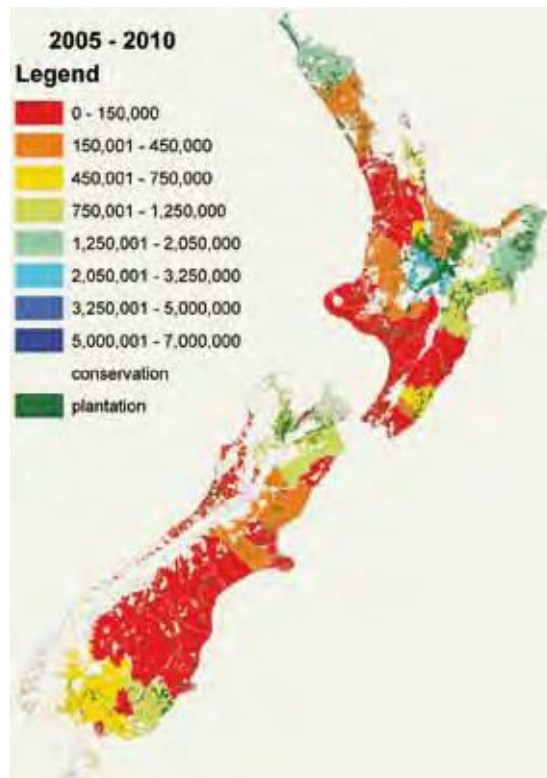


Figure 1: Regional distribution of forest and annual harvest volume (thousands of green tonnes) (SCION, et al., 2007)

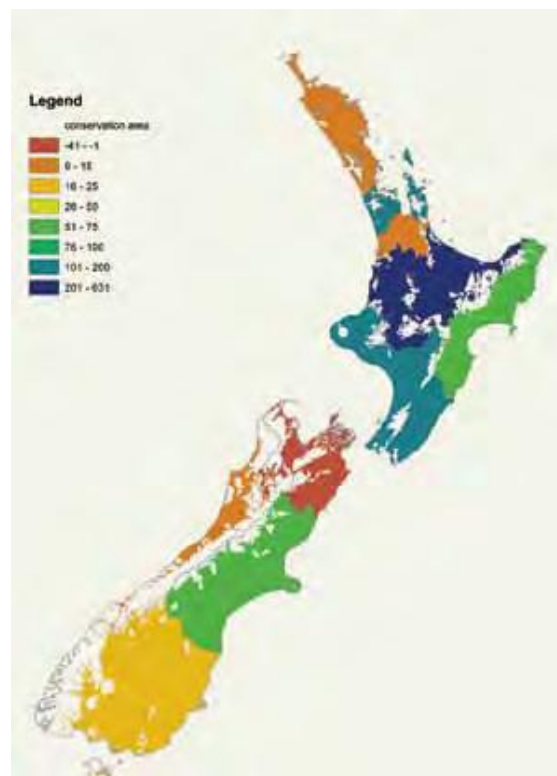


Figure 2: Wood processing residues available for use 2005 (thousands of green tonnes) (SCION, et al., 2007)

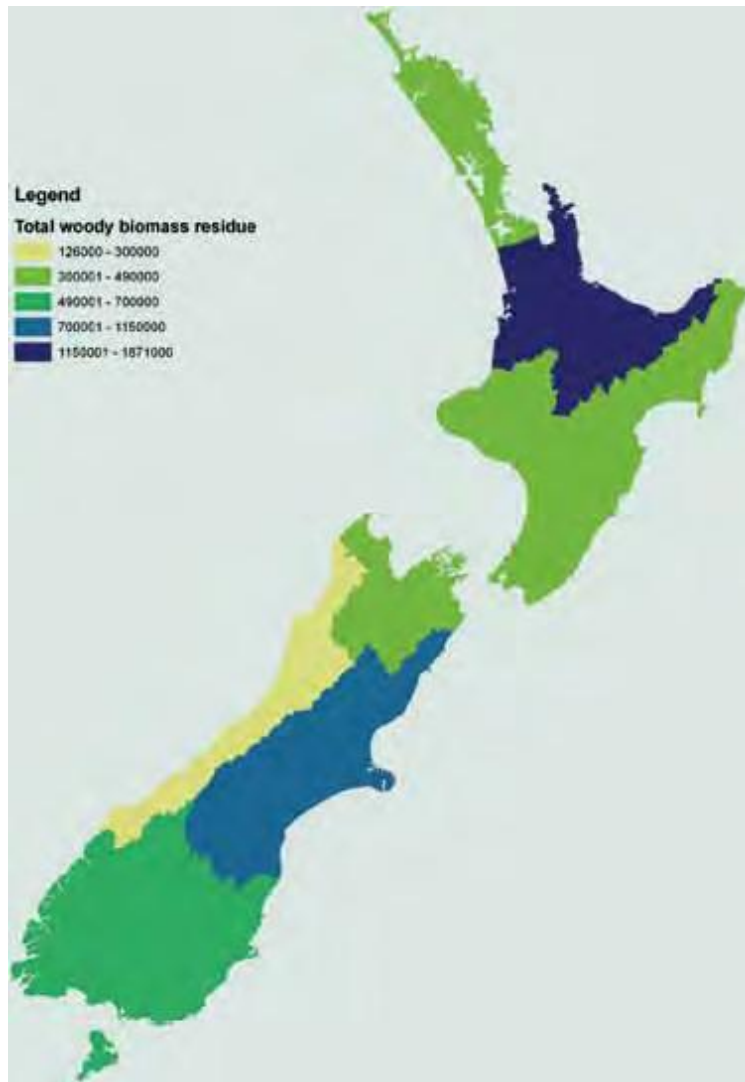


Figure 3: Distribution of all woody biomass resources for New Zealand 2007 (tonnes/year) (SCION, et al., 2007)

The above figures (Figure 1 to Figure 3) give an overview of the resource distribution and are obviously representative of the current scenario. It can be seen that the central North Island and the central South Island have the most resource. What is of significantly more interest to this research is the future trend of the forestry industry. This relates both to the supply of wood, as well as the amount required by end users.

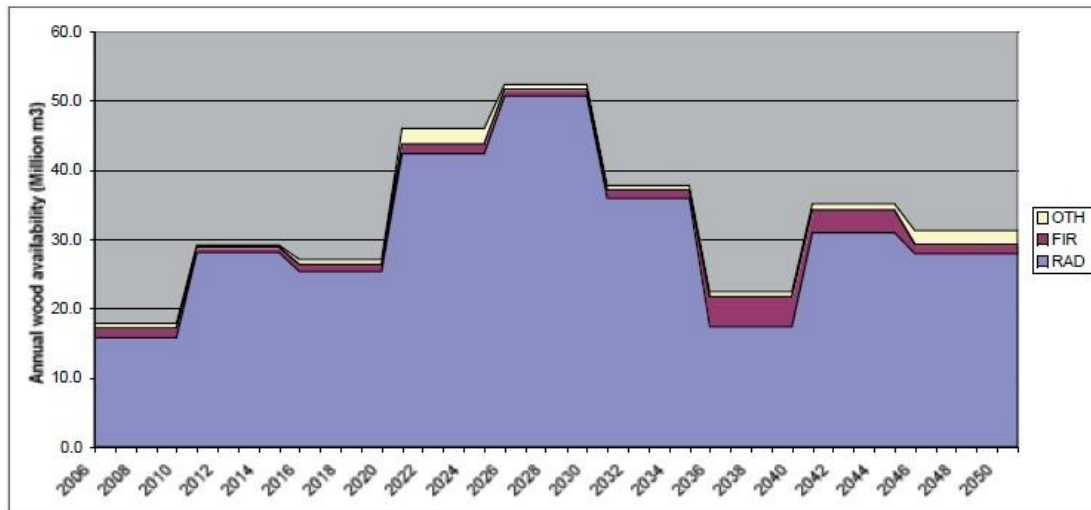


Figure 4: Forecast of annual wood supply with RAD being Pinus Radiata, FIR being Douglas Fir and OTH being other species (million m³/year). (SCION, et al., 2007)

Future predictions as shown in Figure 4 would indicate a substantial increase in wood availability compared to levels from 2006-2010. From 2010-2030 there is an estimated 9.5-14.8 million m³ of surplus wood available which could contribute 12-23% of the national liquid fuel requirement, 33-52% of the national heat demand and 10-19% of primary energy (SCION, Hall, & Jack, 2009).

Post the sawmills, a significant user of wood processing residues is the pulp and paper industry. Sawmill chip is used as a feedstock for pulp and paper production. For example in 2010 Norske Skog Tasman – a newsprint mill in the Eastern Bay of Plenty used 181,000 m³ of roundwood and 497,000 m³ of sawmill chip as its feedstock (Norske Skog, 2010). However, the future of paper mills may be uncertain. Production at Tasman has already reduced from three paper machines to two in recent years with the announcement that another paper machine will be closed in early 2013. Sawmills rely on being able to sell their sawmill chip for financial viability. If such sites reduce production and there is a surplus of feedstock then this increases the viability of a biomass fed energy plant. Incidentally Norske Skog is currently performing in depth investigations into potential biofuels plants at the Tasman site, indicating they see this as the future of wood processing in the region.

A further influence on the residues market would be the significant increase in export of whole logs, particularly to China. China is an easy and lucrative market for our wood and the export of logs to China has quadrupled since 2008. Part of this is due to a booming building

economy in China, as well as significantly reduced log exports from Russia due to an export tariff that was introduced (NZTIF, 2010). Whole log exports naturally do not generate the amount of residues that a milling operation does, as well as limiting the potential polygeneration scenarios available at sawmills. How this situation will develop long term, however, is not entirely clear. The market in China may slow significantly, and the export tariff from Russia could be removed. This naturally would create another significant shift in the market (NZTIF, 2010). Added to this is the fact that there are many sawmills closing or have recently closed (one merely needs to keep up to date with current affairs or discuss with people within the industry) in New Zealand limiting the sink for harvested wood if overseas demand for whole logs decreases. This could play an interesting role in the price of available wood, however, due to the number of variables it should merely be flagged as an area of interest, rather than a reliable prediction for future biomass based bioenergy projects.

2.3. Cost of Residues

Estimation of the cost of residues to a FT plant is important as this will directly affect the bottom line of the process. Table 1 examines delivered cost of residues including transportation costs and the harvesting terrain.

Table 1: Delivered cost of forest residues to a user (\$/m³, 2007) (SCION, et al., 2007)

Transport distance (one way)	Landing residues		Rolling cutover Ground based harvest		Steep terrain Hauler harvest	
	Low	High	Low	High	Low	High
25 km	\$24	\$34	\$36	\$50	\$63	\$78
50 km	\$27	\$39	\$39	\$55	\$67	\$83
75 km	\$30	\$43	\$42	\$59	\$70	\$87
100 km	\$33	\$47	\$45	\$63	\$72	\$91

As a comparison, the internal cost of usage for a sawmill for their own residues is minimal with just a handling cost of \$0.3-\$0.35 per GJ (assuming 8GJ/m³) (SCION, et al., 2007). This is obviously negating any opportunity cost for selling residues.

2.3.1. Transport cost

Further to the data in Table 1 the transportation cost of biomass has been broken down into cost per tonne per km (SCION, et al., 2007).

- Sawdust \$0.18 to \$0.25 per tonne per km
- Offcuts \$0.18 to \$0.27 per tonne per km
- Dry shavings \$0.54 to \$0.81 per tonne per km

This is on top of the purchase price of the residues from the mills. Currently the author hasn't obtained any figures on purchase prices from mills for waste. This is likely a commercially sensitive area so finding values for this may be difficult.

Given from the results above that costs for internal usage are minimal, and the transport cost can increase costs very easily, an energy plant would best suit a scenario where there is a substantial quantity of residues and a limited market for them and therefore low opportunity cost. The areas which have the highest density of biomass residue available such as the central North Island also have a higher concentration of sinks for the residue such as paper mills. However, areas such as the East Cape on the east coast of the North Island may be localised pockets with less use for the residue and therefore potential energy plants would be more advantageous due to this low opportunity cost.

2.4. Offsetting New Zealand's Fossil Fuel Usage

New Zealand had a biofuels obligation, a target for the proportion of biofuels within the total transport fuel supply, beginning at 0.53 % from 1 April 2008, increasing to 3.4 % biofuels by 2012 (Ministry of Economic Development, 2007). However, with the change in government this law was repealed (Brownlee, 2008) and instead a biodiesel grant scheme implemented (Brownlee, 2009). The scheme started on 1 July 2009 with a grant of up to 42.5 c/L of biodiesel for producers. The companies that signed up to the scheme based their feedstock on tallow, cooking oil, or rapeseed oil (Brownlee, 2009).

2.4.1. Carbon neutral fuel source

This research need not explain the current issues of global warming, or the exponential increase in CO₂ in the atmosphere. Due to the attention this subject has received over recent years the issue is now general knowledge. Less well known, however, is how New Zealand compares internationally in terms of CO₂ emissions (based on emissions from fuel

combustion as this is the area of study). Figure 5 shows New Zealand’s emissions per capita are relatively low when compared to other developed countries. However, the rate of change of New Zealand’s CO₂ emissions is concerning. Figure 6 shows the percentage change in total CO₂ emissions from combustion has increased 63% from 1990 to 2005 rating at the second highest OECD country. While a significant proportion of this could be attributed to changing lifestyles such as more commuting and families owning more than one car, regardless these are merely reasons and not an excuse for our accelerated rate of fossil fuel use in this country. New Zealand does have obligations under the Kyoto protocol for CO₂ emission reduction and has implemented the Emissions Trading Scheme (ETS) that currently caps the cost of emissions at a maximum of \$NZ 25/tonne of CO₂ equivalent emitted (Weir, 2012).

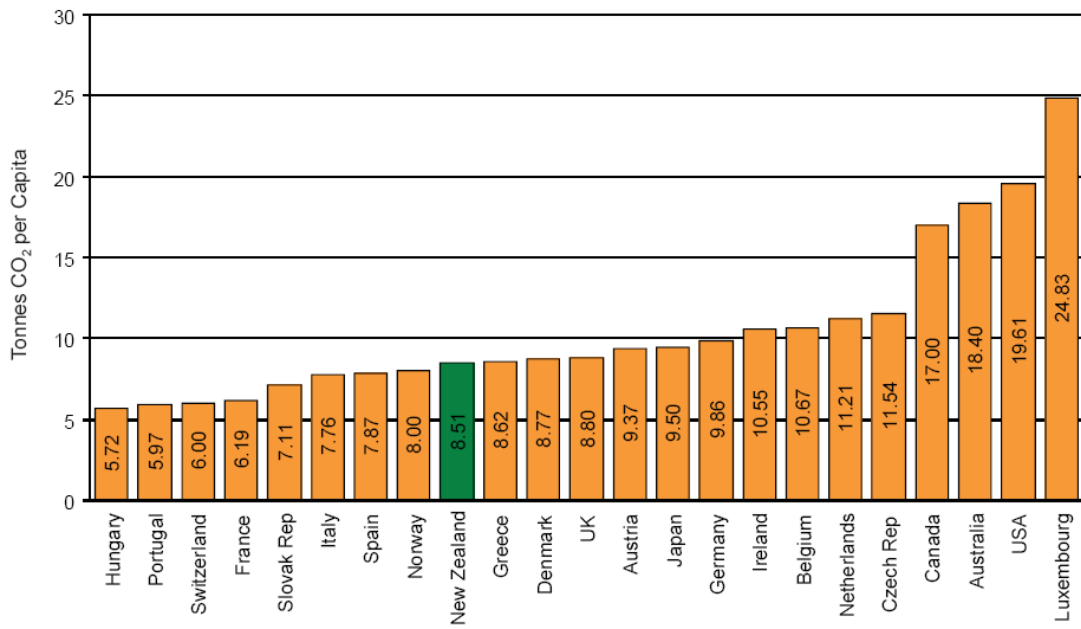


Figure 5: CO₂ emissions from fuel combustion per capita for OECD countries in 2005. (Ministry of Economic Development, 2008b)

Biomass gasification combined with Fischer Tropsch synthesis is a way of producing carbon neutral liquid fuels. The CO₂ produced during production and subsequent combustion of the liquid fuels is balanced by the CO₂ sequestered during the growth phase of the biomass. Figure 7 shows the comparison of greenhouse gas (GHG) reductions for various processes for liquid fuel production. FT from biomass compares very favourably with other technologies with the greatest reduction in GHG emissions compared to fossil fuel.

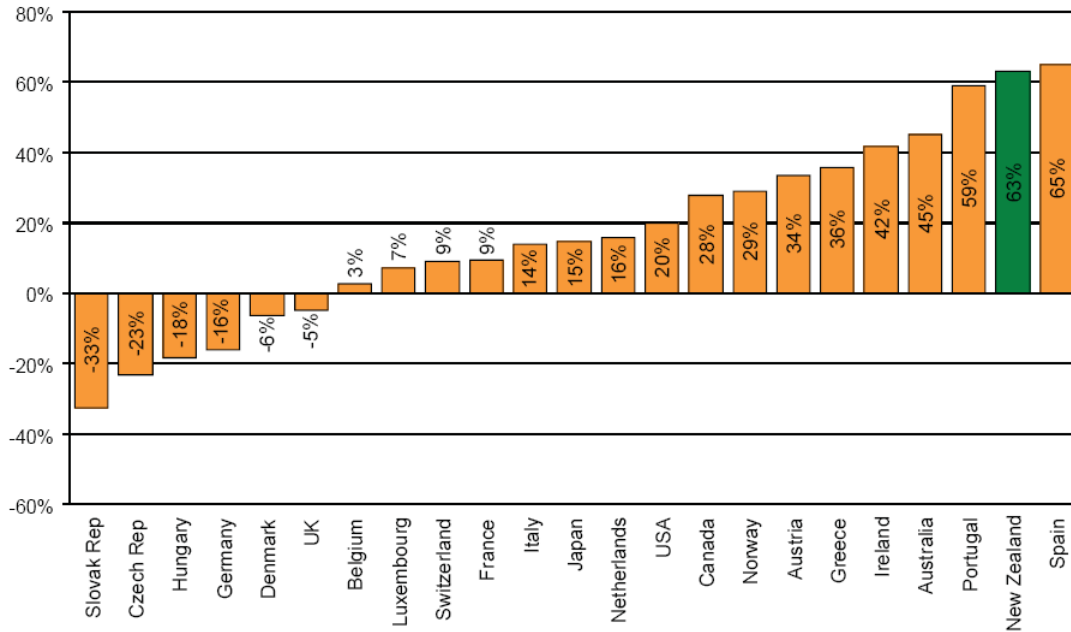


Figure 6: Percentage change in total CO₂ emissions from fuel combustion for OECD countries in 2005 relative to 1990. (Ministry of Economic Development, 2008b)

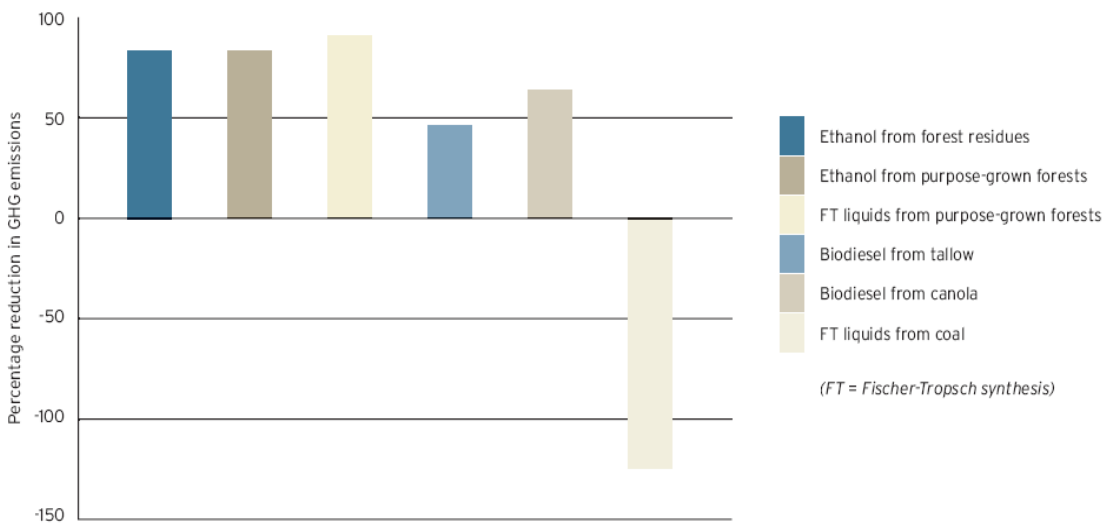


Figure 7: Percentage reduction in greenhouse gas emissions compared to petrol or diesel for various processes. (SCION, Hall, & Jack, 2008)

2.4.2. Oil price

Recent times have seen great volatility in the oil price. During mid 2008 the price for a barrel of crude increased dramatically as shown in Figure 8. Due to the global recession this price has reduced. One would most certainly expect, however, this price will again rise when the economy strengthens. Aside from any environmental performance gain the greatest driver for a FT process is the relative cost of fossil fuels. Logic would argue products

will need to be produced under the cost of existing fossil fuels to attract significant investment in the technology, particularly from private enterprise.

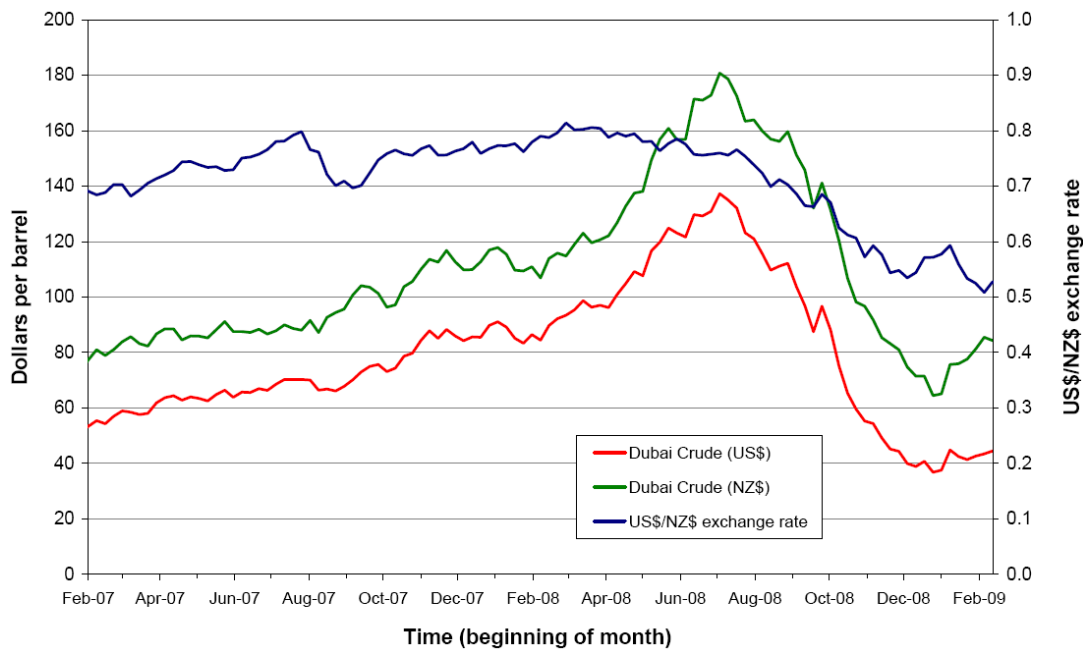


Figure 8: Weekly average Dubai crude incorporating New Zealand exchange rate (Ministry of Economic Development, 2009)

2.4.3. New Zealand industry support

There are several aspects to how biomass to liquid fuel plants can have a positive effect on the New Zealand industry/economy. Production of petrochemicals domestically reduces the need for oil imports. Currently virtually all oil is imported for refining and consumption in New Zealand. This is because all domestic oil bar 3% (in 2007) is exported due to its high quality and subsequent higher value (Ministry of Economic Development, 2008a). Reducing importation by manufacturing and using products domestically or exporting (possibility of exporting higher value FT products) provides better support for the local industry.

2.4.4. Suitability of the technology for New Zealand Infrastructure

There are a number of biofuel technologies being investigated in New Zealand currently. One therefore needs to assess the advantages and disadvantages of each such as relative environmental benefits, economics and the fit with existing infrastructure. In 2010 the Parliamentary Commissioner for the Environment released a report entitled 'Some biofuels are better than others: Thinking strategically about biofuels' (Wright & Bull, 2010). This report was very helpful in taking a broad view of the feedstocks available in New Zealand,

the conversion technologies, and how the final product fits with current infrastructure. The report concluded that technologies should be supported that can utilise wood as a feedstock, and also had the view that technologies that can produce a 'drop in' fuel are superior. The term 'drop in' means that the fuel produced by the technology can be used within the existing systems. For example a car doesn't have to be configured to be able to run on an ethanol based fuel. This is particularly important for a country like New Zealand with an older car population. It would take quite a shift for New Zealand to move to a culture of purchasing predominantly new cars with flexible fuel ability. In addition to being a cultural shift, a substantial proportion of the population could not afford a new car.

Fuel (especially diesel) produced via Fischer Tropsch synthesis has the potential to be an excellent drop in fuel. No modifications to any existing systems are necessary, through the entire supply chain to the end user. Some modification to refineries to accept and process a Fischer Tropsch crude may be necessary but this is not anticipated to be as difficult and costly as that required for alternative biofuels (e.g. Pyrolysis products).

2.5. Fischer Tropsch Background

2.5.1. History of the Fischer Tropsch process

The Fisher-Tropsch process was originally discovered in the 1920's by Professor Franz Fischer and Dr. Hans Tropsch. The Fischer-Tropsch (FT) process is a means of converting synthesis gas (ideally a 2:1 molar ratio of H₂ to CO) into long chain hydrocarbons. This process was widely used in Germany in WWII and in South Africa during oil embargos (Mark E. Dry, 2002). Historically the Fischer-Tropsch process has been based on natural gas and syngas from coal gasification as a feedstock. Current plants in operation or under construction are shown in Table 2. The process with coal or gas as a feedstock is therefore very mature, however, to the author's knowledge there are no significant plants producing biodiesel from biomass via the FT process. There are a small number of smaller scale projects with one of the most notable being the Choren plant in Germany which is a 45 MW plant producing 18 million litres of fuel per annum (Choren, 2011). However, the latest update on this plant is that it is now closed. While difficult to find official information on the closure the grey literature would suggest that the time taken to solve technical issues during commissioning eventually financially crippled the operation (Rapier, 2011).

Table 2: Fischer-Tropsch synthesis plants either in operation or under construction (Guettel, Kunz, & Turek, 2008).

Company	Site	Capacity (bpd)	Raw Material	Commissioning date
Existing Plants				
Sasol	Sasolburg	2500	Coal	1955
Sasol	Secunda	85000	Coal	1980
Sasol	Secunda	85000	Coal	1982
MossGas	Mossel Bay	30000	Natural gas	1992
Shell	Bintulu	12500	Natural gas	1993
Sasol/Qatar Petroleum	Qatar	34000	Natural gas	2006
Under Construction				
SasolChevron	Escravos	34000	Natural gas	2007
Shell	Qatar	140000	Natural gas	2009

Notable is the significant size of the plants in Table 2. The plants represent significant investment and in some cases benefit from the very high end of economies of scale.

2.6. Process Configuration

2.6.1. The process

There are two aspects to consider in discussion of the FT process, the first is the base technology i.e. is it a HTFT (High Temperature Fischer-Tropsch) process or a LTFT (Low Temperature Fischer-Tropsch) process, the second is the plant configuration. These will be described briefly in turn.

2.6.1.1. HTFT

HTFT has a typical temperature range of 300-350°C (Bolhar-Nordenkamp, 2004). Iron catalysts are used in this process and the predominant product is lighter hydrocarbons and high value light olefins (A. Steynberg & Dry, 2004). A typical product distribution for HTFT is shown in Table 3.

Table 3: Typical HTFT product composition (A. P. Steynberg, Espinoza, Jager, & Vosloo, 1999)

Product	(%)
Methane	7
C ₂ -C ₄ Olefins	24
C ₂ -C ₄ Paraffins	6
Gasoline	36
Middle distillates	12
Heavy cut and waxes	9
Oxygenates soluble in water	6

2.6.1.2. LTFT

LTFT has a temperature range of 200-240°C (Bolhar-Nordenkampf, 2004). Heavier waxes are generated in this process and it is more targeted to diesel fuel. Either iron or cobalt catalysts can be used in LTFT but cobalt appears to be the current catalyst of choice (A. Steynberg & Dry, 2004). Both technologies are used in commercial operation. However, for the purposes of this research LTFT will be the process examined further. Because LTFT produces waxy long chain hydrocarbons these are more suitable to deal with on a smaller scale than the HTFT process. HTFT has good petrol production but due to the low selectivity significant offgas is produced necessitating complicated reforming steps to increase productivity. The LTFT long chain hydrocarbons can be treated by hydrocracking to produce biodiesel (Bolhar-Nordenkampf, 2004), as well as having a significant cut of diesel in the syncrude that needs only separation. An example of the fractions produced in LTFT is shown in Table 4.

Table 4: Typical distillation range for LTFT syncrude fractions (A. Steynberg & Dry, 2004)

Distillation Range	FT condensate	FT Wax
	% Vol	% Vol
C ₅ - 160°C	44	3
160 - 270°C	43	4
270 - 370°C	13	25
370 - 500°C	-	40
>500°C	-	25

2.6.2. Process Configuration

There are two different generic configurations for the process (Tijmensen, Faaij, Hamelinck, & Van Hardeveld, 2002).

- Full conversion. The tail gas is recycled into the process to yield maximum output.
- Once through. The tail gas is utilised for production of electricity and heat.

The content of CO₂ in the reactor should be lower than 10 vol% so that the partial pressure of the other components is not significantly lowered (Bolhar-Nordenkampf, 2004). This is where the once through process is most suitable for a small scale operation. In a once through process there is not the cost and complexity of installing and operating a CO₂ separation system on top of the already expensive gas recycle system.

From this brief review of the methods of operation an LTFT once through process is the most likely candidate for the small scale Fischer-Tropsch system in New Zealand. This is due to the simplicity of design of the once through process and the higher selectivity to longer chain hydrocarbons of the LTFT process.

2.7. Techno-economic aspects

The challenge realised in this study is the production of liquid fuels at a suitable scale that meets the balance between production cost and biomass availability. Traditional Fischer-Tropsch fuel plants rely heavily on economies of scale to remain viable. Using either natural gas or coal allows a very concentrated source of feedstock. For the case of a biomass fed Fischer-Tropsch plant there is not the same density of feedstock, therefore a different set of constraints apply compared with traditional plants. Economies of scale becomes a balance with the availability of feedstock at an appropriate price. While a larger plant will produce fuel at a lower price per unit the cost of delivered biomass will increase as the transportation costs increase. Literature can be found (Searcy & Flynn, 2009) on analysis of the optimum size of a plant taking into account scale and biomass cost and this could be applied to the New Zealand scenario. Searcy & Flynn (2009) provide a good graphical summary of this balance between plant size and unit cost as shown in Figure 9 albeit for a biomass to energy plant rather than an FT plant, the same principles apply however.

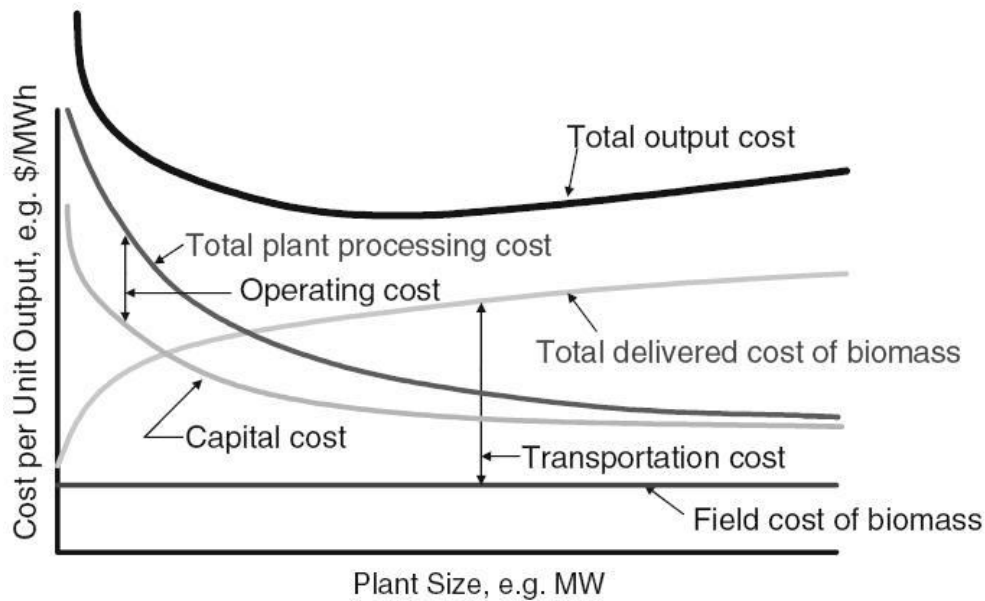


Figure 9: Balance between production cost and plant size for a biomass based energy plant (Searcy & Flynn, 2009)

While Searcy & Flynn (2009) take a logical step towards sizing a plant the design philosophy of this research is different as it involves integration with a sawmill. Rather than attempt to maximise profit in a balance between plant size and biomass cost in a stand alone fuel plant the synergy realised between heat and power requirements of a sawmill being met from a Fischer-Tropsch fuels plant is explored. Williams et al. (2009) take a similar route in examining the advantages of once through polygeneration plant configurations, although they consider a mix of biomass and coal, carbon capture and storage and are not directly integrated into an energy requiring facility. They do however, promote the polygeneration model as a way to produce Fischer-Tropsch liquid at a lower price when sale of electricity is included compared to a plant configured to maximise liquids production. They quote an economic value of lower than \$30 per barrel of crude, although the minimum production in their modelled scenarios is approximately 8,000 bbl/day which is significantly higher than that considered in this research.

There are a number of other techno-economic/feasibility studies of biomass to Fischer-Tropsch plants (Damartzis & Zabaniotou, 2011; Hamelinck, Faaij, den Uil, & Boerrigter, 2004; G. Liu, Larson, Williams, Kreutz, & Guo, 2011; Swanson, Platon, Satrio, & Brown, 2010; Tijmensen, et al., 2002; R. Zwart & van Ree, 2009; R. W. R. Zwart & Boerrigter, 2005). These along with direct costing literature (Bouman, Jesen, Wake, & Earl, 2005; Ulrich & Vasudevan,

2004) and scaling laws assist in costing an FT plant, however, there are no directly correlated scenarios found by the author in terms of FT plant integration into a parent plant as a sink for heat and power.

2.8. The Reaction and Kinetics

The overall reaction commonly used to describe the FT process is (Logdberg, 2007; Tijmensen, et al., 2002)



This reaction by necessity is a multi step reaction with several intermediates, however, the intermediates remain bonded to the surface. In order for the above reaction to complete, at least 10 reactions are required (Schulz, 1999)-

- Associative adsorption of CO
- Splitting of the C/O bond
- Dissociative adsorption of 2H₂
- Transfer of 2H to the oxygen to yield H₂O
- Desorption of H₂O
- Transfer of 2H to the carbon to yield CH₂
- Formation of a new C/C bond

The order of these steps is in question, which can lead to discussion of the mechanism of FT synthesis. However, the mechanism of the FT reaction has not been specifically reviewed in this research. There is sufficient literature available that reviews the development of the FT mechanism (B. H. Davis, 2001; M. E. Dry, 1996; Fontenelle & Fernandes, 2011; Schulz, 1999) if one wanted to investigate further. A fundamental understanding of the mechanism behind the FT synthesis process is helpful, however, in the overall process this detail is not a particularly necessary consideration for this research. Rather than focus on the mechanism of reaction itself, an investigation into the kinetics of the FT reaction(s) is a more tangible area to pursue in regards to comparison and optimisation of various catalysts and reactors. Yates and Satterfield (1991) reviewed a number of published kinetic equations as shown in Table 5 as well as proposing simplified two parameter forms of the kinetic equations with Equation 2 being the most suitable.

$$-R_{CO} = \frac{\alpha P_{CO} P_{H_2}}{(1 + \beta P_{CO})^2} \quad (2)$$

The linearised form of the equation fits their own data well, as well as that of several previous researchers.

Atashi et al. (2010) also provide a summary of kinetic studies that have been performed on cobalt catalysts with the reaction parameters and kinetic expressions shown in Table 6. Also a very good reference providing a literature review of the mechanisms and kinetics of Fischer Tropsch is provided by Van Der Laan & Beenackers (1999).

Table 5: Summary of Kinetic Studies extracted from Yates & Satterfield (1991)

reference	catalyst	reactor type	T, °C	operating conditions		intrinsic kinetic expression ^a	eq
				P, MPa	H ₂ /CO		
Brötz ¹	Co/MgO/ThO ₂ /kieselguhr	fixed bed	185–200	0.1	2	$-R_{H_2+CO} = aP_{H_2}^2/P_{CO}$	3
Anderson ²	Co/ThO ₂ /kieselguhr	fixed bed	186–207	0.1	0.9–3.5	$-R_{H_2+CO} = aP_{H_2}^2P_{CO}/(1 + bP_{H_2}^2P_{CO})$	4
Yang et al. ³	Co/CuO/Al ₂ O ₃	fixed bed	235–270	0.17–5.5	1.0–3.0	$-R_{H_2+CO} = aP_{H_2}P_{CO}^{-0.5}$	5
Pannell et al. ⁴	Co/La ₂ O ₃ /Al ₂ O ₃	Berty (low conversion)	215	0.49–0.8	2	$-R_{H_2+CO} = aP_{H_2}^{0.66}P_{CO}^{-0.33}$	6
Rautavuoma and van der Baan ⁵	Co/Al ₂ O ₃	fixed bed (low conversion)	250	0.1	0.2–4.0	$-R_{CO} = aP_{H_2}P_{CO}^{1/2}/(1 + bP_{CO}^{1/2})^3$	7
Wang ⁶	Co/B/Al ₂ O ₃	fixed bed (low conversion)	181	0.1–0.2	0.25–4.0	$-R_{CO} = aP_{H_2}^{0.68}P_{CO}^{-0.5}$	8
Sarup and Wojciechowski ⁷	Co/kieselguhr	Berty	190	0.2–1.5 ^b	0.5–8.3 ^b	$-R_{CO} = aP_{CO}^{1/2}P_{H_2}^{1/2}/(1 + bP_{CO}^{1/2} + cP_{H_2}^{1/2} + dP_{CO})^2$	9
Wojciechowski ⁸						$-R_{CO} = aP_{CO}P_{H_2}^{1/2}/(1 + bP_{CO} + cP_{H_2}^{1/2})^2$	10

^a *a*, *b*, *c*, and *d* in these equations are temperature-dependent constants. ^b These ranges of operating conditions are estimated from their experimental data.

Table 6: Summary of kinetic studies extracted from Atashi et al. (2010)

Summary of kinetic studies of FTS on cobalt-based catalysts.

Reference	Catalyst	Reactor type ^b	T, °C	P, bar	H ₂ /CO	Intrinsic kinetic expression ^a
[12]	Co-Ru/Al ₂ O ₃	FBR	235–250	45–65	1.7–2.3	$-r_{\text{CO}} = \frac{aP_{\text{H}_2}^{0.5}P_{\text{CO}}^{0.5}}{(1 + bP_{\text{H}_2}^{0.5} + cP_{\text{CO}}^{0.5} + dP_{\text{CO}})^2} \quad (1)$
[13]	Co/ThO ₂ /kieselguhr	FBR	186–207	1	0.9–3.5	$-r_{\text{CO}+\text{H}_2} = \frac{aP_{\text{H}_2}^2P_{\text{CO}}}{1 + bP_{\text{H}_2}^2P_{\text{CO}}} \quad (2)$
[14]	Co/Pt/Al ₂ O ₃	Slurry	230	5–40	1.6–3.2	$-r_{\text{CO}+\text{H}_2} = \frac{aP_{\text{H}_2}^{0.75}P_{\text{CO}}^{0.5}}{(1 + bP_{\text{CO}}^{0.5}P_{\text{H}_2}^{0.25} + cP_{\text{CO}}^{0.5}P_{\text{H}_2}^{-0.25})^2} \quad (3)$
[15]	Co/kieselguhr	Betry (Ic)	190	2–15	0.5–8.3	$-r_{\text{CO}} = \frac{aP_{\text{CO}}^{0.5}P_{\text{H}_2}^{0.5}}{(1 + bP_{\text{CO}}P_{\text{H}_2}^{0.5} + cP_{\text{CO}})^2} \quad (4)$
[16]	Co/kieselguhr	Betry	190	2–15	0.5–8.3	$-r_{\text{CO}} = \frac{aP_{\text{CO}}P_{\text{H}_2}^{0.5}}{(1 + bP_{\text{CO}} + cP_{\text{H}_2}^{0.5})^2} \quad (5)$
[17]	Co/La ₂ O ₃ /Al ₂ O ₃	Betry (Ic)	215	5.2–8.4	2	$-r_{\text{CO}+\text{H}_2} = aP_{\text{H}_2}^{0.55}P_{\text{CO}}^{-0.33} \quad (6)$
[18]	Co/Al ₂ O ₃	FBR (Ic)	250	1	0.2–4.0	$-r_{\text{CO}} = \frac{aP_{\text{H}_2}P_{\text{CO}}^{0.5}}{(1 + aP_{\text{CO}}^{0.5})^3} \quad (7)$
[19]	Co/B/Al ₂ O ₃	FBR (Ic)	181	1–2	0.25–4.0	$-r_{\text{CO}} = aP_{\text{H}_2}^{0.68}P_{\text{CO}}^{-0.5} \quad (8)$
[22]	Co/TiO ₂	FBR	180–240	20	1–4	$-r_{\text{CO}} = \frac{aP_{\text{H}_2}^{0.74}P_{\text{CO}}}{(1 + bP_{\text{CO}})^2} \quad (9)$

^a a, b, c and d are temperature-dependent constants.

^b FBR=Fixed-bed reactor; Ic = low conversion.

2.9. Selectivity

The other significant aspect of the Fischer-Tropsch reaction apart from the activity and subsequent production rate is the selectivity. The selectivity (α) is the term designated to the spread of long chain hydrocarbon products produced. The FTS reaction follows closely the Anderson-Shultz-Flory (ASF) distribution which can be represented by Equation 3 and is based on chain growth probability with the visual demonstration of this shown in Figure 10.

$$\frac{W_n}{n} = (1 - \alpha)^2 \alpha^{n-1} \quad (3)$$

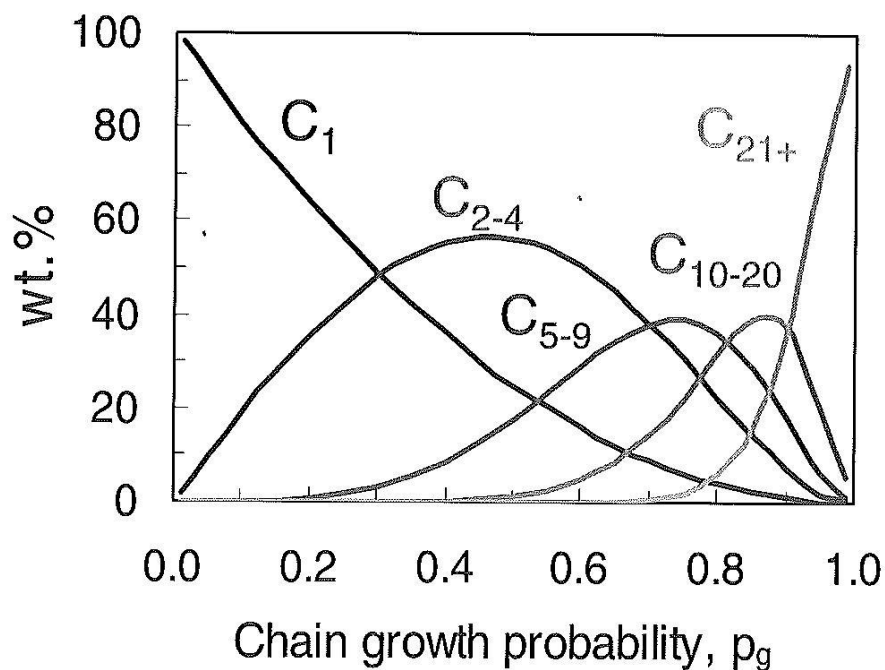


Figure 10: Product composition as a product of chain growth ($p_g = \alpha$) (A. Steynberg & Dry, 2004)

Naturally there is interest in the possibility of modifying this typical product distribution in order to maximise product recovery in a particular range. An example of this can be found later in the literature review under water effects in FT synthesis.

2.10. Catalysts

2.10.1. Fischer-Tropsch catalysts introduction

Literature review for catalysts presents a challenge. The many apparent contradictions and differing opinions when reading literature would lead to the conclusion that catalysis still is, as often quoted, 'a black art' as well as a science. It should also be noted that the information available on catalysis is almost endless, therefore this literature review will attempt to limit the quantity of information by focusing particularly on what is deemed most pertinent to the research and assume a reasonable base knowledge of the reader. This will take the form of an introduction to Fischer-Tropsch catalysts in general. An analysis of the different FT catalysts will allow selection of the most appropriate catalyst for the application allowing further narrowing of the literature review. From there pertinent catalyst properties such as supports, promoters, preparation methods and other areas which affect the performance of catalysts and should be considered in the design and experimentation of a suitable catalyst will be reviewed.

2.10.2. General background

There are four FT catalysts which have the activity required for commercial operation. They are Cobalt, Nickel, Iron, and Ruthenium. Under FT conditions significant amounts of methane are produced using Nickel which renders it unsuitable. Ruthenium although a good catalyst for fundamental studies of FT, is very expensive (around 50,000 times the price of iron) and there are very limited available quantities rendering it unsuitable for large scale operation. Therefore cobalt and iron are the two catalysts that are deemed suitable, and hence have been used in commercial operation (Mark E. Dry, 2002). There are advantages and disadvantages to both iron and cobalt which will be reviewed through the lens of suitability for small scale FT operation in the New Zealand context.

It should be noted that the price of cobalt is about 1000 times that of iron (Mark E. Dry, 2002). However, given that cobalt catalysts are in commercial operation (Khodakov, Chu, & Fongarland, 2007) there must be factors that justify the extra cost. Although cobalt is considerably more expensive than iron it is more resistant to deactivation and tends to last longer (Iron catalyst only lasts for 8 weeks in commercial operation (R. Zwart & van Ree, 2009)). An estimate of the cost per barrel for the cobalt catalyst given the longer lifetime is \$US0.7per barrel. At low conversions the activity is similar, however, water slows the reaction rate with an iron catalyst more so than cobalt. Given that water is a product of FT synthesis, cobalt catalysts have a productivity advantage at

higher conversions (Khodakov, et al., 2007; Schulz, 1999). This would indicate a cobalt catalyst would be more appropriate for a once through process as with iron a significant amount of tail gas recycling is normal due to the conversion being limited because of water inhibition (Schulz, 1999).

The advantage of iron, however, is the water-gas shift activity compared to cobalt. This means that a lower ratio of H₂ to CO can be fed to the FT synthesis reaction. This may be particularly suitable for a biomass gasification scenario (Khodakov, et al., 2007), unless operation of the gasifier can yield a 2:1 H₂:CO ratio suitable for cobalt catalysts.

Based on the advantages and disadvantages and the specific application (LTFT diesel production in a likely once through process) it is deemed that a cobalt catalyst is the most suitable due to its high activity and resistance to water effects. Therefore this review will narrow to focussing on cobalt catalysts with discussion on related areas to this research in terms of development of suitable cobalt catalysts for the small scale FT application.

2.10.3. Supports for cobalt catalysts

Given that cobalt costs significantly more per unit mass than iron a means of minimising the mass by maximising the surface area is required. Cobalt is typically dispersed on high area supports such as Al₂O₃, SiO₂, and TiO₂ with a cobalt loading from 10 to 30 g per 100 g of supporting material (Mark E. Dry, 2002). There have been a number of studies comparing cobalt supported on different metal oxides, (Oukaci, Singleton, & Goodwin, 1999; Storster, Ttdal, Walmsley, Tanem, & Holmen, 2005) to name two good references.

The paper from Oukaci et al. (1999) specifically compares catalysts based as closely as possible to existing patented FT catalysts. It is noteworthy that not one support has been adopted by all manufacturers identifying the potential scope for acceptable FT catalysts with different supports. Gulf/Chevron and Statoil used alumina, Shell used silica and Exxon, titania. This is based on the most common support used in their patents. A summary of the patented catalysts for the various catalysts examined by Oukaci et al. (1999) is listed in their paper and is worth examining by the reader although inclusion in this review would be an excess of information.

2.10.4. Catalyst preparation methods

There are a number of different methods for adding catalytic metal to the support. The most typical for FT synthesis catalysts are impregnation (of which several methods fall under this banner) and precipitation methods. The forms of these will be discussed briefly.

2.10.4.1. *Incipient wetness impregnation*

The simplified concept of incipient wetness impregnation is where a solution of the catalyst precursor is added to the support until the point where visible wetness is observed (Kraum & Baerns, 1999). This is the point at which the pores are saturated with solution. The catalyst is dried and solution added again until the correct loading is obtained. Often for incipient wetness impregnation an aqueous solvent is used (Johan P. den Breejen, Sietsma, Friedrich, Bitter, & de Jong, 2010; Kraum & Baerns, 1999; Oukaci, et al., 1999; Storster, et al., 2005).

2.10.4.2. *Impregnation*

Impregnation is similar to the method above, however, an excess of solvent is added to create a slurry. This is usually agitated and quite often dried in a rotary evaporator with an organic solvent (Kraum & Baerns, 1999; Oukaci, et al., 1999)

2.10.4.3. *Precipitation*

A common method for creating supported cobalt catalysts by precipitation is described. The simple principle is that a solution of the catalyst salt is chemically modified to allow it to precipitate out of solution and onto the support. The specific details of concentration and so forth are not described, rather these will be picked up in experimental sections in this thesis.

A basic precipitation method (Atashi, et al., 2010; Kraum & Baerns, 1999)

- Dissolve $\text{Co}(\text{NO}_3)_2$ in water, add a saturated NaHCO_3 solution
- Adjust pH to 8 by adding HNO_3 dropwise
- Stir and filter cobalt hydroxide precipitated on support
- Wash several times with water and dry

2.10.5. *Novel methods*

Of interest are newer, novel methods for catalyst preparation and support beyond those traditional methods used in industry. Given the challenge of smaller scale FT, novel catalyst methods may have an advantage, particularly if a novel reactor is also incorporated.

2.10.5.1. *Combustion synthesis*

Velocys is an example of a company endeavouring to use novel reactor and catalyst technology to improve the economics of FT synthesis. They are employing microchannel reactors loaded with catalyst prepared by their 'Organic Matrix Combustion' technique (Atkinson, 2010). The catalyst

preparation process is claimed to create higher catalyst loading while still maintaining an optimum small crystal size. The metal salt is combined with an organic component to form a complex, in turn stabilising the metal. During calcination, combustion occurs that fixes the crystallites at a smaller size given the speed of the combustion reaction. This leads to a narrow particle size distribution, avoiding larger crystallites which can lead to lower activity, as well as very small crystallites which can lead to sintering (Atkinson, 2010). Because of the promising nature of this catalyst method it seemed prudent to research further in the open literature the methodology of similar techniques.

There is literature available (Castro, Gayoso, & Rodriguez, 1997; Dinka & Mukasyan, 2005; Ganesh et al., 2005; Gonzalez-Cortes, Rodulfo-Baechler, Xiao, & Green, 2006; González-Cortés, Xiao, Costa, Fontal, & Green, 2004; González-Cortés, Xiao, Rodulfo-Baechler, & Green, 2005), however, none was found that related directly to FT catalysts.

The combustion synthesis technique uses a fast and highly exothermic reaction in a powder mix to generate high temperatures of the order of 1500 K and above for a short period. There are a significant quantity of structural defects that are generated in this process leading to beneficial properties for catalysis (González-Cortés, et al., 2004). The work of González-Cortés et al. (2006; 2004) utilised a cobalt on alumina catalyst (albeit with other metals as well) for a different catalytic application, however, the principles are the same. Urea was mixed with the salts in a 10:1 ratio and a 2:1 ratio of water to precursors before being slurried with the alumina support. Post this the mix was heated at 50°C for 2-3 hours before being ignited at 500°C in a furnace in static air for 10 min. This yields a carbon free light voluminous oxide. For the application of the catalyst the activity was higher than that of catalysts prepared via incipient wetness impregnation.

2.10.5.2. Novel precipitation

Research by Bezemer et al. (2006) investigated the effect of homogenous deposition-precipitation on the catalyst support from a basic solution compared to the conventional application from an acidic solution. They found that the precipitation from the basic solution (using ammonia evaporation) caused less interaction between the precipitate and the silica support. With the acidic precipitation method the interaction with the support required a higher reduction temperature of 600°C which in turn sintered the metal to 35nm. With the ammonia evaporation method the reduction temperature was lower resulting in a catalyst with 13nm cobalt particles on the silica support.

2.10.6. Novel supports for catalysts

Carbon nanotubes/nanofibres as a catalyst support for both cobalt and iron catalysts are currently receiving a reasonable amount of attention (Bahome, Jewell, Hildebrandt, Glasser, & Coville, 2005; Bahome et al., 2007; Bezemer, Radstake, Falke, et al., 2006; Bezemer, Radstake, Koot, et al., 2006; W. Chen, Fan, Pan, & Bao, 2008; Chin, Hu, Cao, Gao, & Wang, 2005; A. Tavasoli et al., 2008; Trepanier, Dalai, & Abatzoglou; Van Steen & Prinsloo, 2002; Zaman, Khodadi, & Mortazavi, 2009).

Tavasoli et al. (2008) reported a significant increase in hydrocarbon yield with cobalt supported on carbon nanotubes compared to an alumina support. The carbon nanotube supported catalyst exhibited better dispersion with lower average cobalt cluster size. Metal-support interactions were reduced with a corresponding increase in the reducibility of the catalyst. A slightly lower selectivity resulted from the carbon nanotube supported catalyst however.

Whereas Tavasoli et al. (2008) used an impregnation method on nanotubes, Bezemer et al. (2006) used a homogeneous deposition-precipitation (HDP) method on carbon nanofibres (CNF) with silica as a support comparison. When precipitation was started from a high pH the CNF supported cobalt catalyst performed very well compared to the other methods particularly in terms of C₅₊ selectivity. These results interestingly are counter to Tavasoli et al. (2008) where lower selectivity was observed.

Trepanier et al. (2010) used a microemulsion technique on CNT's to produce catalysts with very tight Co particle size distributions. They created catalysts with average particle sizes of 2-3nm and 9-10nm. They found an increase in the FTS rate and the C₅₊ selectivity in the larger particle size. Interestingly through TEM analysis they put the reasoning for this lower activity down to the smaller particles being confined into the nanotubes suggesting the confinement affects the typically seen structurally sensitive results. Aside from the suggested reasons for the lower activity with smaller particle size, the results seem to corroborate with that of Den Breejen et al. (2009) in that particle sizes under 6nm result in lower FTS activity as discussed specifically in section 2.14.

Chen et al. (2008) investigated the confinement of iron catalyst within CNTs and although this review is not focussing on iron it makes an interesting comparison. Confinement within CNTs according to their research actually increased the FTS activity compared with that outside of the CNTs. This is attributed to the confinement modifying the redox properties of the encapsulated iron oxides. The iron inside the CNTs tends to exist in the more reduced carbide phase leading to higher FTS activity. The yield of the iron catalyst contained within the CNTs was twice that of iron catalyst outside of the

CNTs. It is interesting that the comparison between Chen et al. (2008) and Trepanier et al. (2010) shows that the FTS activity of cobalt decreases when confined in CNTs whereas the activity of iron increases. This shows the different ways that iron and cobalt act as FT catalysts. Where cobalt has catalytic activity in the pure metal state, iron is regarded as having FTS activity in oxide and/or carbide states.

2.11. Water Effects in FT Synthesis

Given the biggest single product of FTS is water any influence it may have on the process is likely to be significant. It has therefore seen a reasonable amount of attention by researchers (Jinlin Li, Jacobs, Das, Zhang, & Davis, 2002; X. Liu, Hamasaki, Honma, & Tokunaga, 2011; Lögberg et al., 2011; Lualdi, Logdberg, Regali, Boutonnet, & Jaras, 2011).

The effect of water depends on a number of factors such as the support, metal loading, promoters and preparation that all leads to a complex situation (Dalai & Davis, 2008). It is noted that in general water up to a certain concentration actually has positive effects on FTS, leading to higher CO conversion and better C₅₊ selectivity, olefin selectivity, as well as lower methane and CO₂ production. There are variations to this effect however as shown in Figure 11 sourced from Dalai and Davis (2008).

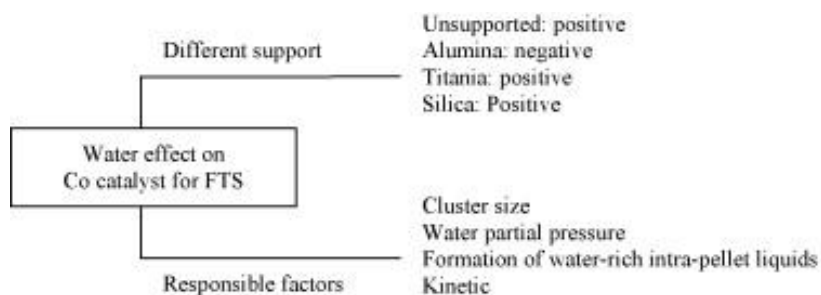


Figure 11: Diagram showing water effects for a Co catalyst for FTS (Dalai & Davis, 2008)

A very interesting application of the water effects was the study by Liu et al. (X. Liu, et al., 2011) where substantial anti-ASF distribution was noted by adding water in a slurry reactor. The catalyst was unsupported cobalt suspended in an n-decane solvent in the reactor at 230°C at 6MPa. Without water addition the system followed usual ASF parameters yielding a C₁₀₊ selectivity of 32%. With water addition the C₁₀₊ selectivity increased to 87.3%. The remarkable results can be seen graphically in Figure 12.

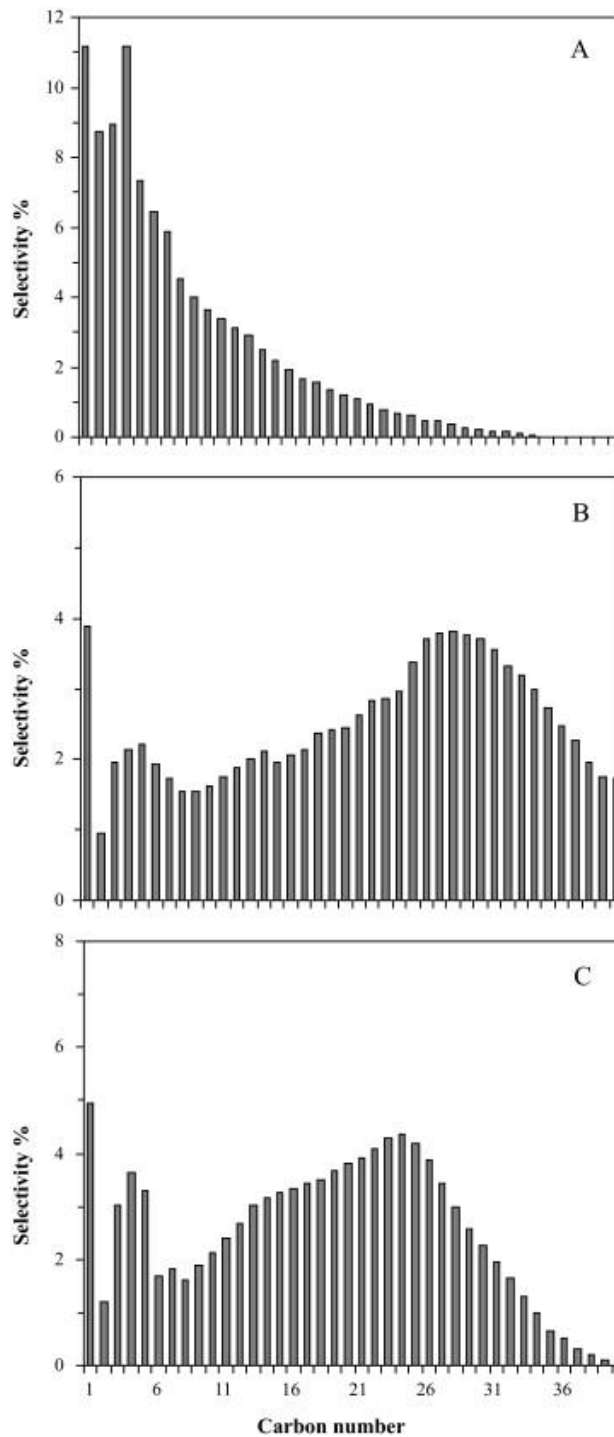


Figure 12: A - no water addition, B - 10 mmol water vapour, C - 10 mmol water as liquid (X. Liu, et al., 2011a)

Luaidi et al. (2011) investigated the importance of indigenous water to the FT reaction. This is somewhat different to the previous mentioned researchers who typically added water on top of the existing FT reaction. To investigate the effect of indigenous water a Cu based water gas shift (WGS) catalyst was incorporated in the reactor. Although it was expected this would increase the activity due to an increase in H_2 partial pressure, the result was in fact a reduction in activity. This led to

Lualdi et al. (2011) postulating the water was contributing in a positive way to the reaction even though the catalyst was a Co on Al₂O₃ which in other research is suggested to be negatively influenced by water. It may be the case, however, that smaller amounts of water (such as that produced in the reaction only) do in fact have a positive influence on a Co/Al₂O₃ catalyst whereas it is the addition of significantly extra water which leads to the lower activity and catalyst deactivation. This seems to be supported by Lögdberg et al. (Lögdberg, et al., 2011) where they suggest water has a positive kinetic effect up to moderate amounts. They go further to suggest the reason for the deactivation at higher partial pressures of water is due to extensive deactivation of the smaller Co particles (explaining why smaller pore γ -Al₂O₃ support may be more prone). They also suggest this deactivation may be caused by formation of hard to reduce cobalt oxides. One could conclude from these studies that the choice of catalyst support in light of water effects could be significant depending on the type of reactor and process chosen for study. For example in a once through process the single pass conversion must be higher which will result in a higher partial pressure of water. The catalyst response to this may become very important.

2.12. Effect of Different Precursors and Solvents

2.12.1. Precursor effects

Different precursors can be used in preparation of cobalt catalysts. Typically cobalt nitrate is the most common. However, research has been performed (Kraum & Baerns, 1999) that compares different precursors for their FT synthesis activity as a final catalyst. Kraum & Baerns (1999) investigated the effectiveness of cobalt(II) acetyl acetonate, cobalt (III) acetyl acetonate, cobalt acetate, cobalt oxalate, Co-EDTA and Co(OH)₂ on a titania support. They found that the oxalate, acetate and acetonate based precursors resulted in a higher activity than the reference nitrate. This was loosely correlated to cobalt dispersion, related to the precursor and the preparation method (incipient wetness, precipitation and spreading). Having different methods of catalyst preparation outside of changing the precursor does make one question the validity of the comparison somewhat. It appears the most common salts used are cobalt nitrate followed by cobalt acetate. Cobalt nitrate is used in virtually every reference found, and when other cobalt salts are used it is usually in a comparison to cobalt nitrate. Madikizela-Mnqanqeni & Coville (2005) compared catalysts produced from both the nitrate and acetate precursors on titania. They found that the most highly dispersed and active catalyst was produced when a mix of the two precursors were used, rather than either of the precursors on their own, albeit with a lower wax selectivity than a catalyst prepared from the

nitrate. Girardon et al. (2005) concluded virtually the opposite with the cobalt nitrate leading to significantly higher dispersion than the acetate. The reason given that the cobalt acetate decomposes exothermically leading to amorphous, barely reducible cobalt silicate. The silica support appears to be the point of difference between the two studies. Sun et al. (2000) similar to Madikizela-Mnqanqeni & Coville (2005) used mixed nitrate and acetate precursors but on a silica support similar to Girardon et al. (2005). They also found a higher activity with mixed salts even though it was on a silica support and inferred that the cobalt from cobalt acetate was highly dispersed and easily reducible. There appears therefore to be an element of contradiction in the literature about precursor effects.

2.12.2. Solvent effects

As well as differing the cobalt salts for catalyst preparation as discussed above another common deviation is that of the solvent used in the preparation of impregnated catalysts (Ho & Su, 1997; C. Li, Ying, Cao, Zhang, & Fang, 2008; Zhang, Liu, Yang, Endo, & Tsubaki, 2009; Zhang, Liu, Yang, Sun, & Tsubaki, 2007). Aqueous impregnation would be considered the control, with the most often seen deviation from this being ethanol. Zhang et al. (2009), however, also consider the effect of acetic acid while C. Li, et al. (2008) also considered methanol and isopropanol. The consensus between the literature shows ethanol solvent catalysts exhibit the highest activity while still maintaining good C₅₊ selectivity. Acetic acid also improved the dispersion and reduction by modifying the support. C. Li, et al. (2008) ranked the activity of the catalysts based on the support as follows ethanol > methanol > water > isopropanol, with the C₅₊ selectivity ranked ethanol > water > methanol > isopropanol.

2.13. Effect of Promoters

Promoters can have a significant effect on the performance of a catalyst and have therefore received much research attention (Bezemer, Radstake, Falke, et al., 2006; Gaube & Klein, 2008; Jacobs, Chaney, Patterson, Das, & Davis, 2004; Morales, de Smit, de Groot, Visser, & Weckhuysen, 2007; Rytter, Skagseth, Eri, & Sjøstad, 2010; Saeys, Tan, Chang, & Borgna, 2010). A review of the promotion of FT cobalt catalysts with noble metals was performed by Diehl & Khodakov (2009) which provides a sufficient summary of the topic.

Promotion with noble metals modifies catalyst structure resulting in differing catalyst performance. The addition of promoters typically helps cobalt reducibility leading to more active metallic cobalt sites. Often as well as the improved reducibility, promoters also lead to a smaller average cobalt

particle size. These effects can be realised with small fractions of noble metal promotion (0.05-0.2 wt %). While the use of promoters seems like an unquestionably logical proposition due to the improvements on performance the counteracting effect is the cost. The most common promoters considered for FT are platinum, palladium, ruthenium and rhenium. Cobalt in itself is an expensive metal (1000 times the price of iron), with these promoters being orders of magnitude more expensive. If there were a significant increase in the uptake of FT and therefore a much higher demand for these metals, then it is likely the price would inflate further (Diehl & Khodakov, 2009). Therefore if a catalyst could be produced, without promotion or at least with less promotion, that had similar activity this would be significant. While a considerable amount more could be said on the use of promoters it is more an area to be aware of and visited later during experimental design.

2.14. Cobalt Particle Size

Research (Ma et al., 2011) has focussed on the effect of support and particle size on the kinetics. Ma et al. (2011) studied cobalt cluster sizes within the range of 8-40nm. They found that in this range that decreasing the average Co cluster diameter by about 30% led to an increase in the intrinsic reaction rate per unit of catalyst of 62-102% on γ -Al₂O₃ and SiO₂ supported catalyst. Further research in this area (J. P. Den Breejen, et al., 2009) examined a smaller size range of cobalt clusters in the range of 2.6-16nm. They used carbon nanofibres as the supports and varied the cluster size by varying the cobalt loading, cobalt precursor and solvent. They discovered that a cobalt particle size smaller than about 6nm caused a decrease in turn over frequency (TOF) and an increase in methane selectivity. Den Breejen, et al. furthered their study in this area and tightened their optimum particle size range to 4.7nm \pm 0.2nm looking at both carbon nanofibre and silica supports (Johan P. den Breejen, et al., 2010). Combining the results of den Breejen et al. (2009; 2010) with that of Ma et al. (2011) one could potentially conclude that a decrease in the particle size increases activity down to the point where particle size drops below 4-6nm at which point the activity decreases. The application to this research drawn from these studies would be to investigate methods of catalyst manufacture that consistently create an optimum cobalt cluster size of around this range if not a little higher.

2.15. Catalyst Deactivation

One significant and more importantly, costly challenge is that of catalyst deactivation. The longer a catalyst will run without losing activity the less cost there is with ongoing catalyst replacement, with

reactor downtime as catalyst is replaced as well as reactors not running to full capacity due to degraded catalysts. Catalyst deactivation is a difficult area of study as it is complicated by many mechanisms contributing to degradation of catalyst performance (Tsakoumis, Rønning, Borg, Rytter, & Holmen, 2010). Catalyst deactivation, therefore, is an issue that has been subject to much research (Bartholomew, 2001), including the area of Fischer-Tropsch catalysts (Moodley et al., 2009; Saib et al., 2010; A. Steynberg & Dry, 2004; Tsakoumis, et al., 2010) to name but a few references. The review by Tsakoumis et al. (2010) is very thorough and demonstrates the vastness of the area by citing over 180 references. Because of this area, as with others discussed in this literature review, the research presented will again be filtered based on the application of the technology. Therefore, detailed account of specific mechanisms and particular complex analysis techniques will not be entered into, rather an understanding gained of the overriding causes of deactivation and the practical ways to combat it.

The main areas contributing to catalyst deactivation are (Moodley, et al., 2009; Tsakoumis, et al., 2010)

- Sintering
- Poisoning
- Cobalt reconstruction
- Carbon deposition
- Re-oxidation
- Metal-support solid state reactions
- attrition

A very good summary of the deactivation mechanisms mentioned above can be found in Tsakoumis et al. (2010) as shown in Table 7.

Table 7: Summary of deactivation mechanisms retrieved from Tsakoumis et al. (2010)

Deactivation Mechanism	Short description
Poisoning	Sulphur in the form of H ₂ S, COS will poison the catalyst. Sulphur content in the feed should be kept below 0.02 mg/m ³ . Feed purification is vital for the process. Nitrogen compounds appear to have a reversible poisoning effect. Other species are accused for catalyst poisoning as well.
Sintering	Exothermicity of the reaction dictates sintering as a possible deactivation mechanism. Coalescence seems to be the prevailing mechanism. Support sintering has been proposed as well.
Carbon formation and fouling	The possibility of pore plugging and catalyst fouling due to carbonaceous species formation is high, since carbon is a key element of the synthesis. The exact nature of the species is still unclear.
Re-oxidation	Thermodynamic calculations shown that re-oxidation is possible only for crystallites less than 5 nm in diameter. Nevertheless, several studies are proposing water-induced re-oxidation as a deactivation mechanism. In contradiction further reduction during FTS has been proposed as well. Other oxygen containing species have been investigated for their oxidizing ability.
Carbidization	Mainly XRD studies are reporting Co ₂ C formation. The formation appears to be reversible.
Metal-support solid state reactions	The formation of mixed compounds of metal and the support is thermodynamically feasible, however kinetically restricted. Water may promote this side effect.
Surface reconstruction	Surface reconstruction has been proposed and connected with the activation of the catalyst. Calculations have shown a link between reconstruction and deactivation, but the phenomenon is lacking experimental evidences.
Leaching of active phase	ICP analysis of spent catalysts used in laboratory units shows that the catalyst components are remaining in the catalyst after operation.
Attrition	Particularly valid for moving beds. Fragmentation of catalyst particles is resulting in secondary effects disturbing proper operation and assisting catalyst loss.

From Table 7 a number of these points can be considered relevant to the application in this research and will be discussed in more detail.

2.15.1. Poisoning

Poisoning is an obvious one to consider, as removal of potential poisons in any plant will be critical and a significant part of the design and capital investment. For the application here this is somewhat outside the scope as the cleaning system is being developed by another member in the overall project team. However, for techno-economic studies in this research cleaning will have to be considered, so investigation of suitable techniques for costing purposes should be investigated. It should be noted that the value of 0.02 mg/m^3 shown in Table 7 is very low therefore significant cleaning will be required to achieve this target. As an aside, however, the cleanliness requirement of the gas, apart from protecting the catalyst has the further advantage of producing a very clean fuel. Therefore, there is limited drive to develop highly sulphur resistant catalysts.

2.15.2. Attrition

Attrition is one parameter which may or may not be relevant depending on the reactor chosen. In the case of a micro-reactor attrition is not relevant which can be seen as a significant advantage. The addition of cobalt influences the attrition resistance of the support. For the most common supports the attrition resistance from most to least is $\text{Co/Al}_2\text{O}_3 > \text{Co/SiO}_2 > \text{Co/TiO}_2(\text{rutile}) \gg \text{Co/TiO}_2(\text{anatase})$ (Wei, Goodwin Jr, Oukaci, & Singleton, 2001).

2.15.3. Sintering

The FT reaction is structure insensitive so any reduction in activity from sintering can be attributed to a lowering of the surface area (Bartholomew, 2001). High temperatures and water increase the rate of the sintering process. It is generally regarded to be an irreversible process but a reduction-oxidation-reduction sequence under certain circumstances can result in redispersion of the cobalt (Tsakoumis, et al., 2010). Sintering rates are exponentially related to temperature (Bartholomew, 2001) therefore adequate temperature control within all parts of a reactor would seem critical in reducing the potential for sintering. Of note is that different supports can change the potential for sintering. Al_2O_3 for example is a strongly interacting support which reduces crystal diffusion (Tsakoumis, et al., 2010). In other literature sintering was attributed as one of the main causes of non recoverable activity after regeneration (Ahmad Tavasoli, Malek Abbaslou, & Dalai, 2008).

2.15.4. Carbon formation and fouling

The deactivation of catalysts via this method is multifaceted. Fouling is the physical deposition of material on the surface of the catalyst which lowers activity due to blockage of active sites or pores (Bartholomew, 2001). Given the cleanliness of the gas required for FT one would expect the likely

means of fouling would result from carbon formation alone. Carbon can form from CO disproportionation (Bartholomew, 2001), an example being the Boudouard reaction (Tsakoumis, et al., 2010), whereas coke is produced via decomposition or condensation of hydrocarbons on the catalyst surface, typically heavy hydrocarbons (Bartholomew, 2001).

The FT reaction is coke insensitive (meaning reactive coke precursors on active sites can be readily removed by hydrogen) and therefore the deactivation rate depends significantly on the relative rates between the formation and gasification of carbon/coke. If the rate of formation is higher, carbon/coke will deposit. The rates of both vary exponentially with temperature, although with significantly varying degrees (Bartholomew, 2001). This can be shown in an Arrhenius plot (Figure 13) obtained from Bartholomew (2001). Interpretation of this figure shows carbon deposition should be insignificant at the lower temperature FT process chosen for study in this research.

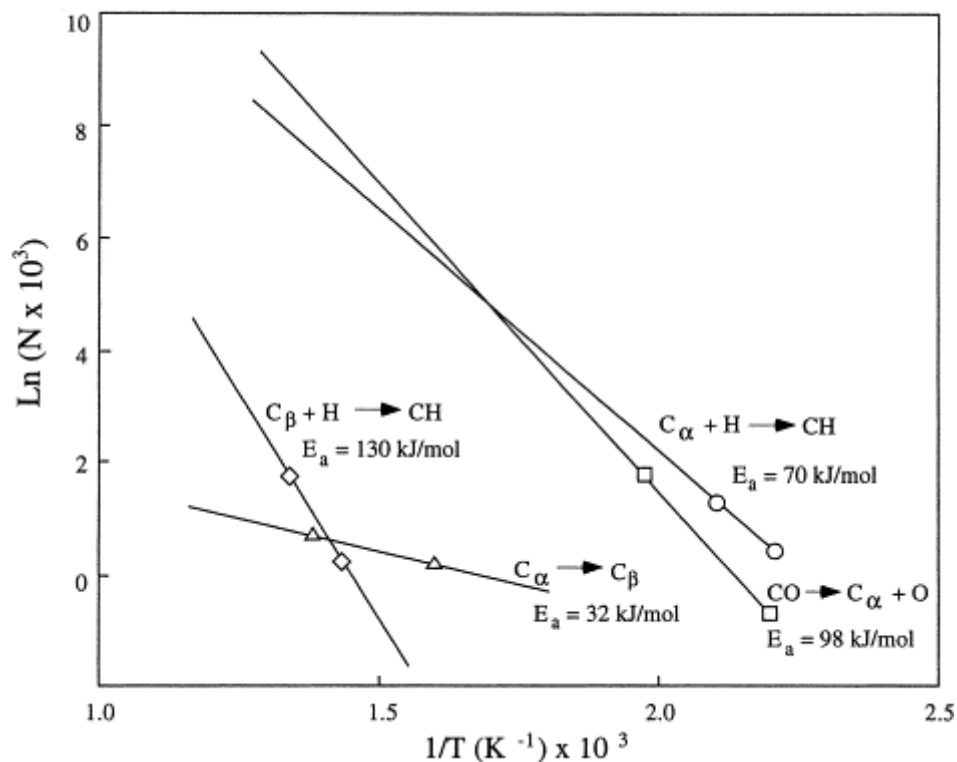


Figure 13: Rates of formation and hydrogenation of carbon (N) vs. inverse temperature (Bartholomew, 2001)

There are several routes for carbon/coke formation in FT however, most of these are specific to hydrogen deficient conditions which at a 2:1 $H_2:CO$ ratio should not be as significant (Tsakoumis, et al., 2010).

Fouling by higher weight hydrocarbons is a potential negative influence in LTFT particularly given that hydrocarbon chains of C_{100+} are possible. Although these would be in very small fractional

quantities, time based accumulation is possible resulting in blocking of microporous channels. While not causing deactivation of the catalyst itself, this fouling has the potential to cause diffusion limitations and therefore slowing of the overall reaction rate (Tsakoumis, et al., 2010). It is assumed, however, in the experimental cases for this thesis that the run time of the catalyst will unlikely be long enough for the negative effects of heavy hydrocarbon build-up to be apparent.

Regarding the effect of promoters there seems to be agreement that noble metals, particularly ruthenium reduces carbon formation (Tsakoumis, et al., 2010).

2.15.5. Metal support reactions

Deactivation is an issue across all typical FT supports. γ - Al_2O_3 appears to be the preferred support, part of this reason being its attrition resistance, which may or may not be of significance depending on the reactor type chosen in this research, as well as the ability to stabilise cobalt clusters which assists against sintering but the relatively strong metal-support interactions lead to formation of hardly reducible cobalt species. On SiO_2 cobalt silicate hardly reducible species are also formed (Tsakoumis, et al., 2010). It is suggested that the presence of water leads to cobalt-support formations. Addition of promoters such as zirconium can lower the cobalt support interactions (at least in silica in the case reviewed), lowering the reduction temperature therefore improving the overall reducibility.

2.15.6. Deactivation by oxidation

Deactivation by oxidation in FT is a subject that appears to have differing views. It is debated whether it is possible to have re-oxidation under typical FT conditions. The debate is based on the fact that water which is a significant byproduct of FTS is an oxidising agent. Bulk cobalt metal will not be oxidised under typical FTS conditions, however, it is supposed that nano sized cobalt particles will function in a different manner from bulk cobalt (Tsakoumis, et al., 2010). van de Loosdrecht, et al. (2007) concluded through use of XRD, XANES and magnetic measurements that oxidation is not a deactivation mechanism during typical FT synthesis using an industrial $\text{Co}/\text{Al}_2\text{O}_3$ catalyst with a cobalt crystal size of 6nm. They also conclude that much of the discrepancy has been due to lack of direct characterisation of the cobalt oxidation state, as well as the catalyst comparison not being made under consistent partial pressures of hydrogen and water. Their final practical conclusion is that oxidation of cobalt can be prevented by the correct hydrogen/water partial pressure ratio, as well as the correct cobalt crystal size. This correct cobalt crystal size appears to be a minimum of

6nm (Tsakoumis, et al., 2010). This is consistent with studies on cobalt particle size in FTS as described previously.

2.16. Summarising the Catalyst Review

While the review of catalysts in part appears to address a number of separate issues they seem significantly interrelated. One of the most influential would be particle size and dispersion of the cobalt. This appears to be the single biggest factor to consider in FT catalysis if one were to be chosen from the fore mentioned literature study. The particle size and dispersion has a significant effect on the activity and selectivity of FT synthesis. Many of the areas studied such as the precursor and the solvent during catalyst preparation as well as promoters at least in part are based around achieving suitable size and dispersion of cobalt particles. Particle size is also attributed to having an effect on deactivation of a catalyst, whether sintering to a large particle, or a small particle re-oxidising. Therefore, whichever route the catalyst production takes in this study, care should be taken to consider the particle size and how this might be affecting the performance of the catalyst.

2.17. Fischer-Tropsch Reactors

Because the Fischer Tropsch process was discovered in the 1920's and has been used commercially for many of the interceding years until now, there has been a significant timeframe to allow for reactor development. In this time there has been periods of significant development but also periods where little development was made (Burtron H. Davis, 2005; Guettel, et al., 2008).

Each type of reactor is designed in a certain way to address particular problems although all have compromises, therefore the reactors used in Fischer-Tropsch will be reviewed with a view to understanding the advantages and disadvantages of each specific to the small scale FT application. The arrangement of the reactor types are also shown in Figure 14 to Figure 17.

2.17.1. Multi-tubular fixed bed

The fixed bed reactor is one of the original designs used for FT synthesis. They consist of many tubes packed with FT catalyst as shown in Figure 14. The advantages and disadvantages of this arrangement are listed below.

Advantages (M. E. Dry, 1996)

- Simple to operate
- Can be used over wide temperature range (liquid or gaseous products are both suitable)
- No problem separating catalyst from liquid product, therefore good for wax production
- If slugs of H₂S come through, the top part of the bed will absorb it minimising overall loss of activity
- Scaling relatively simple as the number of packed tubes can be multiplied with predictable performance in each tube

Disadvantages (M. E. Dry, 1996)

The disadvantages of the fixed bed reactor are mainly economic

- High construction cost and large physical volume requirements
- High gas flow rate results in high pressure drop, as well as necessary recycling resulting in high compression costs
- FT reaction is diffusion controlled, therefore a compromise between particle size and pressure drop is encountered
- Labour and time intensive process to change catalyst

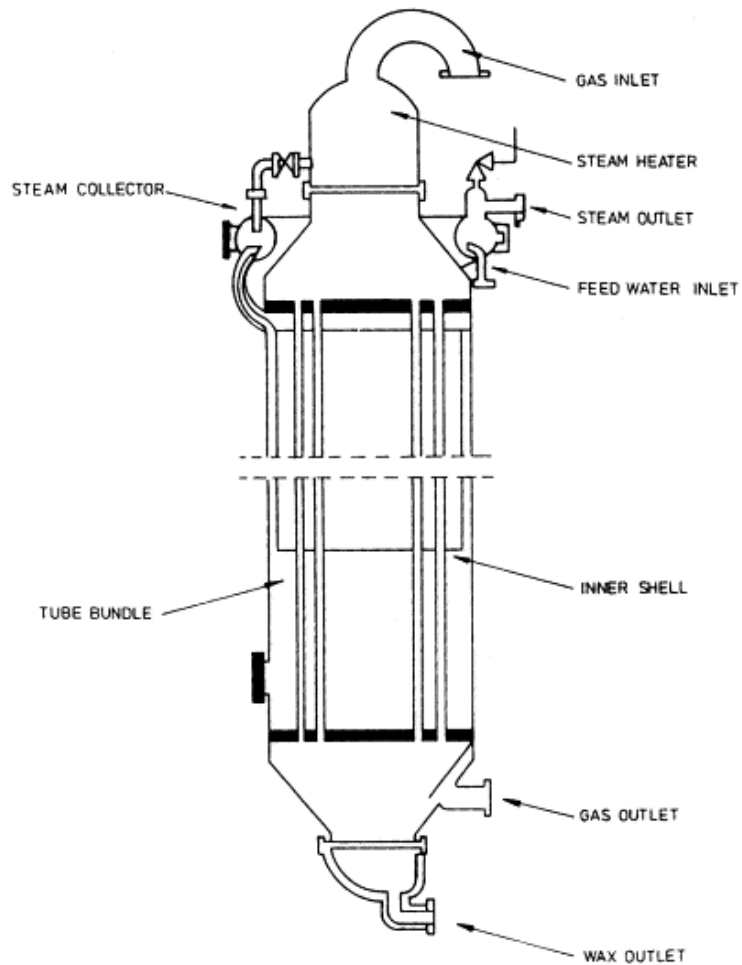


Figure 14: Multitubular fixed bed FT reactor (Mark E. Dry, 2002)

2.17.2. Circulating fluidised bed (CFB)

Circulating fluidised bed reactors were the design of choice for the first Sasol plant. After considerable teething problems, modifications and catalyst formulation changes these reactors operated for around 30 years. Improved versions were used in the Sasol 2 and 3 plants (M. E. Dry, 1996).

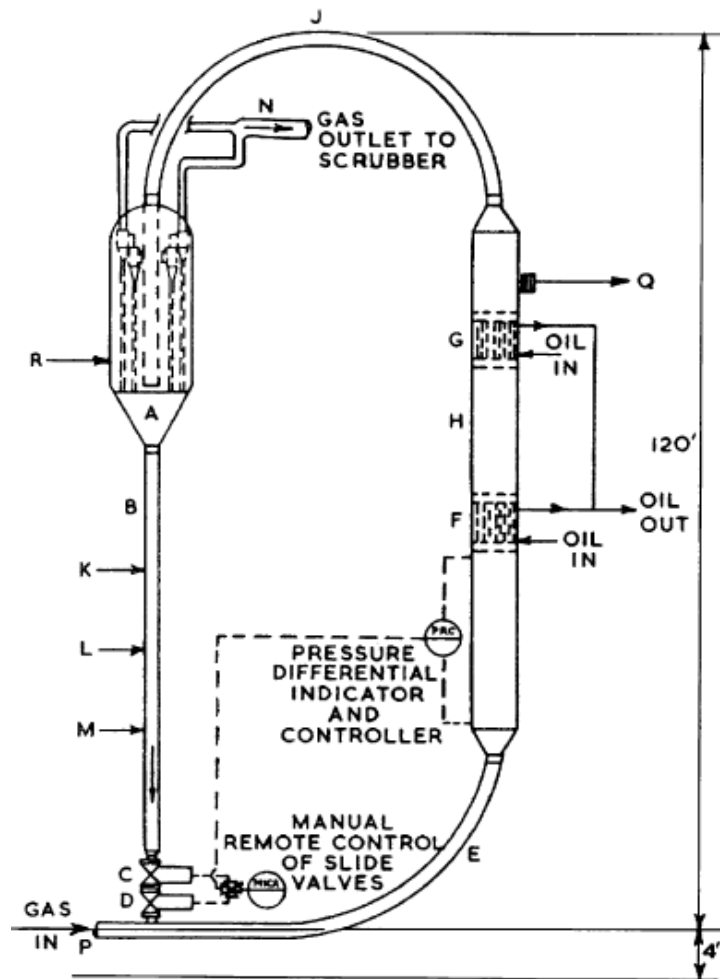


Figure 15: Sasol circulating fluidised bed reactor (Burtron H. Davis, 2005)

As per Figure 15 catalyst was stored in hopper (A) under nitrogen or hydrogen until required. Catalyst in the standpipe (B) was kept aerated through (K), (L) and (M) so that it would flow freely through slide valves (C) and (D) when they were opened. (C) is open in normal operation whereas (D) is controlled to give the required catalyst flow. Feed gas enters at (P). A two phase flow of gas and catalyst travels through (E). The temperature was maintained (288-343°C) by cooling coils (F) and (G). Gas and catalyst travels through the gooseneck (J) before entering the settling area (R) where the gas passed through cyclones to recover small catalyst particles. The larger particles would disengage from the gas stream due to gravity (Burtron H. Davis, 2005).

At high operating temperatures carbon deposition occurs on the catalyst which results in particle breakdown and a decrease in particle density. The higher velocity of the particles lowering the residence time would lead to a reduction in conversion. This could be overcome by introducing fresh catalyst (Burtron H. Davis, 2005; M. E. Dry, 1996).

Wetting of catalyst particles by higher weight hydrocarbons was also an operating problem. This would cause clumping of the catalyst particles which would not fluidise or would create large deposits. Catalyst modifications and process condition optimisation was used to manage the problem (Burtron H. Davis, 2005).

2.17.3. Fixed fluidised bed (FFB)

Several groups helped to develop the fixed fluidised bed reactor in Brownsville, TX, headed by Hydrocarbon Research Inc. Unfortunately the low price of Middle Eastern oil and the high price of natural gas caused the plant to be shut down just as the operating problems were being resolved. Many of the problems related to scale up and the influence this had on gas/solid contacting. This was attributed to large gas bubble formation in the fluidised bed lowering the catalyst surface to gas volume ratio. Channelling of gas through unfluidised parts of the catalyst bed was also considered a factor in lowering the conversion compared to lab scale (Burtron H. Davis, 2005). Sasol, however, seemed to have more success with FFB reactors with a 1m ID demonstration unit that was commissioned in 1984 and a 5m ID commercial unit commissioned in 1989 that both operated well (M. E. Dry, 1996).

Advantages (M. E. Dry, 1996)

- For the same production capacity the FFB has lower capital cost than a CFB reactor mainly due to the smaller physical size
- Lower gas velocity eliminates erosion problems
- Differential pressure and hence compression costs are lower
- Carbon deposition causes bed expansion actually increasing contact time. Therefore conversion over time is more consistent

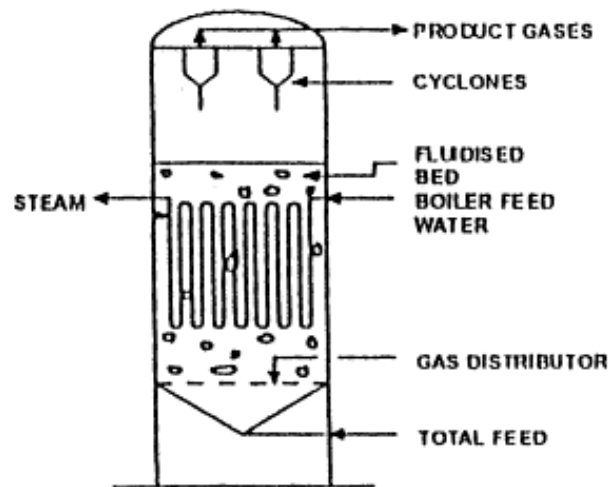


Figure 16: Fixed fluidised bed reactor (Mark E. Dry, 2002)

It is interesting that Dry (1996) seems very positive and only lists the advantages of the FFB reactor as well as pointing out that at the time the paper was written Sasol 2 and 3 CFB plants were being replaced with FFB reactors. Davis (2005) on the other hand focuses primarily on the difficulties of development with only a small mention of the uptake of the design by Sasol.

2.17.4. Slurry bed

The slurry reactor contains fine catalyst particles which are suspended in a liquid in which feed gas is bubbled through. The reactor is used to make high molecular weight waxes, which are liquids at operating conditions. This means the FT product itself makes up the liquid phase (M. E. Dry, 1996).

During WWII and following, Kolbel and his co-workers made significant progress on slurry bubble column reactors both in terms of scientific understanding and engineering technology (Burtron H. Davis, 2005) as can be seen by the graph produced shown in Figure 18. The graph shows the influence on gas velocity through the reactor and the hydrodynamic regime occurring within the reactor. This example shows the in depth research that occurred in the field of slurry reactors at the time.

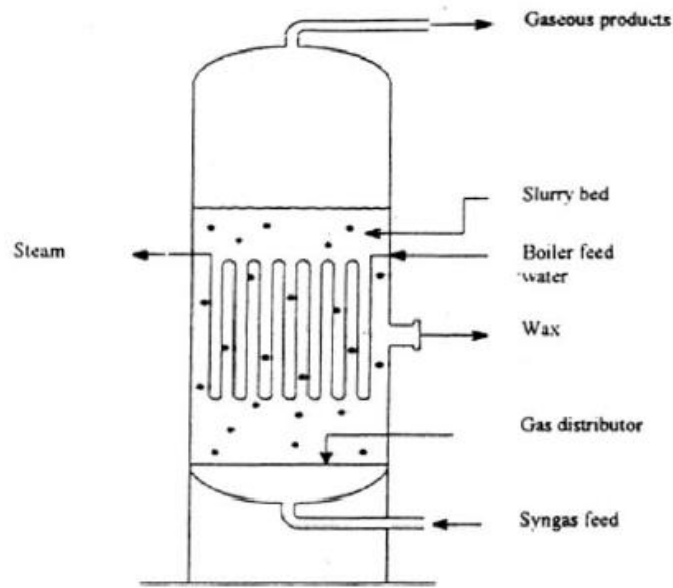


Figure 17: Slurry bed FT reactor (Tijmensen, et al., 2002)

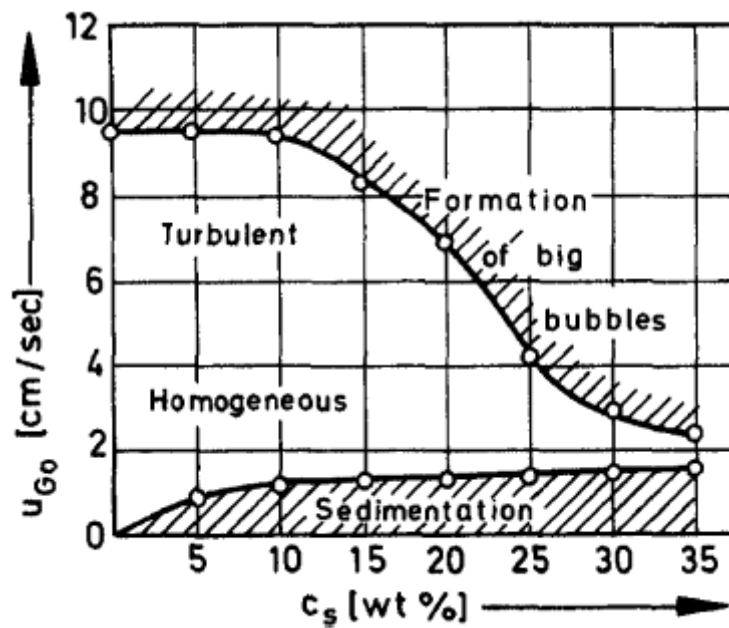


Figure 18: Influence of catalyst loading (C_s) and the superficial gas velocity (U_{Go}) on the flow characteristics in the slurry reactor (Burtron H. Davis, 2005)

Sasol commissioned a 2500bpd slurry reactor in 1993 after a 10 year research programme. It was the development of their proprietary catalyst/wax separation system that allowed the slurry phase reactor technology to be implemented (Espinoza, Steynberg, Jager, & Vosloo, 1999).

Espinoza et.al. (1999) appear to be of the opinion that an efficient slurry phase reactor in combination with a very active cobalt catalyst is a cost effective way forward for Fischer-Tropsch in particular for converting remote natural gas. They quote a figure of \$25,000 of capital per daily barrel for plants with a capacity of 20,000 bpd or more. The construction cost of a slurry reactor is about 40% less than the equivalent multi-tubular fixed bed reactor (M. E. Dry, 1996) and is simpler and far easier to fabricate than a fixed bed reactor (Espinoza, et al., 1999). The pressure drop over the slurry reactor is much lower than a fixed bed reactor lowering compression costs (M. E. Dry, 1996). Because of the much smaller catalyst particles in comparison to fixed bed reactors the pore diffusion rate limitation is all but eliminated. Therefore, the activity per unit mass of catalyst is significantly higher (M. E. Dry, 1996). Also the heat transfer co-efficient for cooling surfaces in a slurry reactor is five times that of fixed bed reactors (A. Steynberg & Dry, 2004).

While slurry reactors are scalable in terms of the large capacities they can be designed to, large scale pilot plants are generally a necessity to sufficiently design a commercial sized system. This is due to the difficulty in predicting operating conditions. Two phase fluidisation is a well understood science now, whereas the complexity of slurry systems means accurate prediction is not yet fully possible. Thus pilot reactors should be 30cm in diameter at a minimum with 1m diameter preferable (Espinoza, et al., 1999). However, The Technical University of Vienna (TUV) has a pilot scale slurry reactor receiving a slipstream of gas from the Gussing biomass gasifier. This reactor is much smaller in diameter than that recommended above, demonstrating their ability to function at smaller sizes. The TUV slurry reactor shows conversions up to 70% with α values up to over 0.9 (Rauch, 2011).

2.17.5. Reactor Perspective

If one were to make a philosophical rather than a technical conclusion about FT reactor technology and development throughout the years it would fit well with the adage of 'necessity is the mother of invention'. It was times such as wars or embargoes limiting oil supplies that pushed ahead development of the technology. It could be suggested that with the heightened interest in global warming and the turn to biomass as a feedstock another 'necessity' is generating interest in further, novel development of FT reactors. That 'necessity' is the ability to economically run FT synthesis at a significantly smaller scale than is currently being used commercially due to the dispersed nature of the biomass feedstock. Interest in microreactor technology could be said to be driven, at least in part, by this necessity. Microreactor technology will be reviewed further in this literature review as a stand alone topic reflective of its importance in reaching the goals of small scale FT.

2.18. Microchannel Reactors

Microchannel reactor technology is seen as part of the solution to economically producing liquid fuels at smaller scale. Currently there is little commercial development of FT based microchannel technology, however, those endeavouring to make it a commercial endeavour such as Velocys (example Patent US7084180) (Briscoe et al., 2006), do claim significant cost effectiveness at smaller scale compared to existing technology (A. Tonkovich et al., 2008). Research is becoming more prevalent in the area of microreactors with at least one very good overview of the topic (Gavriilidis, Angeli, Cao, Yeong, & Wan, 2002).

Microchannel reactors are seen as being very suitable for FT synthesis. The high rate of heat transfer available within a microreactor system is ideal for controlling the highly exothermic FT reaction. The scalability of microchannel reactors is also seen as a significant advantage, especially given the unconventional scale in question in this paper. Scale-up with micro-reactors is more a case of numbering up of either channels or reactor modules (Gavriilidis, et al., 2002). This provides greater confidence in repeatability of lab scale results on a larger scale.

A common question or objection to microchannel reactors is the high potential for plugging with particulates. In FT synthesis this problem is solved by pure virtue of the process – the catalyst requires a very clean syngas feed, therefore the prior rigorous cleanup steps have removed all particulate matter. There is the potential for coking in FT which would be detrimental in the small channels. However, coking is usually caused by higher temperature deviations (A. Steynberg & Dry, 2004), a difficulty that should not be associated with a microchannel reactor due to the high rates of heat transfer.

One of the challenges of microchannel reactors is the ability to appropriately load catalyst into the reactor. There are a number of papers on this subject although much literature involves coating microchannels (or monoliths and other microreactor shapes) outside of the reactor before assembly (Almeida et al.; Pfeifer, Schubert, & Emig, 2005; Visconti et al., 2009). However, research investigating adding catalyst post reactor assembly is deemed important as it is very likely full scale units will be permanently sealed to ensure reliability at the high operating pressures required for FT synthesis. The author therefore sees investigation into several types of catalyst washcoated into an assembled microchannel reactor as an important area of study. Hessel et al. (2009) reviews two main methods of washcoating catalysts – sequential washcoating and one step washcoating. With sequential washcoating a support such as alumina is washcoated first, followed by the active

component precursor before final activating treatment. A relatively low fraction of active component can be used due to the risk of blocking the pores of the support and reducing the catalyst effectiveness. The one step method washcoats a pre-prepared catalyst into the reactor. There are advantages to this method such as being able to prepare and characterise the catalyst before coating, however, there are potential issues with leaching the active catalyst into the solvent, potential negative impacts of milling the catalyst to the right size and whether the deposition procedure as a whole is compatible with the catalyst. While some literature produces high performing catalysts through complex methods (Chin, et al., 2005; Nagineni et al., 2005) (please don't read this as criticism of their work!), the aim of this research is to produce simple, cost effective reactor and catalyst systems at a smaller scale. Therefore complex and potentially difficult to repeat (at least at scale) methods, as well as precious metal promoters have been eliminated as the starting point. The intention is to use this study as a base case to select the most effective catalyst for further washcoating and reactor optimisation that best suits a small scale biomass fed combined heat, power and liquid fuels plant.

2.18.1. Microchannel reactor manufacturing techniques

There are quite a number of different ways to create microreactor structures. These vary from mechanical/machining techniques to chemical etching and electrical discharge methods. A range of techniques are investigated more specifically focussed on those which can be performed on the same materials as would be used in mass manufacture i.e. metals such as stainless steel or aluminium, and which could potentially be performed in New Zealand. Some comment is made as to whether the technology is available locally.

2.18.1.1. Mechanical/machining

There are a number of different mechanical/machining techniques to create microstructures. Many of the techniques are the same or an adaption of typical macro technology (Gavriilidis, et al., 2002; V Hessel, 2011; Mills, Quiram, & Ryley, 2007).

2.18.1.2. CNC milling

Specialist milling machines are available to create microstructures. They feature high precision (0.01 μm) (Gavriilidis, et al., 2002) with spindle speeds up to 60,000 rpm. Minimum dimensions are in the 50 μm range (V Hessel, 2011). This technology is good for rapid prototyping of different designs.

2.18.1.3. *Stamping, rolling, embossing*

These techniques are very suitable for significant mass production. Design changes would be more difficult as punches or formers would need to be remade. Therefore it makes sense that this is a mass production technique for a design that is very proven. One would imagine the cost of the punches/dies etc would be very expensive unless offset by significant production, lowering the cost per unit.

Velocys use stamping as their technique for manufacture and they quote it is the cheapest method of mass manufacture. There are issues which need to be overcome such as distortion, burrs, and edge rollover, but these issues can potentially be designed out from being of consequence (A. Tonkovich et al., 2005).

Availability of this technology in the Canterbury area has not been investigated as this method is far from the early stages of research. There are a number of capable toolmakers in the area, the question is whether the fine structures could be achieved.

2.18.1.4. *Chemical Etching*

Chemical etching is one of the earliest methods used for creating microreactor structures. Often this was performed in silicon, although it can be applied to metal (Gavriilidis, et al., 2002). For isotropic wet chemical etching the minimum width of a structure is two times the depth, plus the width of the mask openings (V Hessel, 2011). This method is reasonable for mass manufacture, and has the advantage that changes in design do not need significant tooling changes, rather simple redesign of masks. This technology can potentially, therefore, be appropriate for all stages from prototyping to mass manufacture. Although literature can be found on the subject (Nageswara Rao & Kunzru, 2007), it is questionable how effective and repeatable chemical etching will be on more chemically resistant materials, such as stainless steel, that would be most suitable for the durability required in an industrial context. However, Ehrfeld et. al. (2004) suggest stainless steel can be etched effectively and cite examples. They also suggest that it is proven technology which external contractors can complete. There is a local company in Christchurch that can perform etching work, however, in early dialogue they were not favourable towards using stainless steel (Photoetch Ltd, 2008).

2.18.1.5. Electrical Discharge Machining

There are different types of electrical discharge machining (EDM). Drilling can produce features in the order of 5-10 μ m, whereas wire cutting in the order of 15-20 μ m. This technology is considered very applicable for rapid prototyping and indirectly for mass production by making moulds (V Hessel, 2011). Typical wire diameter is 0.1-0.3mm therefore limiting the minimum channel size that could be cut using wire EDM. Virtually no burrs are created (XACT, 2012). Wire EDM is better for making smaller external features such as heat exchanger fins. The minimum wire diameter is around 20 μ m (V Hessel, 2011). Canvassing the local area several companies offered wire cutting although certainly not down to 20 μ m wire size.

2.18.1.6. Laser

With laser machining aspect ratios up to 1:50 can be achieved with little surrounding heat stress. The most common lasers in microfabrication are CO₂ and neodymium yttrium aluminium garnet (Gavriilidis, et al., 2002). There is also the ability for laser welding making lasers a very versatile technique. Canvassing the Canterbury area showed plenty of laser cutting equipment, however, the boasting point for most was how thick they could cut not how thin, with none appearing suitable for fine microchannel manufacture.

2.18.1.7. Other

There are other techniques such as thin film deposition and growth, and LIGA which represent the more complicated and specialist manufacture of microstructures (Gavriilidis, et al., 2002). These techniques therefore, while mentioned for completeness, will not be explored further due to a very low likelihood of this technology being pursued in this research.

Ultimately the limitation for selection of a technology to create a microchannel reactor for this research comes from the availability of equipment to achieve a certain technique. This is discussed further in Chapter 4 under reactor construction.

2.19. Product Upgrading/Refining

The complicated nature of upgrading and refining FT syncrude to end products suggests many PhD studies could be completed in the area, and therefore is kept outside the scope of this research. It is more a case of redirecting the reader to where information could be obtained. Research by Leckel (2009) gives a good overview of the history of product upgrading from FT synthesis while Collins et al. (2006) specifically discusses BP's product upgrading history. Other literature is available that addresses more specific topics within refining and upgrading (Bouchy, Hastoy, Guillon, & Martens, 2009; Guo, Liu, & Larson, 2011). The best resource found in the literature search is the full textbook by de Klerk (2011) which specifically addresses Fischer-Tropsch refining.

3. Techno-Economic Study of Small Scale Fischer-Tropsch in the New Zealand Wood Processing Industry

3.1. Introduction

The purpose of this chapter is to investigate the economic feasibility of combined heat, power, and liquid fuels plants based on woody biomass as a fuel. There are multiple drivers for the investigation and development of plant to produce biofuels from woody biomass in New Zealand as has been reported in the literature review. However, one must understand, aside from the obvious drivers, whether the process is likely to be economic (or at least near to) and thus generate commercial interest.

Based on understanding gained through review of the literature the configuration of plant that is assumed to best suit the smaller scale application required in New Zealand is discussed.

LTFT forms the basis of the technology for reasons already described, particularly that although the HTFT process can have good petrol production the necessary recycles and reforming required due to the lower selectivity add expense and complication unsuitable for a smaller scale plant. The LTFT long chain hydrocarbons can be treated by hydrocracking to produce biodiesel (Bolhar-Nordenkampf, 2004).

As the literature suggests (Mark E. Dry, 1999) the most efficient FT reactor currently in commercial application is the slurry reactor, therefore this is the reactor type considered in this study. The operating temperature is usually below 240°C to minimise methane production and maximise wax selectivity and operating pressures are in the region of 20 to 40 bar (Tijmensen, et al., 2002). These parameters will therefore be considered as the baseline for the model. Also as discussed in the literature review a once through process is considered the most appropriate configuration for this scenario due to the elimination of the expensive and complexity of recycles, reforming and CO₂ separation systems. With the once through system the CO₂ content will not elevate beyond that supplied from the gasifier therefore not reducing partial pressure of the reacting components.

Cobalt is also the catalyst of choice for the once through process due to the fact that cobalt does not suffer inhibition from the produced water like iron does, in turn allowing higher conversion per pass (Schulz, 1999).

Due to the compromise considered between economies of scale and biomass availability as investigated in the literature review, a polygeneration scenario which takes advantage of the heat and power requirements of a sawmill is considered. This is a different philosophy of plant sizing and relies more on the size requirements of integration with the sawmill creating a synergy than the more readily investigated plant size/biomass availability compromise scenario. The plant configuration will be considered in the methodology.

3.2. Methodology

The FT synthesis unit operation is only one step to creating FT products from biomass. Figure 19 shows a typical block diagram of the overall process. These will be discussed in further detail as appropriate.

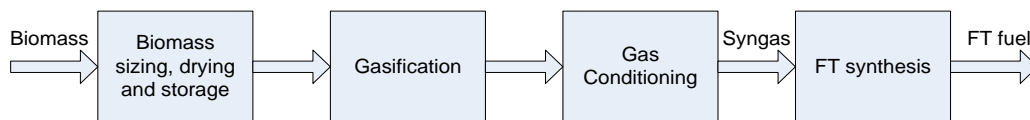


Figure 19: Block diagram of the Fischer-Tropsch process

Biomass sizing, drying and storage is not discussed in detail in this research due to the knowledge already available on commercial technology. For the basis of this study routine costing estimates have been used, either from correlations from literature (Bouman, et al., 2005), or direct discussion with suppliers.

3.2.1. Gasification

There are a number of different gasification technologies available with each having specific advantages and disadvantages in relation to providing syngas suitable for Fischer Tropsch synthesis. Also the advantages and disadvantages shift with scale. The variations in design usually revolve around whether the gasifier is pressurised or running at atmospheric pressure, whether it is oxygen or air blown or whether the gasification process is directly or indirectly heated. Pressurised gasification has the advantage of limiting downstream equipment size, however, this is much more applicable to larger scale. At a smaller scale pressurised gasification is not cost effective. Oxygen blown gasification also is more suitable on a larger scale. There are significant advantages in terms of no dilution from nitrogen which necessitates larger downstream equipment and also has a negative influence on C_{5+} selectivity. However, an oxygen separation plant is necessary which is again expensive at a smaller scale. Indirect has the advantage over direct gasification as N_2 dilution

is limited without the need for an oxygen plant. The disadvantages of this technology is the basic principle of operation of the gasifier itself can be more complex, and there are generally more tars produced (Hamelinck, et al., 2004; Tijmensen, et al., 2002).

The gasifier design selected for this analysis is of a twin fluidised bed type (therefore indirect style). Figure 20 is a simple representation of the operation of the gasifier. Sand is circulated between the two columns as a heat carrying medium. Combustion of char as a byproduct of gasification and additional fuel (recycled producer gas in this case) within the combustion column provides the heat for the sand (to a temperature of around 800°C) before the sand is circulated back into the gasification column. The gasification column is a bubbling fluidised bed where steam is used as the gasification agent. The advantage of this system is there is no nitrogen dilution as occurs in traditional air blown gasifiers. This results in a producer gas with a higher calorific value, or for the case of use as a syngas for Fischer-Tropsch, higher partial pressures of the reacting components. Fluidisation with steam also promotes a higher fraction of hydrogen within the producer gas, ideal for the 2:1 ratio of H₂:CO preferred for Fischer-Tropsch synthesis. Using sand as a heat carrying medium within the gasifier also allows the opportunities for varying the sand composition and using catalytically active materials that can reduce the production of tar and modify the H₂:CO ratio. This gasifier was chosen because although there are some disadvantages in terms of higher tar production and complexity, the negation of an oxygen plant reducing overall complexity and cost, while still producing a syngas with the ideal ratio of H₂:CO, with no nitrogen dilution is seen as a very sensible compromise.

Further details of the operation of this particular design of gasifier can be found in previous work by the University of Canterbury (Brown, 2006; Bull, 2008) and also that by the Technical University of Vienna (TUV, 2009).

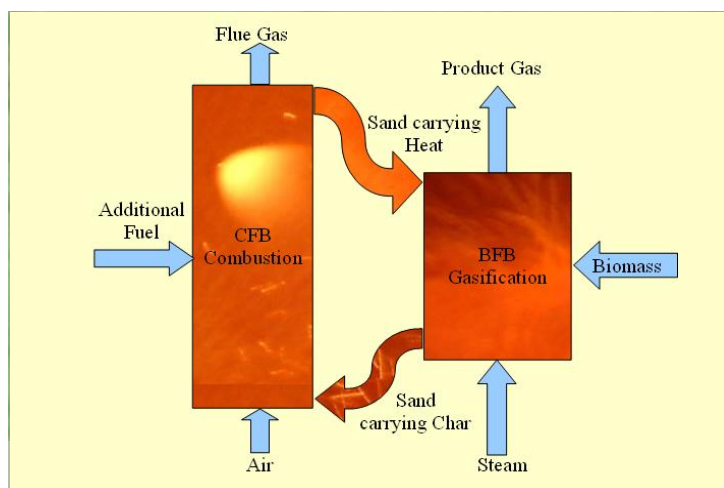


Figure 20: Simple schematic of twin fluidised bed gasifier operation (J. P. Rutherford & Williamson, 2006)

3.2.2. Gas Cleaning

One of the significant, challenging and often overlooked unit operations of a biomass to liquids plant is the gas cleaning component. As mentioned in the literature review FT catalysts are very sensitive to poisoning and require a very clean syngas with sulphur being the main contaminant of concern with very low concentrations (a few ppm) causing catalyst degradation. Compared to coal, biomass releases significant amounts of chlorine and alkali metals as well as H₂S, NH₃, HCN, COS, and tars and particulates (Logdberg, 2007). These contaminants can poison the catalyst lowering the activity in the FT synthesis process (Tijmensen, et al., 2002). Literature focuses on two different methods of cleaning

- Conventional 'wet' low temperature cleaning
- Advanced 'dry' hot gas cleaning

While literature is beginning to surface for high temperature gas cleaning (Leibold, Hornung, & Seifert, 2008) it still appears to be in its infancy in comparison to conventional wet low temperature cleaning.

For the purposes of this study it is seen as prudent to continue with a more proven technology therefore the low temperature cleaning will be the focus. Table 8 from literature shows typical contaminants and cleaning steps. It should be noted from this table, however, that zero ash and tar at ppb level is likely impractical and a <1ppb level is more appropriate.

Table 8: Contaminant concentrations and their maximum values for FT synthesis (Tijmensen, et al., 2002)

Contaminant present in dry syngas	Assumed cleaning requirements (ppb)	Required cleaning steps ('wet' low temperature cleaning)
Ash (particulates)	0	Cyclone separator, bag filters/scrubber
N (HCN + NH ₃)	20	Scrubber (possibly with H ₂ SO ₄), Sulfinol D also removes HCN and NH ₃
S (H ₂ S + COS)	10	Scrubber, possibly COS hydrolysis unit or Sulfinol D necessary, ZnO guard bed
Alkalis	10	During cooling down alkalis condense on particulates, possibly also on vessels (and thereby polluting them)
Cl (HCl)	10	Absorbed by dolomite in tar cracker (if used), reaction with particulates in bag filter, scrubber (possibly with NaOH)
Pb and Cu	Not known	Condense on particulates, but actual behaviour has not been studied
Tars	0	Condense on particulates and vessels (and thereby polluting them) when syngas is cooled below 500°C

3.2.3. Scrubber

A packed scrubbing tower is used fed with chilled biodiesel. The scrubber removes tars, as well as condensing out water in the producer gas. This condensed water also allows water soluble contaminants to be removed. The cost of the tower has been calculated by applying economy of scale relationships to larger scale FT plant cost data available in literature (Hamelinck, et al., 2004). This is a common practice in the process industries to obtain estimates of equipment or plant capital cost and the relationships take the form

$$Cost_{(Size2)} = Cost_{(Size1)} \left(\frac{Size2}{Size1} \right)^{ScaleFactor} \quad (4)$$

where the scale factor usually ranges from 0.6-0.8.

3.2.4. Guard Beds

An active charcoal filter as well as two guard beds to remove contaminants such as COS, HCl and H₂S have been included in the capital costing. The guard beds have the added advantage of being able to remove residual char. As with the scrubber, power factor relationships were applied to larger scale FT plant data (Hamelinck, et al., 2004).

3.2.5. Compression

A compressor is needed to compress the producer gas from approximately atmospheric pressure up to 25 bar for feeding to the FT reactor. The sizing and costing of the compressor are based on the

fluid power required. For electrical use calculations the electrical input to fluid power was assumed to be 70%. Capital cost for the compressor is given by (Bouman, et al., 2005)

$$\text{MPIC } (\$NZ) = 1210w_f \quad (5)$$

Where w_f is the fluid power in kW and the range is approximately 10-1000kW

It should be noted this is a general correlation for compressor costs. It is acknowledged, however, that syngas compression may be more challenging from a design standpoint. Given the general nature of this economic model it is assumed to be an over complication to consider specialised methods at this stage.

3.2.6. FT synthesis

While there have been several reactor types reviewed, the most suitable option selected from reactors in commercial use is the slurry bed reactor. Because the slurry bed reactor has high average once through conversions of up to 80% (necessary for once through conversion), low negative influence on C_{5+} selectivity by inerts, and are less maintenance and labour intensive than fixed beds due to online catalyst replacement abilities (Tijmensen, et al., 2002) it was chosen as the FT unit operation in the techno-economic study.

The costing relationship for the slurry bed FT reactor was again based on economy of scale relationships from literature data for a larger plant (Hamelinck, et al., 2004).

It should be noted that this study does not incorporate any plant for upgrading the liquid fuel product, rather the product is conservatively considered to have the same value as crude oil and breakeven calculations are based on this assumption. It is assumed this is a likely future scenario for such a plant as the added complication of a 'mini refinery' may be beyond the resources of a sawmill. An ideal situation would allow a simple process to separate the diesel fraction for local use while the remaining products are transported to an existing refinery.

3.2.7. Heat exchangers

In general the heat exchangers selected for the plant were of shell and tube type. The reason for selecting this type is they are considered the most suitable for the application, while the capital cost is reasonable when compared to other types such as plate heat exchangers (Bouman, et al., 2005). They are by far the most common heat exchanger configuration (Smith, 2005) and depending on the particular design can be used in most applications (Ulrich & Vasudevan, 2004). They are generally accepted as easy to maintain and clean so are a logical choice for the plant.

The costing data from SCENZ (Bouman, et al., 2005) is based on heat exchanger area. The UniSim model produced provides a UA for the heat exchangers. Values from literature for U were obtained for each scenario to allow an area to be calculated.

The costing relationship for heat exchangers in this study is

$$\text{MPIC (\$NZ)} = 1530A^{0.566} \quad (6)$$

Where A is the heat exchanger area (m²) with approximate range of 5-1000m²

The installation factor used for heat exchangers was 2.

3.2.8. Combined heat, power and liquid fuels concept

As discussed previously the philosophy in selection of scale is to take advantage of the heat and power requirements of a sawmill. Figure 21 shows the process flow diagram for the base case design that allows integration with a sawmill. For a simpler diagram showing major components and energy flows refer to Figure 23 to Figure 25. The advantages of a system such as this revolve mainly around a sink for the heat produced in the process. The Fischer-Tropsch reaction is highly exothermic as shown in Equation 1. Heat can be recovered in the form of steam which when combined with supplementary steam from a boiler running off producer gas can meet the heat requirement for a sawmill kiln drying process. The other benefit of integration with a sawmill is the potential for meeting the electrical needs of the plant. Having a gas engine utilising the off gas of the F-T process allows the plant to be run in a once through configuration reducing potential complications of gas recycle and carbon dioxide removal and it also makes use of the unwanted gaseous products such as methane produced in the F-T reaction. The gas is also very clean as all the tars and other contaminants have been removed prior to the F-T reactor meaning the gas can be fed directly to the engine without any associated capital or operating cost.

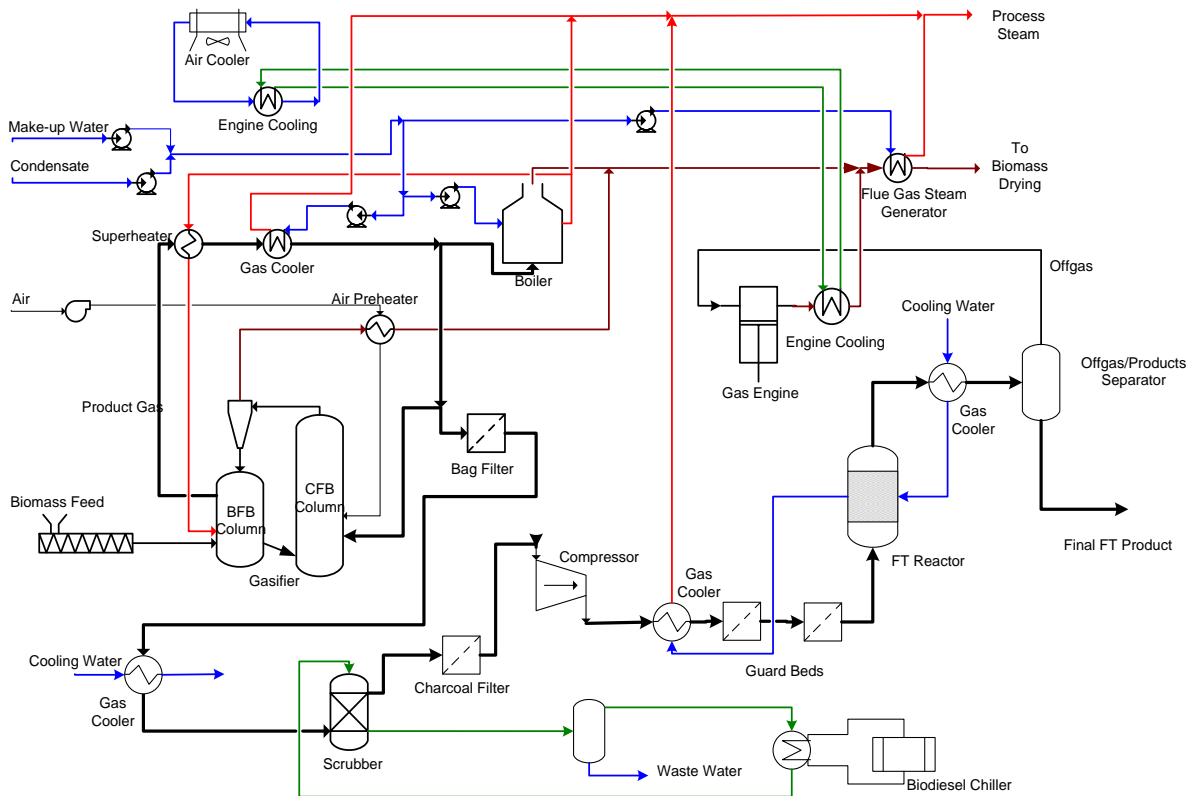


Figure 21: Schematic of combined heat, power and liquid fuels process

3.3. Modelling

3.3.1. Structure of the model

The model is based on a series of interlinked Excel workbooks combined with a UniSim (heat and mass balance software) workbook. Data is imported to UniSim via the Chemical Equilibrium model workbook, and is exported from UniSim to the Economic workbook. Figure 22 shows the overall flow of the modelling process.

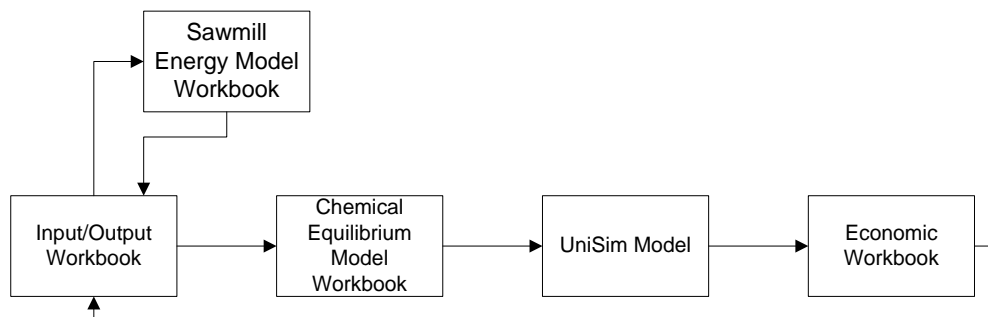


Figure 22: Flow diagram of the economic modelling of the process

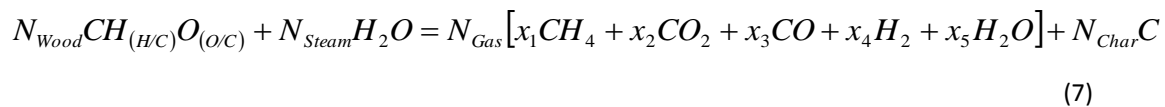
3.3.1.1. *Input/Output workbook*

The Input/Output workbook is the main interface for the combined model. It is a means of collating the necessary information in a single sheet to feed to other workbooks in the model. In this case the main inputs of interest are the biomass feed rate to the overall plant, the fraction of gas sent to the FT process, the once through conversion of CO and the selectivity of the FT products.

3.3.1.2. *Chemical equilibrium model*

The model will not be explored in detail other than a brief description of its function as it was developed in previous research (J. P. Rutherford & Williamson, 2006) and used in previous techno-economic analyses of CHP supply to wood processing plants (Penniall & Williamson, 2009). The importance of the model in this context, however, is to export a gas composition and flow to the UniSim model allowing calculation of various parameters including the FT products.

The model is based on the reaction shown in Equation 7



From Equation 7 there are six unknowns needing solved. Dalton's law and mass balances solve for four of the unknowns, while the CO shift and steam methane reforming reactions solve for the remainder. The model is solved iteratively using Excel solver due to the interdependence of temperature and an equilibrium constant.

The key assumptions used in the model are

- Chemical equilibrium is reached
- The temperature in both the gasification and combustion columns is uniform
- The actual temperature at which the reactions are taking place are equal to the gasification temperature
- The reactions modelled are representative of the actual reactions occurring

The chemical equilibrium workbook allows linking of the Excel models to the UniSim model. Gasifier gas composition and flow, along with other pertinent parameters are exported to UniSim to allow overall plant modelling.

3.3.1.3. *Sawmill energy model*

As with the chemical equilibrium model the sawmill energy model was developed in previous research (Jingge Li, 2007) hence will not be discussed in detail. The importance of the model however is to provide the thermal and electrical requirements of a specific sized sawmill allowing the overall sizing of the combined heat, power, and liquid fuels plant.

3.3.1.4. *Unisim model*

In Unisim the process is modelled in terms of heat and mass flows. It allows sizing of much of the equipment in the overall energy plant, such as heat exchangers and the boiler, also power requirements in the compression step of the FT process. This information can be exported back to Excel for further use in modelling and costing. UniSim is able to model reactions so the conversion of producer gas to FT products is also modelled within the process and is explained in detail below.

The main inputs to the UniSim model are

- Gas composition
- Gas flow
- Gas temperature
- Engine efficiencies
- Engine power required
- Steam required and steam loss
- Gasifier air and steam preheat requirements
- FT selectivity, temperature and pressure

Further description of the UniSim model showing the flowsheets and other pertinent information that relates to the balance and optimisation of the model can be found in Appendix A.

3.3.1.5. *Modelling of the FT process*

The two most important parameters in modelling the FT process are the once through conversion and the selectivity. These parameters are a function of pressure, temperature, reactor design, catalyst, feed composition, and other factors. Because of this complexity the process has been modelled using typical values obtained from literature. The once through conversion has been modelled as the fraction of CO that reacts in a single pass through the reactor. In the model 70% was used (Hamelinck, et al., 2004). For this study a selectivity of 0.87 has been used which corresponds with a plant of similar gasifier and overall design (Bolhar-Nordenkamp, 2004).

In UniSim each individual reaction needs to be set up for modelling. For example the CO and H₂ to CH₄ reaction is modelled multiplied by the once through conversion and calculated selectivity. Because of this, and the limitation of UniSim to C₃₀, reactions for C₁ to C₁₉ were modelled as stated above. The remainder of the FT product was modelled as C₂₀₊. This was modelled by summing the calculated molar fraction of each component multiplied by a molar mass correction from C₂₀ to C₆₀. The result is a range of product fractions from C₁ to C₁₉, with the remainder as C₂₀₊ considered to be

generic waxy product. It is assumed this is a sufficient analysis as it shouldn't affect the gas/products split, and the final product is considered as bulk product for costing purposes.

3.3.1.6. *Economic workbook*

The economic model predicts the capital cost of the plant based on the sizing parameters from the other workbooks. From other imported parameters an operating cost is also calculated. This enables a discounted cash flow analysis to be performed where net present value (NPV) is used as a measure to determine if the plant is economically viable.

3.4. Results and Discussion

There are a number of different strategies for sizing the combined heat, power, and liquid fuels plant based around the varying electrical demand of the sawmill. Typically a sawmill will mill for 8 hours during the day with the associated electrical demand, while drying continues 24 hours per day with a continual heat and electrical demand. The energy plant must meet the heat requirement of the drying process, however, the electrical production of the energy centre has more flexibility as there will still be grid connection. If the energy centre were to meet the full electrical requirements on peak there would be the necessity to sell power back onto the grid for the times when only the drying component of the mill is operating. Depending on the contract with the electrical supplier it is likely the power would be sold back to the grid at a lower than purchase price. The other option is to meet the off peak electrical requirement of the mill. In this case during peak production it will be necessary to purchase electricity but the electricity continually generated will be offsetting a higher realised value than if it were being sold. The trade-off is that the economy of scale suffers with the plant only producing the lower quantity albeit higher value per unit electrical output. On this premise this balance has been investigated and reported. The fuels component adds another complication to the model, however, for the purposes of simplifying variables of investigation the maximum fuels production within the constraints of the model has been used as the basis. In other words, the FT part of the plant is made as large as possible until different flows of heat and syngas or offgas meet the heat and power requirement of the sawmill and other parameters in the model are constrained. The model was based on a mill producing 300m³ per day (approx 100,000 m³/yr) of timber. While this is considered to be at the larger end of sawmills in New Zealand it is unrealistic to assume a significantly smaller sawmill could, or would invest the capital necessary for such a significant energy centre. Based on the energy demand model the sawmill has an electrical demand on peak of 1,400 kW, while the off peak electrical demand is 360 kW. There is a continual need for

7800 kW of heat energy (in the form of steam) for drying and a varying heat requirement to dry the biomass fed to the energy plant.

Because of the potential arrangements in terms of meeting electrical requirements three different scenarios have been modelled and compared for feasibility. The three scenarios are

- Scenario 1. The energy centre will supply all heat that is required for kiln drying in the form of steam and all on peak electrical requirements of the mill (including parasitic use in the liquid fuels operation – mainly for compression). The Fischer Tropsch component of the plant will be sized as large as possible limited by the heat generated by the process to balance with mill requirements. See Figure 23
- Scenario 2. The energy centre will supply all heat required by the mill for kiln drying and off peak electrical requirements of the mill (including parasitic use in the liquid fuels operation). Fischer Tropsch component size will again be maximised limited by heat production. See Figure 24
- Scenario 3. The energy centre will supply all the heat and the maximum liquid fuels production possible within the constraints of the heat production matching that required by the sawmill. No electricity will be produced by the energy centre rather the off gas will be used as boiler fuel. See Figure 25

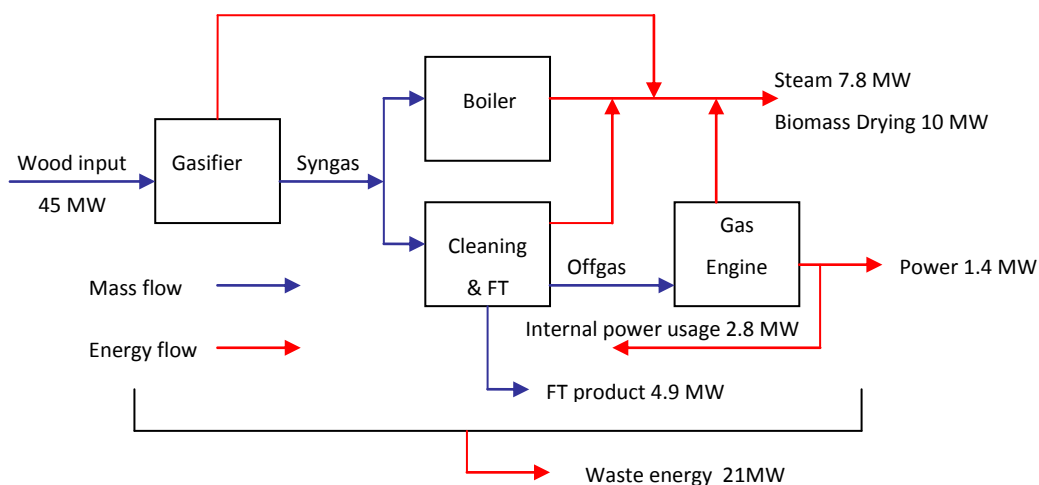


Figure 23: Simplified layout and flows for scenario 1

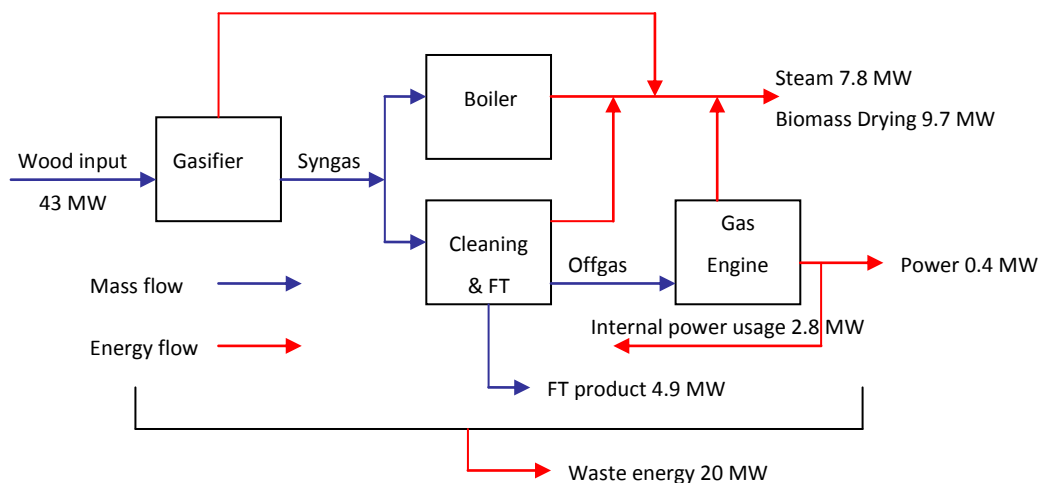


Figure 24: Simplified layout and flows for scenario 2

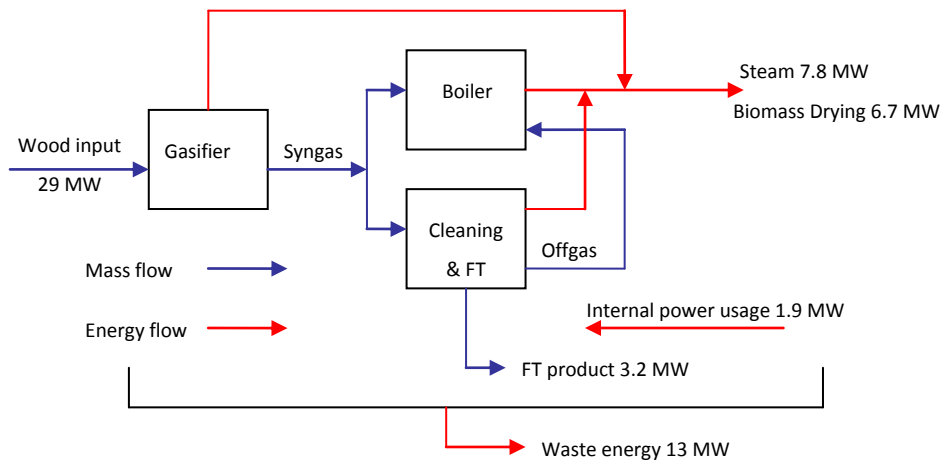


Figure 25: Simplified layout and flows for scenario 3

3.4.1. Capital cost

Capital cost was calculated based on correlations as discussed in methodology. The breakdown of capital cost for the three scenarios is shown in Table 9 and includes all the components of the base gasification plant and the FT plant. It should be noted the method employed for calculating capital cost has a typical error of $\pm 25\%$. Therefore one should refer to the sensitivity analysis for comparison of the effects of a movement in capital cost.

Table 9: Economic breakdown for modelled scenarios

		Capital Cost (\$NZ)		
		On peak	Off peak	No Generation
Biomass Drying		3,060,000	2,890,000	2,090,000
Feed Handling		2,630,000	2,530,000	2,020,000
Gasifier		2,950,000	2,830,000	2,240,000
Gas Engine		7,260,000	5,570,000	-
Boiler		351,000	334,000	439,000
Misc.		160,000	156,000	112,000
Gas Scrubber		1,220,000	1,230,000	1,230,000
Gas filters and Guard Beds		186,000	187,000	187,000
Compressor		2,250,000	2,270,000	1,480,000
Heat exchange		638,000	643,000	469,000
FT slurry reactor		7,440,000	7,500,000	4,890,000
Contingency and Fee		4,220,000	3,920,000	2,270,000
Working Capital		3,240,000	3,000,000	1,740,000
Total		35,600,000	33,000,000	19,200,000
Breakeven price	\$US/barrel	167	173	219
Fuel production	kg/yr	3,330,000	3,350,000	2,190,000
	barrel/yr	27,100	27,400	17,900
	barrel/day	74	75	49
Engine power	kW	4,260	3,250	-
Biomass requirement (dry T/yr)		67,700	63,500	43,400

3.4.2. Operating cost

Operating cost was calculated using typical values from literature (Ulrich & Vasudevan, 2004) or typical assumed values that are applicable to New Zealand. The value for heat that the energy centre would 'sell' to the mill was \$8/GJ (J. Rutherford, 2006). The electricity value had a split value depending on whether the energy centre was offsetting power purchased by the mill, or whether the mill was selling power back onto the grid. The values were 9.8 c/kWh to buy, 8.13 c/kWh to sell based on what the wood processing industry paid on average in 2008 (Ministry of Economic

Development, 2010). Table 10 shows an operating cost and profit breakdown of scenario 1 as an example for all scenarios (capital, operating cost and electrical and heat revenue breakdowns can be found in Appendix B). Note this is with the product value adjusted to achieve breakeven over a 30 year plant lifetime. Worth comment, however, is the value chosen for the wood cost. A value of \$20 per odt has been selected. This may seem very low compared to the typical sale value of wood chip for instance, however, the rationale is this plant would not get installed in a scenario where substantial amounts of biomass would need to be purchased at a premium or transported large distances. Rather, it would suit a scenario where there may be excess biomass and low opportunity cost for selling sawmill chip and other waste biomass. One can examine the effect of increasing the wood price from the sensitivity analysis shown in Figure 26 to Figure 28.

The breakeven fuel price quoted in Table 9 is the value the F-T product would have to sell at to generate \$0 NPV over a 30 year plant lifetime with a 10% discount factor (IRR). The NZ/US exchange rate used in the calculations is 0.73 current at the time of calculation. The modelling results are encouraging with a breakeven price for the F-T syncrude between \$US167 and \$US219 per barrel which at the lower end isn't significantly above historic crude price trends (Ministry of Economic Development, 2011). The first two scenarios produce a very similar quantity of product, and share a similar breakeven price. The decision, therefore, as to which scenario to proceed with could be based on a more detailed study of the variations in power price between on peak and off peak scenarios, specific to a particular site. The third scenario was generated as a comparison, and shows the economic impact of buying electricity for the mill and the F-T process rather than generating electricity to offset the milling processes. It can be seen that the third scenario generates the most expensive crude, which would indicate that the plant is able to generate electricity cheaper than what it can be purchased at, therefore offsetting the cost of producing the F-T syncrude. Also, as a comparison for completeness a breakeven price for a scenario where wood feed to the plant will cost \$40 per odt is \$US 209 per barrel for scenario 1. This would represent a more realistic scenario if a mill was unable to find a cheap source of biomass, or was not constrained in selling its chip or other waste biomass.

Table 10: Operating cost and profit breakdown example for scenario 1

	Annual Use		\$/unit		\$/yr
Raw Materials					
Wood	68000	odt	20		1,360,000
Utilities					
Diesel	540000	L	1	L	540,000
Labour and Maintenance					
Process Operation	13000	hrs	20	hr	260,000
Supervision	15	% of operating labour			39,000
Administrative and General Overhead	60	% of labour + maintenance			610,000
Maintenance	2	% of capital cost			720,000
Local taxes	1	% of capital cost			360,000
Insurance	1.5	% of capital cost			540,000
Operating Supplies	15	% of maintenance cost			54,000
Total Operating Costs (\$NZ)					4,500,000
Revenue from sales					
Product sales (FT syncrude)					5,500,000
Heat revenue					1,700,000
Electricity revenue					1,100,000
Net Annual Profit					
Sales revenue					8,300,000
Less Operating Costs					4,500,000
Net Annual Profit after operating costs, before tax					3,800,000
Less depreciation on fixed capital	10	years straight line			3,200,000
Net annual profit after depreciation					570,000
Less tax	33	c/\$			190,000
Net Annual Profit after tax (\$NZ)					380,000
Add back depreciation					3,200,000
Total Net Annual Cashflow (\$NZ)					3,600,000
<hr/>					
% return on capital investment					10

3.4.3. Sensitivity analysis

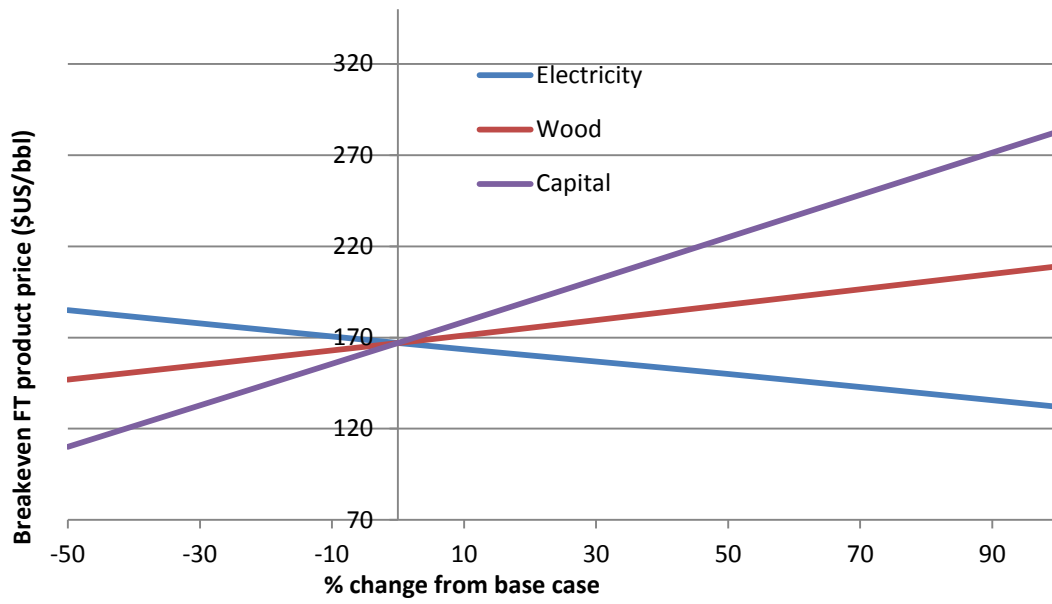


Figure 26: Sensitivity analysis for on peak scenario (Scenario 1)

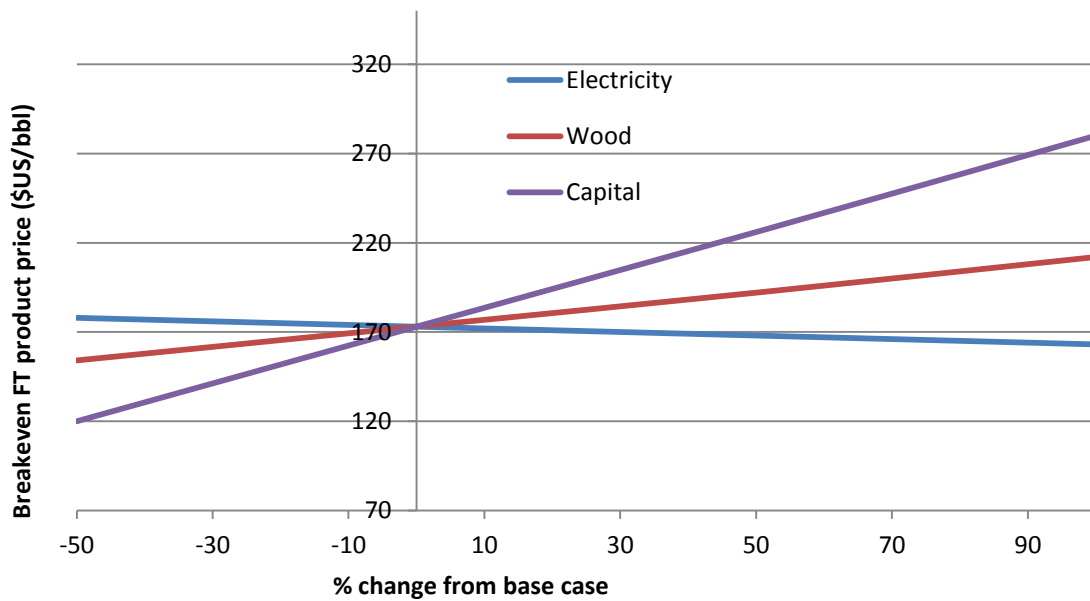


Figure 27: Sensitivity analysis for off peak scenario (Scenario 2)

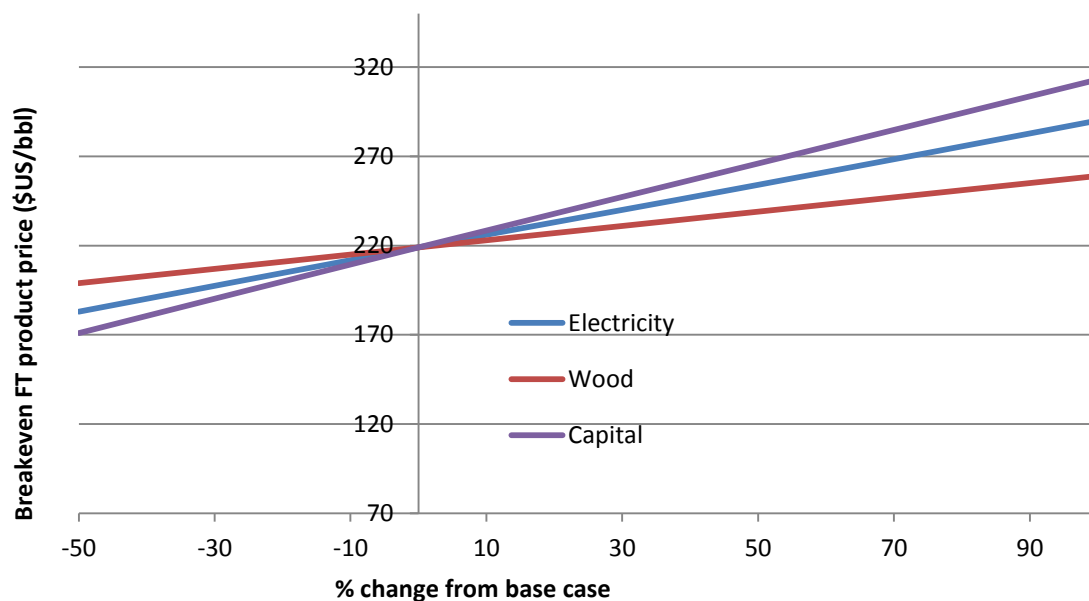


Figure 28: Sensitivity analysis for scenario where no power is generated (Scenario 3)

The sensitivity analysis for the third model as seen in Figure 28 shows a sensitivity to electricity price opposite to the other two scenarios. This scenario relies on buying electricity to produce liquid fuels, therefore, as the electricity price increases the cost of fuel production goes up. In the other two scenarios the plant is offsetting electricity purchased for the mill, consequently as the price increases the price of the fuel goes down, because the power savings are effectively offsetting the fuel production cost.

The third scenario is unprotected from any volatility in the electricity market, whereas the first two scenarios do offer varying levels of protection to the sawmill from such volatility. The third scenario may suit a situation where a mill has a localised source of cheap power such as geothermal generation. However, the purchase price of electricity would have to be over 60% less than the price modelled to allow a scenario where the breakeven FT product price for the non generation scenario is within the range of the other scenarios. This is an unlikely case and coupled with the general expectation of an increased electricity price in the future (Ministry of Economic Development, 2007) the first two scenarios are the most sensible forward looking options.

3.4.4. Expected obstacles

Even if the plant is economically viable there are a number of non-economic factors which need to be considered when gauging the feasibility. The obstacles are not seen in any way as insurmountable but should be kept in mind when considering overall feasibility of an installation.

3.4.4.1. Biomass availability

Currently, in the New Zealand environment, the issue with leftover wood waste for use in a plant is the existing market driven value for the wood. Good chip is usually either exported or used in local pulp, paper, and panel board production. While substantial wood processing residues are generated in New Zealand having those residues available on site in consistent volumes and quality at an economic price is not guaranteed. Currently there isn't an established or well understood infrastructure that allows consistent and economic residue supply. This is often an overlooked difficulty in the development of biomass based technology. Guaranteed feedstock relies greatly on both the location of a plant within a mill that generates its own residues, and the location of the mill as to the value of those residues. Ideally a plant would be situated in a remote location where there is limited market for the residue and therefore biomass disposal is an issue. This would be the ideal areas to target as they would not represent the average and the economics would likely be more favourable.

3.4.4.2. Complexity of plant

The overall plant is a combined heat, power, and liquid fuels process. This complexity can be a potential difficulty especially given the intended setting. This has generally been regarded, in some part, as the downfall of BIGCC (Biomass Integrated Combined Cycle) processes. Also in a sawmill it is likely there is not the expertise to operate and maintain the equipment. This can, however, be overcome with suitable training of existing staff, or employment of appropriate people.

3.4.4.3. Capital investment

A by-product of the plant complexity is the associated high capital cost. While the plant may be economically feasible the likelihood of a sawmill being able to invest \$20 M or more in a heat, power, and liquid fuels plant is limited. In the early stages of development it is likely government support would be necessary to build a demonstration plant, and in the future other investors in partnership with a sawmill to build and run such a process plant.

3.5. Conclusion

The primary advantage offered by this system is that the sizing is not based on an optimum that is a compromise of feedstock cost vs. economies of scale, rather the sizing is based on what meets the heat and power requirements of the associated mill. The sizing and design is configured specifically to suit the scenario, instead of, at least in part, mimicking the design of a plant many orders of magnitude larger. Because of this design principle and the synergy created between the energy plant and the associated mill the breakeven price for the FT crude is not an unrealistic figure (between \$US167 and \$US219 per barrel over the three scenarios) in light of trends in crude oil price. The peak in July 2008 of \$US148 (Ministry of Economic Development, 2011) per barrel of crude demonstrates this technology is not far from being competitive in the on peak scenario if prices do continue to rise. Also to be considered is that FT product will be of higher value and quality than regular crude, but for conservatism is compared directly. It can be concluded that if oil price does in fact trend up as is expected, and scenarios can be found where a lower than average biomass supply cost is available, the technology may be appropriate for New Zealand scenarios.

4. Microchannel Experiments

This chapter is a substantial component of the thesis and considers design and construction of a laboratory scale microchannel reactor as well as construction of the experimental rig and methodology. These sections lead to the results and discussion of the experiments in Chapter 5. The process and results from these two chapters aid in scale up design of the microchannel reactor for the sawmill FT plant.

4.1. Laboratory Microchannel Reactor Design and Construction

4.1.1. Basis for design

The initial design principles for the microchannel reactor were relatively simple. The size chosen (50mm square including sealing faces) was partly dictated by observation of other lab scale microreactors in literature (Ajmera, Delattre, Schmidt, & Jensen, 2002; Commenge, Falk, Corriou, & Matlosz, 2002; V Hessel, 2011; Kolb & Hessel, 2004) as well as assumptions of what flows would be required through the reactor based on the flow metering technology available.

The channel width was chosen based on the minimum it was thought the available technology would allow. The channel height is the thickness of the material used. The thickness chosen was 0.2mm which was a compromise to make a small height channel, with the material still being thick enough to enable handling without damage as well as being in line with other reactors in literature. The material chosen was 316 stainless steel as it was deemed the realistic choice of material for scale up scenarios. Also the stainless steel was considered to be inert for Fischer-Tropsch reactions whereas materials like copper are not (although realistically the surface area wouldn't be significant, therefore this is more seen as a positive byproduct of choosing stainless steel, rather than a reason unto itself). In the design the reactor shim was complimented by a feed shim which takes gas from the feed ports and distributes it across the width of the channels. The stacking arrangement of feed and reactor shim is shown in Figure 29. Note this image also shows how cross flow cooling/heating can be incorporated into the reactor with the same shims.

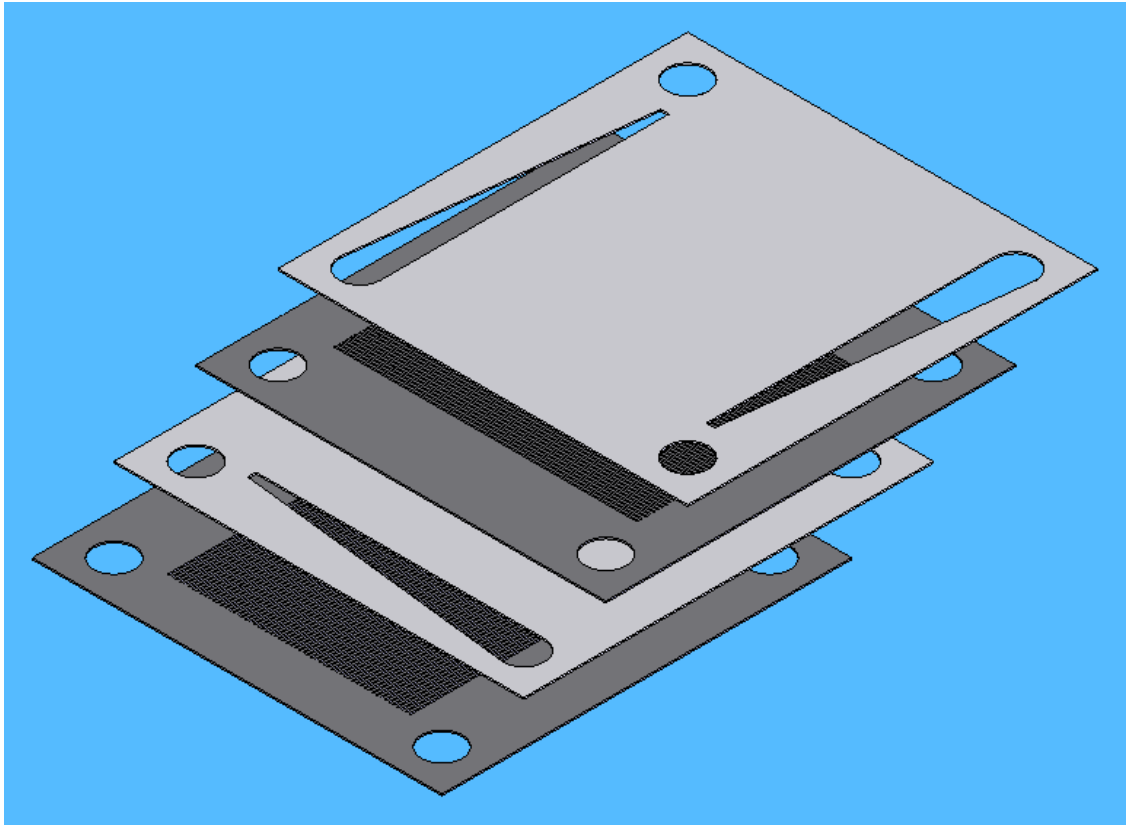


Figure 29: Stacking arrangement of feed and reactor shims, along with cross-flow cooling/heating shims

4.1.2. Construction

4.1.2.1. Chemical Etching technique

The first technique trialed for creating the microchannels was a chemical etching technique. There were a number of reasons for attempting this form of construction.

- This method was often used in literature for creating microchannel reactors (Ajmera, et al., 2002; Ehrfeld, et al., 2004; Gavriilidis, et al., 2002) or at the very least creating detailed fine structures in general use
- The method is very easy to change design with no specialist tooling changes required
- It was believed there was the in house ability to perform the method

The steps described below are the process that was worked through while attempting to develop the chemical etching method. The methods gain robustness and technique as it was discovered each prior step was not sufficient to achieve reasonable results. The overall aim of the chemical etching technique is to expose the surface of the material to the chemical in the areas to be etched. The challenge is to do this in such a way as to maintain the fine features required. Photolithography was chosen as the method to achieve these results. The broad concept of photolithography is shown before a detailed account of the method is given.

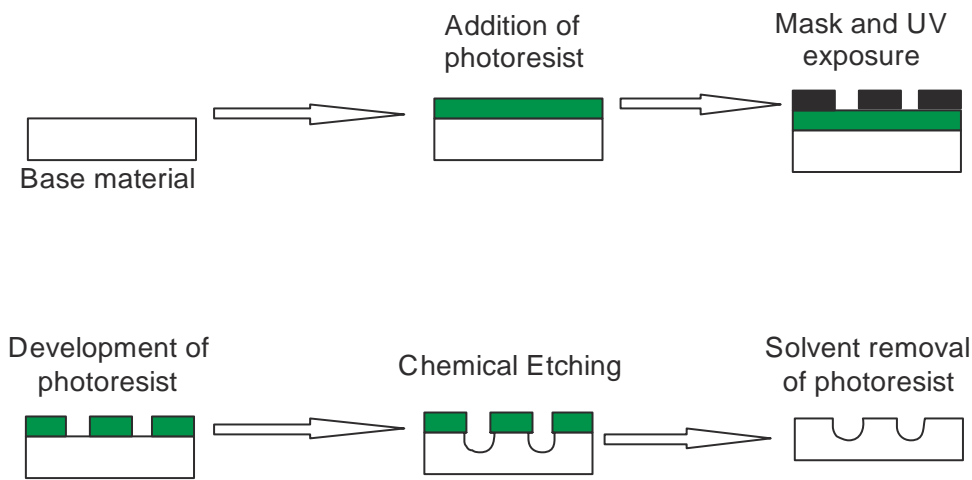


Figure 30: Visual explanation of photolithography process

The method for creating features using photolithography is explained below and in Figure 30

- Coat with photoresist and allow to dry (in dark room)
- apply mask and expose to UV light
- develop with appropriate developing solution
- expose to chemical to etch
- use solvent to remove resist

4.1.3. Methodology used to etch channels

4.1.3.1. Creating the mask

The reactor design was drawn in Solidworks with the external drawing lines eliminated and the reactor shims coloured black so the actual dimensional details are captured. This was saved as a DXF file, then opened in CorelDraw, replicated, and white space filled in as to not waste etch solution. This was then saved as an ai file which is a vector format usable by the printer. The printer (Precision Lithographics) then transferred the design to a film to be used as the mask for developing the photoresist. The design can be seen in Figure 31.

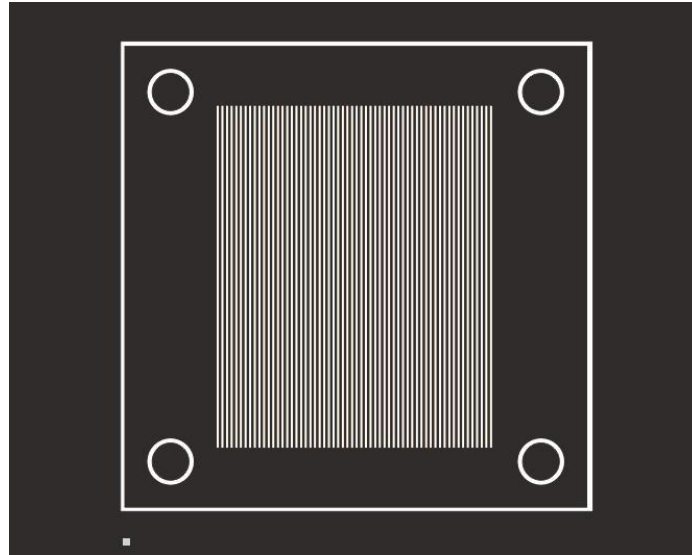


Figure 31: Example of mask filmwork

4.1.3.2. Preparing the shim

Firstly the shim was cut to size and cleaned, then in a dark room a photoresist spray (Electrolube PRP positive photoresist) was applied to the shim and allowed to dry. The mask was sandwiched with the shim and exposed to UV light. Either with a UV lamp or with sunlight. This was a crucial step as too much UV would remove photoresist under the mask, too little and the parts that were to be removed were not exposed enough. Once the shim had been exposed for sufficient time it was returned to the dark room where it was developed in a weak sodium hydroxide solution.

4.1.3.3. Etching the shim

A recipe for etchant solution for stainless steel was found in literature (Nageswara Rao & Kunzru, 2007) with the recipe being FeCl_3 10 wt%, HCl 10 wt%, HNO_3 5 wt% at 40°C . Leaving a stainless steel test piece in this solution for several hours did achieve noticeable dulling and thinning of the material, indicating it would in fact etch the material. The control of the etching was to be the more challenging aspect of the process however. It was also noted that the rate of etching appeared to slow greatly over time. It was assumed that there was sufficient solution as to not be spent therefore there were localised pockets of spent solution at the stainless steel interface. This required agitation.

Searches of the grey literature (chemical etching is often used in model making) suggest air agitation as the best solution that allows sufficient agitation without causing undue shear which could damage or lift the resist mask. A fish tank air pump, and a foam aerator tube were used in the base of a plastic container as shown in Figure 32. The air flowrate was adjusted to give fine bubbles, and

the shim to be etched was held at an angle that allowed the bubbles to pass up the face to be etched.

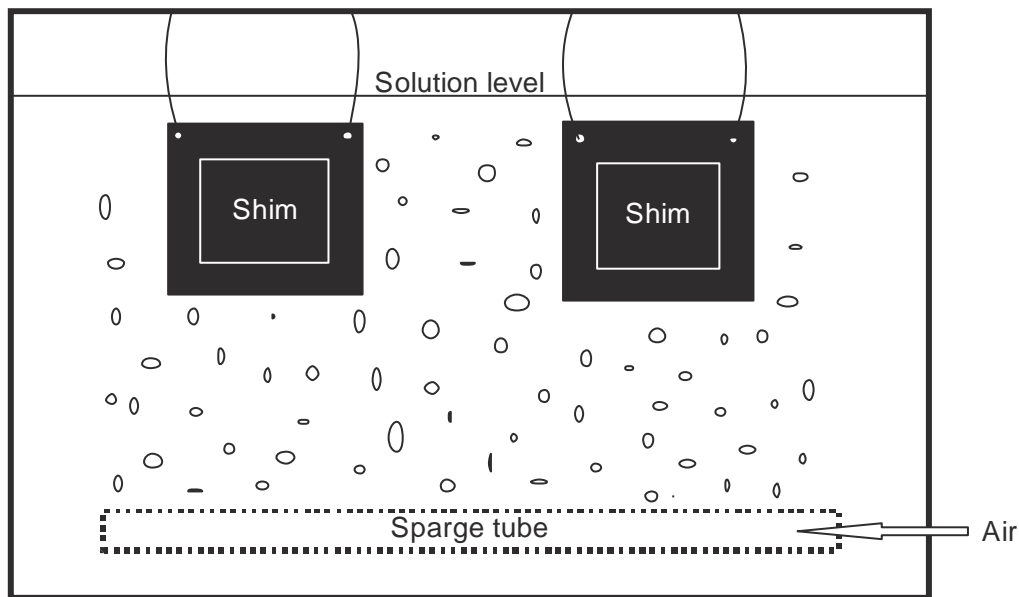


Figure 32: Schematic of etch tank arrangement

Trial etching of the resist coated shim proved to be quite unsuccessful. The main issue was that the etching would not remain within the boundaries of the resist mask. In fact etching appeared to preferentially happen where the etchant could be between the metal and the mask. This obviously was not ideal and any pinholes in the mask (which were very hard to avoid) became substantial voids early on, while the surfaces to actually be etched appeared relatively unscathed.

It is assumed a significant amount of the difficulty can be attributed to the thickness of material that was intended to be removed, along with the type of material. For example, the often used application of this technology is circuit boards where very thin copper is removed. Because of the fast etch rate of the copper, as well as the small thickness that has to be removed, the exposed areas are easily removed before undercutting of the mask becomes a problem.

4.1.3.4. Further photolithography development

The electrical engineering department at the University of Canterbury has the very sophisticated nanofabrication laboratory. Utilisation of their training and equipment was performed in an attempt at improving the technique to a useable technology.

Significantly greater care was taken in the preparation and cleaning of the reactor shim prior to applying the photoresist. Acetone was used, followed by methanol and then IPA. The photoresist was spun on rather than the crude spray on method. This provided a significantly improved finish. Again the etching step was not particularly successful. While the resist layer was an improvement there were still issues with pinholing and undercutting. Another issue which presented itself was the effect of the etchant penetrating right through the metal. The back of the shim was painted to protect it from being etched, however, when the etchant reached the back coating it began to etch sideways. This showed that in an ideal situation there would be etching from both sides. This is common in a commercial etching process. An attempt was made to create an envelope of the reactor filmwork to allow development of photoresist on both sides of the shim. However, there was great concern for the difficulty of maintaining accurate registration of the two faces.

It can be concluded that while there was an ease in changing design the time required to produce each shim and the consistency and repeatability of etching between each shim was a significant barrier. It may have been possible with significant numbers of trials and time spent to perfect the method, however, it was deemed best to investigate other options at the same time to see whether there were simpler, more repeatable and time effective methods.

4.1.4. Laser cutting

As discussed in the literature review a short amount of time spent canvassing local companies about laser techniques showed no-one in the Canterbury area believed their laser cutter could produce the small channels required without consuming the 'land' between the channels.

4.1.5. Wire cutting

Because of the lacklustre results of the above techniques attention was turned to electro-discharge machining technology. While this project was pushing the limits of the technology there was still far more confidence in the reproducibility of the channels than by the chemical etching technique. The channel width was chosen as the minimum dimension possible that would allow the wire cut to be produced (Wilson, 2008). This was 0.3 mm. Within the dimensions of the reactor shim this allowed a total of 50 channels per shim. In order to be able to feed the wire to make the cut for each channel an EDM drill was used to open the smallest hole possible that would allow an open circuit when the wire was fed through. Because this hole is slightly larger than the channel cut the holes were drilled at alternate ends for adjacent channels. This can be seen in Figure 33.



Figure 33: Close-up of channels revealing EDM start holes

This prevents each EDM drilled hole breaking through into the next hole. For 50 channels this is obviously a very time consuming process, however, the advantage is multiple shims can be stacked then drilled and cut at once. For this project 42 shims were stacked together and sandwiched between 3 mm gauge plate as shown in Figure 34.

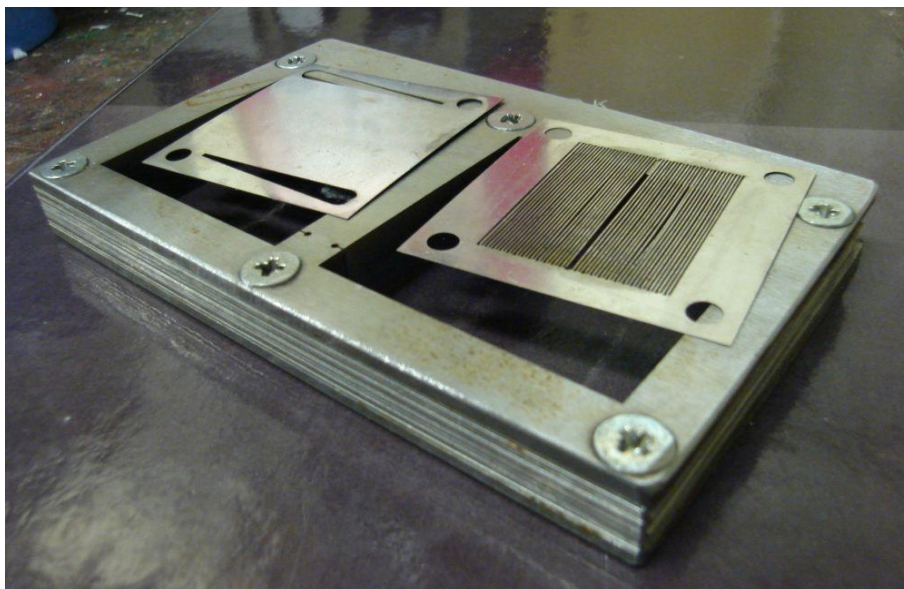


Figure 34: Arrangement of shims sandwiched between gauge plate for wire cutting with the feed shim on the left and reactor shim on the right

The shim and gauge plate was cut large enough to allow for both the reactor and the feed shims to be produced as well as leaving sufficient land for the screw supports. The cost of creating the reactor shims was \$1325 + GST and the feed shims cost \$220 + GST. This gives a per shim cost of \$32 + GST for the reactor shims and \$5 + GST for the feed shim. This indicates, as expected due to the work involved, the cost for the reactor shim is relatively high. However, the feed shim is quite

cost effective and well within the capabilities of the wire cutting technology. Therefore, even if there are future developments at the University of Canterbury for creating microchannels such as micromachining or improved wet etching techniques, fabrication of the feed shims using wire cutting may still be the most practical approach.

4.1.6. Reactor top and bottom plates

To seal the reactor it was determined a relatively significant clamping pressure would be necessary. As shown in Figure 35 there were areas where the effective sealing face is quite small. Therefore, substantial top and bottom plates for the reactor were produced that could provide significant clamping pressure. The plates were initially manufactured from 10 mm stainless steel plate. The thick top and bottom plates also had the advantage of being able to mount ports for the reactant and coolant streams. The contact faces were ground and polished. The plates are shown in Figure 36.

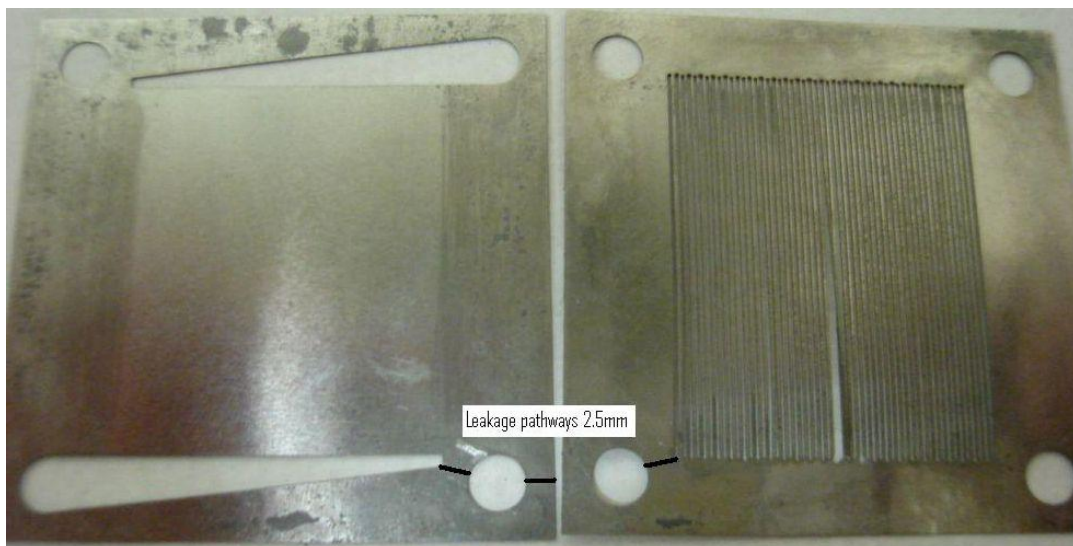


Figure 35: View of feed and reactor shims demonstrating smallest sealing faces

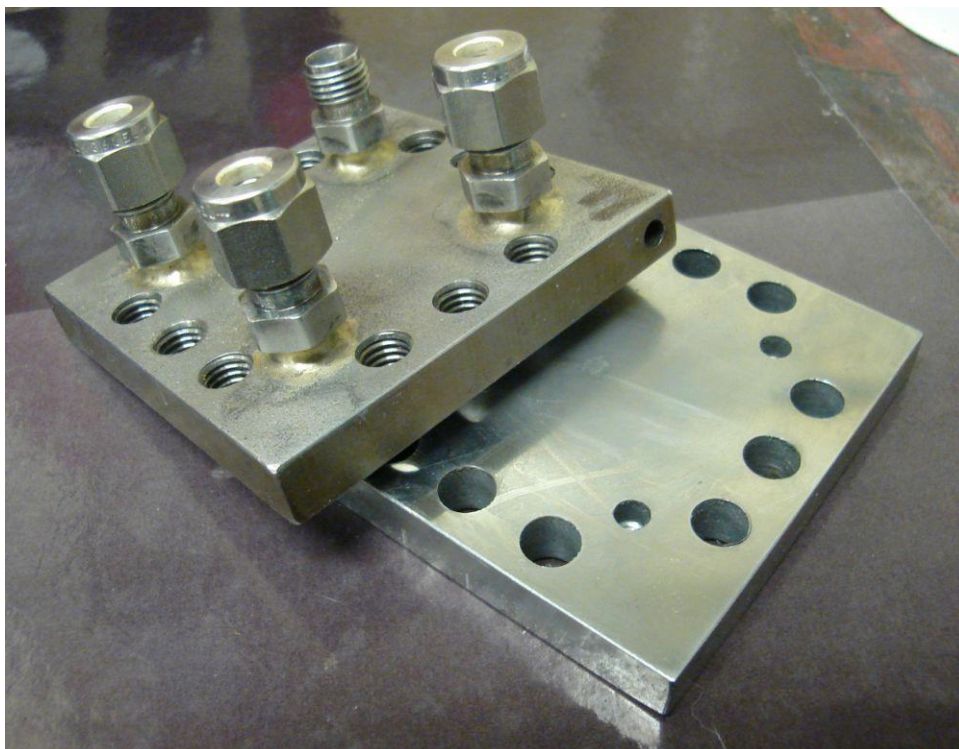


Figure 36: First reactor created using 316 stainless steel

These plates proved unsuccessful as the stainless steel was too soft and bowed and indented. External sealing of the reactor was relatively successful due to the softness of the stainless steel compressing around the edges of the shim, however, the internal sealing (between reactant and coolant streams) was poor due to the bowing meaning there was very little to no compression on areas that needed to internally seal. Because of these limitations new reactor top and bottom plates were fabricated in an attempt to alleviate the inadequacies of the first design. 25 mm thick Stavax (tool steel) plate was used. Stavax is easily machineable but can be hardened to 55 rockwell. Because the heat release from the Fischer-Tropsch reaction at the volumes used in the initial work is almost certainly less than any heat loss from the reactor, ports for cartridge heaters were also machined into the top plate. These plates are shown in Figure 37 compared to the original reactor design.



Figure 37: Second reactor model constructed from Stavax on left, in comparison to stainless steel model on right

For assembly blind 5mm holes were drilled in the bottom plates which allowed 4.9 mm drill bits to be used as dowel pins for alignment of shims and top reactor plate as shown in Figure 38.

Note that ports are now welded in as the thread tape would not be adequate for the temperature required. The sequence of construction of the top and bottom plates were as follows. The sequence is important due to the hardening step negating the possibility of further machine work.

- Machine all features necessary in the top and bottom plates
- Grind the faces of the reactor
- Mill the other side of the reactor to ensure faces are parallel
- Get the reactor hardened
- Weld in the feed and outlet ports
- Grind the plates again to obtain final flatness
- Polish the reactor faces using emery paper on a flat surface

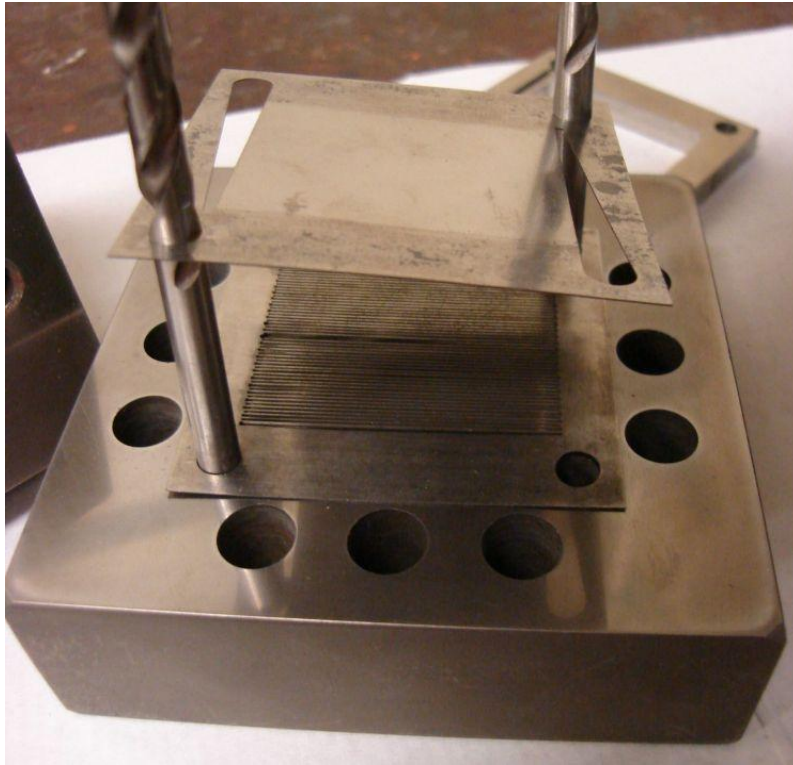


Figure 38: Demonstration of the use of 4.9mm drill bits as 'dowel pins' for accurate alignment of plates

4.1.7. Reactor proof testing

With the completed reactor, pressure testing and any necessary sealing development was required. As previously stated the stainless steel top and bottom plates were soft enough to indent around the shim. While creating internal leakage the stainless was self sealing due to the softness. With the Stavax top and bottom plates this was not the case, therefore, a form of gasketing was required. Graphite powder was trialed, however, the repeatability of the coating was not sufficient and leakage was common. Metal foils were the obvious next solution. Copper is a very common gasket material, however, copper can have a potential influence on FT activity (O'Brien & Davis, 2004) therefore it was reserved as a secondary solution if another wasn't found.

A very simple solution was trialed with the use of aluminium foil (standard kitchen foil). The advantages of this material is the lack of FT activity, the ease of workability (gaskets can be cut with a scalpel using a feed and reactor shim as a template), and the extremely low cost and easy availability. This solution proved to be more than adequate. When the aluminium foil gaskets were used there was complete sealing up to the maximum potential operating pressure of 500psi using compressed nitrogen. With this proving to be a successful solution no other forms of gasketing were investigated.

There were lessons to be learnt concerning assembly of the reactor, especially when the equipment had been through heat cycles up to 400°C. This was particularly relevant to the torquing down of the bolts that hold the top and bottom plates together. The M8 bolts were torqued to a setting of 25 ft lb based on a value of approximately $\frac{3}{4}$ the yield strength of the grade 12.9 bolt. However, after heating cycles the bolts were binding during tightening, reducing the actual torque rate. This was solved by wire brushing the bolts and coating the threads with an anti seize compound before assembly.

Another interesting point to note was that post the 400°C heat cycles of calcination and reduction, the aluminium tended to bond to the adjacent faces. It would appear the material was beginning to diffusion bond due to the high pressure from bolting together and the temperature around $\frac{2}{3}$ of the melting point. This creates a difficulty upon disassembly as it is a challenge to remove the top and bottom plates and separate the shims without causing damage to the catalyst layer. However, upon separation there was still sufficient catalyst remaining to perform SEM analysis so this problem was far from insurmountable for the experiments conducted as part of this thesis.

4.2. Microchannel Reactor Experimental Methods

The purpose of this section is to describe the process by which the experimental methods were developed and subsequently performed. The construction of the microreactor has been discussed previously, whereas this section discusses the necessary equipment and techniques to analyse the performance of the reactor. Initially the trial rig will be described, followed by the processes for forming the catalyst in the microchannels. There is also discussion on powdered catalysts created for comparison and the associated fixed bed reactor. The final step in the process is analysis and this is discussed in terms of analysing the gaseous and liquid products, as well as analysis techniques for the powdered catalysts.

4.2.1. Rig setup

The trial rig used was a single stream system due to the use of pre-mixed gas. The gas mix is 64% H₂, 32% CO and 4% N₂. This limits the system to being unable to change the ratio of the feed gases. However, this is not seen as a significant issue as this is the optimum ratio for Fischer-Tropsch and is also achievable from the gasifier. There is still significant scope for testing and development outside modifying the syngas ratio. The N₂ is used as a tracer gas to enable mass balance closure and error analysis. The flow schematic for the system is shown in Figure 39.

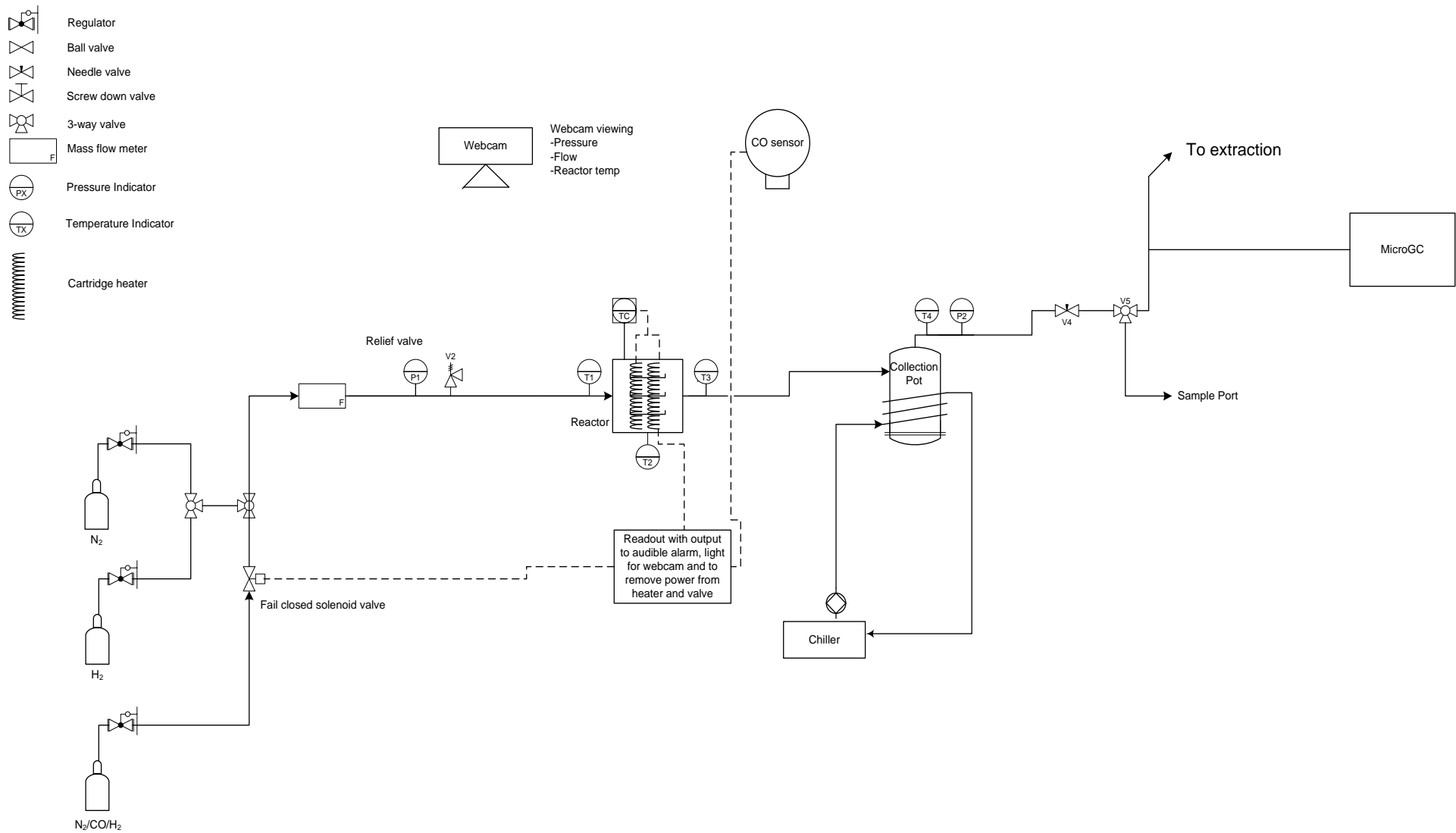


Figure 39: Schematic of lab scale Fischer Tropsch Rig

Hydrogen and Nitrogen bottles were also incorporated into the rig for reduction and inert gas pressure testing respectively. The three gas bottles were manifolded as shown in Figure 40 which eliminates the possibility of back filling gas bottles.

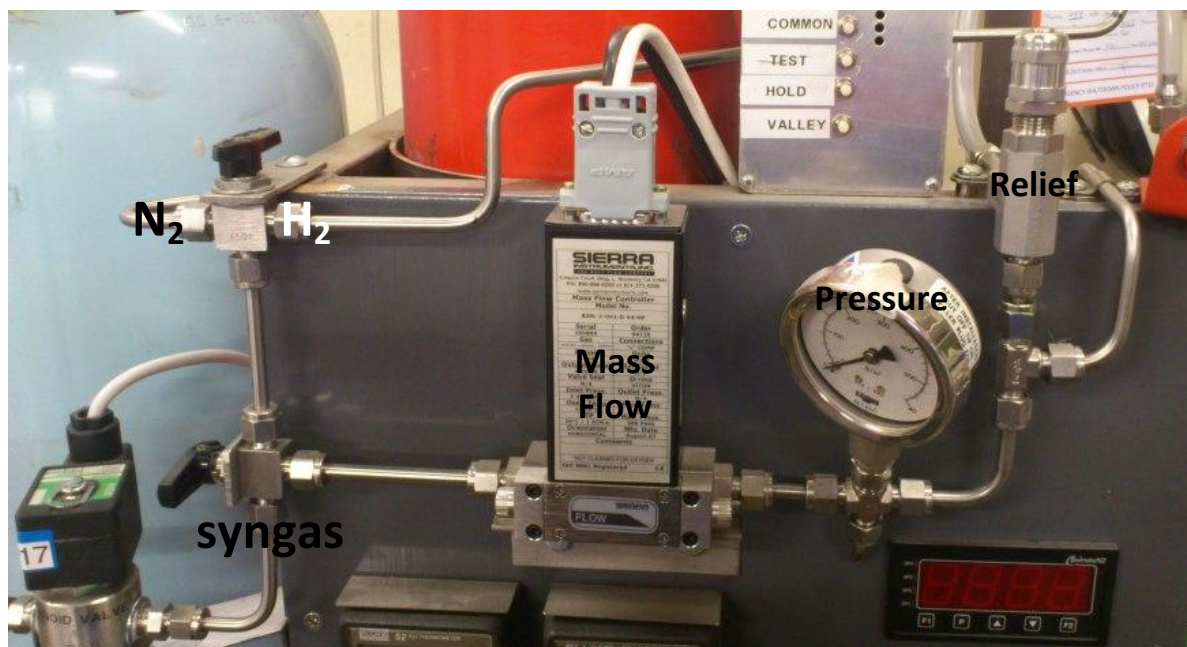


Figure 40: Picture showing the manifold system to allow only one gas to flow at a time (N_2 top left valve, H_2 top right, syngas from bottom of lower valve) as well as the mass flowmeter, pressure indication and pressure relief valve.

Upstream of the reactor an electronic mass flow meter measured the flow, while post the reactor and collection system a syringe displacement test was used to measure the flow of the gaseous products (Figure 40 and Figure 42) from the open port post the three way valve.

Figure 41 shows the reactor is mounted so the feed and outlet ports face downwards. This is to facilitate the movement of any liquid products through the outlet ports of the reactor to the collection pot. The tube run from the reactor to the collection pot was kept as short and vertical as practicable and insulated during operation to minimise product condensation in the line. It should be noted that the reactor is also insulated during the run in order to minimise heat loss and avoid overloading the cartridge heaters.



Figure 41: Arrangement of reactor showing outlet to collection pot. Note the line is separated and capped between runs to eliminate air oxidising the catalyst

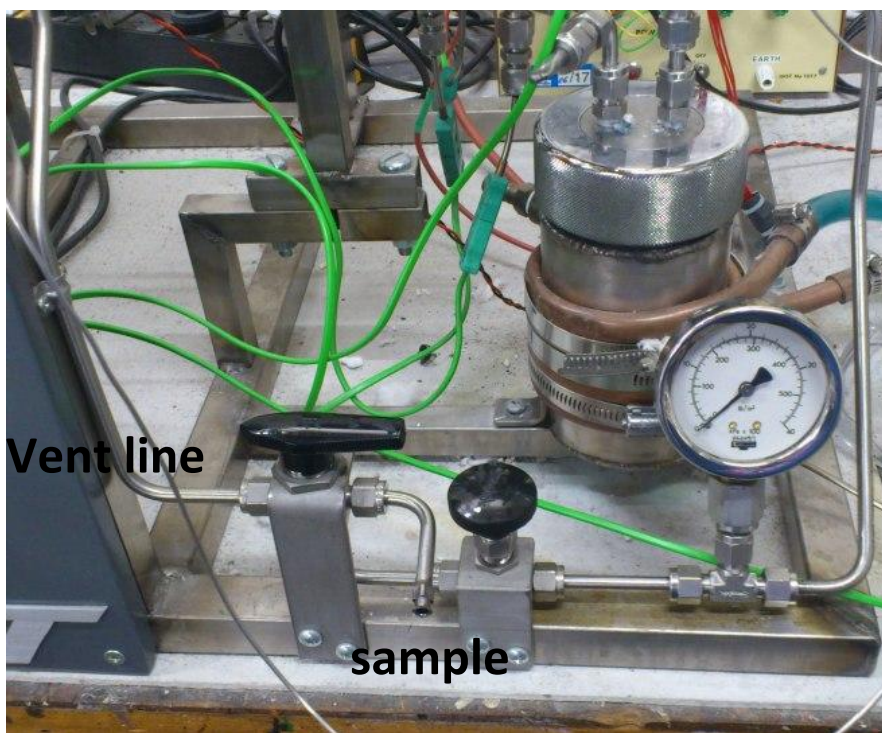


Figure 42: From the collection pot the outlet flows through the manual flow control valve before entering the three way valve where the valve can be turned to obtain a manual sample. Otherwise the line going vertical to the left of the picture is the vent, which has a take-off point for the micro-GC.

The collection system consisted of a stainless steel vessel to contain the pressure, while a smaller glass vial was contained in the vessel to collect the sample as shown in Figure 42 and Figure 43.



Figure 43: The glass vial inside the collection pot. The tube to the left is the inlet directly into the vial, the outlet of the vial is to the larger collection pot

The vessel used was the main section of a bomb calorimeter with a new top machined that was dimensionally similar to the original, but with more suitable porting. Although the vessel is somewhat oversized it was deemed an appropriate choice from a safety point of view as the vessel had a pressure rating that was far in excess of the pressures used in the experiments. The glass vial was immersed in ethylene glycol to provide efficient heat transfer to cooling coils external to the collection pot. The temperature of the collection pot was approximately 5°C while the gas space in the pot was held at 8-10°C.

The rig was constructed using ¼" 316 stainless tube with Swagelok fittings. The system was leak checked under pressure prior to each run for safety and experimental accuracy.

4.2.2. Catalyst addition

A cobalt based catalyst was chosen as the basis for this study. Although the cost is significantly higher than iron the increased activity is seen as critical in supporting the once through process

envisioned in the small scale FT system. Also given the longer lifetime of the cobalt catalyst the amortised cost of the catalyst is assumed to be insignificant.

One of the challenges of microchannel reactors is the ability to appropriately load catalyst into the reactor. There are a number of papers on this subject although much literature involves coating microchannels (or monoliths and other microreactor shapes) outside of the reactor before assembly (Almeida et al., 2011; Pfeifer, et al., 2005; Visconti, et al., 2009). However, research investigating the addition of catalyst post reactor assembly is deemed important as it is very likely full scale units will be permanently sealed to ensure reliability at the high operating pressures required for FT synthesis. This paper therefore investigates several types of catalyst washcoated into a microchannel reactor. This research intentionally keeps the catalyst preparation method relatively simple. While some literature produces high performing catalysts through complex methods (Chin, et al., 2005; Nagineni, et al., 2005) , the aim of this research is to produce simple, cost effective reactor and catalyst systems at a smaller scale. Therefore complex and potentially difficult to repeat (at least at scale) methods, as well as precious metal promoters have been eliminated. The intention is to use this study as a base case to select the most effective catalyst for further washcoating and reactor optimisation that best suits a small scale biomass fed combined heat, power and liquid fuels plant. The most effective catalyst being the one which exhibits the highest activity and best selectivity to diesel range fuels.

Three variations of cobalt catalyst in the microchannel reactor were investigated and the process of washcoating for each is described as follows. The first is an unsupported cobalt washcoat. This was chosen as the simplest form of washcoating to provide a base case for comparison. The second was a cobalt on titania catalyst selected to represent a more typical catalyst supported on a metal oxide. Titania was washcoated followed by cobalt nitrate rather than washcoated together so that the cobalt would have the most active sites exposed to the gas flow through the channel, rather than locked in near the walls. The third method of washcoating was a combustion synthesis form of catalyst. Auto ignition upon heating of the cobalt nitrate/urea mix was intended to quickly form the oxide state and lock in crystal size producing a uniform catalyst with high specific surface area (Atkinson; Ge, Ran, Shao, Zhu, & Liu, 2009). While this method would often have a metal oxide support, the method was trialled without support as a means of comparison to the neat cobalt washcoat.

4.2.2.1. *Neat cobalt*

As a means of creating a simple base catalyst for comparison cobalt nitrate without a support was washcoated into the reactor. Temporary transparent tubing was inserted into the feed and outlet ports of the reactor during assembly. A solution containing equal weights of deionised (DI) water and $\text{Co}(\text{NO}_3)_2 \cdot 6\text{H}_2\text{O}$ was injected into the temporary tubing until there was a level in both the feed and outlet tubing. The syringe was pulsed back and forth while connected to the temporary tubing to ensure any air trapped in the reactor was removed.

The reactor was heated to 80°C for 6 hours using the cartridge heaters which were incorporated in the reactor, before the transparent temporary tubing is removed and the temperature is ramped to 400°C for a period of 5 hours for calcination. It should be noted that the temperature controller is of a basic design that provides full power when the temperature drops below the setpoint, and turns off completely above the setpoint. This results in continual temperature fluctuations of approximately $\pm 3^\circ\text{C}$ around the setpoint. The mass of cobalt in the channels was estimated from the channel volume and concentration of the cobalt nitrate solution to be 16.4mg. This is assuming there was no carry-out of catalyst due to evaporation of the water.

4.2.2.2. *Titania support*

P25 titania (SGE International Ltd) was slurried in DI water to 13% by total mass. The solution was injected into the reactor with temporary tubing as per the other trials. The titania was dried at 80°C . Cobalt nitrate was then washcoated over the dried titania using a 30% by total mass $\text{Co}(\text{NO}_3)_2 \cdot 6\text{H}_2\text{O}$ in DI water solution. This was again dried at 80°C before calcination for several hours at 400°C . Via calculation, the mass of titania in the channels was estimated at 14.4mg and the mass of cobalt at 8.3mg giving a cobalt loading of 37% by total mass.

4.2.2.3. *Combustion synthesis method*

Urea was used as the fuel in the combustion synthesis method. The quantity of urea required was calculated based on balancing valencies using methods from propellant chemistry (Castro, et al., 1997; Ganesh, et al., 2005). A 2 times mol excess of urea was added to an equal weight DI water and $\text{Co}(\text{NO}_3)_2 \cdot 6\text{H}_2\text{O}$ solution. The solution was washcoated into the reactor by the method described previously. The solution was dried at 80°C for 6 hours before heating to 500°C for auto ignition (temperature ramp and hold time 1.5 hours total), then the temperature was reduced to 400°C for 3.5 hours.

4.2.3. Fixed bed reactor

As a means of comparing the performance of the microchannel reactor with traditional technology a small fixed bed reactor (channel dimensions 4mm by 6mm by 30mm) was fabricated from 316 stainless steel (Figure 44). The fixed bed reactor plate was designed to bolt into the top and bottom reactor plates using aluminium foil gaskets as used in the microchannel reactor. This was done in order to replicate the conditions as closely as possible so that the only variables for comparison were the channel dimensions and form of the catalyst. The catalyst was held in the channel by ceramic wool (Kaowool) packing at either end. Approximately 0.4 g of catalyst was packed in the reactor. It should be noted that in each case the catalyst was crushed to a point where it was assumed intraparticle mass transfer limitations would be minimal.

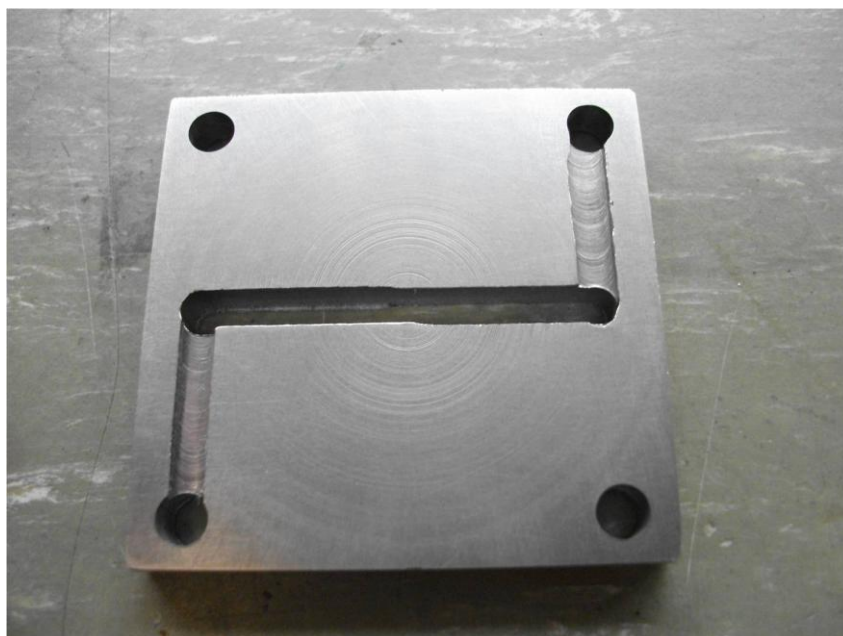


Figure 44: Fixed bed reactor plate. Photo shows the inlet and outlet ducts to the horizontal reactor space

4.2.4. Catalyst production for the fixed bed reactor

4.2.4.1. Precipitation

A method for producing a supported cobalt catalyst was obtained from Kraum and Baerns (1999) that utilised a precipitation method. This method was followed in preparing a catalyst for comparison as is described below.

- $\text{Co}(\text{NO}_3)_2$ is dissolved (0.33 mol/ml) by stirring in deionised water containing titania (1.1 mmol/ml) at 60°C
- then a saturated NaHCO_3 (1mmol/ml) solution was added to the slurry.

- The pH value was adjusted to 8 by adding aqueous HNO₃ drop-wise.
- After 2 hr of stirring the solid catalyst precursor containing hydroxide precipitated on titania was separated by filtration from the solution,
- The precursor was washed five times with water (each time 3 ml H₂O per gram of catalyst) and then dried in air at 130°C for 12h.
- The catalyst was then crushed and calcined at 400°C in air for 6 hours

4.2.4.2. *Impregnation and freeze drying*

A simple catalyst using a 12% cobalt loading on titania (P25 SGE international Ltd) prepared by impregnation and freeze drying was used in the reactor. This is a development of a typical impregnation method for catalyst preparation. The basic method is described as follows

- Co(NO₃)₂ is dissolved (0.33 mol/ml) by stirring in deionised water containing titania (1.1 mmol/ml) at 60°C
- The precursor was agitated in an ultrasonic bath for 20 minutes
- Immediately after removal from the bath the vessel with the precursor was immersed in liquid nitrogen
- The catalyst was freeze dried overnight
- After drying the catalyst was crushed and calcined at 400°C in air for 6 hours

4.2.4.3. *Alumina supported catalyst*

An alumina supported catalyst was also prepared for comparative analysis, particularly for TPR, to gauge whether the given TPR profiles compared with literature with differing supports. The catalyst was made using a typical precipitation method the same as the titania supported catalyst described above with a 20% cobalt on alumina loading.

The reduction step for all the catalysts was performed in the same manner. Hydrogen was passed over the catalyst at 400 kPa with the reactor ramped to 400°C for 2 hours. While this reduction time appears short previous experimentation discovered a longer reduction time severely reduced catalyst activity.

4.2.5. *Analysis methods*

4.2.5.1. *Analysis of gaseous products*

Gas products (CO, H₂, N₂, CO₂, CH₄, C₂H₄, C₂H₆) were analysed during the run at 30 minute intervals using an Agilent 3000A micro GC. There are two columns in the microGC, a molecular sieve and a

Plot Q (DVB column that separates targeted apolar and polar compounds). H₂, CH₄, CO and N₂ are separated and analysed by the first column, while CO₂, C₂H₄ and C₂H₆ are resolved in the second column. The microGC utilises TCD detection. Calibration of the microGC was performed using a gas mixing rig that enabled dilution of the above components to concentrations that spanned the expected readings during operation. This gives confidence in the accuracy of the data.

Analysis of gaseous products enables calculation of conversion based around gas flows and concentrations in and out of the system, along with the N₂ tracer. The following show the calculation method for characterising the flows of individual components and a check on experimental accuracy.

Flow of components in and out of the system can be calculated using Equations 8 and 9

$$Fin_i = xin_i Fin_{tot} \quad (8)$$

$$Fout_i = xout_i Fout_{tot} \quad (9)$$

The flow out of the reactor is calculated using the N₂ balance as shown in Equation 10 because there isn't online measurement out

$$Fout_{tot} = Fin_{tot} \frac{xin_{N_2}}{xout_{N_2}} \quad (10)$$

The accuracy of the flow out calculated in Equation 10 is estimated based on the error between the flow in and the flow out of N₂ based on a measured flow out (using a syringe and stopwatch test every few hours) rather than calculated and is shown in Equation 11

$$N_2 \text{error} \% = \frac{Fin_{N_2} - Fout_{meas_{N_2}}}{Fin_{N_2}} 100 \quad (11)$$

Where the flow out of N₂ is calculated by Equation 12

$$Fout_{meas_{N_2}} = F_{out_{tot_{meas}}} xout_{N_2} \quad (12)$$

Once the flows of all the components in and out have been calculated conversions and relations between components can easily be quantified.

4.2.5.2. Analysis of liquid products

Liquid samples (C₈ to C₃₀₊ hydrocarbons) were analysed post run in a Varian CP 3800 GC using a Varian Factor Four capillary column (30m x 0.25mm ID). Hexane was used as the solvent to dissolve the waxes as well as providing a means of dilution of the products to a suitable level for the GC to give acceptable peak resolution. Typically 2-3mL of hexane was used to dissolve the products in the collection vial, with 20-40µL sampled and added to a GC vial with 1.5mL of hexane. The excess of hexane masked the FT products in the C₆-C₈ range, however, there were enough products post this range to establish suitable ASF distributions.

The method used on the GC is as follows

Injector temperature 300°C

Detector type FID
Split ratio Splitless injection, split ratio 5 after 2 minutes
Injection volume 1.0 μ L

Oven temperature ramping parameters are shown in Table 11

Table 11: GC oven temperature parameters

Temp	Rate	Hold	Total
$^{\circ}$ C	$^{\circ}$ C/min	min	min
35	0	5	5
180	15	0	15
280	30	12	30

4.2.5.3. Calibration of GC

The GC was calibrated for analysing the hydrocarbons from the FT synthesis by using an aliphatic hydrocarbon standard from Restek (cat. Number 31459). The standard contained a range of 14 aliphatic hydrocarbons from C₉ to C₃₆ at a concentration of 1,000 μ g/mL per compound in hexane. This standard was further diluted to a range of concentrations and used to gain calibration curves for each component. Note that although the FT process does produce some olefins with the majority as paraffin, the paraffin standard has been used and the products are considered as clumped for each carbon number. This is based on the assumption that the products will be used for fuel, and therefore an overall mass distribution of products within fuel ranges is of most importance. Thus the difficult challenge of separate analysis of olefins and paraffins is considered unnecessary.

4.2.5.4. Catalyst analysis methods for powdered catalysts

The benefit of the powdered catalyst in the fixed bed reactor compared to that washcoated into the microchannel reactor is the ability to perform ex-situ analysis. This allowed the powdered catalyst to undergo typical catalyst analysis techniques, at which point the catalyst could be compared on line for FT productivity to that of the washcoated catalyst therefore vicariously giving some comparability.

4.2.6. TPR method

For the powdered catalyst a temperature programmed reduction (TPR) rig was constructed using available equipment. Due to the high cost and lack of availability of TPR equipment it was decided an attempt at constructing a TPR rig in house was worthwhile. The schematic of the TPR rig is shown in Figure 45 with the actual equipment shown in Figure 46. Note that the tube runs were all flexible PVC with Teflon tubing connecting at either end of a 6mm quartz tube that ran through the oven with the catalyst placed in the middle.

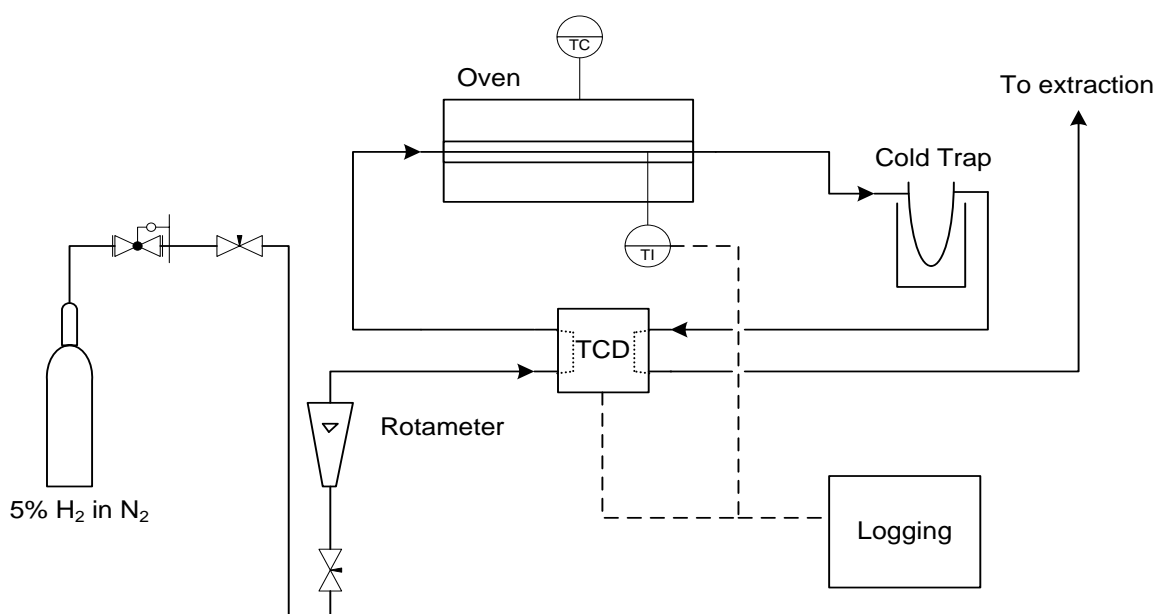


Figure 45: Schematic of TPR rig arrangement



Figure 46: Physical arrangement of TPR system

Approximately 100mg of catalyst was loaded into the quartz tube and contained with Kaowool at each end. Much care had to be taken not to compact the catalyst as this prevented flow. The ramp rate was set at 10°C per minute up to a temperature of 800°C. 5% hydrogen in Nitrogen was used at a flowrate of approximately 30cc/min. The thermal conductivity detector (TCD) signal was logged and the temperature recorded over the course of the experiment which allowed plotting of the TPR profiles vs time and temperature.

4.2.7.XRD diffraction

XRD analysis was also performed on the titania based catalysts (both the precipitation and freeze dried catalysts). There were two reasons for performing the XRD analysis. The first was to compare the reported composition to that of the calculated composition from catalyst preparation. The second was to estimate the cobalt crystal size using the Scherrer equation.

The XRD diffraction patterns are shown in Appendix D. The composition generated in the analysis showed both anatase and rutile titania which was to be expected, however, the 5% cobalt manganese oxide is obviously incorrect as there is no manganese present. Therefore the XRD analysis (at least on this particular equipment) was not suitable for quantification.

The Scherrer equation is a method used to estimate the crystal size of a component based on the peak width in the XRD diffraction pattern and is shown in Equation 13.

$$\beta(2\theta) = \frac{K\lambda}{L\cos\theta} \quad (13)$$

Where

β is the full width half maximum (FWHM) of the peak (rad)

K is the constant of proportionality (typically 0.94)

L is the crystal diameter (nm)

θ is the Bragg angle

XRD diffraction pattern analysis gave an estimated cobalt crystal size of 13 nm for the freeze dried cobalt on titania catalyst. Even though the elemental analysis proved incorrect it is assumed the particle size analysis is correct given it is calculated directly from the diffraction pattern.

As discussed in the literature review there has been research focussing on the effect of particle size on the kinetics (J. P. Den Breejen, et al., 2009; Ma, et al., 2011). Between both papers cobalt cluster size effects were examined in the range of 2.6-40nm. From the combined research it is shown that decreasing cluster size leads to an increase of reaction rate per unit of catalyst until lower than 6nm at which point the turn over frequency (TOF) decreases and methane selectivity increases. For this research a value of 13nm is therefore considered to be in an appropriate range, i.e. small enough to take advantage of the higher reaction rate but well outside of the range of decreasing activity due to smaller particle size.

4.2.8. Rig safety

One of the most important aspects of the experimentation was the safety element, particularly with the use of carbon monoxide. Due to a limitation of detection and active safety devices in the initial stages, experiments were limited to within a single day so as not to leave the equipment unattended for significant lengths of time. Due to the need for longer runs to gauge catalyst activity over time the safety concerns were addressed in the following ways.

- A permanent CO sensor was installed that provided a 4-20mA output. This output gave provision for a display of CO concentration as well as an alarm limit to perform active safety functions
- A control unit would shut off power to a fail closed solenoid valve on the syngas bottle outlet as well as shutting off power to the reactor heating system. This shutoff procedure would occur if the alarm limit was reached on the CO sensor or there was a loss of flow in the extraction (monitored by a flow switch). If the control unit was tripped either by the

above sensors, or a power loss, it would require a manual reset to return power to the valve and heating

- Two portable CO sensors with a concentration readout and audible alarm are available in the lab to be worn if working around the rig, or hung in front of the webcam.
- A webcam was installed that logs a picture of the rig every 30 seconds. This can be accessed anywhere with an internet connection and shows CO concentration in the lab, flow, temperature and pressure as well as a light to show if the hardwired CO sensor is alarming. An example of the webcam picture is shown in Figure 47



Figure 47: Example image provided by webcam every 30 seconds

5. Microchannel Experimentation Results and Discussion

This section has been broken into sub-parts recognising the staged approach that was taken with the experiments. The first stage is the analysis of the powdered catalysts before investigating the Fischer-Tropsch synthesis. The second is a series of shorter Fischer-Tropsch synthesis runs comparing various washcoats and the fixed bed over a range of temperatures. The third section incorporates online performance analysis of pressure and temperature based variables over a neat cobalt nitrate and a cobalt on titania washcoat with significantly longer run times. These latter runs were performed based on conclusions from the shorter runs and are therefore considered in a separate discussion.

5.1. Ex-situ Analysis

5.1.1. TPR

Figure 48 shows TPR profiles for the main titania catalyst used, as well as an alumina catalyst prepared for comparison. TPR in this case is most useful when multiple catalysts are compared with the same equipment (given it is a custom apparatus). It allows comparison of the reducibility of the catalyst as well as showing the stages of reduction through the oxides until cobalt metal is obtained. The TPR response for the cobalt catalyst supported on titania with two main absorption peaks (approximately 375°C and 560°C) could be considered typical (Jones & McNicol, 1986). The alumina catalyst showed significantly less reducibility particularly in the higher temperature range where the lower oxides such as CoO were reduced to cobalt metal. This is a typical response for a cobalt on alumina catalyst where the metal-support interactions are considered stronger than that of titania leading to greater difficulty in reduction (Jones & McNicol, 1986). TPR was also performed on the Kaowool packing blank to ensure there was no interaction from the packing. Often promoters are included to assist in the reducibility of a catalyst. In the interests of maintaining a simple approach to catalyst production these promoters have been intentionally excluded. Therefore, the best catalyst for the application, inferred from these results, would be the most reducible one which is the cobalt on titania catalyst prepared by freeze drying.

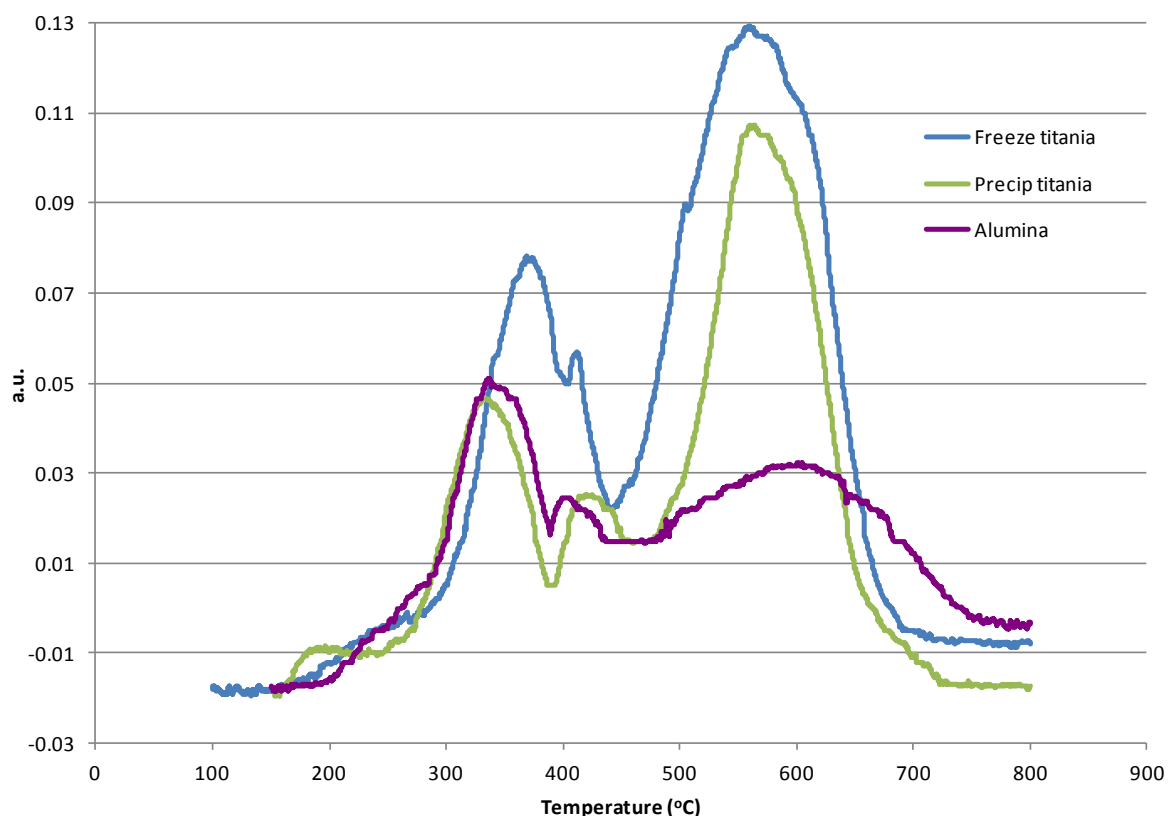


Figure 48: TPR profiles for freeze dried titania, precipitated titania and alumina based cobalt FT catalysts

5.2. Ease and Repeatability of Washcoating

Because of the intended use of the washcoats in a simple Fischer-Tropsch system it seems prudent to comment on the ease of catalyst incorporation in the reactor. It should be noted the injection process was chosen as one that could be replicated in a larger scale than the lab scale in use. This is because the coating can be incorporated in a completely assembled reactor. The neat cobalt nitrate and combustion synthesis methods were the simplest to washcoat due to the one step nature of the injection process. Also, as the washcoat precursor is a solution rather than a suspension there were no difficulties with settling while trying to inject the precursor. The combustion synthesised method may be limited in repeatability due to the rapid evolution of gases upon ignition carrying catalyst out of the channels. Visual comparison of the reactor plates upon disassembly would tend to support this hypothesis.

The effectiveness of the slurry injection and drying phases was investigated with the use of a reactor constructed with glass top and bottom plates. This allowed visual observation of the injection and drying processes within the channels. Interestingly, on injection, the flow of slurry between channels was very similar which indicated that the reactor doesn't have a preferential flow path

which would effectively reduce residence time. It also demonstrated that with a few cycles of the injection syringe it was possible to remove any air pockets in the channels ensuring an even distribution ready for drying. A concern was the possibility that during the drying step, water exiting the reactor would cause the support to coat heavier at either end of the channels, while depositing very little support in the middle of the reactor. However, observation of the transparent reactor has shown this not to be a significant problem attributed to the fact that the temperature used for drying was 80-85°C. Keeping the water below boiling temperature better manages the driving force of the vapour leaving the reactor carrying catalyst material with it.

5.3. SEM Analysis

SEM analysis was performed on the washcoatings to gain a visual understanding of the deposition and structure of the catalyst within the reactor. The reactors were prepared using the washcoating methods previously described but not run online with syngas so as not to create any hydrocarbons that could adversely affect the SEM. The cobalt on titania washcoated catalyst had to be carbon coated for the SEM analysis due to the non-conductive nature of the titania. The reactors were disassembled after reduction. Because of the temperature and clamping force of the reactor the gaskets bonded to the shims in places, therefore separation was not completely clean. This explains the partially broken and cracked catalyst layer in the images. Energy dispersive spectrometry (EDS) was used to identify the elemental composition of the washcoats to demonstrate the various morphologies presented were in fact composed of cobalt.

Figure 49 shows a lower magnification view of one of the gasket surfaces of the microreactor. Note that this is after separation of the reactor shim. This is therefore representative of one of the two sides of each channel which have deposition on the aluminium foil gasket. Even from the low magnification of Figure 49 one can see there appears to be heavier deposition and different structure towards the edges of the channel of the neat cobalt washcoat. This is shown more clearly in Figure 50 when focussing on an individual channel. Figure 51 shows the centre of one such channel. It can be seen there is a very consistent fibril structure of length in the order of 300nm and width estimated at 15nm. One would expect this to be quite a high surface area arrangement. Figure 52 and Figure 53 show the transition from the centre of the channel to the edge where the structure changes significantly. Higher magnification of the structure in Figure 54 shows the jagged mountainous form with openings ranging from approximately 1µm and smaller. This method of deposition shows a similar appearance to that produced by electrosynthesized cobalt coatings (Dinamani & Kamath, 2000) which is unusual given this is a thermal decomposition deposition method. It is acknowledged this is very un-intuitive and further development or experimentation in

the area of cobalt deposition in the microchannels could be a valuable area of investigation in regards to identifying this unusual behaviour. This deposition structure is, however, a positive result as one could assume both these methods of deposition seen in the micro reactor would exhibit relatively high surface area albeit for different reasons – one for the aspect ratio of the fibrils (Figure 51), the other for the porous nature (Figure 54).

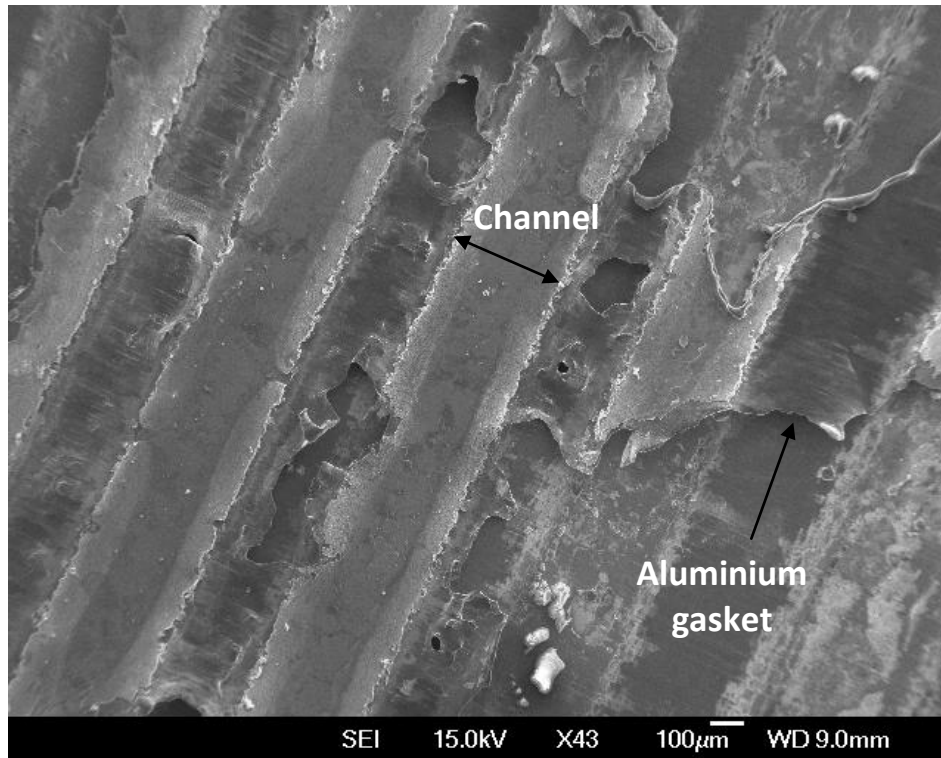


Figure 49: SEM micrograph showing the gasket material with a straight cobalt washcoat. Note the damaged layer is due to separating the reactor post run

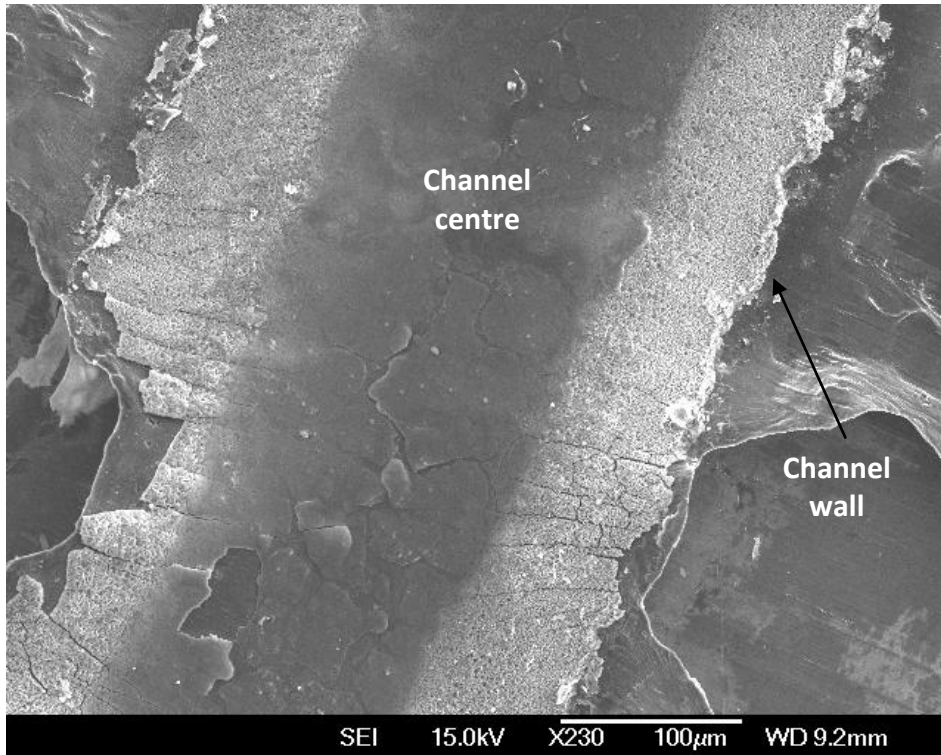


Figure 50: View of an individual channel of the straight cobalt washcoat showing the different formations on the wall to the centre of the channel

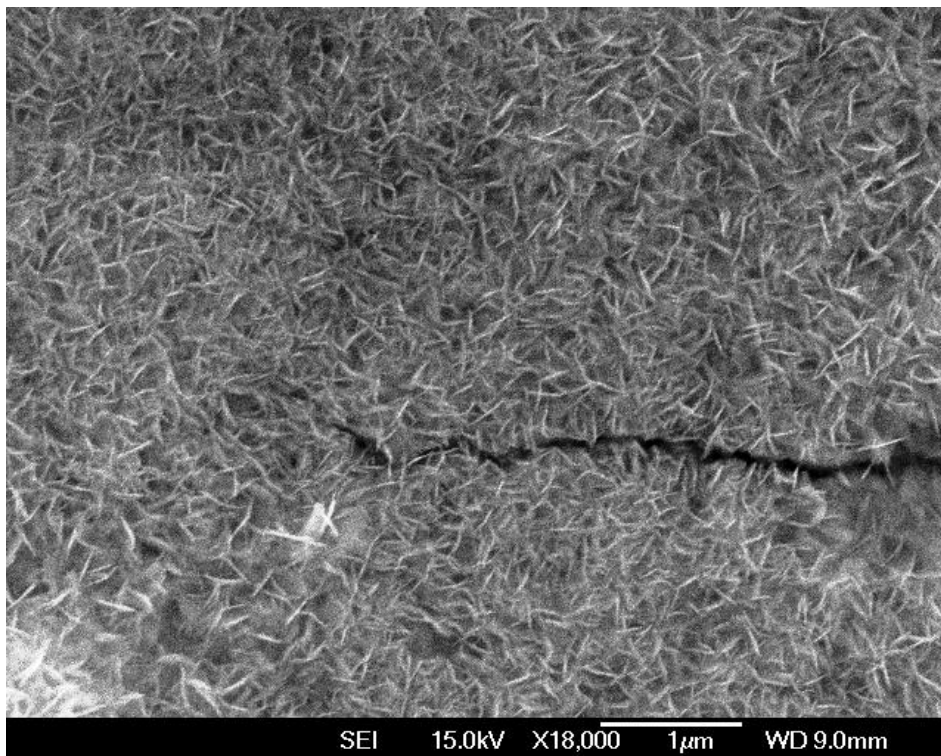


Figure 51: Close up of the centre channel of the straight cobalt washcoat

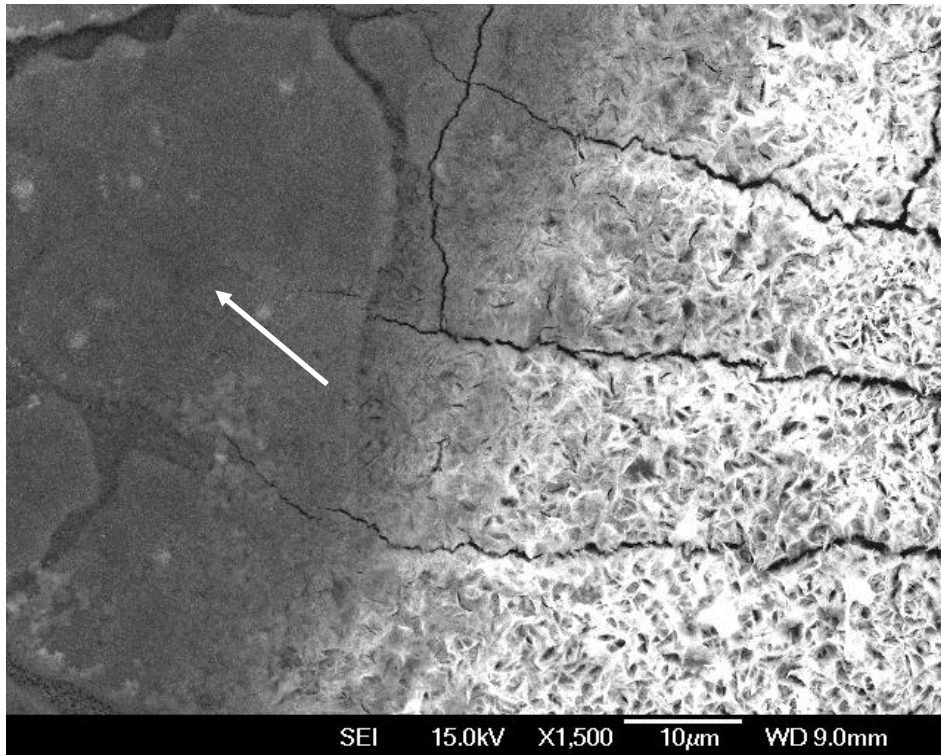


Figure 52: SEM micrograph showing the boundary between the centre and outside edges of the channel for the straight cobalt washcoat. Note the microfibril structures can just be seen in the left side of the image

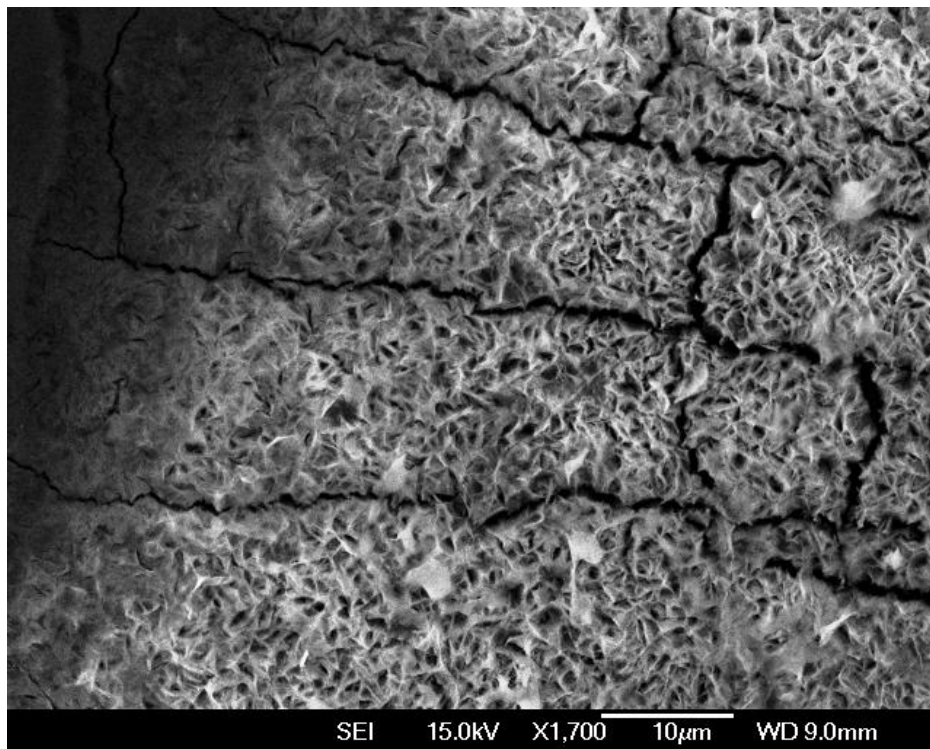


Figure 53: Closer view of the structure of the cobalt washcoat near the edges of the channel

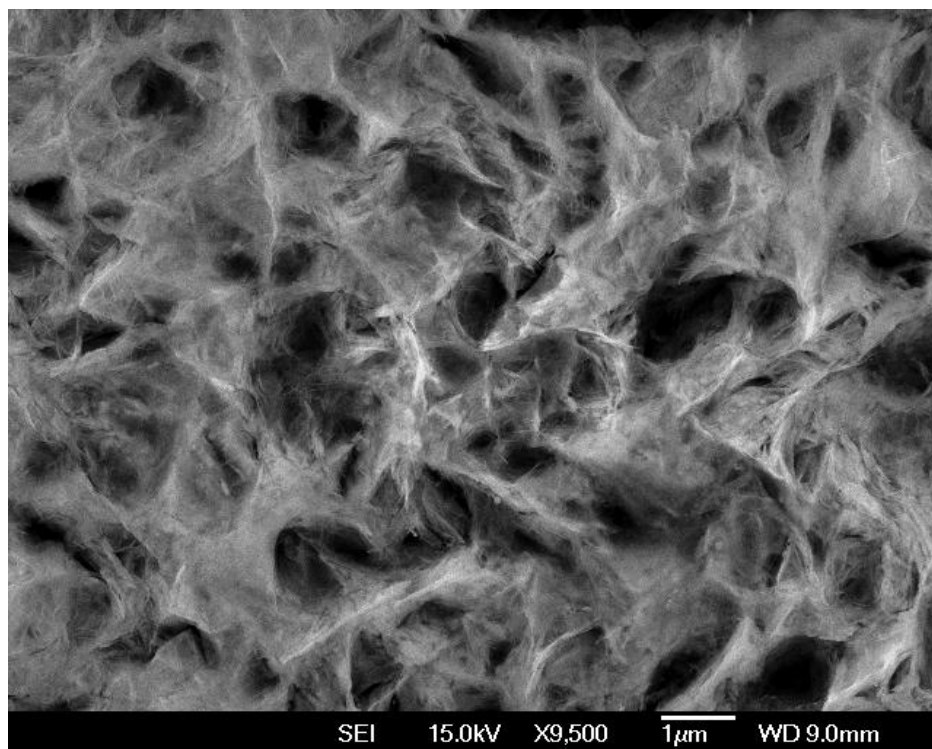


Figure 54: Further magnification of the straight cobalt washcoat near the channel edges showing the high surface area structure

5.3.1. Cobalt on titania washcoat

The cobalt on titania washcoat showed some structural similarities to that of the neat cobalt washcoat but also some significant differences. Figure 55 and Figure 56 show an increasing magnification of the centre of the channel. Some of the fibril nature in the straight cobalt washcoat can be seen but there appears to be more depth and spacing around what one would presume are titania particles. The jagged structure of Figure 54 was not noted in the cobalt on titania washcoat. The way the reactor separated in this test allowed a view of the bottom (foil gasket surface) and side (stainless wire cut shim surface). Figure 57 and Figure 58 show this wall surface. It is very different to any other structure seen. There is an abundance of spherical particles under 20nm with little sign of the fibrils seen in other images. One would expect from visual comparison of the two washcoats that the cobalt on titania catalyst should exhibit a higher surface area than the neat cobalt washcoat, although they both appear high.

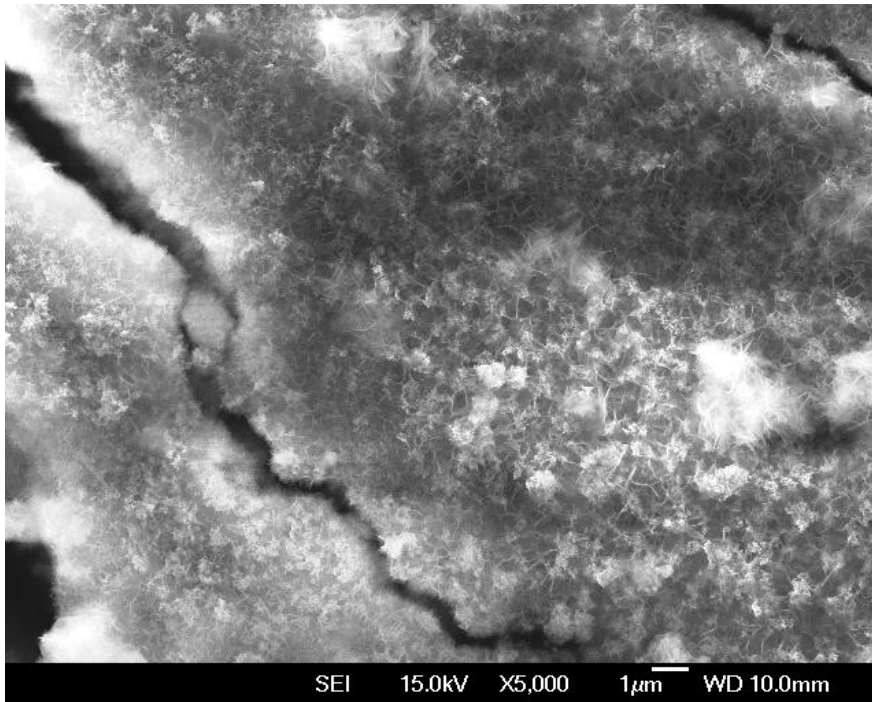


Figure 55: SEM micrograph of cobalt on titania washcoat

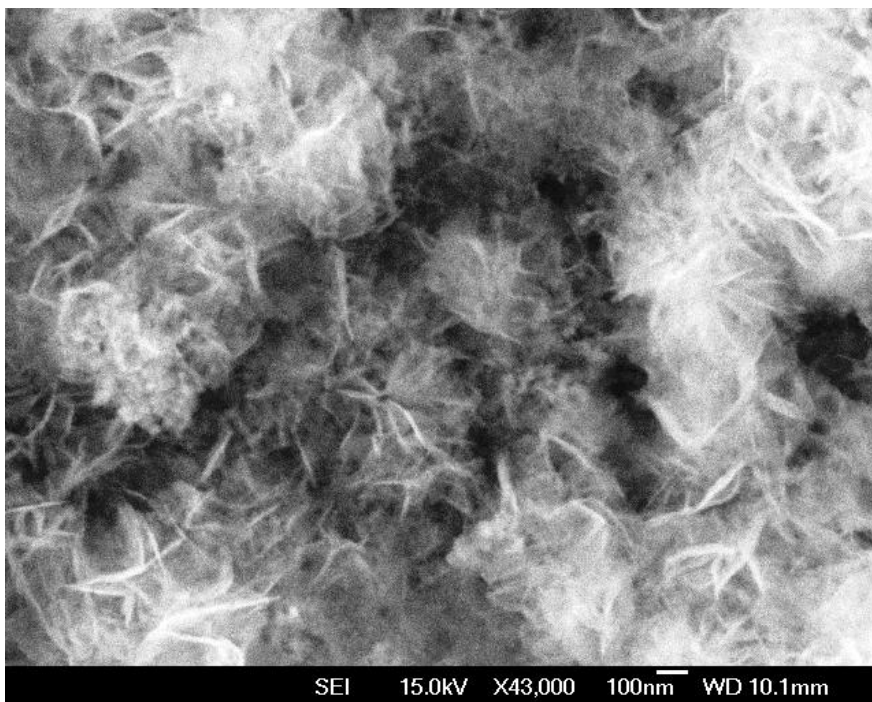


Figure 56: Closer view of cobalt on titania washcoat showing the differing structure to that of the straight cobalt washcoat

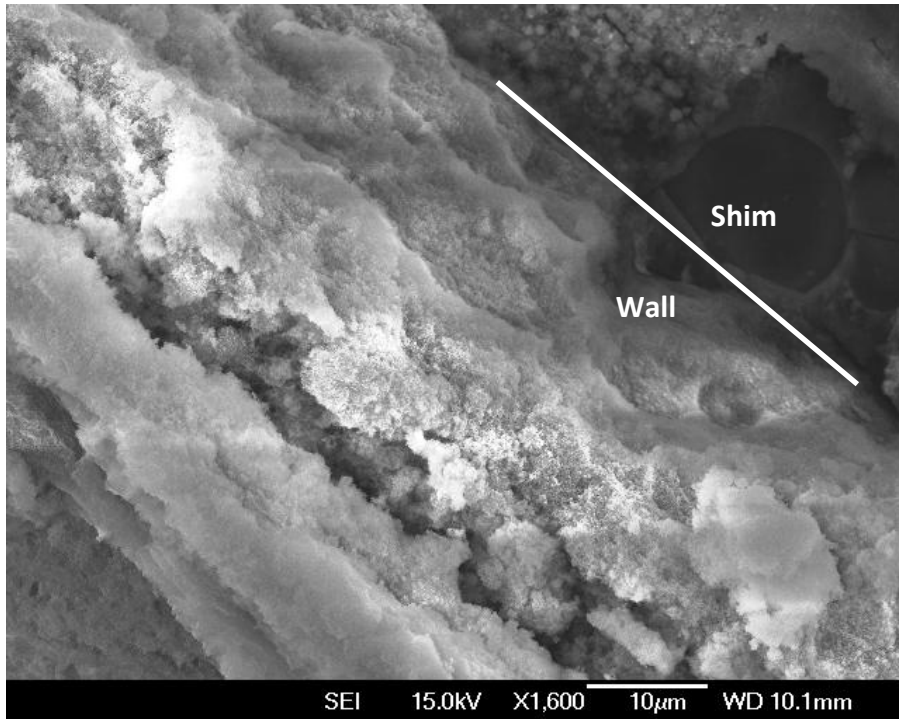


Figure 57: This image was of a channel with the stainless steel shim still in place with the focus being on the cobalt on titania washcoat on the vertical wall

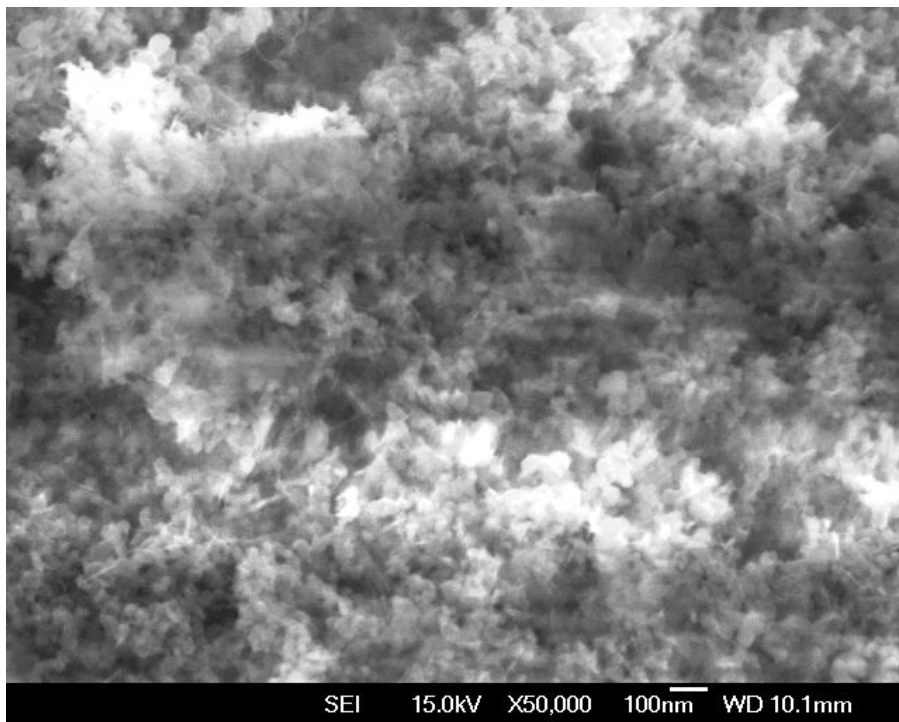


Figure 58: Higher magnification of the wall structure of the cobalt on titania washcoat showing a significantly different structure to that of the straight cobalt washcoat on the gasket surfaces

5.3.2. Combustion synthesis washcoat

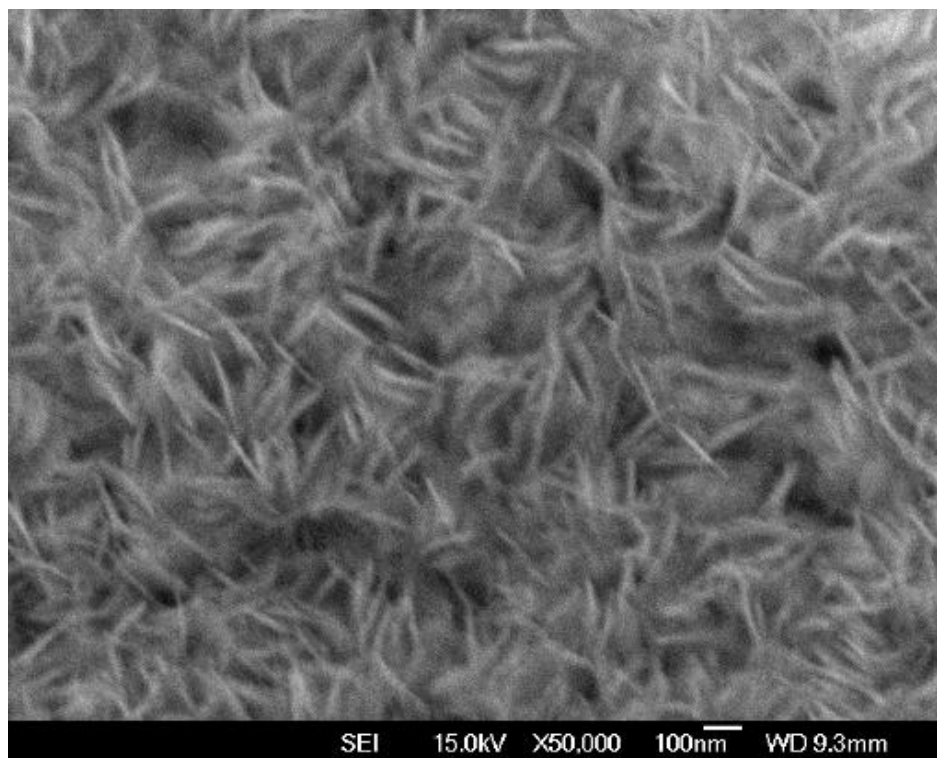


Figure 59: SEM micrograph of the channel centre in the combustion synthesis washcoat showing identical structure to the straight cobalt washcoat

Interestingly, the combustion synthesis catalyst (Figure 59) showed a similar microfibril arrangement to the unsupported cobalt washcoat (Figure 51). However, the fibrils may be slightly finer in the combustion synthesis method, although not by any order of magnitude. There appeared to be little difference in the resultant structure between the combustion synthesis and the neat cobalt washcoat. This suggests the expected advantages of the combustion synthesis were not realised and the additional complication of the method is potentially unwarranted compared to the simpler neat cobalt washcoat.

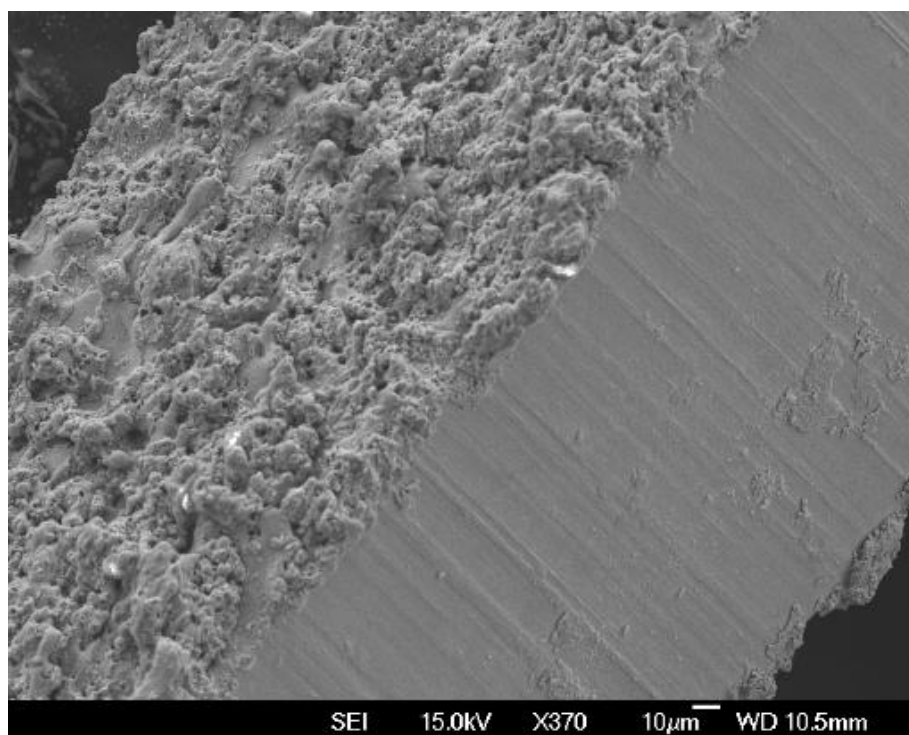


Figure 60: Image of a wire separator between the channels. The rough surface to the left is the wire cut surface, while the surface to the right is the polished mill finish of the stainless steel shim

Further support of the method chosen for microchannel manufacture is shown in Figure 60. This shows the surface of the stainless steel both from the mill on the right, and the wire cut surface on the left. It shows the wire cut surface to be a very rough surface. This theoretically will improve surface area and the adherence of the washcoat.

An unfortunate limitation of the SEM analysis is the inability to confidently use post reaction samples due to hydrocarbon buildup as mentioned previously. This would have allowed a greater understanding of the reasons for deactivation by looking for sintering/crystallite size change or any other changes in the physical properties of the catalyst surface. Future work could investigate the ability of multiple solvent washes to remove residual hydrocarbons to allow post run analysis.

5.4. Online Performance

5.4.1. Short time frame catalyst comparisons

Short time frame catalyst comparison runs were performed for the various washcoats for Fischer-Tropsch synthesis over three temperatures (210°C, 225°C, 240°C) at a pressure of 20 bar. Four runs were conducted for each catalyst in the order of 240°C, 225°C, 210°C, 240°C. The repeat of the

240°C run allowed a comparison of performance between the first and last run after more time on stream and reduction steps which took place before each run.

The performance of the microchannel reactor in terms of conversion compared to the fixed bed reactor is of significant interest. While conversion is often reported as a percentage it was deemed more appropriate to compare conversion per hour in relation to the mass of catalyst in the reactor for two main reasons. 1) Gas Hourly Space Velocity (GHSV) was noted to have little influence on conversion per unit mass of catalyst within the range of flows the equipment would allow and 2) GHSV was adjusted to allow better measurement. i.e. for a catalyst with low conversion the GHSV was reduced to provide a higher fractional conversion allowing more accurate determination of conversion via measurement on the micro GC. GHSV was in the range of 8000-19000 hr⁻¹ for the microchannel reactors and 1200-2500hr⁻¹ for the fixed bed reactor, while CO conversion was in the 5% - 35% range. Note the GHSV was calculated based on the channel volume rather than catalyst volume. Also of note was that no noticeable pressure drop was seen in the microchannel reactor at any of the space velocities tested.

A challenge to reporting conversion in terms of unit mass of catalyst is the ability to accurately measure the mass of catalyst in the microchannels. Due to the large mass of the microchannel reactor as a complete unit an accurate before and after loading mass measurement is not possible. Therefore, the mass in the reactor is calculated as the product of the solution concentration and reactor volume. This method relies on the assumption that the channels are full, and upon drying, the catalyst precursor solution dries and deposits without either concentrating in the channels or evacuating from the channels. The system was run for at least 5 hours to reach steady state before calculating conversion.

Conversion in terms of gram of C₂₊ product per gram of catalyst per hour is shown in Table 12 and was calculated based on CO consumption and stoichiometry. The microchannel reactor in all cases is operating with significantly higher activity (up to 40 times) than a more traditional fixed bed arrangement and this substantial difference is shown visually in Figure 61. Literature survey yields comparable results. Cao (2009) reports productivities up to 1.7 g C₂₊/g catalyst/hr at 224 °C and 25 bar. This was based on a powdered Co/Re catalyst supported on alumina packed in the microchannels. Our research at 225°C and 20 bar yields a maximum productivity for the neat cobalt washcoat of 2.2 gC₂₊/g catalyst/hr. Myrstad (2009) investigated a slightly different type of micro reactor incorporating pillar structured catalyst foils, however, like Cao (2009) the catalyst was

packed into the reactor and was Co promoted with Re on an alumina support. At 240°C the $\text{gC}_{5+}/\text{g catalyst/hr}$ productivity was 2.6, while at 225°C productivity was 1.7 $\text{gC}_{5+}/\text{g catalyst/hr}$. Our research compares with 5.7 and 1.6 $\text{gC}_{5+}/\text{g}_{\text{catalyst}}/\text{hr}$ respectively with the neat cobalt washcoat. Given the lack of precious metal promotion used in this research, the productivity per unit catalyst results are shown to be encouraging.

Catalyst activity was very dependent on temperature and activity followed a logarithmic trend in relation to temperature, as is expected with typical reaction kinetics. Temperature, however, appeared to have a more dramatic affect on productivity compared to that reported in the research by Myrstad (2009).

Table 12: Product conversion (gC_{2+} product/g catalyst/hr) over temperature range for various washcoats established in this experimental research

	240°C	225°C	210°C	240°C
Cobalt	7.4	2.2	1.4	3.6
Cobalt on titania	2	0.8	0.54	1.3
Combustion synthesis	2.5	0.61	0.67	1.8
Fixed bed	0.19	0.067	0.04	0.12

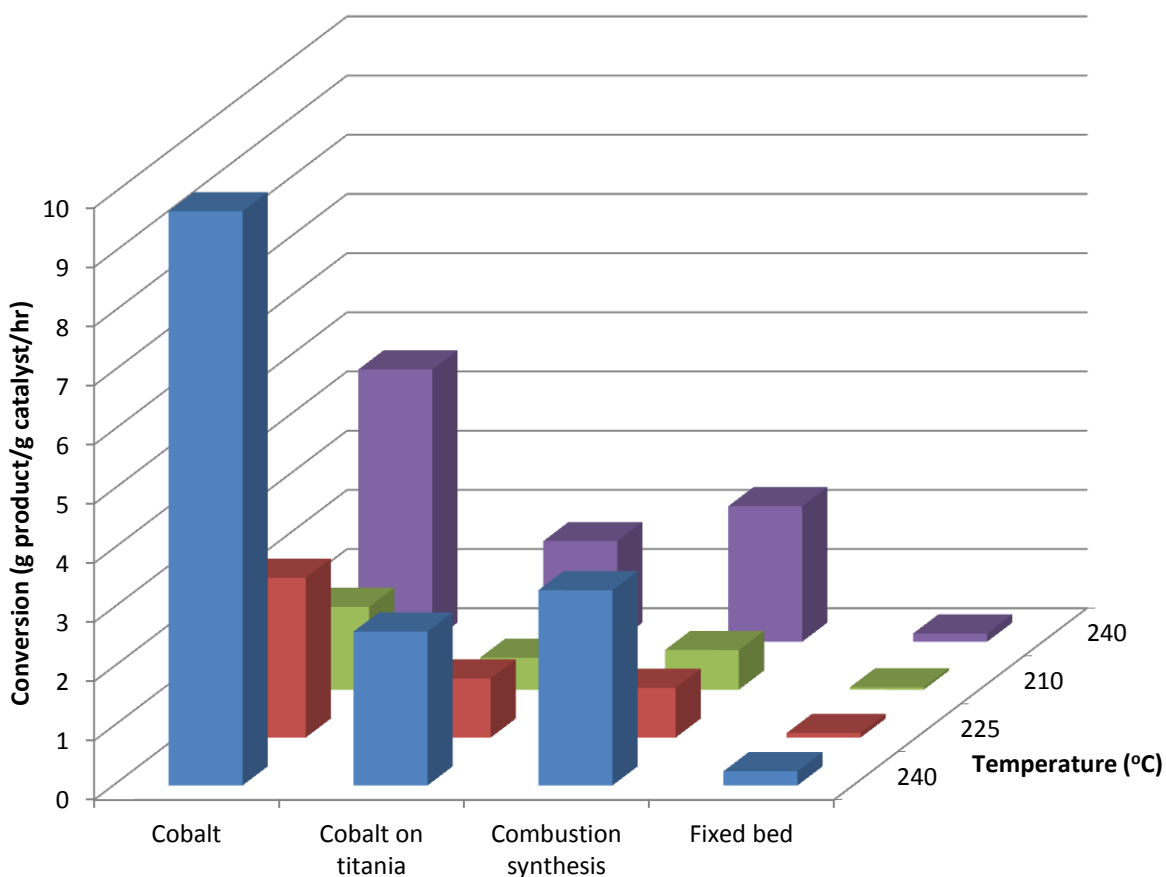


Figure 61: Visual comparison of relative catalyst activities

Comparison of the various microchannel washcoats showed the simplest method of neat cobalt nitrate to be the highest performing coating in terms of conversion per unit of catalyst. It was hypothesised that the titania supported method would yield the highest performing catalyst due to the expected extra surface area. Even on comparison of conversion per actual Co loading (rather than total catalyst mass) the neat Co still outperformed the titania supported catalyst. From comparison of SEM results one possible conclusion is that the microfibril and jagged mountain geometry generated in the neat cobalt washcoat provided sufficient surface area to be comparable or better than that provided by the titania supported catalyst. If different loading concentrations were investigated it would be interesting to note if there is a changeover point at which the titania supported method would outperform the neat cobalt. With the high loading the neat cobalt is providing its own high surface area support. At lower loadings this may not have such an effect and cobalt spread over the high surface area titania may be more advantageous. However, while it has been termed 'high loading' there is still very high activity per unit catalyst requiring little catalyst for conversion compared to traditional technology. Therefore, it is seen as being no advantage to try and significantly reduce the catalyst in the channels. Rather, it is considered beneficial to maximise

as much as possible the active sites within the microchannels, even at the expense of catalyst utilisation efficiency. On this premise, if pure cobalt is its own best high surface area support, then this should be pursued. One question of the unsupported washcoats will be their resistance to deactivation over significant run periods, which is addressed later in this thesis.

Results were fitted to an Anderson-Shultz-Flory (ASF) distribution to determine the selectivity (α). The most accurate fit was possible in the C_8 to C_{22} range particularly in the 240°C runs where higher activity resulted in a greater quantity of sample. This is within the fuels range so the most accurate analysis is within the range of interest. With the higher weight hydrocarbons there is a drop off from the expected mass fraction which is attributed to product drop out in the collection pot feed, however, this does not affect identification of a suitable product distribution.

An approximation for α in relation to temperature from Song (2003) yields 0.77 for 240°C, 0.81 for 225°C and 0.85 for 210°C. Selectivity varied significantly from these predictions as can be seen in Table 13. Selectivity in most cases trended opposite to typical FT prediction in relation to temperature. Some of this may be attributed to error, especially at the lower temperatures where less activity resulted in less product. It is likely there would be some buildup of heavy product throughout the apparatus skewing the distribution particularly when there is very little product produced. However, due to the accuracy at which the 240°C runs fit the ASF distribution one can assume an accurate value. This is an encouraging result as the α value in the mid 0.8's is much higher than predicted at that temperature and is an appropriate range for high fuel production, while operating at a higher temperature and therefore increased catalytic activity. Comparing results to Cao (2009) who achieved an average α of 0.87 at 225°C this research is shown to be in a similar range. Methane selectivity as seen in Table 13 could be considered on the high side, particularly at the higher temperature of 240°C, however, it was very consistent over all the different washcoats in the microchannel reactor. Surprisingly the fixed bed reactor exhibited the lowest methane production. Note the %CO converted to methane is not shown at 210°C due to low activity at this temperature not producing enough methane to register on the microGC.

Table 13: Values of α and % of converted CO converted to methane over temperature range

	240°C		225°C		210°C		240°C	
	α	%CO to CH ₄	α	%CO to CH ₄	α	%CO to CH ₄	α	%CO to CH ₄
Cobalt	0.83	21	0.74	16	0.72	n/a	0.83	20
Cobalt on titania	0.82	21	0.73	15	0.64	n/a	0.77	22
Combustion synthesis	0.89	21	0.84	16	0.87	n/a	0.71	17
Fixed bed	0.87	17	0.85	10	0.84	n/a	0.89	15

Table 14: Product distribution (mass %) for various catalysts over temperature range calculated from α

	240°C		225°C		210°C		240°C	
	C ₅ -C ₁₉	C ₂₀₊	C ₅ -C ₁₉	C ₂₀₊	C ₅ -C ₁₉	C ₂₀₊	C ₅ -C ₁₉	C ₂₀₊
Cobalt	68	12	59	1.9	56	1.2	68	12
Cobalt on titania	68	9.0	58	1.6	41	0.16	64	3.7
Combustion synthesis	58	27	67	13	63	22	53	0.86
Fixed bed	63	22	67	15	67	14	57	29

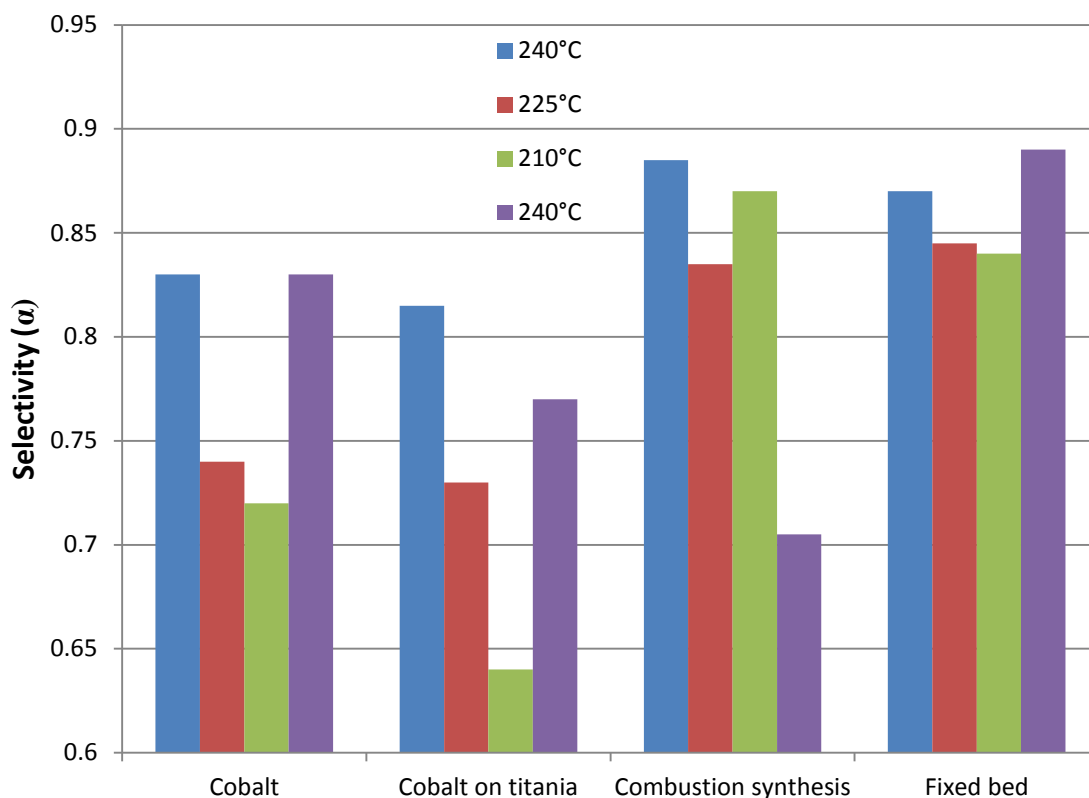


Figure 62: Graphical comparison of selectivities for different catalysts and varying temperature

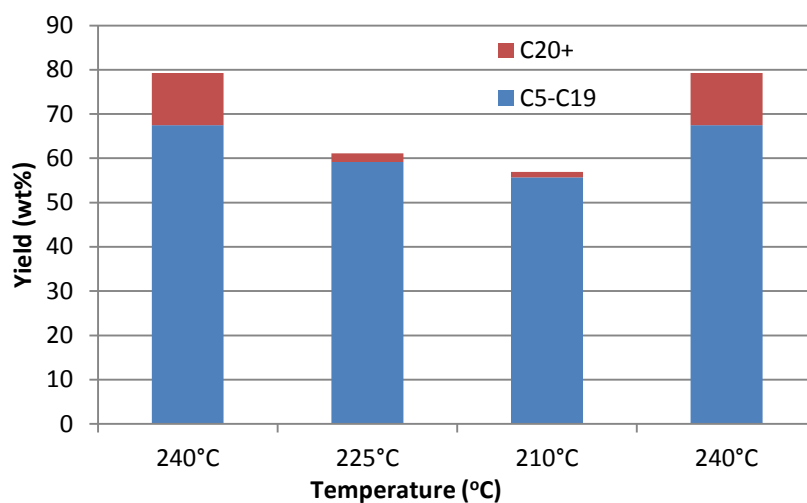


Figure 63: Product fractional yield vs. temperature for the neat cobalt washcoat

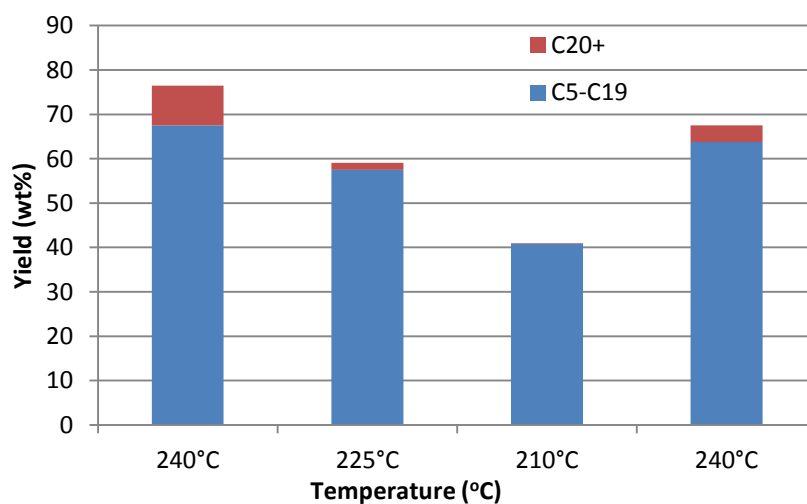


Figure 64: Product fractional yield vs. temperature for the cobalt on titania washcoat

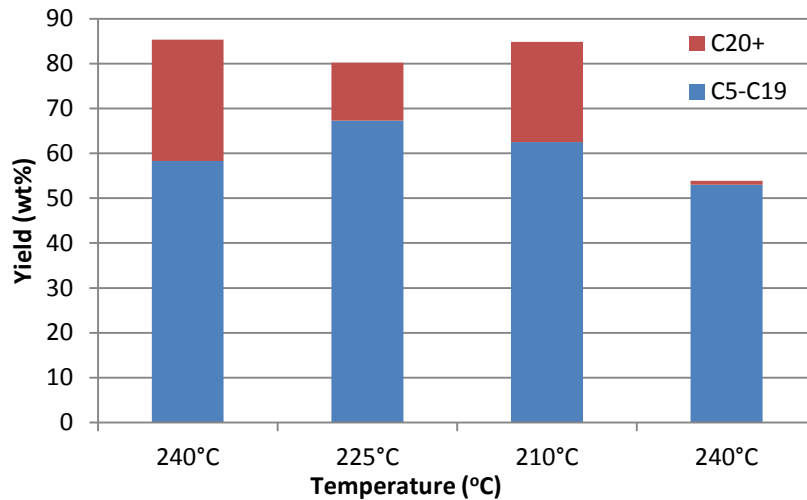


Figure 65: Product fractional yield vs. temperature for the combustion synthesis method

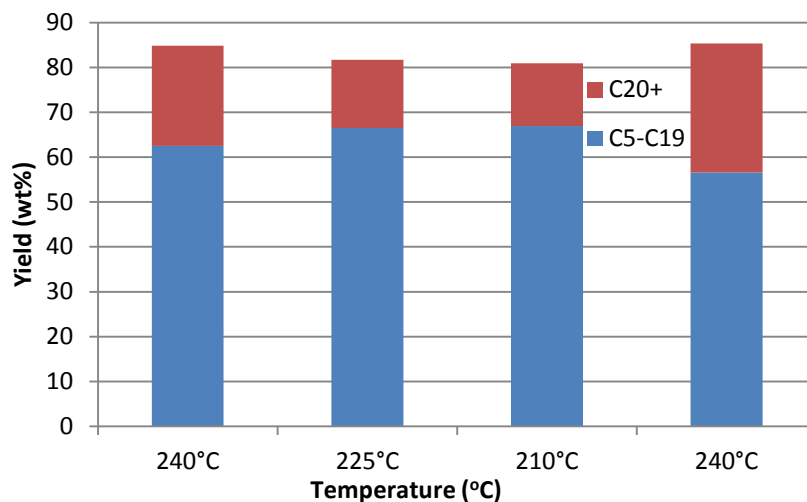


Figure 66: Product yield vs. temperature for the fixed bed reactor

Table 14 shows in most cases the product distribution was quite favourable for fuels production. The selectivity and product distribution can also be seen represented visually in Figure 62 to Figure 66. Again one must remember the application of this technology is small scale, localised FT. It is anticipated the FT syncrude would be transported to a central refinery, however, if a significant fraction is within a useable fuel range then some simple separation on site may be a suitable option. Separation would especially focus on diesel fuels due to the high need for diesel in the local forest industry, and due to the high quality of diesel available from the FT process (Mark E. Dry, 2002).

5.4.2. Shorter runs conclusion

A microchannel reactor was constructed which allowed comparison of various types of washcoating of Fischer-Tropsch catalysts, as well as comparison with a fixed bed reactor and powdered catalyst. The microchannel reactor was found to function at productivities per unit of catalyst 32 to 40 times higher compared to the fixed bed reactor. The productivities of the washcoated catalysts were also comparable to other microreactor FT work in literature using packed beds (Cao, et al., 2009; Myrstad, et al., 2009). Experimental research established that a simple washcoat of unsupported cobalt was the most effective catalyst in terms of productivity. Temperature was also shown to have a significant influence on productivity. In addition, at higher temperature (240°C) product selectivity was found to be still within a range suitable for fuels production. Therefore, it can be concluded in a small scale combined heat, power and fuel plant with a once through arrangement the process should be run at this higher temperature to maximise productivity per unit catalyst. In this scenario the benefits of higher temperature and productivity may outweigh any disadvantages in terms of product selectivity, but this should be investigated further.

5.5. Longer Time Frame Comparison

For the longer time frame comparison, two of the washcoats were utilised. As the neat cobalt washcoat proved to have the highest activity, this was the main catalyst considered for further study. However, a cobalt on titania washcoat was also considered to provide a comparison of the neat catalyst to that of a supported catalyst with a view to examining the long term catalyst performance changes over the two. One could hypothesise the supported catalyst may suffer less deactivation as the metal-support interactions could assist against sintering. Temperature was the only modified parameter for the short term runs, whereas it was considered more important to analyse another parameter, namely pressure, in the longer trials. Temperature and pressure are the key elements to consider when configuring the plant for integration with a sawmill. If the temperature could be kept as high as possible to increase quality of steam, and the pressure as low as possible to reduce compression costs, while not causing significant negative effects on catalyst lifetime or selectivity this would be a favourable outcome.

The temperatures investigated were again 210°C, 225°C and 240°C. The pressure range investigated was 2 bar, 5 bar, 10 bar and 20 bar. A summary of the data for reference can be found in Table 15.

Table 15: Summary of pertinent data from longer runs

Date	Cumulative time (hrs)	Catalyst	Temp °C	Press bar	CH4 sel. % of CO	R_{CO} mol/s/m³	C₂₊ g/g/hr	Selectivity α
10/04/2012*	72	Neat Co	240	10	23.4	15.29	9.2	0.75
26/04/2012	143	Neat Co	240	20	24	4.61	4.7	0.78
7/05/2012	214	Neat Co	240	20	25	4.57	4.2	0.77
21/05/2012	286	Neat Co	240	5	31.2	3.27	1.9	0.74
18/06/2012	355	Neat Co	240	2	21.7	2.43	1.8	0.725
1/07/2012	452	Neat Co	240	10	25.7	4.22	2.35	0.72
16/07/2012	524	Neat Co	225	10	22	1.45	0.889	0.75
30/07/2012	597	Neat Co	210	10	12.9	0.702	0.507	0.777
3/09/2012*	99	Co on TiO ₂	240	10	19	7.82	3.29	0.8
9/09/2012	171	Co on TiO ₂	240	20	20.2	4.85	2.05	0.81
28/09/2012	241	Co on TiO ₂	240	5	20.2	3.58	1.56	0.78
6/10/2012	313	Co on TiO ₂	240	2	28.7	1.95	0.86	0.79
12/10/2012	388	Co on TiO ₂	240	10	17.8	2.03	0.92	0.79
20/10/2012	458	Co on TiO ₂	225	10	11.8	0.92	0.407	0.8
2/11/2012	528	Co on TiO ₂	210	10	-	0.625	0.333	0.805

*initial catalyst settling runs shown for completeness but excluded from analysis

Experimental error has been estimated from the propagation of assumed errors through the system. This method is chosen as statistical methods were unable to be used due to a lack of sufficient repeat data. Two main sources of error were considered in the analysis for calculating the error. That of the potential mass discrepancy within the microchannel reactor and that of the experimental error determined through the nitrogen tracer gas balance. The largest error considered for the system is that of the mass of catalyst in the microchannels as it is an estimation based on the volume of cobalt nitrate solution filling the channels and evaporating. The expected error comes from either the cobalt nitrate solution concentrating and therefore the mass of cobalt increasing compared to the estimate, or the solution being forced out due to evaporation leading to less cobalt in the microchannels. This error has been cautiously estimated at 20%. The error calculated from the nitrogen balance for all scenarios fell into the 1-5% mass balance error range. Therefore, for visual representation the sum of the maximum of these errors (25%) has been shown as the vertical error

bars in all graphs. The horizontal bars shown on the temperature based graphs represent a conservative estimate of error based on maximum fluctuations about the setpoint of the temperature controller.

5.5.1. Fitting a kinetic equation to the experimental data

It is advantageous to attempt to fit a kinetic equation to the experimental data obtained from the CAPE microchannel reactor to assist in characterisation for scale up. To do this the same method was employed as from Yates and Satterfield (1991). Langmuir-Hinshelwood kinetics based on partial pressure were represented by a number of different equations. The partial pressures were based on ideal gas laws utilising the known volume fraction and total pressure of the reacting system. In keeping with the Yates and Satterfield study five different forms of the equation were fitted to the data in order to find the best fitting result. The equations used are Equations 14 to 18.

$$-r_{CO} = \frac{\alpha P_{H_2}^2 P_{CO}}{1 + \beta P_{H_2}^2 P_{CO}} \quad (14)$$

$$-r_{CO} = \frac{\alpha P_{H_2} P_{CO}^{1/2}}{(1 + \beta P_{CO}^{1/2})^3} \quad (15)$$

$$-r_{CO} = \frac{\alpha P_{CO}^{1/2} P_{H_2}^{1/2}}{(1 + \beta P_{CO}^{1/2})^2} \quad (16)$$

$$-r_{CO} = \frac{\alpha P_{CO} P_{H_2}^{1/2}}{(1 + \beta P_{CO})^2} \quad (17)$$

$$-r_{CO} = \frac{\alpha P_{CO} P_{H_2}}{(1 + \beta P_{CO})^2} \quad (18)$$

In order to establish the constants representative of the data the equations were modified into a linearised form as shown in Equations 19 to 23. This enabled graphing of the results and application of linear lines of best fit. The left hand side of Equations 19 to 23 were graphed against P_{CO} or $P_{CO}^{1/2}$ and are shown in Appendix E. The intercept of the fitted equation is equal to that of $1/\alpha^{1/2}$ while the slope is equal to $\beta/\alpha^{1/2}$. The fitted results for the experimental data can be seen in Equations 24 and 25.

$$\frac{P_{H_2}^2 P_{CO}}{-r_{CO}} = \frac{1}{\alpha} + \frac{\beta P_{H_2}^2 P_{CO}}{\alpha} \quad (19)$$

$$\left[\frac{P_{H_2} P_{CO}^{1/2}}{-r_{CO}} \right]^{1/3} = \frac{1}{\alpha^{1/3}} + \frac{\beta P_{CO}^{1/2}}{\alpha^{1/3}} \quad (20)$$

$$\left[\frac{P_{H_2}^{1/2} P_{CO}^{1/2}}{-r_{CO}} \right]^{1/2} = \frac{1}{\alpha^{1/2}} + \frac{\beta P_{CO}^{1/2}}{\alpha^{1/2}} \quad (21)$$

$$\left[\frac{P_{H_2}^{1/2} P_{CO}}{-r_{CO}} \right]^{1/2} = \frac{1}{\alpha^{1/2}} + \frac{\beta P_{CO}}{\alpha^{1/2}} \quad (22)$$

$$\left[\frac{P_{H_2} P_{CO}}{-r_{CO}} \right]^{1/2} = \frac{1}{\alpha^{1/2}} + \frac{\beta P_{CO}}{\alpha^{1/2}} \quad (23)$$

5.5.2. Establishing values for selectivity

Selectivity was determined by fitting the obtained data to the ASF distribution. An example of the fit is shown in Figure 67. The fitting process is performed by plotting $\log (W_n/n)$ vs. carbon number which yields a straight line. The theoretical selectivity is modified until the best correlation between the theoretical and experimental data is obtained. An example of this graph is shown in Figure 68.

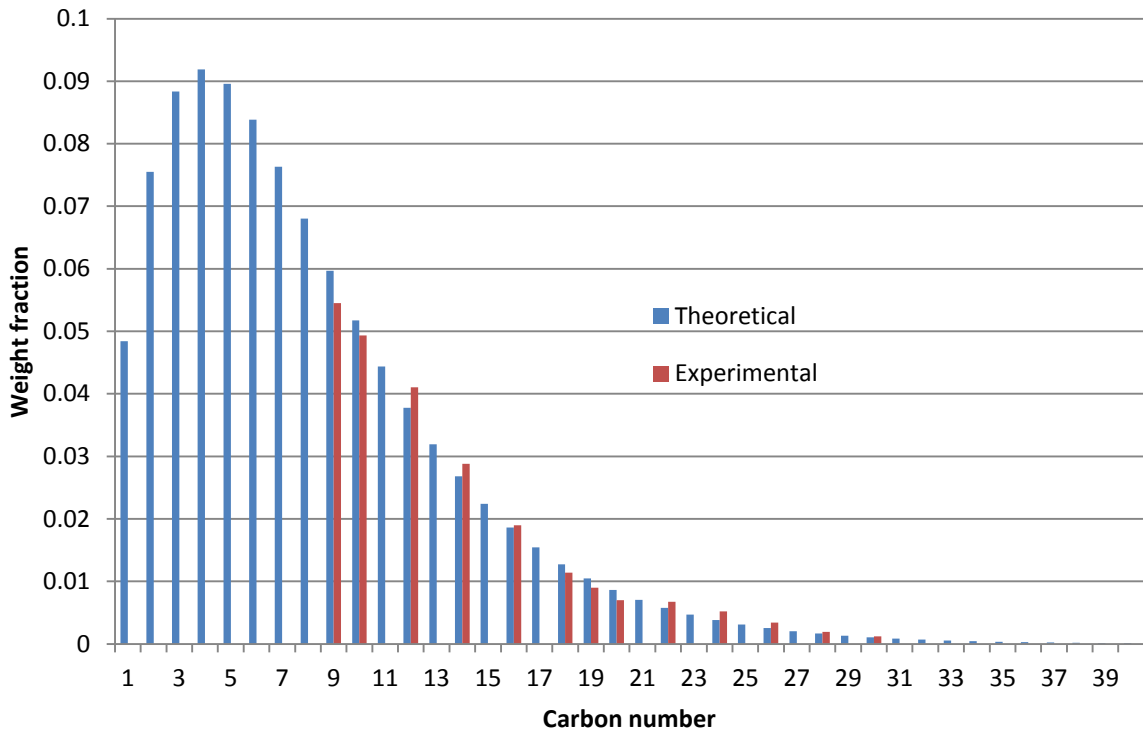


Figure 67: Example of fit of experimental liquids analysis to ASF distribution. Run 26/04/2012 20 bar 240°C neat cobalt washcoat with an α value of 0.78

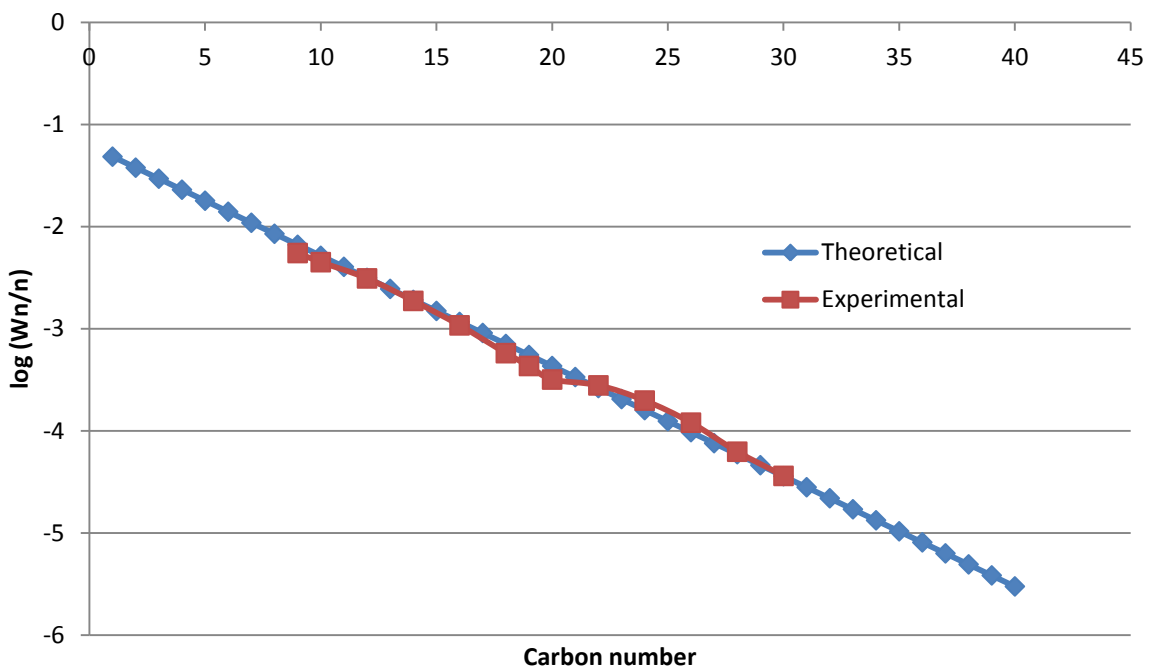


Figure 68: Example of methodology of fitting an α value to experimental data. Run 26/04/2012 20 bar 240°C neat cobalt washcoat with an α value of 0.78

Presentation of the results for kinetics and selectivity have been subdivided into the individual washcoats before comparison is made between the washcoats with the established data.

5.5.3. Neat cobalt washcoat

The neat cobalt washcoat runs were performed between the 10th April and 30th July 2012 with a total run time spanning 600 hours as shown in Table 15.

Of the results Equation 19 showed the best fit. However, the majority of the values were very near the x-y intercept making one question the validity of using this equation. Subsequent interpretation of the graphical results into equations showed the plot for Equation 23 to be significantly more accurate than Equation 19 when compared to experimental data (Figure 70). The resultant equation with the constants established from the graphical interpretation of Figure 69 in this section is shown in Equation 24. This is the same equation form that Yates and Satterfield (Yates & Satterfield, 1991) deemed to have the best fit giving confidence in the match to benchmark literature. Note that the units of $-r_{CO}$ are in mol/s/m³, where the m³ refers to the volume of the reactor. These units were chosen based on what is deemed the simplest for further design/scaleup modelling.

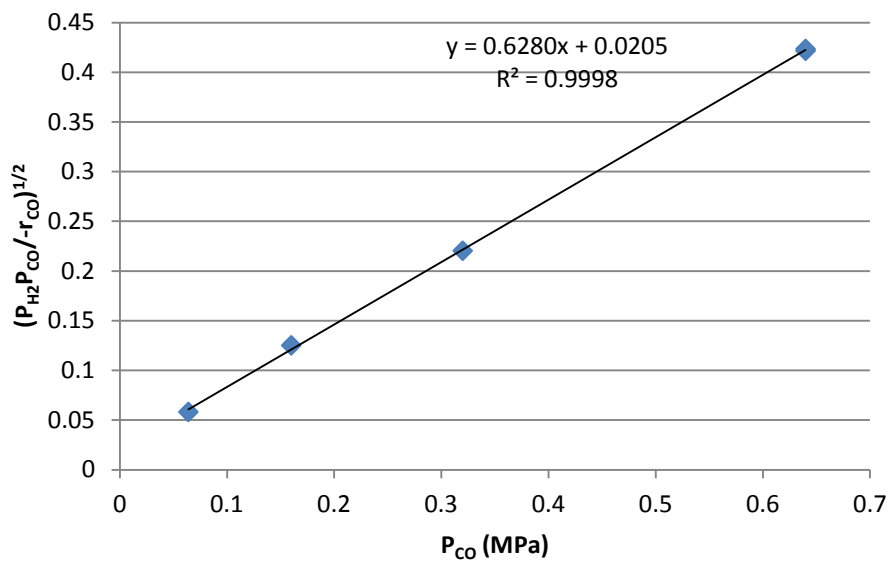


Figure 69: Plot of linearised equation 23

$$-r_{CO} = \frac{2367 P_{CO} P_{H_2}}{(1 + 30.56 P_{CO})^2} \quad (24)$$

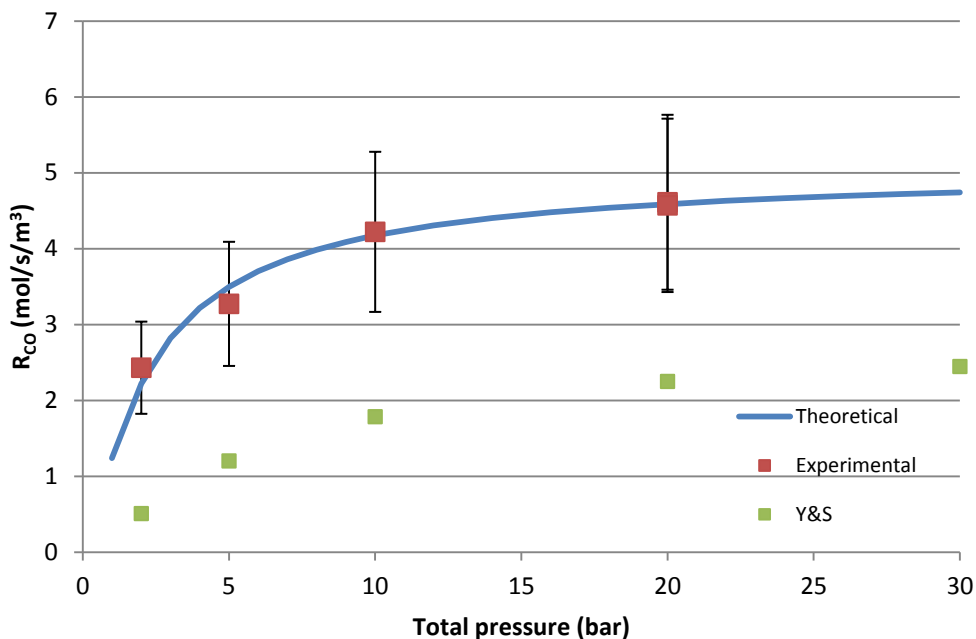


Figure 70: Productivity vs reactor pressure with the theoretical kinetic equation fit to the data along with comparative data from Yates and Satterfield (1991). Note the units of volume in the productivity refer to the reactor volume in this case

Converting the data from Yates and Satterfield into the same units and also plotting on Figure 70 shows the increased activity of the microchannel experimental work. While the microchannel work shows activity above Yates and Satterfield it must be acknowledged that their powdered catalyst (in a slurry reactor) had significantly better activity than that of the fixed bed powdered catalyst produced in this research.

It is interesting that there is a significant fall away in the catalyst activity lower than 5 bar total pressure, while there is a relatively small difference in the range of 5 to 20 bar. This shows that a process could be run at a much lower pressure than traditional technology while still maintaining comparable activity. The other significant consideration, however, is the selectivity effect with the lower pressure. It can be seen in Figure 72 that selectivity (apart from the outlier at 10 bar possibly due to catalyst degradation) with the neat cobalt washcoat also reduces when the pressure is lowered, from 0.78 at 20 bar to 0.725 at 2 bar. While this doesn't appear a substantial drop in α the fraction of recoverable FT product can be affected significantly. Figure 71 also shows the effect of temperature on productivity and selectivity for the neat cobalt washcoat. As anticipated there is an inverse correlation between temperature and selectivity. As the temperature increases there is, however, a significant increase in activity. This balance between selectivity and activity based on

temperature is an important variable and is one that can be addressed in modelling and techno-economic studies.

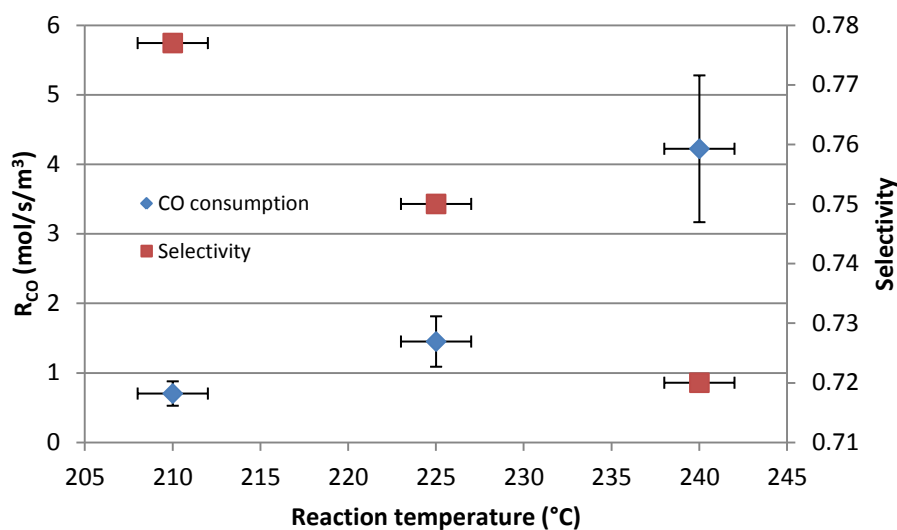


Figure 71: Reaction rate and selectivity as a function of temperature for the neat cobalt washcoat

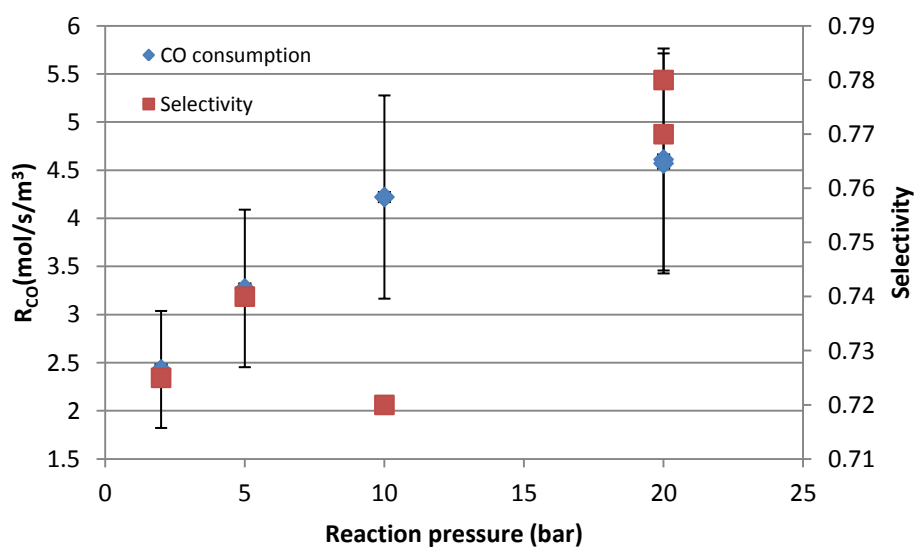


Figure 72: Reaction rate and selectivity as a function of reaction pressure for the neat cobalt washcoat

5.5.4. Cobalt on titania washcoat

The second washcoat compared was that of a cobalt on titania washcoat as described in the methodology and performed between 3rd Sep and 2nd Nov 2012 spanning a total run time of 530 hours. As with the neat cobalt washcoat, investigation of a kinetic model was performed on the cobalt on titania washcoat using the method from Yates and Satterfield (1991). Figure 73 shows the data collected showing an obvious outlier at 10 bar. This was the last of the four runs performed.

The sudden drop cannot be explained by typical gradual catalyst deactivation seen throughout the experiments as there was no trend but a rather apparent stepchange. It is suspected there was a blockage or other issue created between cooldown of the prior run and the startup of the 10 bar run that removed a certain quantity of catalyst from active production. Therefore for the purposes of calculating the kinetic model, the 10bar run has been eliminated in the calculations, however, is still shown on the final graph in Figure 75.

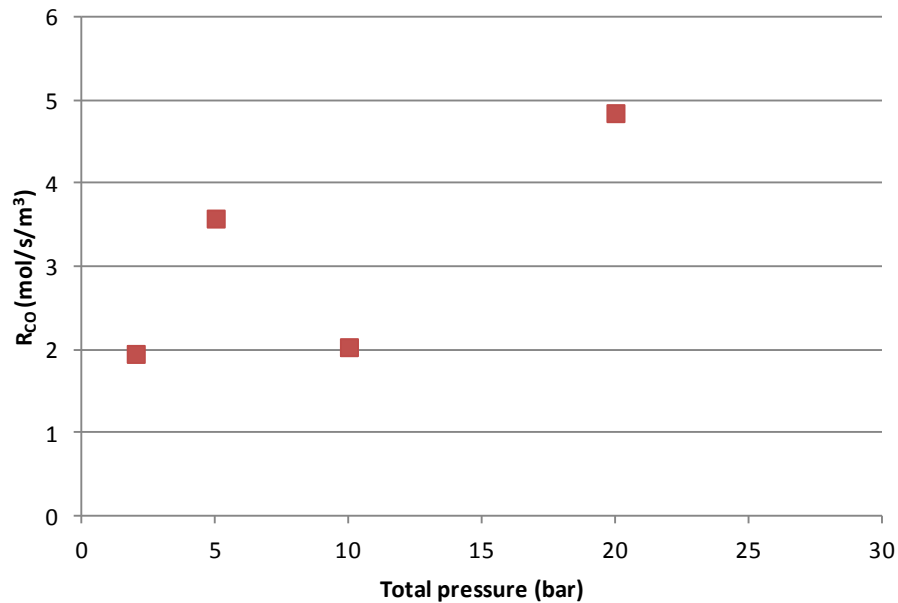


Figure 73: Raw data of reaction rate as a function of reaction pressure for the cobalt on titania washcoat

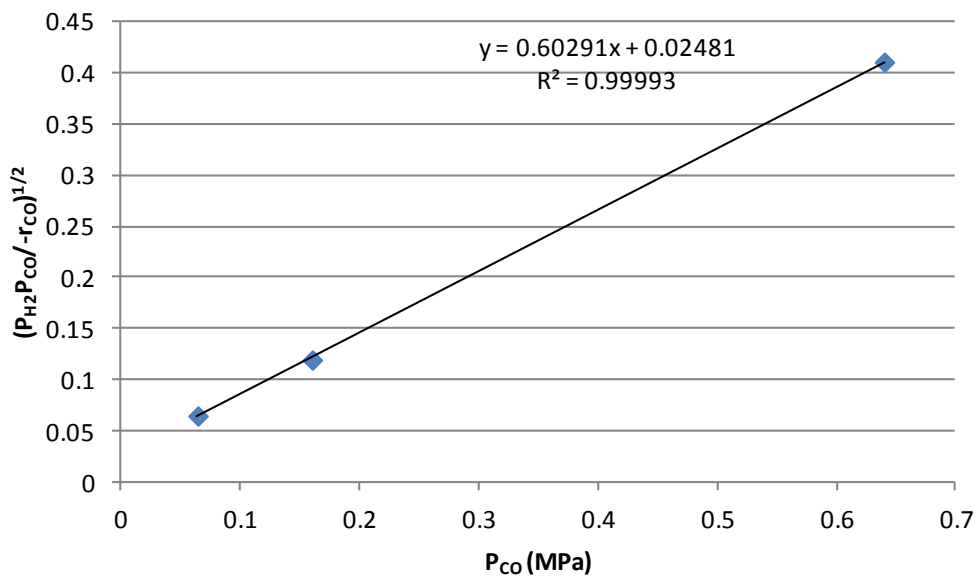


Figure 74: Best linearised fit of cobalt on titania data ignoring 10 bar outlier

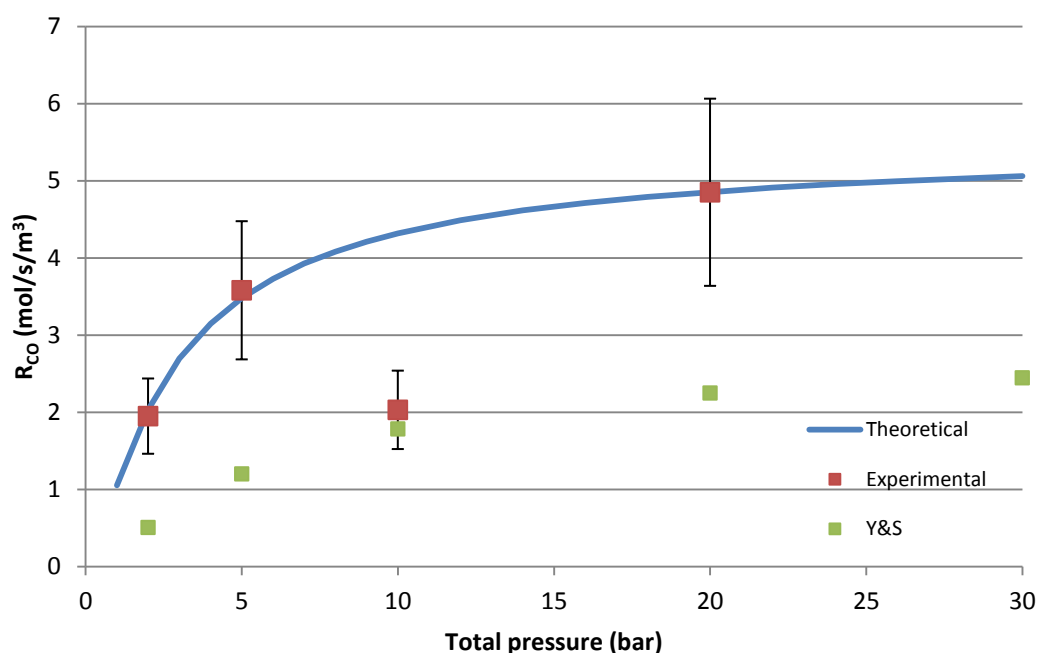


Figure 75: Theoretical equation comparison to raw data and Yates and Satterfield data for reaction rate as a function of reaction pressure

Again the kinetic model provided by Equation 19 and shown on Figure 74 provided the best fit for the data. The equation obtained is shown in Equation 25.

$$-r_{CO} = \frac{1625P_{CO}P_{H_2}}{(1 + 24.3P_{CO})^2} \quad (25)$$

Comparison of catalyst activity to reaction temperature has been shown visually in Figure 77. Note that from the comments earlier, the 10 bar 240°C run on the 12/10/2012 suffered from an unexpected lower activity in comparison to the previous results. Note however, that this value corresponds well with the other temperature points. These experiments were performed after the 10 bar 240°C run indicating the cause of lower activity remained consistent throughout the remaining experiments. One could assume therefore, if the activity step change was caused by a certain fraction of the catalyst being rendered unproductive, then for comparison sake the temperature dependent data in Figure 77 could be scaled up in a linear fashion based on the ratio between the actual data obtained in the 10 bar 240°C run on the 12/10/2012 and the value obtained at that pressure from the kinetic model fitted to the data.

As with the neat cobalt washcoat the selectivity followed typical expected trends with respect to temperature and pressure as shown in Figure 77 and Figure 78. These selectivity results, while

somewhat contrary to the shorter runs, are deemed to be considerably more accurate due to the amount of product available as well as having more certainty that steady state is achieved. From what can be seen in these figures one certainly needs to consider the balance between productivity and selectivity. The obvious balance being, the lower the temperature the higher the selectivity giving a higher fraction of retrievable and usable products, but requiring a greater amount of catalyst and larger reactor to achieve the same productivity. This is particularly pertinent to the scenario in this research due to the once through system as well as the higher cost of feedstock compared to traditional scenarios. Because there isn't a valuable use for gaseous products other than electricity or heat generation, as well as a lack of recycle/reforming to ensure good utilisation of feedstock, any balance between selectivity and productivity should be examined very carefully through a techno-economic lens and this is examined in Chapter 8. The same applies for the comparison of pressure to productivity and selectivity, although in this case as can be seen in Figure 72 for the neat cobalt and Figure 78 for the cobalt on titania, the compromise is not between the two catalyst parameters, but the cost of compression of the syngas. This is another aspect warranting techno-economic evaluation. The values for selectivity (α) are, however, for this experimental work quite low in comparison to some values that can be found in literature (Bezemer, Radstake, Falke, et al., 2006; Bolhar-Nordenkamp, 2004; Cao, et al., 2009; Kapteijn, de Deugd, & Moulijn, 2005; Knochen, Güttel, Knobloch, & Turek, 2010; Oukaci, et al., 1999). However, from the same literature there are some comparable values of α suggesting the catalyst is in the same order as others, although there is significant room for improvement of the catalyst performance in terms of selectivity. A small variation in values of α causes a significant shift in the available liquid or higher products available post the FT reactor and therefore the economics. An example of the affect of a changing α can be seen in Figure 76 showing the significant difference in cut with a varying selectivity. Therefore, while the activity produced by the washcoated catalyst in the microchannel reactor is very encouraging the α value is certainly an area that requires further development before it could be considered a commercial catalyst, at least in the once through LTFT scenario explored in this research. In this light, the values of α from experimentation will not be directly transferred to the techno-economic analysis. Rather, a sensitivity analysis will be performed to show the influence of α on the overall economics to highlight the affects of variation. It is not difficult to find literature which addresses FT selectivity (Lualdi et al., 2011; Teiseh, Capareda, & Rezenom, 2012), however, one very pertinent paper refers to the effect on the selectivity of adding water vapour to the feed gas with outstanding results (X. Liu, et al., 2011) as mentioned in the literature review. Their results showed a C_{10+} selectivity of 32% without water vapour and 87.3% C_{10+} with water vapour. This is a significant shift from an ASF distribution and if this could actually be harnessed in the once through scenario

considered in this thesis it would have an immensely positive effect on the overall feasibility. One would need to replicate the experiments with the microchannel reactor as a comparison to the slurry batch tests performed in the paper in question, based mainly on how significant the change is to the typical product distribution, as well as the questionable accuracy of a batch slurry FT experiment.

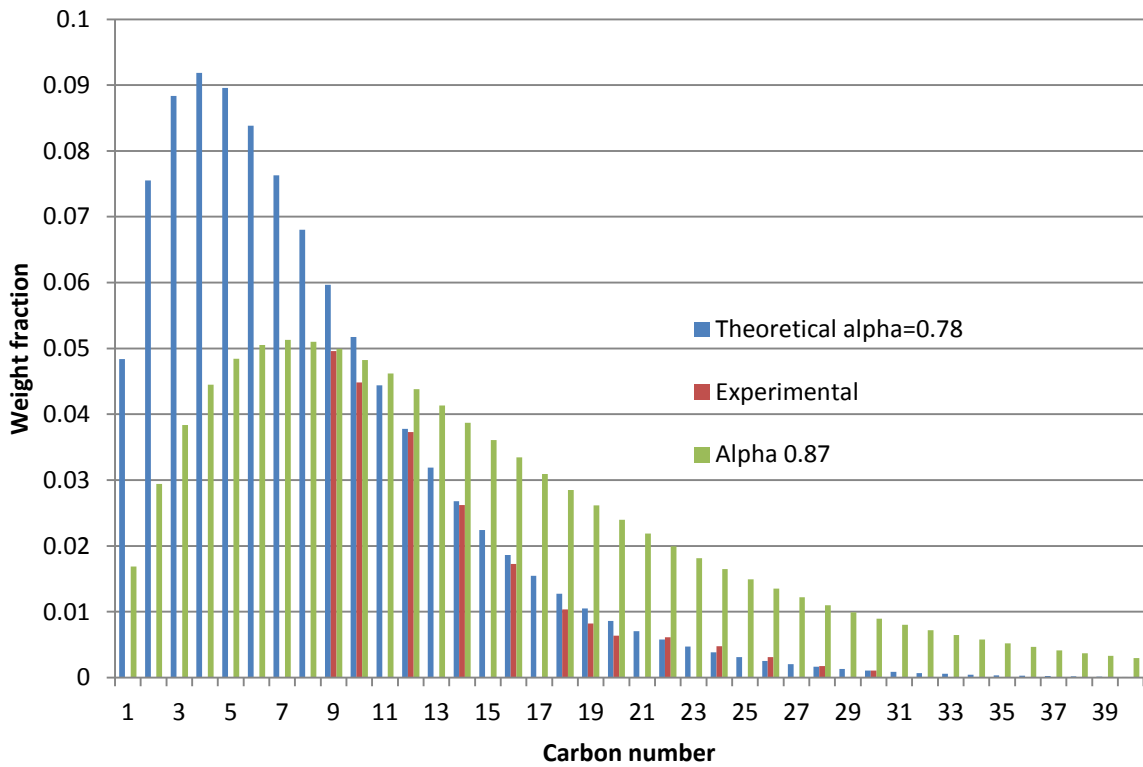


Figure 76: Graph to enable visualisation of ASF distribution with experimental results fitted to an α of 0.78 and comparison made to an α of 0.87

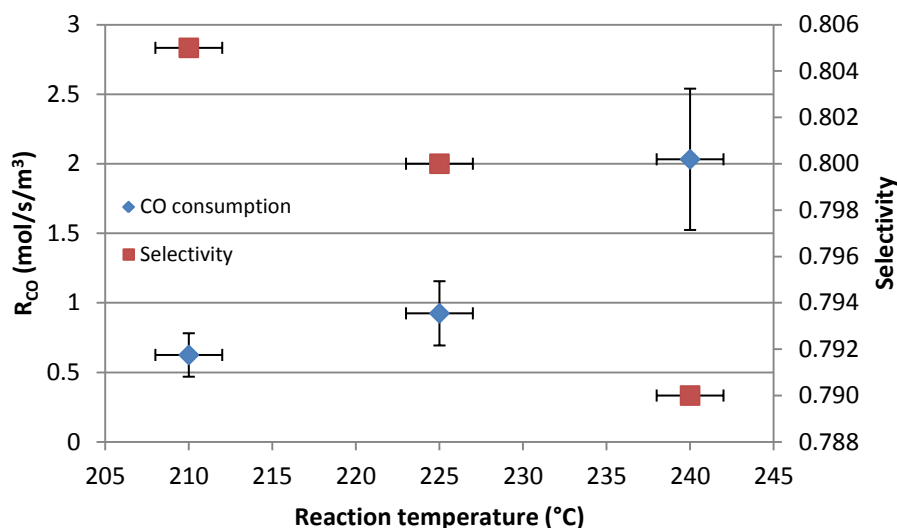


Figure 77: Reaction rate and selectivity as a function of reaction temperature for the cobalt on titania washcoat

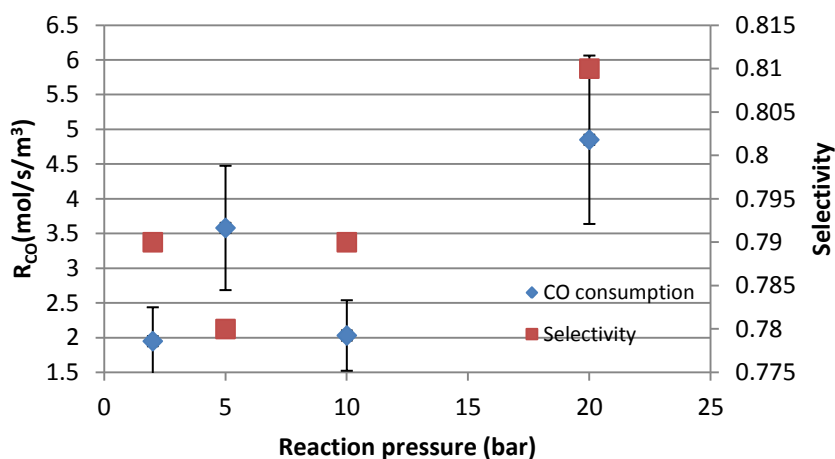


Figure 78: Reaction rate and selectivity as a function of reaction pressure for the cobalt on titania washcoat

5.6. Washcoat Comparison

While the two washcoats have been discussed somewhat individually a direct comparison of the two is important to gauge the relative performance. The neat cobalt washcoat has always been considered preferable by the author due to the simplicity of the catalyst production. The fact that it is a solution rather than a suspension as in the case of the titania washcoat as well as being only a single stage washcoat are examples of this simplicity. Therefore, unless the cobalt on titania washcoat were to exhibit markedly improved performance compared to the neat cobalt washcoat, the latter would be most preferred.

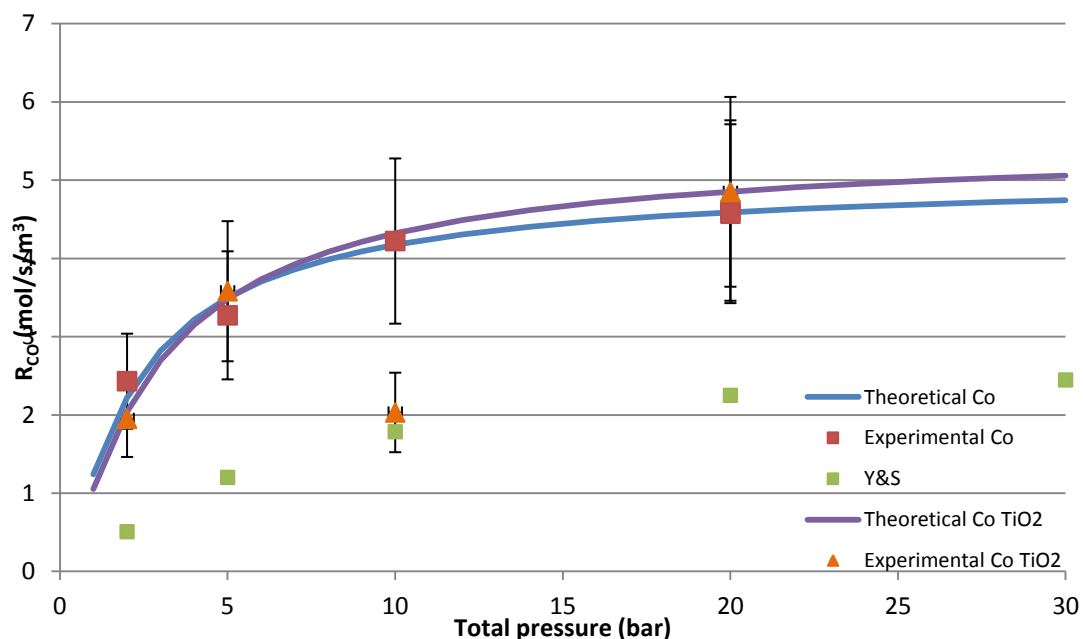


Figure 79: Comparison of the two washcoats in terms of conversion per unit volume of the reactor as a function of reaction pressure

Two main measures have been considered for the comparison. The first is performance per reactor volume and the second performance per mass of catalyst. The data reported graphically thus far for the two washcoats has been based on a conversion of CO per unit volume of reactor. This is a useful comparison as it shows what total reactor volume would be required based on the exact same method and concentrations of washcoating as performed in the experimentation. Productivity per unit mass of catalyst, however, is a very common form of performance reporting and is the one utilised in the shorter runs to allow literature comparability. This will therefore be compared to complement the shorter runs and further aid comparison of the two washcoats.

Figure 79 shows the comparison based on volume of reactor, and when the erroneous 10 bar result from the cobalt on titania washcoat is ignored the performance of the two washcoats is very similar. Although the performance is showing slightly higher for the cobalt on titania washcoat, the difference is so negligible that one wouldn't make a catalyst choice based on these results alone and at this comparison, the author would still prefer the neat cobalt washcoat.

Figure 80 and Figure 81 make the comparison of the pressure and temperature effects of the catalyst productivity per unit mass of catalyst and these results certainly show a more pronounced trend. It can be seen that for unit mass of catalyst the neat cobalt is more effective. However, this refers to the total mass of catalyst, thus for the cobalt on titania washcoat this includes the mass of

titania and not just the mass of cobalt. It is fairly typical for the reporting to be based on the total catalyst mass, however, it is the cobalt that is the active (and likely more expensive) component of the catalyst thus it is also helpful to make the comparison between the two catalysts based on the cobalt mass alone and is shown in Figure 82 and Figure 83.

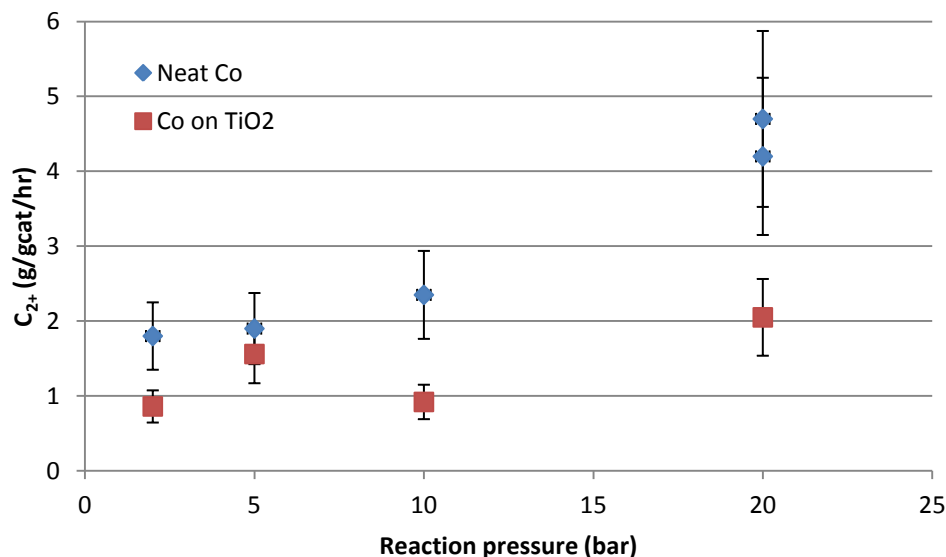


Figure 80: Comparison of reaction rate in terms of C_{2+} products per gram of catalyst per hour as a function of reaction pressure

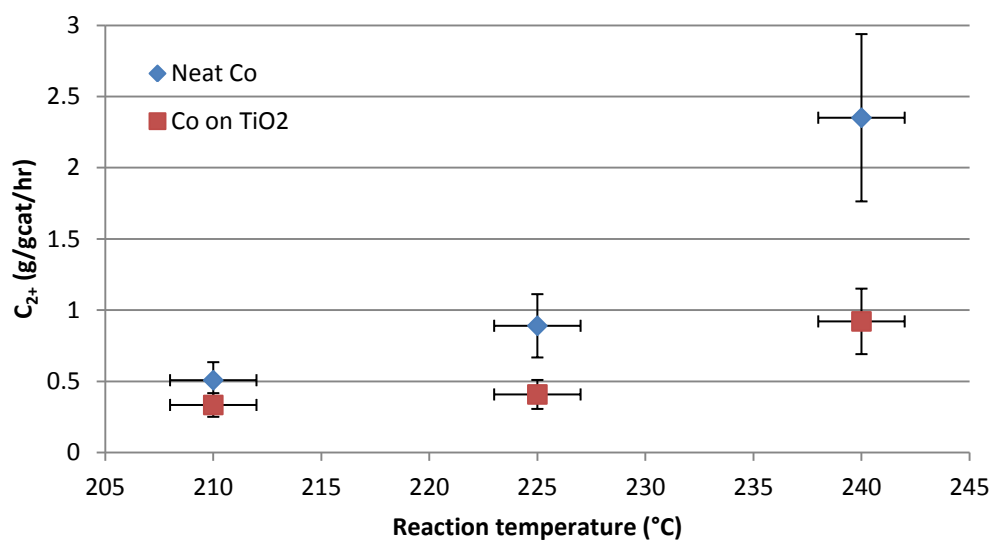


Figure 81: Comparison of reaction rate in terms of C_{2+} products per gram of catalyst per hour as a function of reaction temperature

This comparison of catalyst performance per unit of cobalt mass alone is shown in Figure 82 and Figure 83 for both pressure and temperature variation. It can be seen the comparison shifts

somewhat with the cobalt on titania washcoat exhibiting a slightly higher production rate per unit of cobalt mass than the neat cobalt washcoat. The difference, however, except for the 5 bar value shown in Figure 82 is not significant. This shows the titania is not having a particularly significant affect towards enabling a higher fraction of active sites of cobalt in comparison to the neat cobalt washcoat. Based on this one could still consider the neat cobalt washcoat the preferred option of the two at this stage, relying on the ability to further develop the catalyst to generate higher α values without the need for a support.

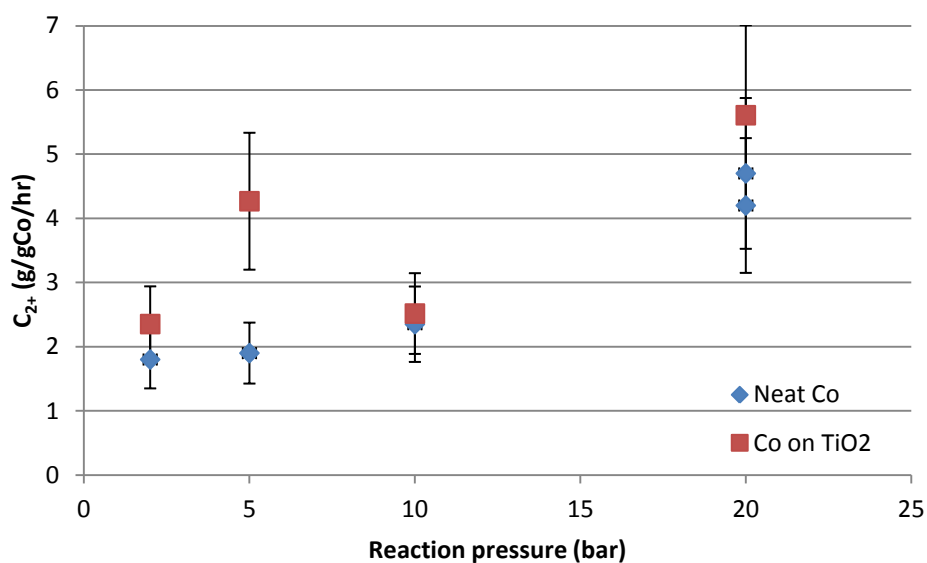


Figure 82: Comparison of reaction rate in terms of C₂₊ products produced per gram of cobalt per hour as a function of reaction pressure

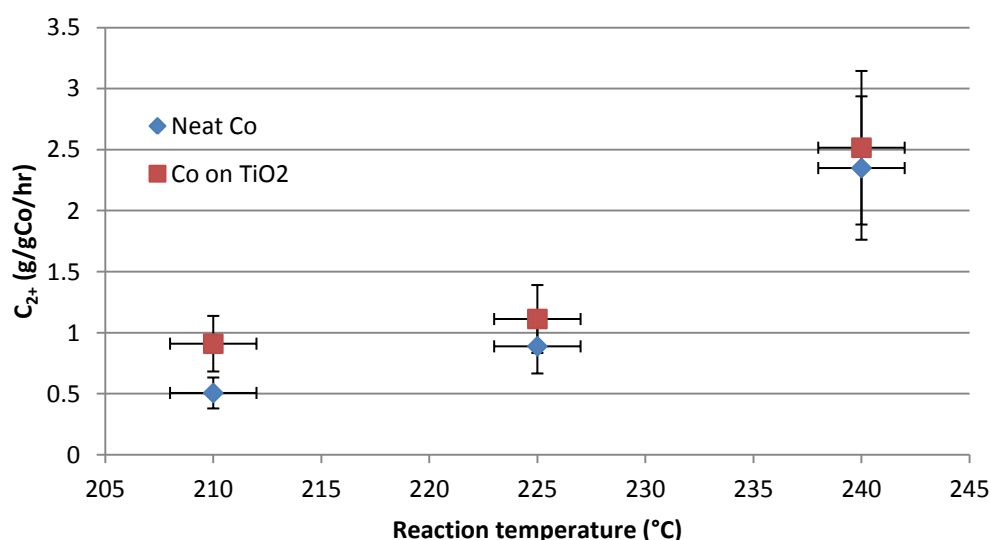


Figure 83: Comparison of reaction rate in terms of C₂₊ products produced per gram of cobalt per hour as a function of reaction temperature

5.7. Deactivation

One of the most significant advantages of the longer runs over 70 hours or more, in comparison to the shorter runs of several hours, has been the ability to view the behaviour of the catalyst over time. Because the same catalyst/reactor system was reused for each run for the two separate catalysts, the neat cobalt catalyst had over 570 hours of run time, while the cobalt on titania catalyst had over 500 hours of run time. Running for longer has proven that the shorter run results, while still useful for comparison with one another, were certainly still in a settling in period for the catalyst. For the longer runs the first 10bar 240°C run for each was considered to be a settling run, as even part way into the next run the catalyst activity was still settling down. It therefore took approximately 100 hours before the catalyst could be considered to be operating at a normal ongoing performance. Because of the differing conditions tested over the course of the experiments it is difficult to get an absolute gauge on the long term performance of the catalyst. One can, however, examine the performance over a 72 hour run. Inspection of the performance over the course of the runs shows difficulty in determining the level of deactivation within the noise of the data. Ultimately for an accurate view of the rate of deactivation of the catalyst it is the recommendation that the catalyst be run under the same conditions for 500 hours at an absolute minimum, preferably 1000 hours (over 40 days) continuously.

5.8. Conclusions and Recommendations of Experimental Work

While there has been significant discussion of the observations of the experimental work, the ultimate goal is further application. This takes the form of useable conclusions from the experimental work, as well as concrete recommendations for further work that would add considerable value to the area of research. These observations are presented below.

Virtually all of the SEM images showed a catalyst surface with the appearance of a high surface area which is an encouraging result, albeit a little surprising at the differing forms this high surface area catalyst took. One aspect that could be very valuable for further work is SEM imaging of a catalyst after it has settled down from its initial high activity to view any structural changes in the catalyst. Because of the danger of causing damage to the SEM due to the presence of hydrocarbons the author has been exceedingly wary of performing this analysis. Therefore the catalysts examined in the SEM were completely prepared but not used for FT synthesis. Subsequent researchers, however, may deem post FT synthesis SEM analysis valuable enough to perfect techniques for washing all traces of hydrocarbons out of the catalyst sample.

The results for the productivity of the catalyst are encouraging in two ways. Firstly they are above current literature values for a cobalt catalyst from a slurry reactor (Yates & Satterfield, 1991), as well as fitting kinetic equations very well from the same reference. The equation for the neat cobalt washcoat based on productivity per unit reactor volume is shown in Equation 26.

$$-r_{CO} = \frac{2367P_{CO}P_{H2}}{(1 + 30.56P_{CO})^2} \quad (26)$$

While the productivity per unit reactor volume for the cobalt on titania washcoat can be represented by Equation 27.

$$-r_{CO} = \frac{1625P_{CO}P_{H2}}{(1 + 24.3P_{CO})^2} \quad (27)$$

Of the two catalysts presented for longer runs, the performance was very similar when considered on a per volume of reactor basis. Therefore, the author would conclude that the neat cobalt washcoat, at least in its current fraction of reactor loading is the most appropriate catalyst for further consideration from a CO conversion point of view. Due to the long timeframe required to obtain multiple results, the quantity of results to provide statistical error analysis is limited. While the kinetic results of this study have been used for further design work one should bear in mind that further repeated results would improve the confidence in the scaled up design.

An area of the experimental work that would benefit from further research is improvement of the α values. The effects of the α value on plant performance is demonstrated in the techno-economic study in Chapter 8, and shows a definitive need for a high α catalyst in the plant arrangement evaluated. Further work into traditional methods of modifying catalysts such as preparation methods and promoters could be considered, however, more novel methods such as water vapour addition may produce the most significant improvements and thus should be investigated further.

The longer runs have been useful to analyse the catalyst performance once initial catalyst activity has settled down, as well as ensuring adequate steady state, however, a beneficial further experimental process would be to run with the same conditions for an extended period (suggest 500-1000 hours minimum) to be able to examine long term catalyst washcoat deactivation beyond the noise of the data.

The parameters that have been examined in this research have currently excluded variation of the quantity of catalyst loaded into the reactor. Further investigation into the effects of a higher catalyst loading are presented in the modelling section (Chapter 6) along with variations in reactor size. There is an obvious benefit to modification of either of these as it has the potential to reduce the reactor size and complexity of manufacture significantly. Post the discussion on the modelling findings, conclusions have been drawn as to the benefit of further experimentation considering increased catalyst loading.

6. Modelling of the CAPE Microchannel Reactor

6.1. Introduction

It is often claimed that microchannel reactors exhibit significantly better heat and mass transfer than traditional reactor technology (Atkinson, 2010; Gavriilidis, et al., 2002; A. L. Y. Tonkovich, Yang, Perry, Fitzgerald, & Wang, 2007). However, rather than simply rely on this 'common knowledge' the intention of this work is to model microchannel reactors to provide a theoretical context for the results being seen in the experimental work. This also will allow comparison of experimental work with literature.

The other benefit of being able to closely model the experimental system is to gain an understanding of potential scale up. While microchannel reactor scale up is normally considered a case of 'numbering up' the channels, compared to the lab scale CAPE reactor, length considerations also need to be taken into account. Channel dimension modifications are also an important consideration for the manufacturability. The modelling should help somewhat towards answering these questions. The modelling will focus on the reaction and mass transfer aspects rather than heat transfer as literature would suggest heat transfer resistance will be insignificant in this research. Myrstad et al. (2009) suggest in their reactor system that modelling shows fully isothermal behaviour in more than 97% of channel length, with their reactor being of greater dimensions (400 μm height and 800 μm between pillars) than this research. Visconti et al. (2011) studied a circular monolith with coated walls inserted into a 25mm fixed bed reactor tube. They found less than 0.2 $^{\circ}\text{C}$ temperature difference in either the radial or axial direction and increasing the catalyst activity by 10 gave a 6 $^{\circ}\text{C}$ temperature deviation in the axial direction with minimal difference in the radial direction. Cao et al. (2009) utilised a microchannel reactor packed with fine catalyst particles (45 μm and 150 μm). They have produced a useful correlation in regards to temperature profile through a catalyst particle as shown in Figure 84. While this isn't a direct correlation to this research, one could consider the washcoating thickness to be relative to the diameter (or half the diameter) of a catalyst particle. It can be seen in Figure 84 the particle diameter at which there begins to be noticeable temperature differences is actually above the dimensions of the reactor channels in this research. All of the above lead to the conclusion that sufficient work has been performed in the area of heat transfer, showing negligible affect, and thus it can be assumed that heat modelling in this thesis would be an unnecessary repeat of existing work for little gain. Rather, modelling of mass transfer in the microchannel reactor is the selected focus.

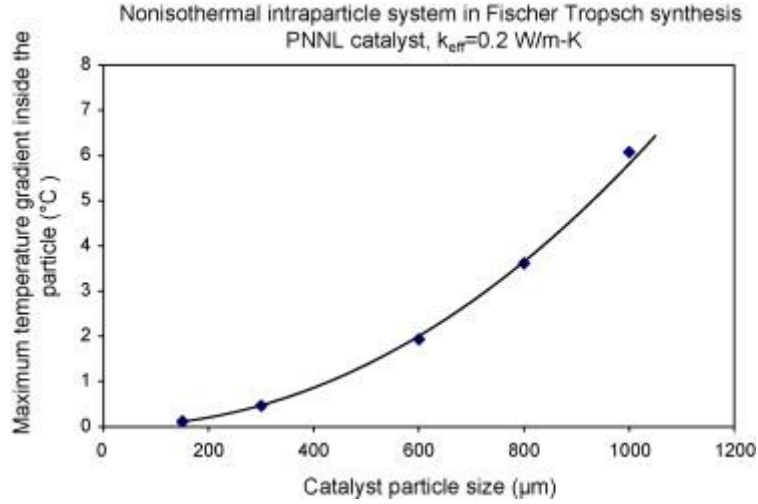


Figure 84: Intraparticle temperature gradient vs. catalyst particle size (Cao, et al., 2009)

6.2. Theory and Modelling

Before a particular model is selected, one has to review the flow regime. It is generally assumed to be laminar flow in a microchannel reactor, however, this is checked for completeness by ensuring the Reynolds number is <2000. Note that d is based on the hydraulic diameter of the channels. This parameter was chosen due to the fact that the catalyst is wall coated, so the channel dimensions become the parameter of interest.

$$Re = \frac{d \cdot v \cdot \rho}{\mu} \quad (28)$$

In order to calculate the Reynolds number it is necessary to obtain a viscosity for the mixed gas. This is calculated from equations 29 and 30 (Poling, Prausnitz, & O'Connell, 2001). Because of the low fraction of nitrogen in the feed gas the viscosity is only calculated for CO and H₂.

$$\mu_m = \frac{y_1 \mu_1}{y_1 + y_2 \phi_{12}} + \frac{y_2 \mu_2}{y_2 + y_1 \phi_{21}} \quad (29)$$

$$\phi_{12} = \left(\frac{M_2}{M_1} \right)^{0.5} = \phi_{21}^{-1} \quad (30)$$

After confirmation of laminar flow, the model can be selected. In this case a plug flow reactor (PFR) is selected. Literature (Visconti, et al., 2011) suggests this is a reasonable assumption for gas phase microchannel reactors. The informed assumption by Visconti et al. (2011) is based on a calculated measure of axial dispersion from Equation 31

$$\left(\frac{D_{eaCO}}{v \cdot L} \right) \ll 1 \quad (31)$$

Where D_{eaCO} is the effective axial diffusivity and is calculated from Equation 32

$$D_{eaCO} = D_{CO} + \frac{v^2 \cdot d^2}{192D_{CO}} \quad (32)$$

For the lab scale scenario based on 25cc/min flow the axial dispersion is 0.08. This is with a short reactor, therefore any increase in reactor length in longer modelled scenarios will serve to lower this value further. While literature and Equation 31 do suggest the PFR model is appropriate, it does seem somewhat counter-intuitive for a laminar flow based system. If one were to require significantly accurate results for scale up or other more detailed analysis then it is suggested that pulse experiments be completed to validate the plug flow assumption.

A significant assumption made is that there are no liquids present that need to be taken into consideration in the model i.e. not having to consider diffusion through FT product to reach the catalyst surface. This is based on work by Philippe et al. (2009) who suggests that under typical FT conditions (20 bar 230°C) more than 99 mol % of the reacting species are in the gaseous phase based on thermodynamic equilibrium calculations and therefore a gas-solid system can be assumed.

Another important assumption is that the catalyst layer is thin enough to negate any intraparticle mass transfer resistance based on the data shown later in Figure 92. Therefore the mass transfer from the bulk phase to the catalyst particle is the only mechanism considered for mass transfer resistance.

Therefore to find the mass transfer coefficient the Sherwood number relationship can be employed using the channel diameter and diffusion to relate convective to conductive diffusion rates.

$$\text{Sherwood number } Sh = \frac{k \cdot d}{D} \quad (33)$$

Diffusion is calculated as the rate of CO diffusing through H₂ from Equation 34 (N. H. Chen & Othmer, 1962). Equation 35 checks the validity of the diffusion equation. The equation is valid between 0.7-20.

$$D_{12} = \frac{0.43 \left(\frac{T}{100} \right)^{1.81} \left(\frac{1}{M_1} + \frac{1}{M_2} \right)^{0.5}}{Patm \left(\frac{T_{c1} T_{c2}}{10000} \right)^{0.1405} \left[\left(\frac{Vm_{c1}}{100} \right)^{0.4} + \left(\frac{Vm_{c2}}{100} \right)^{0.4} \right]^2} \quad (34)$$

$$0.7 < \left(\frac{\frac{T}{100}}{\left(\frac{T_{c1} T_{c2}}{10000} \right)^{0.453}} \right) < 20 \quad (35)$$

The value for the Sherwood number depends on the shape of the duct. The following relationships relate to a square duct with Equation 36 (van Male, de Croon, Tiggelaar, van den Berg, & Schouten, 2004) and Equation 37 (Visconti, et al., 2011) showing slightly different values. To be conservative the lower of the two was selected. Note that there are entrance effects which raise the value of the Sherwood number. These entrance effects relate to the Graetz number as defined in Equation 38 which takes into account the added convective diffusivity due to the disruption of entering the channel.

$$Sh = 2.43 \left(1 + \left(\frac{Gz}{132} \right)^{0.835} \right) \quad (36)$$

$$Sh = 2.977 + 6.874 \left(\frac{1000}{Gz} \right)^{-0.488} \cdot \exp \left(\frac{-57.2}{Gz} \right) \quad (37)$$

$$\text{Graetz number } Gz = \frac{v \cdot d^2}{zD} \quad (38)$$

From Equations 28 to 38 the mass transfer coefficient, k , can be calculated for the given system which then relates to the actual mass transfer flowrate, n_A , of a component (in this case CO) via Equation 39. For the given situation the Graetz number has little effect therefore just the constant of Equation 36 is used for further calculations.

$$\dot{n}_A = Ak(C_g - C_i) \quad (39)$$

While the bulk gas concentration C_g is known, the concentration at the catalyst interface C_i is not and is dependent on the reaction kinetics. The rate of CO consumption based on reaction kinetics is calculated initially using C_g . C_i , the more relevant concentration, is then calculated using Equation 39 and compared with C_g to see if there would be an appreciable difference in rate calculated if C_i were used in the kinetic expression.

The kinetic equation (Equation 40) used to describe the rate of consumption of CO was obtained from Yates and Satterfield (1991) and given its substantial use in papers appears to be somewhat of a benchmark. This equation has been fitted to the experimental data as seen in the experimental section.

$$-R_{CO} = \frac{\alpha P_{CO} P_{H_2}}{(1 + \beta P_{CO})^2} \quad (40)$$

As the reactor is being evaluated as a plug flow reactor the rate was converted to that of a volume of reactor basis rather than per mass of catalyst. The equation used is shown in Equation 41 which incorporates the experimental parameters of the neat cobalt washcoat.

$$-r_{CO} = \frac{2367 P_{CO} P_{H_2}}{(1 + 30.6 P_{CO})^2} \quad (41)$$

Having to account for all the products produced from the Fischer-Tropsch reaction would overly complicate the model therefore a lumped stoichiometry (Visconti, et al., 2011) based on the ASF distribution from experimental data was used giving values for a, n and m in Equation 42.



In this scenario a typical value for α was selected from experimental work of 0.78 as well as 20% of CO being converted to methane. From weighted proportioning of consumption of the reactants and the generation of products into bulk stoichiometry gave values of a = 2.57, n = 3.1 and m = 9.7.

From Equation 42 the relative rates for the components can be established based on CO as shown in Equations 54 to 56.

After calculating the CO consumption based on the kinetics, the value for the concentration at the catalyst-gas interface can be calculated. This is determined by rearrangement of Equation 39 based on the fact that $-r_{CO}$ must equal n_A in equivalent units. The concentrations have also been converted to partial pressures to be consistent with the kinetic equation. This is shown in Equation 43.

$$P_{COi} = P_{COg} - \frac{r_{CO} RT}{Ak\rho_b 10^6} \quad (43)$$

A set of equations for solving the system was produced based on an algorithm by Fogler (2011). These are shown from Equation 44 to 58. The set of equations were solved in Polymath 6.1 using the Burlirsch-Stoer (BS) algorithm which is an extrapolation method.

Differential Equations

$$\frac{dF_{CO}}{dV} = r_{CO} \quad (44)$$

$$\frac{dF_{H_2}}{dV} = r_{H_2} \quad (45)$$

$$\frac{dF_{prod}}{dV} = r_{prod} \quad (46)$$

$$\frac{dF_{H2O}}{dV} = r_{H2O} \quad (47)$$

Explicit Equations

$$P_{CO} = P_{To} \frac{F_{CO}}{F_T} \quad (48)$$

$$P_{H2} = P_{To} \frac{F_{H2}}{F_T} \quad (49)$$

$$P_{prod} = P_{To} \frac{F_{prod}}{F_T} \quad (50)$$

$$P_{H2O} = P_{To} \frac{F_{H2O}}{F_T} \quad (51)$$

$$F_T = F_{CO} + F_{H2} + F_{prod} + F_{H2O} + F_{N2} \quad (52)$$

$$-r_{CO} = \frac{2367 P_{CO} P_{H2}}{(1 + 30.6 P_{CO})^2} \quad (53)$$

$$r_{H2} = ar_{CO} \quad (54)$$

$$r_{prod} = -\frac{1}{n} r_{CO} \quad (55)$$

$$r_{H2O} = -r_{CO} \quad (56)$$

$$X = \left(1 - \frac{F_{CO}}{F_{COo}}\right) 100 \quad (57)$$

$$P_{COi} = P_{COg} - \frac{r_{CO} RT}{Ak\rho_b 10^6} \quad (58)$$

6.3. Results and Discussion

Results from the model are generated from using the kinetic rate equation established from experimental work as shown in Equation 41. It should be noted that the equation was based on a molar conversion of CO per second on a reactor volume basis. This is shown again in Figure 85. However, for the course of the modelling results, the output that will be compared will be in terms of % CO conversion. When making comparisons over the same system the % CO conversion is an easier measure to visualise and becomes an important parameter in reactor design.

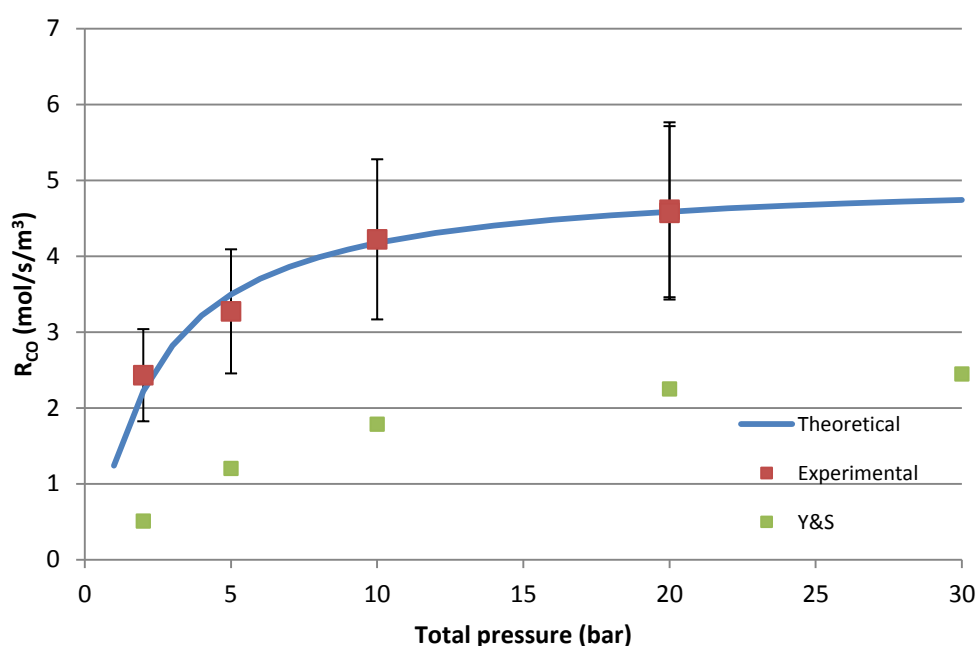


Figure 85: Reaction rate in terms of reactor volume as a function of reaction pressure showing the experimental data in red, with the fitted kinetic model in blue, while the green is the comparison with Yates and Satterfield's work

Modelling results for CO conversion vs. reactor volume are shown in Figure 86. It can be seen over the length of the reactor the conversion is virtually linear at the reactor volumes and flowrates used in the experiments. This is a positive result as it simplifies analysis of the actual reaction rate within the reactor, based on the conditions of the experiment, and shows that there needn't be any back calculation to the kinetic rate, rather the overall rate measured is representative of the kinetics. This certainly is the advantage of performing FT synthesis experiments at a lower conversion rate where there isn't a significant enough drop in partial pressure of the reacting components to cause noticeable overall conversion rate change in the system.

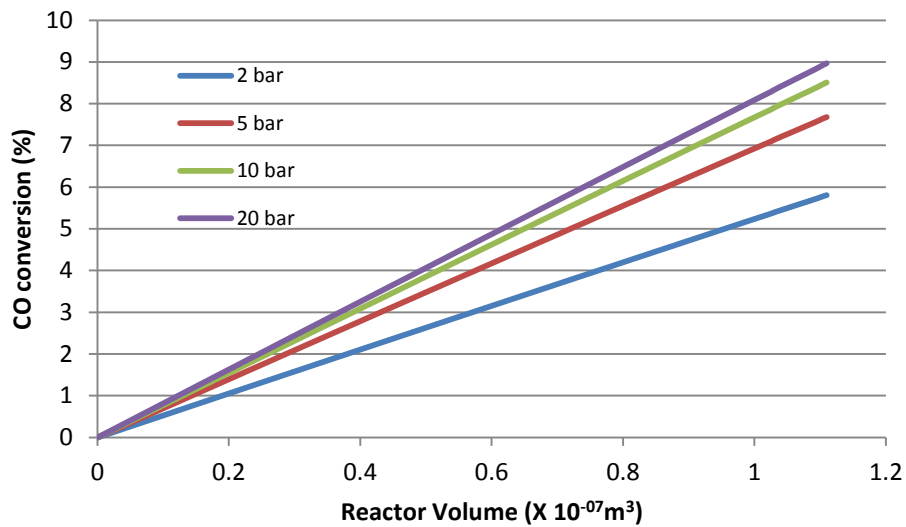


Figure 86: Estimated conversion of CO over the reactor volume at various total pressures. 240°C, 25cc/min feed

The modelled performance of the reactor with a larger volume (a reactor 370mm long yielding 10 times the volume) at the same flowrate is shown in order to see the effects of a higher conversion and begin to understand scale up challenges. Figure 87 shows that as the conversion goes up the partial pressures of the reacting gases (H₂ and CO) are dropping to the point that it is affecting the reaction rate, and therefore creating nonlinear conversion over the length of the reactor. From Figure 88 it can be seen that the lower pressure has less of an effect with the 5 bar conversion being only a relative 11.2 % lower than the 20 bar conversion, whereas, in the shorter reactor shown in Figure 86 the difference is a relative 14.4 %.

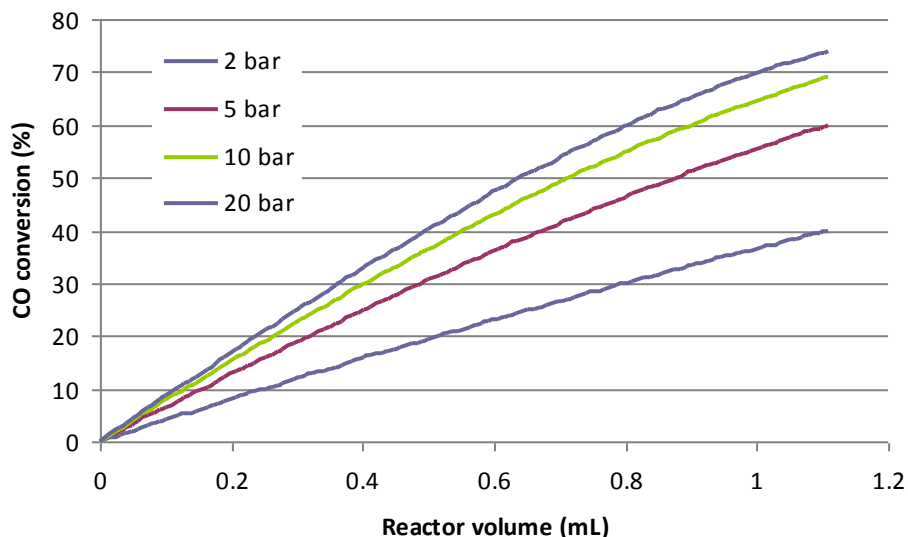


Figure 87: Comparison of CO estimated conversion over the length of the reactor at various pressures based on a reactor ten times the volume of the experimental reactor. 240°C, 25cc/min feed

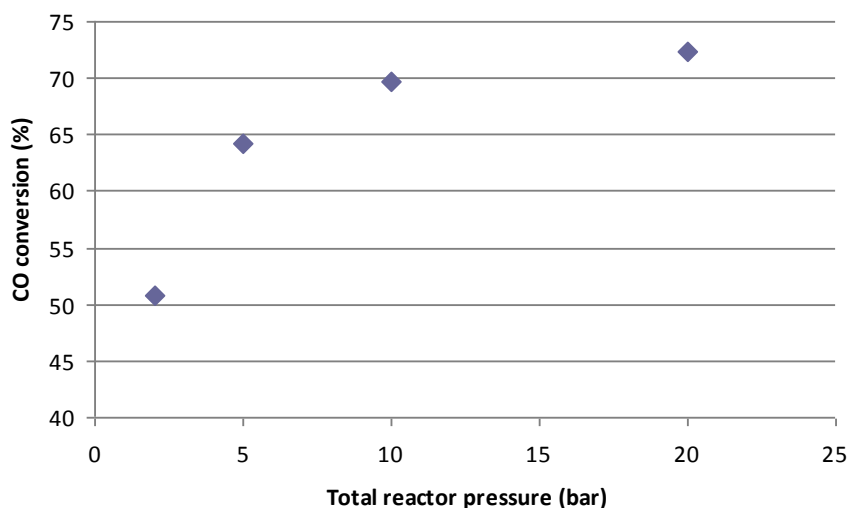


Figure 88: CO estimated conversion vs. reactor pressure based on a reactor ten times the volume of the experimental reactor. 240°C, 25cc/min feed

A consideration worth investigating is the effect of a higher conversion over the same volume of reactor, based on a higher reaction rate per unit volume. This scenario could come from either a more active catalyst per unit mass, or more catalyst loaded into the reactor per unit reactor volume. The results of this model are shown in Figure 89 for a longer reactor of 10 times the volume of the lab scale for the same flow.

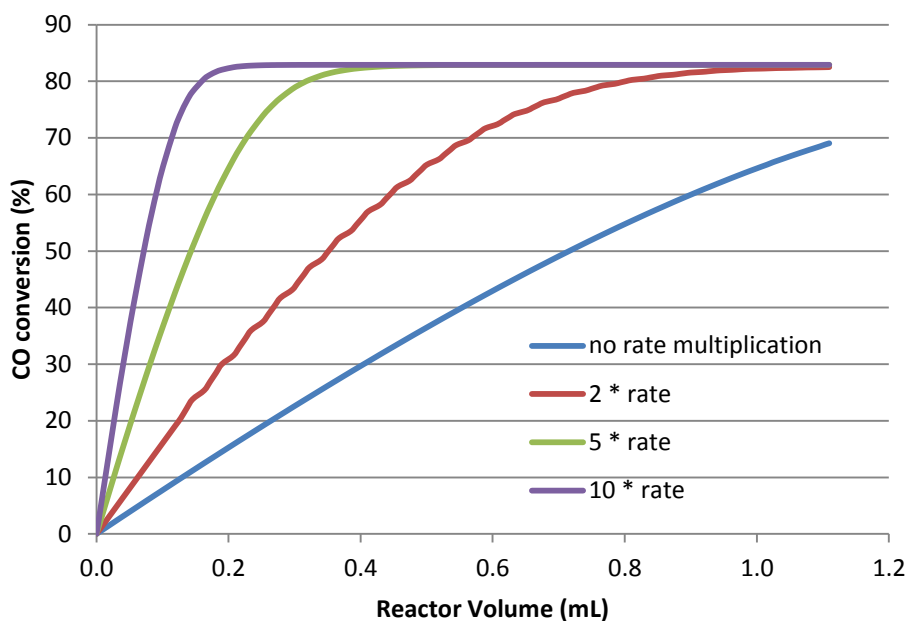


Figure 89: Analysis of estimated conversion over a longer reactor with varying multiplications of the reaction rate per unit volume

As can be seen in the higher rate scenarios the CO conversion tends to asymptote at an approximate value of 75%. This was due to the almost complete consumption of H₂ lowering the partial pressure to the point where the rate was greatly inhibited. The cause of this complete H₂ depletion before complete CO conversion was that the feed gas was at a 2:1 H₂:CO ratio whereas the consumption was at a 2.56:1 H₂:CO ratio based on parameters derived from the selectivity chosen. This shows the importance at higher conversions of a correct H₂:CO feed ratio matched to the consumption ratio.

6.3.1. Mass transfer effects in the microchannel reactor

Thus far only the effects of the kinetics have been discussed, whereas one of the main reasons for performing this modelling work was to investigate whether mass transfer would have a significant effect or whether the commonly held view that microchannel reactors are not limited by mass transfer was applicable to this case.

The simplest method of investigating the effects of mass transfer is to calculate what the concentration of CO would be at the surface of the catalyst compared to the bulk phase, based on the rate of consumption from the kinetics calculated. Ultimately the rate of reaction is based on the concentration at the catalyst surface, therefore, comparison of the concentrations would allow a comparison of the expected rate of reaction. As described in the methodology a combination of Equations 10 and 12 allows one to solve for the partial pressure of CO at the interface.

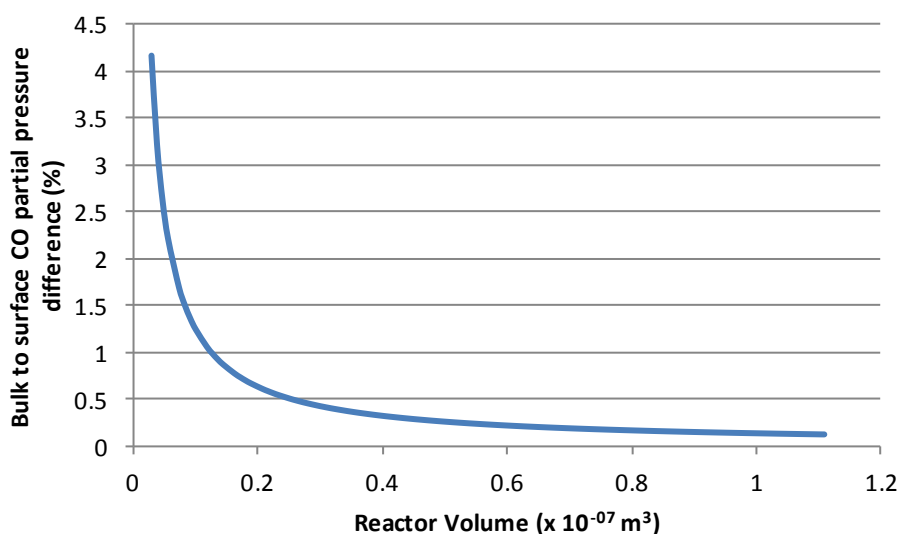


Figure 90: Graph showing the estimated difference in bulk phase to surface partial pressure of CO over the length of the reactor at 240°C, 20 bar, 25cc/min feed

Figure 90 shows that the difference between the bulk phase and surface partial pressure of CO drops off to be very insignificant within a short length of the reactor. The difference is less than the accuracy that the total pressure can be measured experimentally. One could conclude, therefore, that the effects of mass transfer are in fact insignificant in the microchannel reactor. As the channel size increases this will obviously change. The model should give an indication of what channel sizes could be obtained without inflicting significant mass transfer limitation. An increase of channel dimensions, even minor and in the width direction only, would greatly increase the manufacturability of the reactor. This therefore has been examined in Figure 91. It can be seen on fitting an equation the relationship between the partial pressure difference and hydraulic diameter is a squared function. It can be seen that even at a hydraulic diameter of 4mm (compared to 0.26mm hydraulic diameter from experimental work) the mass transfer resistance from the bulk phase to the catalyst surface is still less than 0.5% indicating there is most certainly the potential for increases in the dimensions of the channels in a scaled up scenario.

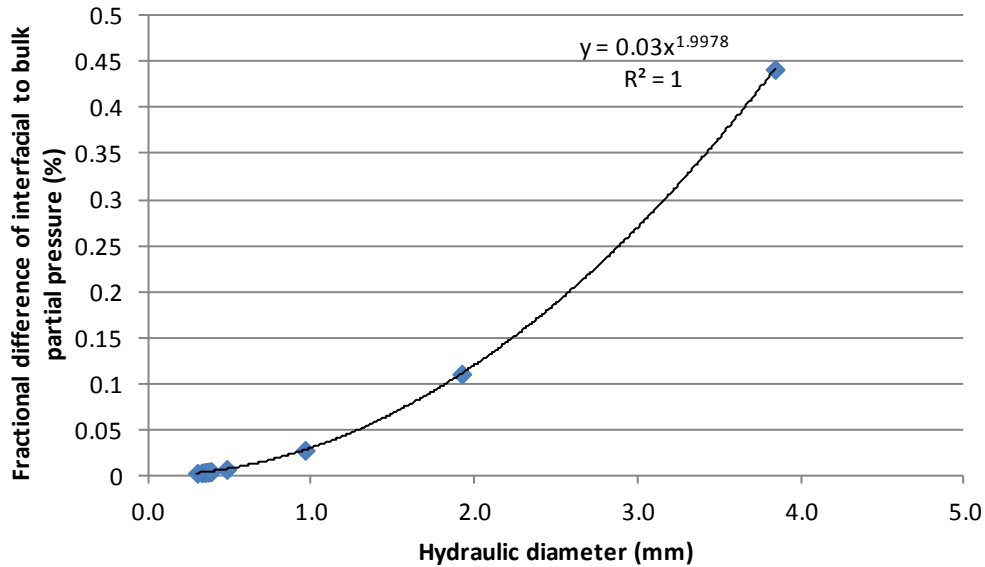


Figure 91: Estimated fractional difference in partial pressure between bulk gas phase and catalyst interface as a function of channel hydraulic diameter. Based on kinetic data at 240°C and 10 bar

The inhibiting factor upon increasing dimensions in this case may become the intraparticle mass transfer resistance, because, to keep the same catalyst mass per unit volume the washcoating layer will be thicker. Investigation of this effect analytically, involves another complete model and is therefore considered outside the scope of this current work. Comment will, however, be made on research into the effects of catalyst layer thickness. Kapteijn et al. (2005) investigated FT synthesis in monolithic coated wall reactors with varying catalyst layer thicknesses from 20 μm to 110 μm . Their conclusion and that of previous work they referred to (Hilmen et al., 2001) suggest that diffusion limitations in the catalyst layer begin to become apparent at thicknesses great than 50 μm . Figure 92 retrieved from Kapteijn et al. (2005) shows the influence on both activity and methane selectivity vs. catalyst layer thickness.

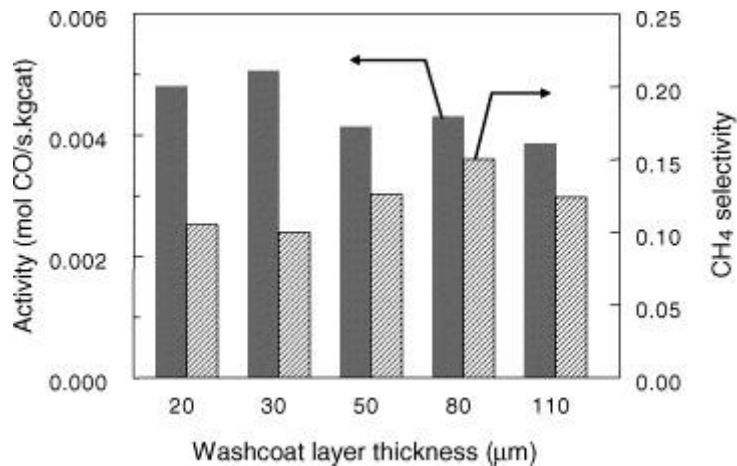


Figure 92: Affect on catalyst activity and methane selectivity with increasing washcoat thickness (Kapteijn, et al., 2005)

One of the effects of a thicker catalyst layer is an increase in methane production and a lower selectivity. This is due to hydrogen having a faster rate of diffusion than CO resulting in a higher H₂:CO ratio at the catalyst surface. The thickness of the washcoat in the microchannel reactor in this research is estimated at 20μm or less suggesting these effects should not be an influence in the experimental work. However, upon increases in catalyst thickness there may need to be consideration for intraparticle mass transfer limitations. This increasing thickness will be a result of increased channel dimensions and should be considered when scaling up the reactor.

6.4. Conclusion

The results of the modelling study allow several conclusions to be made about the microchannel reactor system.

- At lower conversions the rate of reaction throughout the system is virtually linear simplifying rate calculations from experimental data
- The effect of pressure on reaction rate is only significant at pressures below 5 bar. This indicates a lower pressure than typical could be used with still suitable activity
- If targeting higher conversions in the reactor, the feed ratio of H₂:CO needs to be as close as possible to that of the consumption ratio in order to prevent rate inhibition from a low concentration component
- Mass transfer has an insignificant effect, well within experimental accuracy
- The modelling allows further design of larger reactors
- The modelling allows conclusions on the impact of larger channel sizes leading to improved manufacturability of larger scale systems

7. Scale Up Design of the Microchannel Reactor for Small Scale Biomass to Liquid Fischer Tropsch Plants

The intention of this section is to consider the challenges and practicalities for scale up and after consideration of these, along with review of current technology, propose a concept design. From the scaled up design estimation of the cost of various manufacturing techniques can be performed, in turn yielding a cost estimate for the microchannel reactor at the scale required.

7.1. Reactor Scale Up

The intention of this sub-section is to consider the parameters necessary for scaling up of the microchannel reactor. Although microchannel reactors are regarded as being 'simple' to scale up due to the 'numbering up' approach and the predictability of the function of each channel whether on lab or industrial scale, there are still a number of important design variables to be considered. The most pertinent of these are considered in turn.

7.1.1. Reactor volume vs. channel length

The lab scale reactor had a channel length of 37mm. While the width and height of the reactor channels may potentially be held constant during scale up the length certainly can not and therefore estimation of a scaled up length is required. The reactor volume vs. channel length balance is not addressed in the reactor modelling as this considers a volume only. There are practical constraints with channel length in regards to mechanical design, however, these are not particularly tightly limited. For instance if the reactor was designed as a high aspect ratio rectangle the reactor stream could either be cross flow or lengthwise flow. The main consideration therefore is the velocity through the reactor channels. A longer channel will result in a higher velocity per channel, with fewer overall channels, giving the same volume and hence residence time as a lower velocity shorter channel where there are more channels. Due to lack of limitation in mass transfer either should theoretically produce exactly the same conversion. However, the question then becomes what practical influence the velocity will actually have. A higher velocity could be useful to assist in keeping the reactor clear of significant liquids buildup which could cause at the least some minor mass transfer interference, but at worst cause channel blockage. If the velocity is too high there is the potential for creating too much shear and removing the catalyst washcoat. Also a higher velocity may change the flow regimes making the current model void. Therefore, in making the decision two

estimated extremes of channel dimension will be considered under a realistic volume and flow scenario to gauge the impact.

The two extremes examined will be a reactor with channel lengths of 200mm and 2m respectively. The data for the cases are shown in Table 16. Note that a case was also examined where there is 10 times the productivity per unit volume. This is an extrapolation to a case where there is a higher productivity due to either increased catalyst performance per mass unit, or an increased loading of the catalyst in the reactor.

Table 16: Velocity and Reynolds numbers within microchannel reactor with varying activities per volume and reactor length while maintaining consistent residence time

	Case A	Case B	Case C	Case D
CO consumption (mol _{CO} /s/m ³ reactor volume)	4.2	4.2	42	42
Reactor length (m)	0.2	2	0.2	2
Velocity (m/s)	0.019	0.19	0.19	1.9
Reynolds number	0.63	6.3	6.3	63

As can be seen in Table 16 there is quite a significant variation in velocity between Case A and Case D. However, it can be seen that the Reynolds number in all cases places the system well within the laminar flow regime.

Knochen et al. (2010) describe a millistructured reactor scale up prediction with inlet gas velocities of 0.05 – 0.15 m/s in combination with reactor lengths of 0.365 – 1.73 m. These velocities are of similar order to those in Table 16 calculated for the chosen design cases A-C. The reactor lengths described are also similar between this research and that of Knochen. The logical conclusion is that in the range considered, variations of length are not going to have a significant affect on parameters and therefore the channel length could be decided on the practicality of physical reactor dimensions.

7.1.2.Channel dimensions

The channel dimensions created for the lab scale microchannel reactor were effectively based on the smallest that could be technically achieved using the chosen manufacturing technology. Continuing with these channel dimensions, while potentially achievable, may significantly add to the cost of the reactor construction. Chapter 6 showed that in the modelling there was negligible bulk phase to

catalyst surface mass transfer resistance even up to 4-5mm hydraulic diameter. If there are no significant losses in mass transfer performance over larger channels then it would be very sensible to increase the channel size appropriately. This would increase the effective volume of reactor compared to the overall physical reactor size. The other significant advantage, however, is that it opens up further manufacturing directions, where typical macro forming or machining tools may be suitable. The downside, however, of increasing channel dimensions is if catalyst washcoats are used the specific wall surface area to volume ratio will decrease, in turn increasing the required thickness of the washcoating layer for a given reactor volume. If this becomes the case driven by manufacturability or economics then one may need to consider other methods of increasing the surface area of a washcoat such as incorporating metallic foams or similar in the reactor.

7.1.3. Preheating and calcination/reduction heating

In the lab scale system the reactor is heated with electric cartridge heaters which for a somewhat larger lab scale could be suitably scaled up, however, for the scale in question this is not a feasible solution. While the FT reaction is very exothermic and necessitates cooling during online operation, there is the need for preheating as well as calcination and reduction during catalyst preparation which requires temperatures upwards of 400°C. Due to the pressure or level of superheat required it is not feasible to use steam in the cooling channels to achieve this temperature. A proposed system design is one where a gas fired hot air stream is used during the catalyst preparation and preheating stages that utilises the cooling channels. Figure 93 provides a schematic of the design.

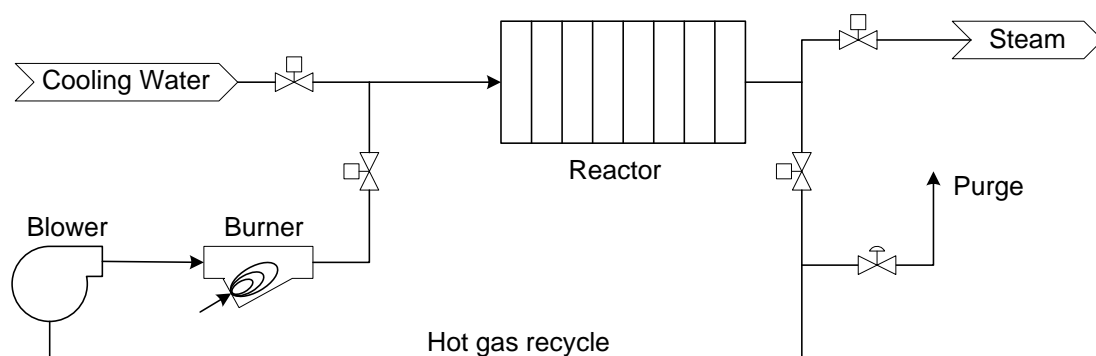


Figure 93: Schematic of gas fired heating of the scaled up microchannel reactor

The cooling system would be shutoff and the heating system engaged to heat the reactor. Once the exothermic FT reaction begins to take place the system can be switched back to steam production to provide the necessary cooling. In this concept it is imperative the gas flame is clear and that water of boiler feed quality is used in order to prevent fouling of the channels.

7.1.4. Catalyst loading

The washcoating method of catalyst addition in the lab scale work was intentionally chosen as one that could be easily scaled up. The method only requires the ability to add a cobalt solution to the reactor and then heat the reactor to the point at which the solvent evaporates and then to a point at which the cobalt salt decomposes to the cobalt oxide. In this case it isn't seen as a significant hurdle to scale up.

7.1.5. Catalyst unloading

While discussing catalyst loading some consideration should be given to catalyst unloading. This is necessary as given the expected catalyst lifetime of approximately 2 years (not withstanding process deviations causing catalyst degradation) it is not long enough to consider the reactor to be an expendible item along with the catalyst. Therefore, it is proposed a solvent wash is first employed to remove the organics in the reactor. This would then be followed by an acid wash that would return the cobalt in the reactor to a soluble salt. The reactor could then be reloaded and put back into service. This certainly isn't a trivial matter and experimental work to determine the success of this method should be performed if a serious path of scale-up is pursued.

7.1.6. Number of reactors vs. size of reactor

This question somewhat comes down to engineering judgement. Multiple reactors would be easier to fabricate although the total cost due to repeated fabrication may be more expensive than the equivalent capacity in a single reactor. However, if specialist equipment such as vacuum ovens are required for diffusion bonding, or for stamping/rolling technology and so forth, smaller reactor sizes may bring down the tooling and equipment costs significantly.

Repetition of process control equipment would increase the cost of multiple reactors. However, the process benefit of having multiple reactors is the ability to take a reactor offline and only lose the appropriate fraction of production depending on the number of reactors installed. This has particular advantage in a newer technology, such as proposed in this research, as an individual reactor problem/optimisation/investigation need not result in entire plant shutdown.

From the above reasoning, until proven otherwise in further studies, the base assumption is that multiple reactors would be a preferential scenario. As a starting point four 25 bbl/day reactors to make a total capacity of 100 bbl/day will be investigated.

7.1.7.Reactor mechanical design

Post answering the questions related to reactor parameters, attention must turn to the mechanical design of the microchannel reactor. The most important considerations are the manufacturability, serviceability, performance and cost of the reactor. Any failing in any of the four will negate any benefit realised by the others. Each of these will be considered in turn.

7.1.8.Manufacturability

As seen in the methodology section wire cutting was used to produce the microchannels in the lab scale reactor. This proved a very suitable technology in this instance as it allowed excellent repeatability between reactor shims, important for experimental comparability. It was also considered to be a realistic method for scale up, at least to a larger lab scale scenario.

Investigation of the cost of manufacture for a significantly larger reactor was undertaken in collaboration with AAA Technology who performed the wire cutting for the lab scale equipment. Figure 94 shows the design that was submitted to AAA Technology for costing. Additional instructions were that each shim would be cut in a stack of 500, where at 0.2mm thick per shim would give a stack of 100mm thick. This is still a small reactor (would need approximately 340 of these to give 100bbl/day production at current production per volume calculations) but was sized to ensure it was compatible with the wire cutting machinery to enable initial costing. Rather than a final design this was an exercise to gauge an order of magnitude idea of costing which could then be scaled up.

The wire cutter costing is based on the length of the cut required. With so many channels the 'perimeter' is approximately 188m which is a very significant length. The suggested cutting rate by AAA technology is an absolute best of 1.2mm/min meaning it will take 2570 hours of machine time. Even at a low price of \$50/hr this equates to nearly \$130,000 just for the wire cutting alone, before any materials have been considered. This would total \$44million in wire cutting alone for sufficient production capacity, which obviously negates using this technology further. Therefore, in further concept design specific attention will be paid to manufacturability.

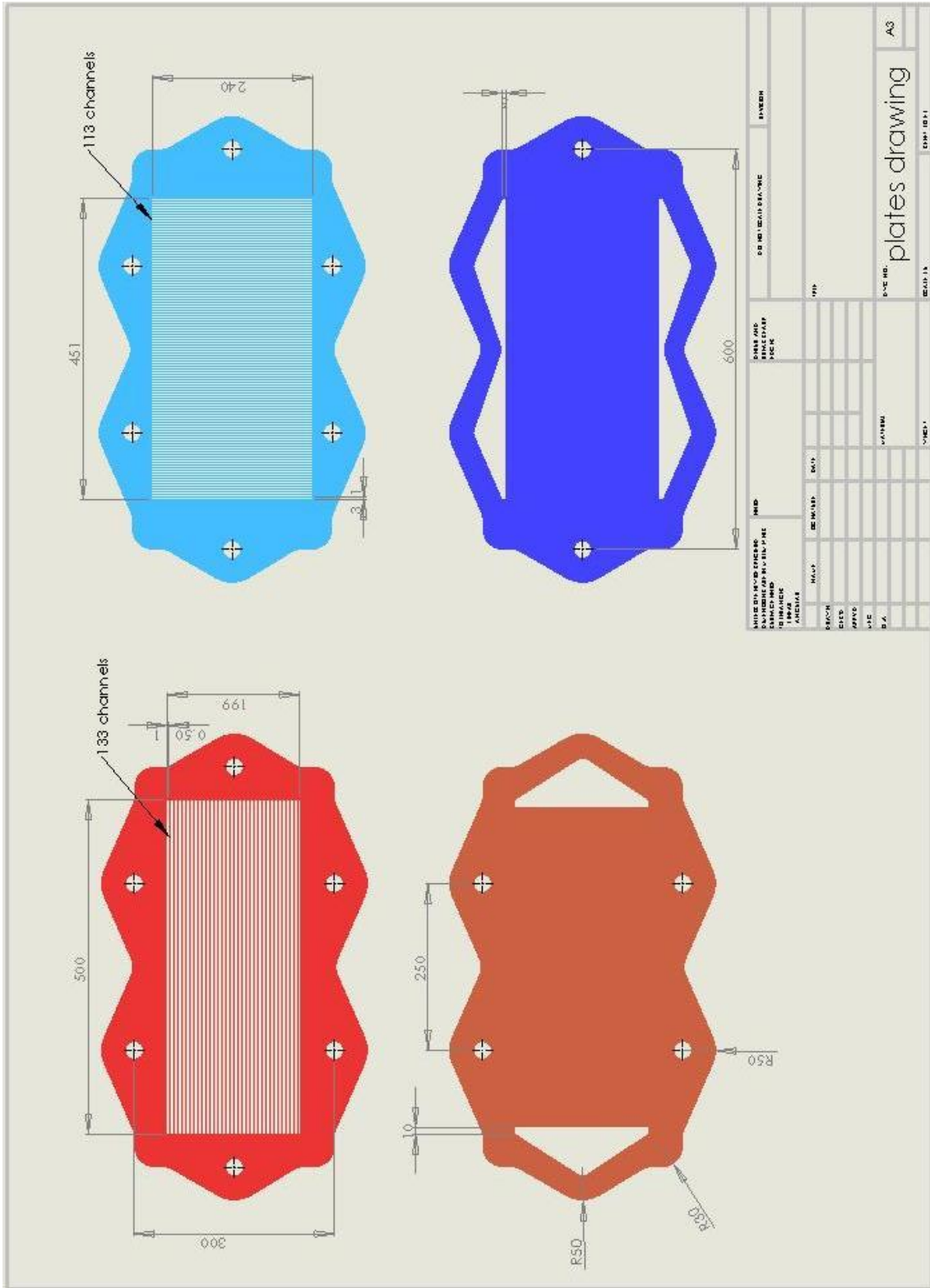


Figure 94: Design basis for wire cutting cost estimation

7.1.9. Serviceability

The ongoing serviceability of the reactor is also deemed important. For longevity and to be sure of leak free operation the reactor shims should be bonded together. This presents difficulties in cleaning the channels in the reactor if required, other than solvent or acid washing. An intermediate solution may be to have a reactor core that is bonded, but with removable manifolding that exposes the channels. One could question, however, other than the above mentioned washes, as to whether there would be the need to access the reactor to clean it.

7.1.10. Performance

The reactor performance depends not only on catalyst activity, but also on the amount of catalyst loaded into the reactor as well as its heat and mass transfer capability with the extra catalyst loading. This becomes particularly relevant with increasing channel dimension, as to keep the same catalyst per reactor volume ratio a thicker catalyst layer will be required. It is assumed the catalyst could still be loaded in the same manner, with a solution followed by evaporation, however, before any actual attempts at scale up are performed this should be investigated experimentally.

7.1.11. Cost

In order to establish the cost a relatively robust idea of final design is necessary. Therefore, before returning to the question of cost, the scaled up design should be established and this will be considered next.

7.2. Current Similar Technology Comparisons

Ideal scaled up design is as yet an unsolved problem as there are many avenues possible to manufacture a microchannel reactor with the required features within the constraints just outlined. A review of similar technology for commercial scale provides a suitable starting point. The commercial equipment examined is based on both reactor and heat exchanger technology due to the overlap in potentially applicable technology.

7.2.1. *Velocys*

As mentioned in the literature review Velocys are attempting to commercialise microchannel based Fischer-Tropsch technology. Changes to their website (Velocys, 2012a) over time create the impression that their reactor design has undergone many iterations to arrive at what is shown today. However, the nature and justification for these design iterations remains confidential. Although information is limited it is possible to gain ideas from a review of their current microchannel reactor design.

Figure 95 and Figure 96 show images of the reactor core showing the channels where a powdered catalyst is loaded and the smaller cross flow cooling channels.

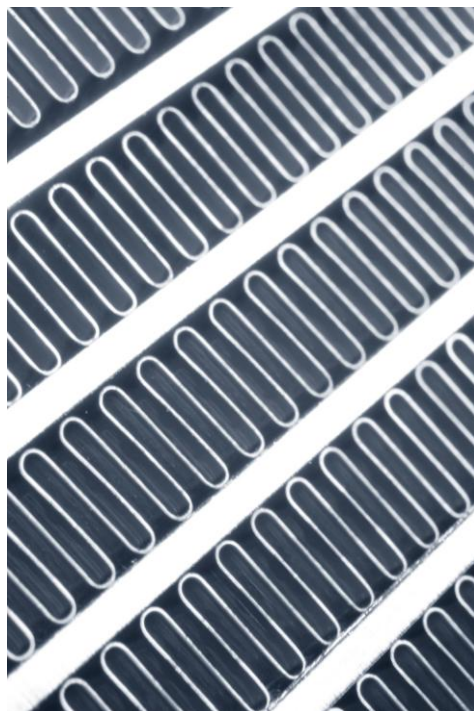


Figure 95: Velocys reactor showing reacting channels (Velocys, 2012b)

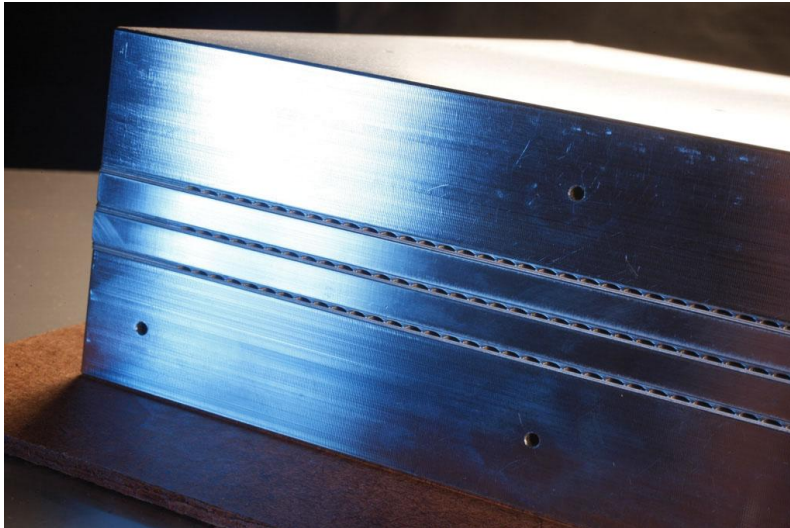


Figure 96: View of reactor showing cooling channels (Velocys, 2012b)

The reactor block shown in Figure 97, and encased in its housing in Figure 98, is reported to produce in the order of 30 bbl/day (Velocys, 2012a). Three of this size would provide sufficient production for the process proposed in this research showing the actual physical size of the microchannel reactors required is quite small.



Figure 97: Core reactor block to produce 30 bbl/day estimated at 600mm in all dimensions (Velocys, 2012b)



Figure 98: Reactor housing for microchannel core (Velocys, 2012b)

It should be noted again, however, that Velocys employ a powdered catalyst in the reactor in a fixed bed form rather than the washcoat as used in this research. This shows why the reactor in Figure 95 exhibits the formed channel structure which appears to have a significantly higher volumetric capacity than that of the cooling channels in order to hold the catalyst required.

7.2.2.Heatric

Heatric could be considered to be the closest comparison to Velocys although they focus more on heat exchange than reaction engineering. They have, however, diversified and proposed case studies for microchannel reactor systems (Johnston, Levy, & Rumbold, 2001). Of interest is the two different options for reactor/heat exchanger production that are employed. The first being chemically etched channels (Figure 99), whereas the second is die formed channels from a sheet (Figure 100). They also produce a heat exchanger which is a combination of the two methods and is shown in Figure 102. Notable is that, apart from the parallel flow of this exchanger, that it is virtually identical in form to that of the Velocys reactor.

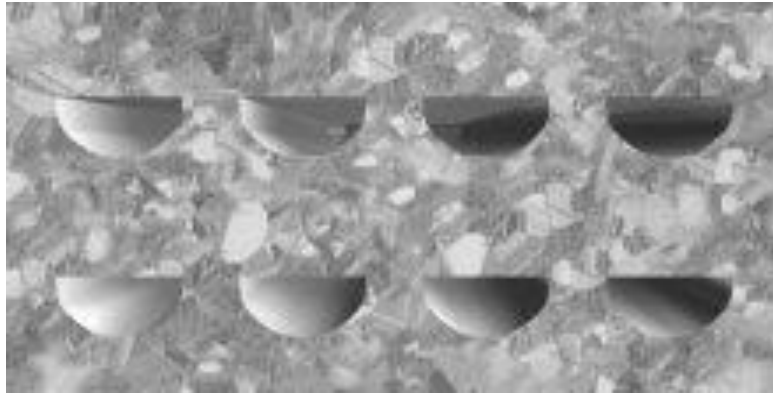


Figure 99: Close-up of Heatric etched channels bonded together (Southall, Le Pierres, & Dewson, 2008)



Figure 100: Example of formed channels for Heatric heat exchangers (Southall, et al., 2008)

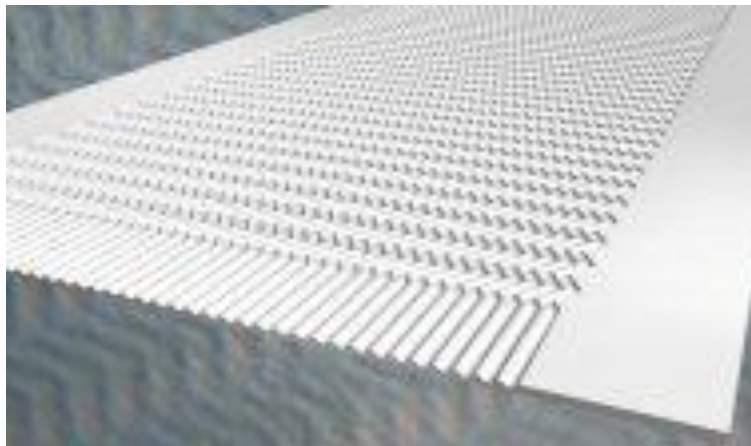


Figure 101: Example of zig-zag etched pattern for Heatric heat exchangers (Southall, et al., 2008)

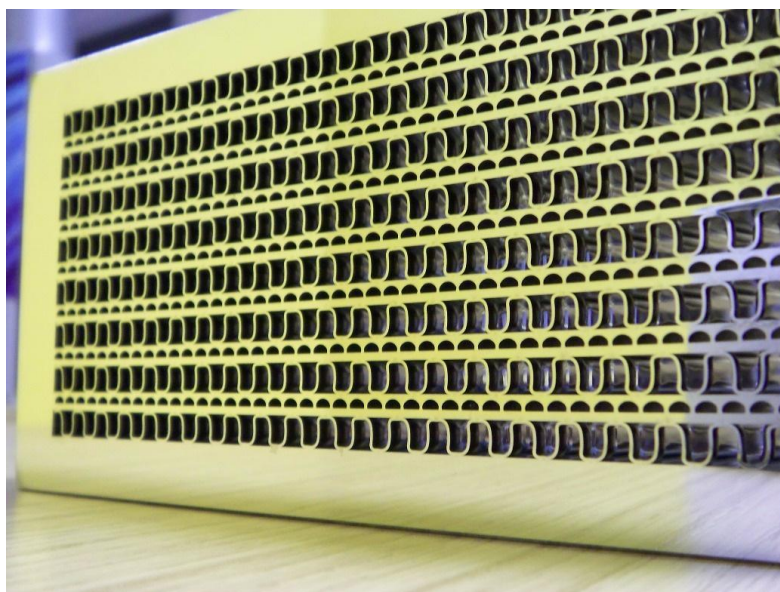


Figure 102: Heatric H2X heat exchanger. It is estimated the folded channels are in the order of 2mm (Southall, et al., 2008)

7.2.3. Plate heat exchangers

An idea proposed by the author is investigation of bonded plate heat exchangers as a reactor. There are a number of variations of heat exchanger on the market which may be suitable for the application and some will be reviewed.

7.2.3.1. Micro plate heat exchangers

One such exchanger type is that produced by Danfoss. Their micro-plate heat exchangers (MPHE) are a very compact design featuring dimpled plates (see Figure 103). Examining their product website and brochures (Danfoss, 2012) shows exchanger thicknesses relating to number of plates \times 1.24mm in the lowest case indicating that when material thickness is taken into account, the actual plate gap must be quite small, most likely sub 1mm. With the dimpled arrangement of the plates this is likely to yield a relatively high surface area to volume ratio suitable for the washcoating method of catalyst loading. The downside to this reactor is that it is only brazed with copper rather than welded with the parent material. Therefore, the temperature handling of this heat exchanger is lower than that required for FT synthesis and reduction/calcination steps.



Figure 103: Expanded view of Danfoss MPHE (Danfoss, 2012)

7.2.3.2. Fusion bonded exchangers

Alfa Laval have a series of heat exchangers called AlphaNova (Alfa Laval, 2012) which are ‘fusion-bonded’ plate heat exchangers (Figure 104). These demonstrate the necessary temperature handling characteristics due to the bonding being between the stainless steel parent material. However, they are not micro by design. One would assume, however, that the two technologies could be combined to make a micro fusion bonded heat exchanger which could be suitable for use as a washcoated reactor.



Figure 104: Example of Alfa Laval fusion bonded heat exchanger (Alfa Laval, 2012)

7.2.3.3. *Welded heat exchanger*

The last example of a heat exchanger presented as part of thinking through scaled up reactor design is that of a welded plate heat exchanger by GEA (GEA, 2012). The benefit of this heat exchanger as can be seen in Figure 105 is the ability to be able to remove panels in order to access the channels for cleaning. Depending on the gasketing on the panels there is potential for high temperature handling, with complete sealing between plates, but still the potential for what would be 'reactor core' access.

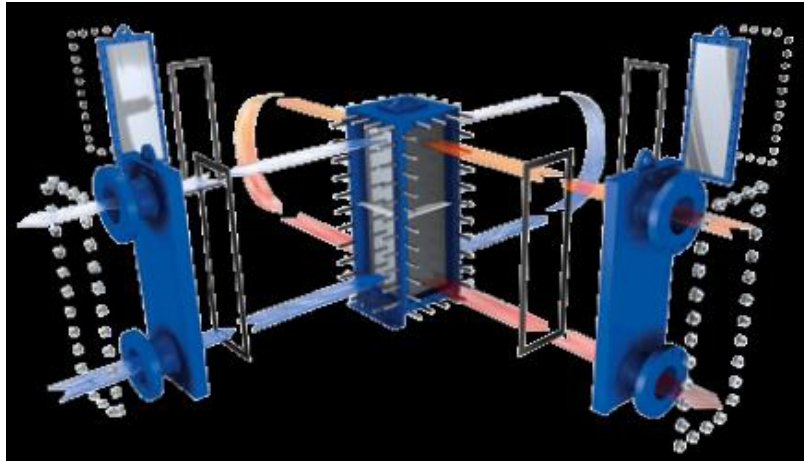


Figure 105: GEA welded plate heat exchanger exploded view (GEA, 2012)

An important parameter when comparing the above reactor/heat exchanger technologies is the surface area to volume ratio. This is particularly relevant due to the proposed washcoated catalyst. The higher the surface area to volume ratio the thinner the catalyst layer possible helping to lower any potential for intra-particle mass transfer limitations. With the 0.3mm by 0.2mm channels used in the experimental work the surface area to volume ratio is 16,700 m²/m³. As a comparison an estimate of the surface area to volume ratio for the Danfoss MPHE is 1,100 m²/m³ minimum but within that order. In literature by Heatric (Johnston, et al., 2001) 2000 m²/m³ is quoted in a reactor design which, as a comparison, is equivalent to 2mm by 2mm channels.

This comparison shows the reactor used in experimentation to be around an order of magnitude higher in specific surface area to what is readily available market technology. If the system could suit this technology, it may be a better avenue to investigate compared to trying to configure the technology to suit a smaller channel reactor system. Therefore, the model produced in Chapter 6 will be utilised to further investigate the effect of larger channels to determine if these, along with their smaller surface area/volume ratio will still provide the performance required for the reactor system. The model has produced a formula that relates the percentage difference between the bulk and interfacial partial pressures to that of hydraulic diameter and is shown in Equation 59.

$$\%diff = 29583d^2 \tag{59}$$

With this formula it can be shown that a hydraulic diameter of 5mm yields a value of 0.74% showing that even at this much larger channel dimension the model predicts very low mass transfer resistance. This shows the attention must certainly turn to the catalyst layer and the optimisation between reactor loading/thickness/surface area.

Despite the above the view is still held that there are significant advantages to a washcoated catalyst as described in this research compared to that of a micro fixed bed reactor. Not least of these being simplicity of catalyst formation and minimal pressure drop. Therefore for continued investigation into scale up costs a reactor with 2mm square channel dimensions will be employed.

7.3. Concept Design for Scaled Up Reactor

The concept design proposed as a relatively simple, and what should be technically feasible, method of increasing the surface area per unit volume is to use a stainless steel mesh to form the channels. An example is shown in Figure 106. Use of the wire mesh in place of shim will lead to a higher surface area available for washcoating. Calculation of the surface area to enable comparison is considered below.

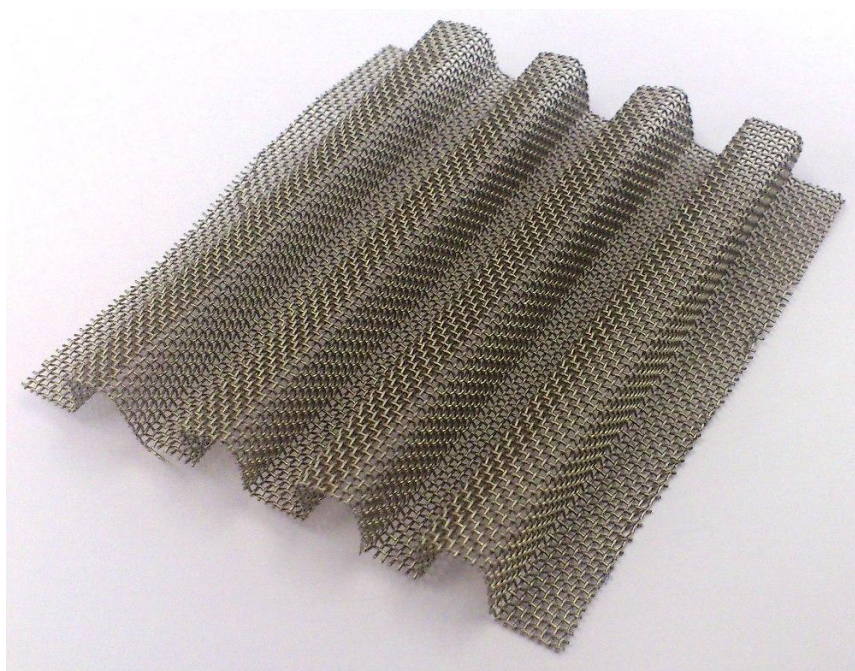


Figure 106: Example of woven stainless steel wire mesh formed into channels

Calculation of the surface area was performed using the following assumptions

- Each wire in the mesh is perfectly round
- The crossover is subtracted from the total wire surface area as a square face
- The wire face touching the parting shim is only just a small part of the face and therefore doesn't lessen the surface area

From these assumptions the surface area of a mesh based microchannel for a 2mm by 2mm channel is $2820 \text{ m}^2/\text{m}^3$ compared to $2000 \text{ m}^2/\text{m}^3$ for a standard shim. This could be considered a substantial improvement. Use of the mesh has other assumed advantages, such as the potential for better turbulence creation and catalyst adherence as well as lower weight and material cost compared to solid shim. While there are still channels there is the possibility of flow being able to pass from one channel to another. This isn't seen as a disadvantage, however, as it may help even out potential

flow imbalances between channels. Also, it partly eliminates the 'double thickness' scenario where a corrugated section is mounted between plates meaning there will be one face in each channel where the heat transfer needs to be through the thickness of the corrugation shim as well as the dividing shim. It is assumed that the cobalt would deposit in the same fashion on the mesh as it would on the wire cut channels. Investigation of this assumption forms part of further investigations into a scaled up design.

An overall arrangement of the concept is shown in Figure 107. It shows cooling channels and mesh reacting channels in a crossflow pattern. It is anticipated on a full scale plant the layers would be diffusion bonded together in order to prevent bypassing and distortion. On a lab scale TIG welding of the external joining edges of the reactor should provide sufficient sealing and mechanical strength.

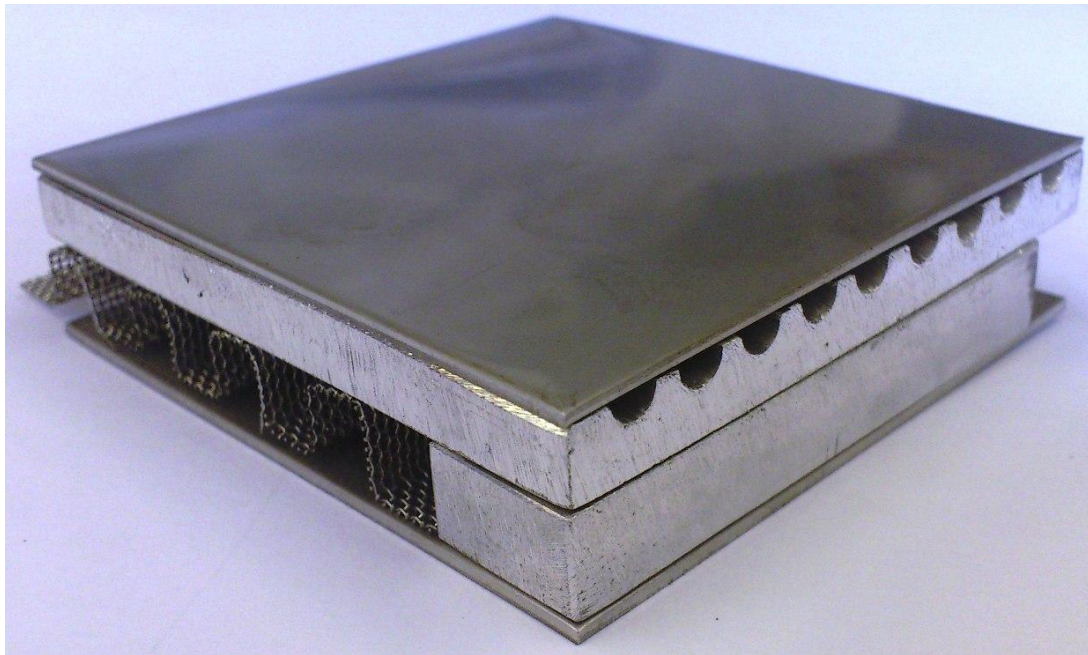


Figure 107: Assembled concept reactor design showing mesh channels and cooling channels in a crossflow pattern. Please note this is not to scale, rather this model was constructed at a size to allow easy visualisation

The arrangement of the overall reactor core with the feed pipework is intended to allow access to the reactor core providing the opportunity for maintenance as well as variations in catalyst loading. The layout is shown in Figure 108.

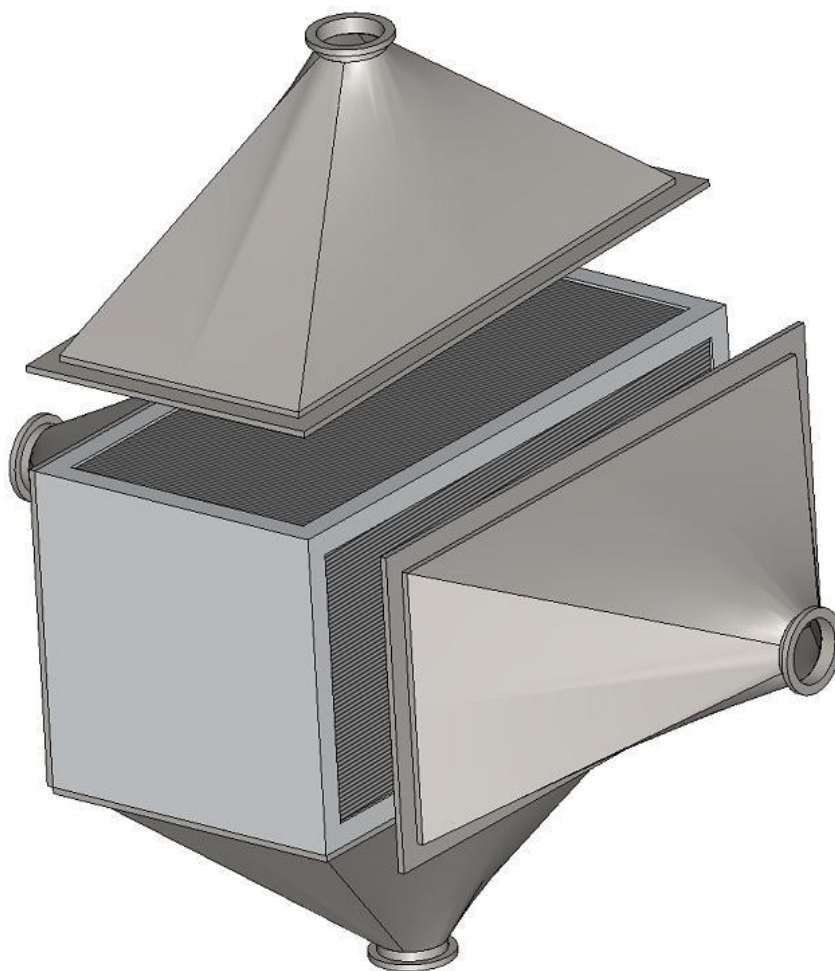


Figure 108: Solidworks drawing showing manifold and reactor core arrangement

Note that in the case of loading the catalyst in situ, a likely scenario would be to change the feed and exit manifolds for the reactor ports to a situation where dead volume is minimised. This is so when a cobalt solution is dried and deposited in the reactor, a significant volume is not ‘wasted’ depositing on the manifolds. This is a waste of catalyst, as well as being unhelpful if it were to provide FT synthesis without appropriate cooling. Changing the manifolding is still a relatively simple job when combined with the simple methodology of catalyst creation/loading.

7.3.1. Estimating reactor construction costs

One of the most significant questions is whether the reactor can be produced at a cost that is more than competitive with existing technology. Because of the specialist manufacturing nature of some aspects of the reactor technology, cost estimation hasn’t been a straightforward task. Rather than relying on likely non-existent correlations for scale vs. price of a microchannel reactor, cost was estimated from first principles of material and manufacturing aspects. This is further explored below.

7.3.2. Costing methodology

7.3.2.1. Material costs

The cost of the raw materials was estimated by design and quantity estimation of the reactor combined with material costs retrieved from New Zealand material suppliers. The design basis being the required volume of reactor with the physical material requirements worked from this point.

The main material requirements estimated for the reactor core are as follows with the items shown in Figure 109.

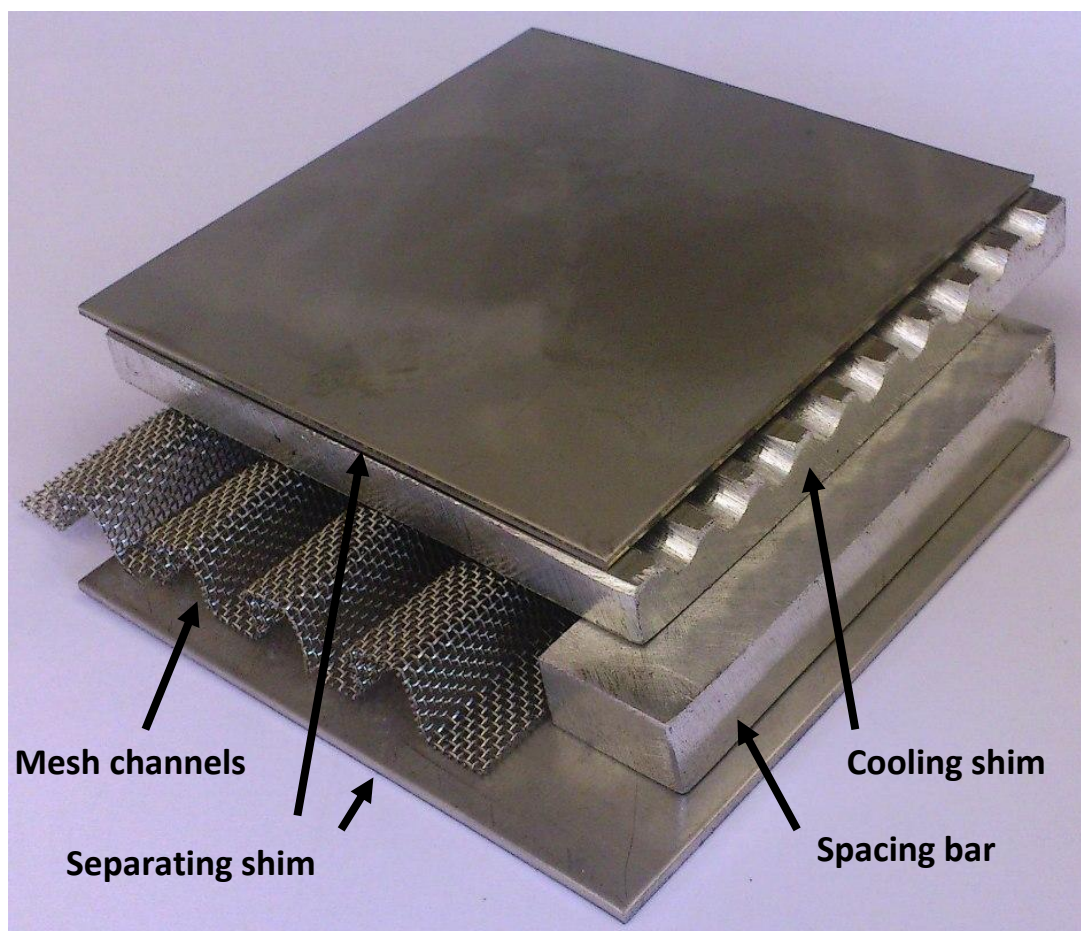


Figure 109: Exploded view of reactor concept showing the individual components

Mesh

The stainless steel mesh chosen is a Steel and Tube Stainless supplied product. The catalogue number is M4100G42. This has 100 by 100 openings per inch, with a wire diameter of 0.1mm, an aperture of 0.15mm and a weight of 0.47kg/m². The product is supplied in a 30m roll 1m wide at a rate of \$37.74 per metre.

Separating shim

There were two avenues of pricing the separating shim. One was the thinnest 316SS sheet that could be supplied from Steel and Tube Stainless at 0.55mm in a 1220mm by 2440 mm sheet. A single sheet is \$124. The second avenue was shim from ACL in Auckland. The shim code was SSS008-12.00 and is 0.2mm thick. The limiting factor of the product is that it comes in 305mm width (with 610mm wide available ex UK). The product is sold by the lineal metre at \$67.97.

It can be seen from the pricing structures of the two materials that the thicker material is significantly cheaper than the shim, surprising given the relative material quantities. The reactor will be priced with both alternatives and the difference compared. One could assume for the shim (as well as any of the other materials priced here) that given the quantity requested significant discounts may apply.

Cooling shim

It is the intention to etch cooling shims from 316SS material. As a base case the thickness of material selected for this sheet is 1mm. This is obtainable through Steel and Tube Stainless at \$225.80 per 1220mm by 2440mm sheet.

Spacing bars

Due to the mesh being used as the reactor channel medium, spacer bars are required that will form part of the diffusion bonding process to seal the reactor from outside leakage, as well as leakage between channels. The material chosen for this exercise is 2mm 316SS from Steel and Tube Stainless, again supplied in a 2440mm by 1220mm sheet at a cost of \$433.59.

Top and bottom plates

The top and bottom plates are to provide mechanical integrity to the reactor, as well as mounting points for reactor support. This is 316SS plate at a thickness of 12mm (chosen as the thickest currently available in New Zealand through Steel and Tube Stainless, thicker may be preferable and would be supplied on an indent basis), supplied in a 3000mm by 1500mm sheet at a cost of \$2950.

7.3.2.2. *Manufacturing costs*

Accurate estimation of the manufacturing cost is seen as a significant challenge due to the potential variables involved. Because there is specialist manufacture such as specific sized corrugations in the

mesh, machinery and tooling costs need to be estimated as part of the manufacturing cost. An assumption has to been made, however, that this could be considered an nth plant costing scenario and the tooling capital for reactor production can be amortised over further production. It was assumed a conservative estimate that 50% of the tooling cost can be amortised over the reactors in question in this study which equates to four reactors producing approximately 80bbl/day of syncrude.

The main operations involved in producing the reactor core are

- Trimming/sizing/cleaning/general handling of material
- Corrugating mesh
- Etching channels
- Diffusion bonding

While the general operations are simple and can be handled on typical equipment the last three are more specialised, with the mesh corrugating requiring a specially tooled press. This corrugation process will therefore be briefly considered.

Corrugating mesh

The simplest method of performing this operation would be to have a press with top and bottom plates with teeth of the dimensions of the channels. Apart from the tooling faces, this is relatively standard and available machinery. The limitation here, however, is that when multiple channels are pressed at once, there would be significant stretching of the material. While this would be unhelpful in the case of a shim, it could prove disastrous for a mesh where the non-welded woven wires would likely be badly distorted. Therefore, consideration of a system where the mesh is pulled into the corrugation as it is formed is necessary. One such system is a set of twin rollers with the corrugation pattern milled into the rollers as shown in Figure 110. Estimating the capital cost of such a system is difficult, although consultation with toolmakers/fitters and machinists provided an approximate estimation of \$80-100,000. Therefore a cost of \$100,000 has been used for this item of specialist equipment. It should be noted that the estimated costing is based around this corrugation tooling producing channels of 2mm square dimensions.

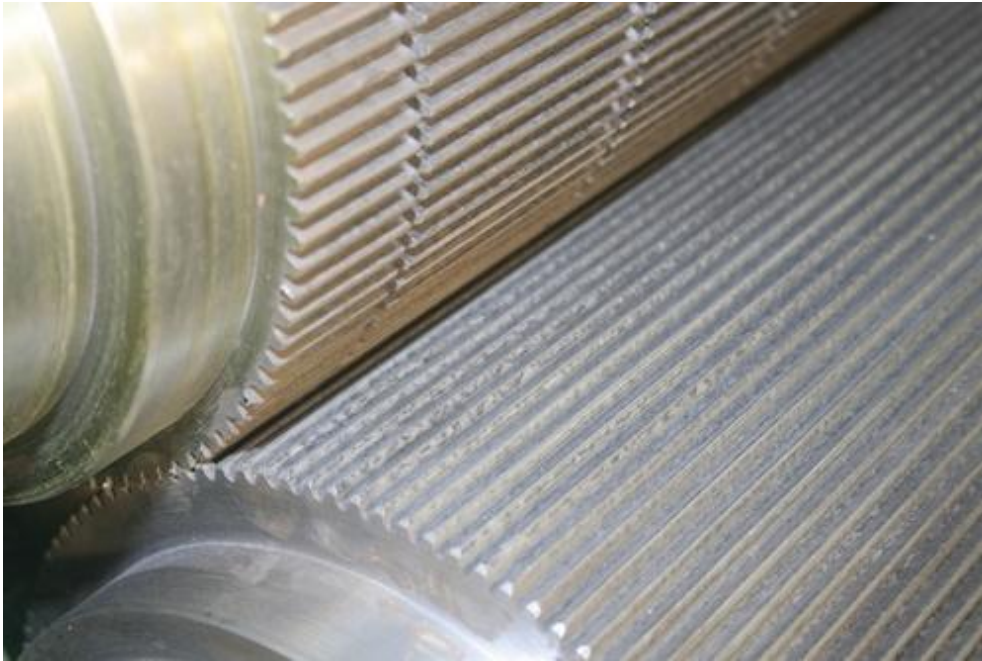


Figure 110: Example of roller style for forming corrugations in the stainless steel mesh (Shree Krishna Engineering Works, 2012)

As suggested earlier it is intended 50% of this capital cost would be amortised against the reactors produced in this study. Also necessary for inclusion is the operational time component for this system. Once the system is running one would assume the plates could be produced on a continuous basis rather expediently. An initial estimate using \$50 per hour gave an operational time cost of less than \$2 per plate. For conservatism and to include other costs such as cleaning and trimming this was upgraded to \$5 per plate.

Etching cost

While not requiring such specialist tooling, the etching process is still a potentially complicated one given the fact that it is not an overly common manufacturing technique, at least in the application given. Rather than trying to calculate a cost an assumed value was produced from inference from literature. Heatric stated (Southall, et al., 2008) that forming saves on material costs and is used for expensive materials whereas etching is suitable when not such a high cost of material is being used. This would tend to indicate the methods are relatively equivalent in terms of cost. Therefore for the purpose of this costing exercise it will be assumed the cost of preparing and etching a cooling layer will be equivalent to that of the cost of the formed layer.

The \$5 handling/cleaning cost per plate has been carried over to the separating shims. A nominal estimation of the cost to have the reactors diffusion bonded is \$20,000 each.

The manifolding has not been priced separately in terms of material cost or manufacturability rather it is considered to be 30% of the reactor core cost. This is assumed to be a conservative over-estimation as this involves relatively routine fabrication work. The combined material and manufacturing costs for the reactors are shown in Table 17.

Table 17: Cost of base reactor and support unit operations for 100 bpd scenario

Productivity	100	bpd
Required reactor volume	9.1	m ³
Split into four reactors	2.3	m ³
Height per reactor	4.2	m
Mass per reactor	15000	kg
Material costs per reactor (\$NZ)		
Mesh	84,000	
Separating shim	46,000	
Cooling shim	84,000	
Spacing bars	6,500	
Top and bottom plates	2,600	
		223,000
Manufacturing costs per reactor (\$NZ)		
Embossing mesh	18,000	
Etching cooling channels	18,000	
Handling/cutting/ shim layer	5,500	
Diffusion bonding	20,000	
		62,000
Framing, pipework at 30% reactor cost		85,000
Total mechanical cost per reactor		370,000
Total for all four reactors (\$NZ)		1,480,000

As can be seen from Table 17 the total cost per reactor is \$370,000 or \$1,480,000 for all four. Note this is the purely mechanical components and does not consist of any control hardware or other peripheral equipment. This will be considered later in the overall costing of the complete plant.

As a comparison Heatric suggested an 8m³ printed circuit heat exchanger used as a reactor to cost in the order of \$US1.5-2m (Johnston, et al., 2001). Taking the volume ratio of 9.1m³ to 8m³ and a NZ to US exchange rate of 0.8 the comparative value estimated in this study is \$US1.04m. This places the estimation of this research slightly below the range quoted from another supplier. It should be noted there is no revenue margin included in this price as would be expected from vendors of such a product, therefore, this estimate appears relatively consistent with that quoted.

To assist in estimating cost for differing reactor sizes a plot has been generated using the costing data as shown in Figure 111. Note that the values in this figure incorporate a factor of 2.5 to give an installed reactor cost.

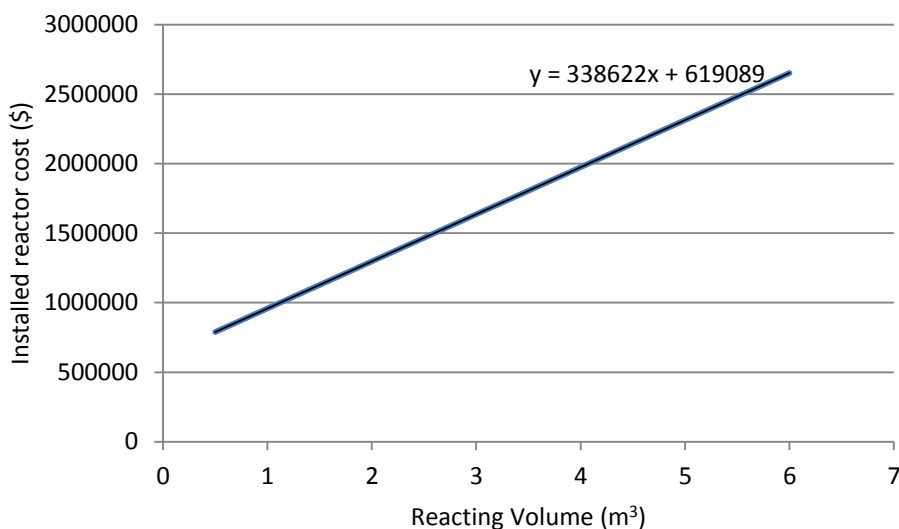


Figure 111: Costing relationship of reactor to reacting volume

From the plot it is possible to obtain an equation for reactor cost per unit reacting volume shown in Equation 60.

$$\text{Installed Reactor Cost (\$)} = 339000 \cdot \text{Vol} + 619000 \quad (60)$$

Where Vol is the reacting volume in m³

One could therefore conclude this design and costing exercise for the microchannel reactor is sufficient to move forward with the techno-economic study based on the cost vs. reactor volume relationship established in this work.

8. Techno-economic Evaluation and Optimisation of Plant Incorporating the Microchannel Reactor

8.1. Introduction

The economic model for the base case, the development of the microchannel reactor and experimental work to obtain operational parameters and allow modelling of a scaled up reactor, as well as the scaled up design and costing of the reactor, all lead to this section of optimising the initial scenario proposed in Chapter 3. While this chapter may be the shortest of the thesis due to the development and methodology occurring in other sections it could be considered the most significant and represents a data based conclusion. This section pulls together the sections to provide perspective into the actual feasibility of a FT based biomass to liquids plant in the New Zealand sawmilling industry based on the research presented in this thesis.

There are effectively two aspects to this Chapter. The first being the influence of changing parameters, particularly pressure, on the overall economics of the existing plant and the second being inclusion of the microchannel reactor in the overall costing. The reasoning, methodology and results of these stages will be reviewed. While the focus is on inclusion of both fore mentioned aspects to generate an overall optimisation, light review will be made of the pressure change affects in the FT plant based on a slurry reactor to enable comparison with the initial work in Chapter 3. From Chapter 3 it was shown the most suitable scenario from an economic perspective was that of the polygeneration arrangement where all the heat and power requirements of the sawmill were met. This meant in off peak times the surplus electricity produced was being sold back to the grid. This scenario has been carried forward and forms the basis for the pressure effect analysis. It should be noted for comparison that the original study in Chapter 3 was based on a 20 bar reactor operating pressure for all of the plant arrangements.

8.2. Optimising for Small Scale – Pressure Effects

One of the significant items of capital cost is the compression stage required to elevate the syngas to a pressure required for effective FT synthesis. The operating cost for the compression stage is also significant due to the high electrical power requirement. On the other hand, as seen in the experimental results, variations in pressure affect both catalyst productivity and selectivity, with lower pressure requiring a larger catalyst load and reactor volume to achieve the same productivity, with higher gas fractions subsequently lowering overall conversion of biomass to liquid fuels. This balance is therefore investigated using the techno-economic model in combination with the experimental data for pressure effects. It should be noted that due to the lower selectivity from the experimental results and the significant negative affect it would have on the techno-economic study the selectivity has not been carried forward from the experimental work. This is reasoned on the basis that further development work is needed on the catalyst in this area before it could be considered sufficient to meet commercial requirements. Rather, the same value of α of 0.87 from the initial techno-economic study has been retained for consistency. It is believed this value is a realistic α target with further catalyst development. In the sensitivity analysis section, modelling has been performed to allow visualisation of the effect of variation in selectivity. Also a scenario with a lower temperature and higher α value has been performed in order to model a typical FT temperature vs. selectivity compromise to gauge the effect.

8.2.1. Slurry reactor based plant pressure effects

A brief comparison of production rate, capital and breakeven crude prices as a function of reaction pressure (2, 5, 10 and 20 bar) have been produced in Table 18 to enable reflection on the initial techno-economic study performed in Chapter 3. Note the model was further optimised by modification of general model variables which has brought down the breakeven cost at 20 bar from \$US 167/bbl to \$US 161/bbl. It can be seen that as the pressure is decreased there is a definitive drop in the breakeven crude price. However the drop is not as significant between the 10 bar and 5 bar scenario. Also noteworthy is the higher production rate at the 5 bar scenario in comparison to the 10 bar scenario. This reflects the optimisation of a complex model. The results are not necessarily as expected or easily able to be fitted to a trend due to the complex interactions within the model. As the pressure is lowered, the cost of compression decreases, as does the parasitic power requirement of the plant therefore lowering the size of the gas engine. At this point the ratio of syngas going to the FT synthesis step has to be modified to optimise the scenario within the model constraints, all while meeting both the heat and power requirements of the sawmill. A caveat for this analysis, however, is that it does not take into account slurry reactor size (and therefore

capital cost) changes for differing pressures. Therefore, due to this fact and the main focus being the economics of a plant with microchannel reactor based technology, further examination of the pressure effects will be based on this arrangement.

Table 18: Changes in production, capital cost and breakeven crude price for a slurry reactor plant as a function of reaction pressure

Operating pressure	Production	Capital Cost	Breakeven crude price
bar	bbl/day	\$NZm	\$US/bbl
2	63	26.5	121
5	88	35.4	146
10	81	34.0	147
20	78	35.6	161

8.3. Incorporation of the Microchannel Reactor into Plant Economics

In the previous Chapter, a methodology was developed for sizing and costing a microchannel reactor. Costing was based on 100bpd production split over four reactors as basis for discussion with this representing the upper end of sizing in the scenarios examined in this thesis. However, the correlation produced for estimating the total reactor cost based on the reacting volume required can be used as shown in Equation 61. This calculation includes a 2.5 installation factor to take into account extra capital expenditure above the base microchannel reactor unit operations for items such as civil works and process control.

$$\text{Installed Reactor Cost (\$)} = 339000.Vol + 619000 \quad (61)$$

Where Vol is the reacting volume in m³

From analysis in the modelling section (Section 6), one can ascertain that the conversion over the length of the reactor remains virtually linear until a little over 70% conversion at which point the partial pressures begin to diminish to a point where the kinetics are affected substantially. Therefore, given that the target once through conversion of the reactor is 70%, for the purposes of calculating the required volume, the kinetic equation established from experimental data (Equation 41) which gives molar conversion of CO as a function of reactor volume will be used to calculate the total required reactor volume at the different pressures examined. The Unisim model as part of the techno-economic model provides flows and composition in and out of the FT reactor. These, along

with the kinetic equation can be used to establish the required volume, at which point the cost can be estimated and included in the economic calculations.

The results of the optimisation for the microchannel reactor scenario are shown in Table 19. It can be seen the capital cost and therefore breakeven price is significantly lower for the microchannel based scenario due to the lower capital cost of the reactor unit operations. Note that as stated previously the slurry reactor based economic estimations did not include varying reactor size for pressure changes. However, the volume vs. pressure relationship has been included for the microchannel reactor scenario. In this case, with lowering pressure, the rate of the reaction reduces in turn requiring the extra capital cost of a larger reactor. This increases the precision of the analysis and produces the results seen in Table 19. Notable here is that the decreasing pressure produces a different breakeven crude price trend compared to that of the slurry reactor scenario in Table 18. One can see that as the pressure drops from 10 bar to 5 bar in the microchannel scenario the breakeven crude price actually increases. This displays a variance in the capital and operating cost balance compared to the slurry reactor scenario in which the increasing capital cost of the microchannel reactor for the lower pressure outstrips the capital and operational advantages gained from lower compression rates. A visual representation of this phenomenon can be seen in Figure 112 which shows the balance between the pertinent model parameters.

Table 19: Parameters of the techno-economic analysis based on differing reaction pressures at 240°C

		Capital Cost (\$NZ)			
		2 bar	5 bar	10 bar	20 bar
Biomass Drying		2,600,000	3,200,000	3,100,000	3,100,000
Feed Handling		2,400,000	2,700,000	2,600,000	2,700,000
Gasifier		2,700,000	3,100,000	3,000,000	3,000,000
Gas Engine		4,200,000	5,800,000	5,800,000	7,000,000
Boiler		460,000	360,000	350,000	340,000
Misc.		170,000	160,000	160,000	160,000
Gas Scrubber		1,100,000	1,400,000	1,300,000	1,300,000
Gas filters and Guard Beds		160,000	220,000	200,000	190,000
Compressor		280,000	1,500,000	1,500,000	2,100,000
Heat exchange		630,000	670,000	670,000	650,000
FT micro reactor		4,300,000	3,900,000	3,100,000	2,800,000
Contingency and Fee		2,800,000	3,500,000	3,300,000	3,500,000
Working Capital		2,200,000	2,700,000	2,500,000	2,700,000
Total		24,000,000	29,000,000	28,000,000	29,000,000
Breakeven price	\$US/barrel	106	120	118	131
Fuel production	kg/yr	2,800,000	3,900,000	3,600,000	3,500,000
	barrel/yr	23,000	32,000	30,000	28,000
	barrel/day	63	88	81	78
Engine power	kW	2,450	3,420	3,410	4,100
Biomass requirement (dry T/yr)		58,000	72,000	68,000	68,000

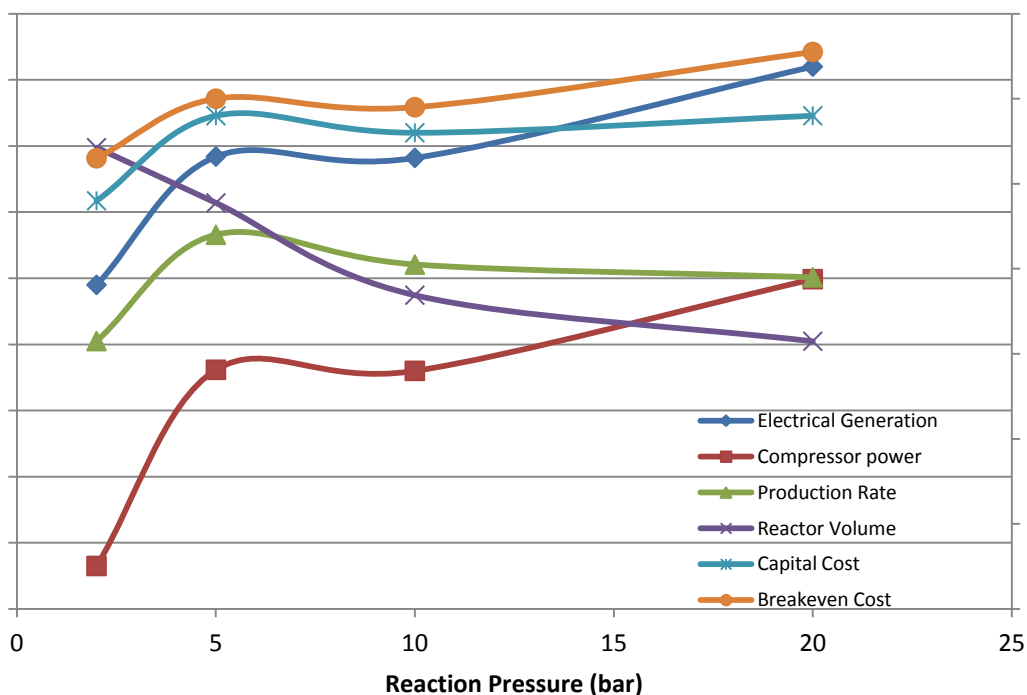


Figure 112: Comparison of the parameters in the techno-economic model at varying reaction pressure. Note the units are ratioed to allow comparison

As can be seen in Figure 112 there is a balance of parameters leading to a relatively flat capital and breakeven syn crude price. As the pressure increases, the compressor power requirement increases requiring higher electrical generation. These increases in capital costs are offset somewhat by the reduction in required reactor volume hence lower reactor capital cost. In the 5 bar scenario the balance of the flows within the model allowed the liquid fuels production to be maximised further than the other scenarios. This can be seen to upset the trend but gives an insight into the effects of a higher fuels production ratio to the heat and electrical production.

While the 2 bar scenario shows the lowest breakeven price overall the author would consider the 10 bar scenario the preferable target. This is due to the fact that while the selectivity was held constant for this analysis, in reality the selectivity will be lower for a 2 bar scenario than a 10 bar given the same catalyst. As can be seen in the sensitivity analysis in Figure 117 this is likely to have a significant affect on the economics.

The overall result of lowering the pressure, performing further model optimisation and including the microchannel reactor concept design has provided a very positive outcome for the economics when compared to the original scenarios from Chapter 3. In comparison to the 20 bar slurry reactor

scenario with a breakeven crude price of \$US 167 per bbl the 10 bar microchannel scenario with a breakeven crude price of \$US 118 per bbl represents a 29% drop in breakeven price, a significant reduction. More importantly, however, the breakeven crude price now falls well within historical crude price trends.

8.4. Sensitivity Analysis

An important aspect is the sensitivity analysis to see the effect of a (likely) change of parameters. The three items selected are the same as in previous sections, the biomass feed cost, the electricity price and the capital cost. The optimised scenario for the microchannel reactor based plant is the basis for the sensitivity analysis.

Figure 113 gives an example of the sensitivity analysis of all parameters for the 10 bar scenario. This is shown to visualise the relative impact of each parameter on the breakeven price. It can be seen that the capital cost, as one may expect, has the most significant affect. While the wood cost doesn't have as significant affect it is likely the area of most vulnerability due to likely price instability.

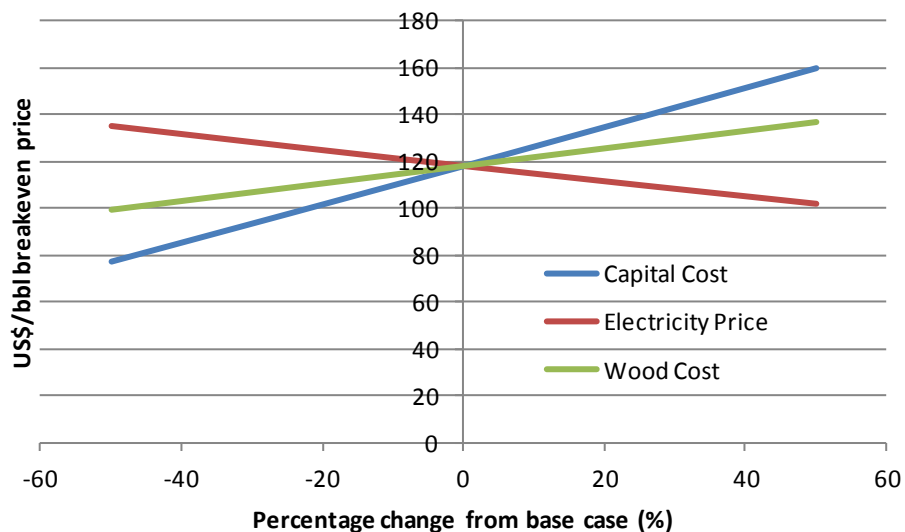


Figure 113: Sensitivity analysis for the 10 bar scenario

Figure 114 to Figure 116 show the sensitivity analysis for each parameter separately so the influence on each can be compared between scenarios. Most situations show a relatively parallel response to changing parameters, only offset by the existing breakeven price differences. However, the 2 bar scenario is the most notable exception, particularly with the electricity price analysis. The reason for

this deviation is that the overall plant is smaller in the 2 bar scenario, although the electricity requirement is still the same, therefore any changes in revenue from electricity sales has a larger impact by proportion on the overall economics of that particular case.

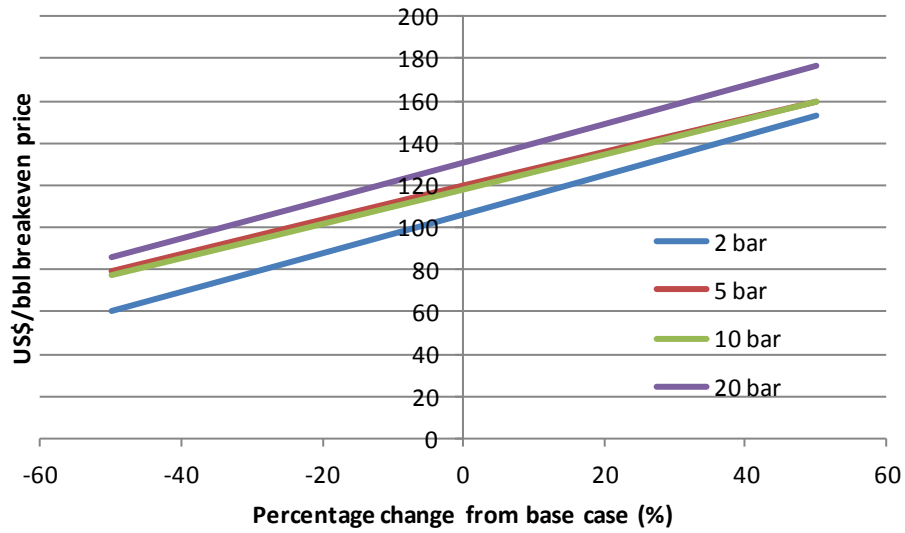


Figure 114: Sensitivity analysis for capital cost for differing pressure cases

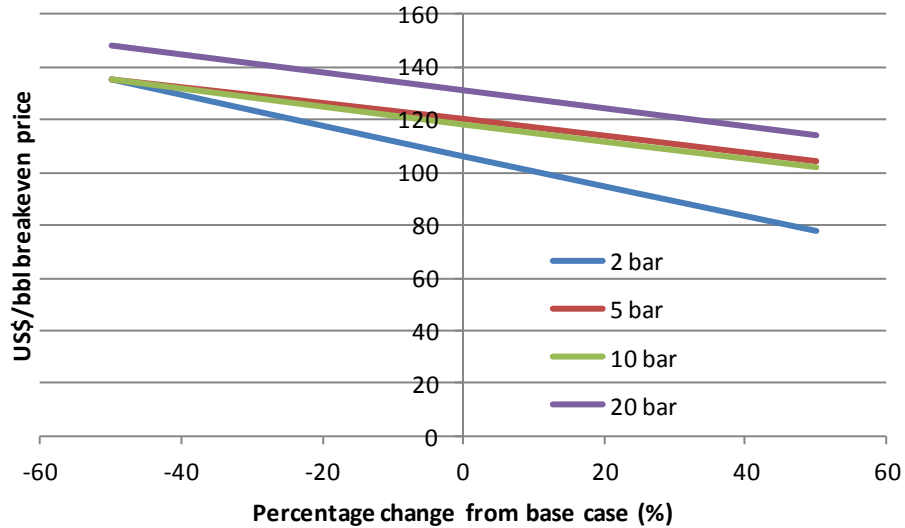


Figure 115: Sensitivity analysis for electricity price for differing pressure cases

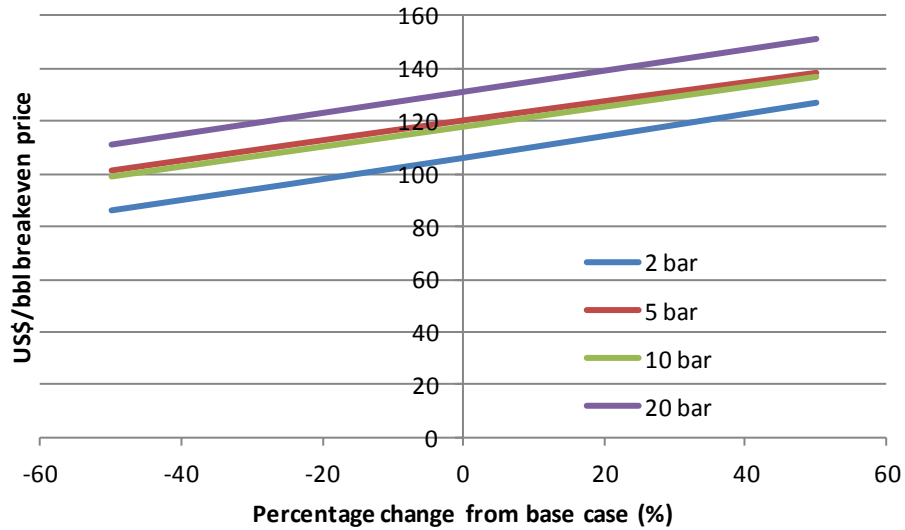


Figure 116: Sensitivity analysis for wood cost

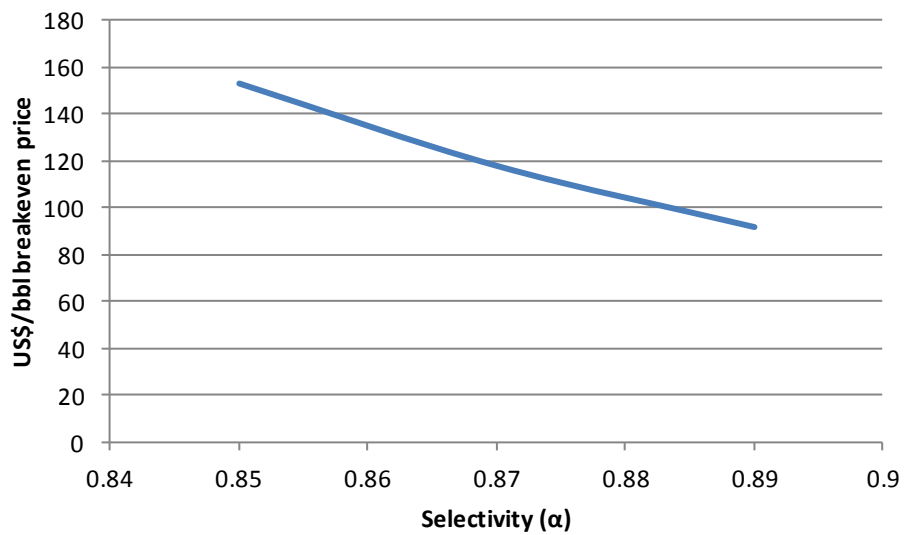


Figure 117: Sensitivity analysis for selectivity for the 10 bar scenario

As shown in Figure 117 a sensitivity analysis for changes in the value of α has been performed on the 10 bar 240°C scenario. It can be seen that in a small range (0.85-0.89) the breakeven syncrude price varies from \$US153/bbl to \$US92/bbl. The reason for the model prediction of this phenomenon is due to the production of 'collectable' products vs. production of off gas. With a lower alpha value, a higher fraction of the gas that goes through expensive cleaning and compression steps simply becomes gaseous fuel for the gas engine, in turn lowering the overall economics. Given that the α value does in fact have a tremendous effect on the economics of the process anything that can be done to improve the α value obtainable by the catalyst in question should be performed. There can

afford to be a reasonable sunk cost in catalyst development or other more expensive catalyst components to achieve this higher α value. Consideration can also be given to lowering the operating temperature of the reactor. This will lower the catalyst/reactor productivity but the increased reactor volume and catalyst cost may very well be offset by the improved process performance from the higher selectivity.

8.4.1. Varying temperature and selectivity

As a final comparison for completeness a scenario where the temperature is lowered, but the selectivity is increased, is compared in order to replicate an assumed realistic scenario based on the known relationship between temperature and selectivity. The temperature and selectivity selected are 225°C and an α of 0.89. This is compared to the 10 bar scenario with a temperature of 240°C and an α of 0.87. To account for the differences the UniSim model temperature has been changed and a new kinetic rate for the lower temperature established which will in turn affect reactor volume and capital cost. The modelling results are shown in Table 20.

It can be seen in Table 20 that even though the kinetics at 225°C are only 45% of that at 240°C the breakeven price is lower than for the higher temperature, lower α scenario. Table 20 shows the capital cost of the reactor has increased significantly in this scenario, once again highlighting the need for the combination of high activity and high selectivity. This area of catalyst development has the most potential for affecting the economics in a positive way.

Table 20: Parameters of the techno-economic analysis based on a 10 bar, 225°C, $\alpha = 0.89$ scenario

		Capital Cost (\$NZ)
	Biomass Drying	3,200,000
	Feed Handling	2,700,000
	Gasifier	3,000,000
	Gas Engine	5,800,000
	Boiler	350,000
	Misc.	160,000
	Gas Scrubber	1,300,000
	Gas filters and Guard Beds	210,000
	Compressor	1,600,000
	Heat exchange	690,000
	FT micro reactor	6,400,000
	Contingency and Fee	3,800,000
	Working Capital	2,900,000
	Total	32,000,000
Breakeven price	\$US/barrel	107
Fuel production	kg/yr	4,800,000
	barrel/yr	40,000
	barrel/day	108
Engine power	kW	3,410
Biomass requirement (dry T/yr)		71,000

9. Conclusions, Recommendations and Perspective

9.1. Conclusions of current work

From the literature review, some main conclusions were made that shaped the development of the research in the thesis. These were

- Commercial plants are all of significant scale necessitating a shift of thinking to allow financial viability on a smaller scale
- Catalyst nano-particle size is important
- Microchannel reactor technology is a promising development for FT synthesis

Three techno-economic scenarios were investigated using a polygeneration design based with a traditional slurry reactor and sawmill integration. Firstly, one that meets all the on peak electrical needs and the heat needs of the sawmill, secondly one that meets the off peak electrical requirement and all the heat needs of the sawmill and thirdly one with no power generation but meeting the heat needs of the sawmill. The most economic scenario was the first where all on peak electrical and heat needs are met, yielding a capital cost of \$36m with a breakeven syncrude cost of \$US167 per barrel. The economics show high sensitivity to capital cost changes, however, although the sensitivity is less for wood price variation, this has the most potential for significant fluctuation and is therefore seen as the area of most vulnerability.

The chemical etching technique for producing microchannels is difficult to perform reliably and repeatably on stainless steel. Either significant development of the technique, or a change in material would be required to pursue this method further. The wire cutting technique for forming microchannels proved very appropriate for the lab scale scenario used.

SEM analysis of the microchannels with catalyst showed an excellent fibril arrangement which would exhibit high surface area. The fibrils were in the order of 300nm long and approximately 15 nm wide. A further development in regard to these observations would be to view images both before and after online running of the catalyst. This will require developing techniques to be sure there are no hydrocarbons remaining in the after sample.

Kinetic rates based on volume per unit of reactor were generated for both the neat cobalt and the cobalt on titania washcoat. They are shown in Equations 62 and 63 respectively.

$$-r_{CO} = \frac{2367P_{CO}P_{H_2}}{(1 + 30.56P_{CO})^2} \quad (62)$$

$$-r_{CO} = \frac{1625P_{CO}P_{H_2}}{(1 + 24.3P_{CO})^2} \quad (63)$$

The catalysts showed similar performance per unit of reactor volume, leading to the conclusion that the neat cobalt washcoat for similar performance, is a simple and robust method of catalyst preparation and is therefore considered the preferable catalyst of the two.

Although the total run timeframe of each catalyst was several hundred hours, changing conditions made analysis of deactivation difficult. Therefore a longer run where the catalyst is maintained under consistent conditions for 500-1000 hours would be seen as beneficial to gauge the long term performance.

While the performance was presented on a per volume of reactor basis, ultimately the productivity is produced by the actual mass of active and available catalyst sites. Therefore, further investigation into the amount of catalyst that can be loaded into the channels, while still providing adequate performance per unit mass of catalyst could be investigated. This has a direct inversely proportional relationship to reactor volume therefore is an important parameter to consider.

In order for the catalyst to be considered useful in a commercial context the selectivity to higher weight hydrocarbons needs to be increased. When considered in the economic analysis the selectivity had the most significant affect on economics out of any parameter. Therefore, this could be considered to be the most important focus of catalyst improvement in this context.

The modelling of reaction rate over the length of the microchannel showed that at lower conversions the rate is virtually linear. This shows that the rate measured in the experiments is representative of the actual kinetic rate so back calculation from measured rate to actual rate on the catalyst particle using the model in Section 6 is not necessary.

From plotting of a longer reactor with higher conversion it is shown that little productivity per unit volume is lost by reducing the reaction pressure from 20 to 10 bar, therefore this is seen as potential economic leverage for a smaller scale plant.

The H₂:CO ratio of the feed gas being close to that being consumed in the reaction is very important at high conversion, otherwise one component will significantly lower in partial pressure, in turn slowing the reaction rate.

The mass transfer resistance was shown to be insignificant from the bulk gas to the catalyst surface at the channel dimensions in the experimental work. Even increasing the channel dimensions up to 4-5mm doesn't have a significant effect, although the relationship developed by the model showed mass transfer resistance to be a squared relationship in relation to channel hydraulic diameter. Therefore above these dimensions the mass transfer resistance would increase very quickly.

The capital cost per unit volume was estimated on the total reactor volume being split between four reactors. A formula of reactor cost per reacting volume has been proposed as shown in Equation 64.

$$\text{Reactor installed cost (\$NZ)} = 339000 \times \text{Vol} + 619000 \quad (64)$$

Where vol is in m³

The techno-economic study performed in Chapter 3 was further developed by incorporation of the microchannel reactor as well as changing the reaction pressure. This was based on a plant that met all the on peak electrical and heat requirements on the premise that this arrangement showed the most potential in the first study. Lowering the pressure and incorporating the microchannel reactor reduced the breakeven syncrude price to \$118 per barrel in the 10 bar reaction pressure case. Again, as with the economics in Chapter 3, the sensitivity analysis showed similar trends with capital cost variation having the most affect, followed by electricity and wood with similar sensitivity. Selectivity was found to have the most profound effect on economics. For example, even a drop in temperature to 225°C with a much lower reaction rate, with an increased α from the assumed value of 0.87 to 0.89, still lowered the breakeven syncrude price (\$US107 per barrel).

9.2. Recommendations

One of the most significant challenges realised by the author in the completion of this work was to contain the scope of the work, knowing there were more avenues that would be of benefit to investigate, but at the same time being realistic about the time and resources available. Therefore this section will reflect on some of this, as well as recommendation as to further application of the conclusions generated in this work.

Further development in an attempt to raise the α value is seen as one of the first priorities in continuing work on this project due to the significant affect on the economics. This could take the form of catalyst modification such as the addition of precious metal promoters or operational changes such as water vapour addition with the feed gas. With further optimisation of the selectivity, consideration should be given to inclusion of variations of selectivity with operating conditions within the economic model. This will lead to a tightening of the real life applicability of the economic model.

Experimental investigation of changes in channel dimensions and catalyst loading/catalyst thickness would assist in validating the modelling work particularly around the 2mm channel dimension area, or showing need for further, more complex models to account for other resistances to mass transfer than bulk phase to catalyst interface mass transfer. This will assist in adding robustness and verifying assumptions in scale up to reactors of several m³.

An improvement to the experimental rig would be the incorporation of a mass flow controller, rather than the mass flow meter currently installed. In conjunction with this a back pressure regulator instead of the current needle valve would provide greater experimental accuracy. This is obviously a significant expense and the system certainly is workable in its current state, however, it is noted as a worthwhile improvement to continue improving experimental robustness. Development of a method for accurately quantifying the mass of catalyst in the reactor channels is also seen as an area that could help improve experimental accuracy and may be of consideration if someone were to continue with rigorous catalyst development. As part of this an increased suite of experimental data would improve the robustness of kinetics for scale up, acknowledging the current scale up calculations are based on limited data.

If there is sufficient progression in these fore mentioned areas and continued interest is generated in the project then two aspects could be seen as an opportunity to push forward. The first being a slightly scaled up lab scale reactor using the full scale design proposed in this thesis configured to run with the University of Canterbury dual fluidised bed gasifier. The second being a fuller techno-economic model with more detailed design and costing in order to improve the accuracy of the capital and operating cost estimation. It is believed these two aspects will assist in decision making as to whether further avenues are progressed in terms of actual scale up of the process.

9.3. Final Perspective

The first thing that must be said is the author has become more convinced throughout the course of this research that something must be done to address the current consumption of fossil fuels. Regardless of whether it is FT or pyrolysis, mixed alcohols or any other combination of technology, the fact that research needs to continue into these technologies is paramount. However, the author regards FT to be near the top of the list of renewable liquid fuels due to the 'drop in' ability of the product. While other technologies can produce fuel, there often needs to be modifications to the vehicle to enable the ability to run such fuels. Biodiesel from FT is a superior fuel, able to be run in conventional engines and is cleaner burning than fossil based diesel.

New Zealand is very well placed in terms of renewable resources for energy. Much of this has been harnessed for electricity production such as hydro, however, taking advantage of these resources for liquid fuels production is certainly lagging. A continuing backtrack from the government on targets and incentives for biofuels production adds to the frustration. However, as seen in this research the predicted breakeven price for the microchannel reactor based polygeneration scenario is lower than recent crude oil price peaks. This allows financial justification for the process outside of subsidies. This reasoning, along with the fact the microchannel reactor based polygeneration design while novel, requires no specialist forms of manufacture that aren't already available in industry, leaves one to hope the technology will garner investment interest.

10. References

- Ajmera, S. K., Delattre, C., Schmidt, M. A., & Jensen, K. F. (2002). Microfabricated Differential Reactor for Heterogeneous Gas Phase Catalyst Testing. [doi: 10.1006/jcat.2002.3584]. *Journal of Catalysis*, 209(2), 401-412.
- Alfa Laval. (2012). Fusion bonded heat exchangers. Retrieved from <http://www.alfalaval.com/solution-finder/products/alfanova/pages/howitworks.aspx>
- Almeida, L. C., Echave, F. J., Sanz, O., Centeno, M. A., Arzamendi, G., Gandía, L. M., et al. Fischer-Tropsch synthesis in microchannels. [doi: DOI: 10.1016/j.cej.2010.09.091]. *Chemical Engineering Journal, In Press, Corrected Proof*.
- Almeida, L. C., Echave, F. J., Sanz, O., Centeno, M. A., Arzamendi, G., Gandía, L. M., et al. (2011). Fischer-Tropsch synthesis in microchannels. [doi: 10.1016/j.cej.2010.09.091]. *Chemical Engineering Journal*, 167(2-3), 536-544.
- Atashi, H., Siami, F., Mirzaei, A. A., & Sarkari, M. (2010). Kinetic study of Fischer-Tropsch process on titania-supported cobalt-manganese catalyst. [doi: 10.1016/j.jiec.2010.04.005]. *Journal of Industrial and Engineering Chemistry*, 16(6), 952-961.
- Atkinson, D. (2010). Fischer-Tropsch reactors for biofuels production: new technology needed! *Biofuels, Bioproducts and Biorefining*, 4(1), 12-16.
- Bahome, M. C., Jewell, L. L., Hildebrandt, D., Glasser, D., & Coville, N. J. (2005). Fischer-Tropsch synthesis over iron catalysts supported on carbon nanotubes. *Applied Catalysis A: General*, 287(1), 60-67.
- Bahome, M. C., Jewell, L. L., Padayachy, K., Hildebrandt, D., Glasser, D., Datye, A. K., et al. (2007). Fe-Ru small particle bimetallic catalysts supported on carbon nanotubes for use in Fischer-Tropsch synthesis. *Applied Catalysis A: General*, 328(2), 243-251.
- Bartholomew, C. H. (2001). Mechanisms of catalyst deactivation. [doi: 10.1016/S0926-860X(00)00843-7]. *Applied Catalysis A: General*, 212(1-2), 17-60.
- Bezemer, G. L., Radstake, P. B., Falke, U., Oosterbeek, H., Kuipers, H. P. C. E., Van Dillen, A. J., et al. (2006). Investigation of promoter effects of manganese oxide on carbon nanofiber-supported cobalt catalysts for Fischer-Tropsch synthesis. *Journal of Catalysis*, 237(1), 152-161.
- Bezemer, G. L., Radstake, P. B., Koot, V., Van Dillen, A. J., Geus, J. W., & De Jong, K. P. (2006). Preparation of Fischer-Tropsch cobalt catalysts supported on carbon nanofibers and silica using homogeneous deposition-precipitation. *Journal of Catalysis*, 237(2), 291-302.
- Bolhar-Nordenkamp, M., Vogel, A., Hofbauer, H., Kaltschmitt, M. (2004). *Analysis and Evaluation of the Production of Fischer-Tropsch Fuels from Biomass*. Paper presented at the 2nd World Conference and Exhibition on Biomass.
- Bouchy, C., Hastoy, G., Guillon, E., & Martens, J., A. (2009). Valorisation des cires de Fischer-Tropsch par hydrocraquage et hydroisomérisation sélective. *Oil & Gas Science and Technology - Rev. IFP*, 64(1), 91-112.
- Bouman, R. W., Jesen, S. B., Wake, M. L., & Earl, W. B. (2005). *Process Capital Cost Estimation for New Zealand 2004*. Christchurch: Society of Chemical Engineers New Zealand.
- Briscoe, M. D., Cao, C., Chin, Y.-H., Daly, F. P., Gano, N., Hu, J., et al. (2006). US Patent No. US 7084180 B2.
- Brown, J. (2006). *Biomass gasification : fast internal circulating fluidised bed gasifier characterisation and comparison*. University of Canterbury, Christchurch.

- Brownlee, G. (2008). Biofuel Obligation Law Repealed. Retrieved from <http://www.beehive.govt.nz/release/biofuel-obligation-law-repealed>
- Brownlee, G. (2009). Biodiesel Grants Scheme off to a strong start. Retrieved from <http://www.beehive.govt.nz/release/biodiesel-grants-scheme-strong-start>
- Bull, D. (2008). *Performance improvements to a fast internally circulating fluidized bed (FICFB) biomass gasifier for combined heat and power plants*. University of Canterbury, Christchurch.
- Cao, C., Hu, J., Li, S., Wilcox, W., & Wang, Y. (2009). Intensified Fischer-Tropsch synthesis process with microchannel catalytic reactors. *Catalysis Today*, 140(3-4), 149-156.
- Castro, S., Gayoso, M., & Rodriguez, C. (1997). A study of the combustion method to prepare fine ferrite particles. *Journal of Solid State Chemistry*, 134(Copyright 1998, IEE), 227-231.
- Chen, N. H., & Othmer, D. F. (1962). New generalized equation for gas diffusion coefficient. *Journal of Chemical and Engineering Data*, 7(1), 37-41.
- Chen, W., Fan, Z., Pan, X., & Bao, X. (2008). Effect of confinement in carbon nanotubes on the activity of Fischer-Tropsch iron catalyst. *Journal of the American Chemical Society*, 130(29), 9414-9419.
- Chin, Y.-H., Hu, J., Cao, C., Gao, Y., & Wang, Y. (2005). Preparation of a novel structured catalyst based on aligned carbon nanotube arrays for a microchannel Fischer-Tropsch synthesis reactor. *Catalysis Today*, 110(1-2), 47-52.
- Choren. (2011). Beta Plant. Retrieved 30 March, 2011, from <http://www.choren.com/en/carbo-v/references/beta-plant/>
- Collins, J. P., Font Freide, J. J. H. M., & Nay, B. (2006). A history of Fischer-Tropsch wax upgrading at BP - From catalyst screening studies to full scale demonstration in Alaska. *Journal of Natural Gas Chemistry*, 15(Compendex), 1-10.
- Commenge, J. M., Falk, L., Corriou, J. P., & Matlosz, M. (2002). Optimal Design for Flow Uniformity in Microchannel Reactors. *AIChE Journal*, 48(2), 345-358.
- Cox, B. (2008). Where May Gasification Fit in the New Zealand Bioenergy Market, *Presentation at Biomass Gasification Technology and Biomass Energy Conference: 13 February 2008*. University of Canterbury, Wood Technology Research Centre.
- Dalai, A. K., & Davis, B. H. (2008). Fischer-Tropsch synthesis: A review of water effects on the performances of unsupported and supported Co catalysts. *Applied Catalysis A: General*, 348(1), 1-15.
- Damartzis, T., & Zabaniotou, A. (2011). Thermochemical conversion of biomass to second generation biofuels through integrated process design-A review. *Renewable and Sustainable Energy Reviews*, 15(Compendex), 366-378.
- Danfoss. (2012). MPHE Product description. Retrieved from <http://heating.danfoss.com/Content/3602F3CE-F2F0-43B2-82C3-87340E6A4457.html>
- Davis, B. H. (2001). Fischer-Tropsch synthesis: Current mechanism and futuristic needs. *Fuel Processing Technology*, 71(1-3), 157-166.
- Davis, B. H. (2005). Fischer-Tropsch synthesis: Overview of reactor development and future potentialities. *Topics in Catalysis*, 32(3), 143-168.
- Den Breejen, J. P., Radstake, P. B., Bezemer, G. L., Bitter, J. H., Frseth, V., Holmen, A., et al. (2009). On the origin of the cobalt particle size effects in Fischer-Tropsch catalysis. *Journal of the American Chemical Society*, 131(20), 7197-7203.
- den Breejen, J. P., Sietsma, J. R. A., Friedrich, H., Bitter, J. H., & de Jong, K. P. (2010). Design of supported cobalt catalysts with maximum activity for the Fischer-Tropsch synthesis. [doi: 10.1016/j.jcat.2009.12.015]. *Journal of Catalysis*, 270(1), 146-152.

- Diehl, F., & Khodakov, A. Y. (2009). Promotion par les métaux nobles de catalyseurs Fischer-Tropsch à base de cobalt : une revue. *Oil & Gas Science and Technology - Rev. IFP*, 64(1), 11-24.
- Dinamani, M., & Kamath, P. V. (2000). Electrocatalysis of oxygen evolution at stainless steel anodes by electrosynthesized cobalt hydroxide coatings. *Journal of Applied Electrochemistry*, 30(Compendex), 1157-1161.
- Dinka, P., & Mukasyan, A. S. (2005). In situ preparation of oxide-based supported catalysts by solution combustion synthesis. *Journal of Physical Chemistry B*, 109(Copyright 2006, The Institution of Engineering and Technology), 21627-21633.
- Dry, M. E. (1996). Practical and theoretical aspects of the catalytic Fischer-Tropsch process. *Applied Catalysis A: General*, 138(2), 319-344.
- Dry, M. E. (1999). Fischer-Tropsch reactions and the environment. *Applied Catalysis A: General*, 189(2), 185-190.
- Dry, M. E. (2002). *The Fischer-Tropsch process: 1950-2000*, Kruger Park.
- Ehrfeld, W., Hessel, V., & Löwe, H. (2004). Modern Microfabrication Techniques for Microreactors *Microreactors* (pp. 15-39): Wiley-VCH Verlag GmbH & Co. KGaA.
- Espinoza, R. L., Steynberg, A. P., Jager, B., & Vosloo, A. C. (1999). Low temperature Fischer-Tropsch synthesis from a Sasol perspective. [doi: 10.1016/S0926-860X(99)00161-1]. *Applied Catalysis A: General*, 186(1-2), 13-26.
- Fogler, H. S. (2011). *Essentials of chemical reaction engineering*. Upper Saddle River, NJ: Prentice Hall.
- Fontenelle, A. B., & Fernandes, F. A. N. (2011). Comprehensive Polymerization Model for Fischer-Tropsch Synthesis. *Chemical Engineering and Technology*, 34(Compendex), 963-971.
- Ganesh, I., Johnson, R., Rao, G. V. N., Mahajan, Y. R., Madavendra, S. S., & Reddy, B. M. (2005). Microwave-assisted combustion synthesis of nanocrystalline MgAl₂O₄ spinel powder. *Ceramics International*, 31(Copyright 2005, IEE), 67-74.
- Gaube, J., & Klein, H. F. (2008). The promoter effect of alkali in Fischer-Tropsch iron and cobalt catalysts. *Applied Catalysis A: General*, 350(1), 126-132.
- Gavriilidis, A., Angeli, P., Cao, E., Yeong, K. K., & Wan, Y. S. S. (2002). Technology and applications of microengineered reactors. *Chemical Engineering Research and Design*, 80(1), 3-30.
- Ge, L., Ran, R., Shao, Z., Zhu, Z. H., & Liu, S. (2009). Low-temperature synthesis of La_{0.6}Sr_{0.4}Co_{0.2}Fe_{0.8}O₃- perovskite powder via asymmetric sol-gel process and catalytic auto-combustion. *Ceramics International*, 35(Compendex), 2809-2815.
- GEA. (2012). GEA PHE systems. Retrieved from http://www.gea-phe.com/fileadmin/user_upload/documents/brochures/GEAPHE_Prod-Image-Broschuere_EN_72dpi_180511_rel.pdf
- Girardon, J.-S., Lermontov, A. S., Gengembre, L., Chernavskii, P. A., Griboval-Constant, A., & Khodakov, A. Y. (2005). Effect of cobalt precursor and pretreatment conditions on the structure and catalytic performance of cobalt silica-supported Fischer-Tropsch catalysts. [doi: 10.1016/j.jcat.2004.12.014]. *Journal of Catalysis*, 230(2), 339-352.
- Gonzalez-Cortes, S. L., Rodulfo-Baechler, S. M. A., Xiao, T., & Green, M. L. H. (2006). Rationalizing the catalytic performance of -alumina-supported Co(Ni)-Mo(W) HDS catalysts prepared by urea-matrix combustion synthesis. *Catalysis Letters*, 111(Compendex), 57-66.
- González-Cortés, S. L., Xiao, T.-C., Costa, P. M. F. J., Fontal, B., & Green, M. L. H. (2004). Urea-organic matrix method: an alternative approach to prepare Co---MoS₂/[gamma]-Al₂O₃ HDS catalyst. [doi: DOI: 10.1016/j.apcata.2004.05.006]. *Applied Catalysis A: General*, 270(1-2), 209-222.

- González-Cortés, S. L., Xiao, T.-C., Rodulfo-Baechler, S. M. A., & Green, M. L. H. (2005). Impact of the urea-matrix combustion method on the HDS performance of Ni-MoS₂/[gamma]-Al₂O₃ catalysts. [doi: DOI: 10.1016/j.molcata.2005.06.055]. *Journal of Molecular Catalysis A: Chemical*, 240(1-2), 214-225.
- Guettel, R., Kunz, U., & Turek, T. (2008). Reactors for Fischer-Tropsch synthesis. *Chemical Engineering and Technology*, 31(5), 746-754.
- Guo, X., Liu, G., & Larson, E. D. (2011). High-octane gasoline production by upgrading low-temperature Fischer-Tropsch syncrude. *Industrial and Engineering Chemistry Research*, 50(Compendex), 9743-9747.
- Hamelinck, C. N., Faaij, A. P. C., den Uil, H., & Boerrigter, H. (2004). Production of FT transportation fuels from biomass; technical options, process analysis and optimisation, and development potential. *Energy*, 29(11), 1743-1771.
- Hessel, V. (2009). *Micro process engineering : a comprehensive handbook*. Weinheim: Wiley-VCH.
- Hessel, V. (2011). *Micro Process Technology: Microfabrication*. Eindhoven University of Technology.
- Hilmen, A. M., Bergene, E., Lindvåg, O. A., Schanke, D., Eri, S., & Holmen, A. (2001). Fischer-Tropsch synthesis on monolithic catalysts of different materials. *Catalysis Today*, 69(1-4), 227-232.
- Ho, S.-W., & Su, Y.-S. (1997). Effects of Ethanol Impregnation on the Properties of Silica-Supported Cobalt Catalysts. [doi: 10.1006/jcat.1997.1614]. *Journal of Catalysis*, 168(1), 51-59.
- Jacobs, G., Chaney, J. A., Patterson, P. M., Das, T. K., & Davis, B. H. (2004). Fischer-Tropsch synthesis: Study of the promotion of Re on the reduction property of Co/Al₂O₃ catalysts by in situ EXAFS/XANES of Co K and Re LIII edges and XPS. *Applied Catalysis A: General*, 264(2), 203-212.
- Johnston, A. M., Levy, W., & Rumbold, S. O. (2001, Nov). *Application of Printed Circuit Heat Exchanger Technology within Heterogeneous Catalytic Reactors*. Paper presented at the AIChE Annual Meeting 2001.
- Jones, A., & McNicol, B. D. (1986). *Temperature-programmed reduction for solid materials characterization* (Vol. 24). New York: M. Dekker.
- Kapteijn, F., de Deugd, R. M., & Moulijn, J. A. (2005). Fischer-Tropsch synthesis using monolithic catalysts. [doi: 10.1016/j.cattod.2005.06.063]. *Catalysis Today*, 105(3-4), 350-356.
- Khodakov, A. Y., Chu, W., & Fongarland, P. (2007). Advances in the development of novel cobalt Fischer-Tropsch catalysts for synthesis of long-chain hydrocarbons and clean fuels. *Chemical Reviews*, 107(Compendex), 1692-1744.
- Klerk, A. d. (2011). *Fischer-Tropsch refining* ([1st. ed.]). Weinheim, Germany: Wiley-VCH.
- Knochen, J., Güttel, R., Knobloch, C., & Turek, T. (2010). Fischer-Tropsch synthesis in milli-structured fixed-bed reactors: Experimental study and scale-up considerations. [doi: 10.1016/j.cep.2010.04.013]. *Chemical Engineering and Processing: Process Intensification*, 49(9), 958-964.
- Kolb, G., & Hessel, V. (2004). Micro-structured reactors for gas phase reactions. [doi: 10.1016/j.cej.2003.10.005]. *Chemical Engineering Journal*, 98(1-2), 1-38.
- Kraum, M., & Baerns, M. (1999). Fischer-Tropsch synthesis: The influence of various cobalt compounds applied in the preparation of supported cobalt catalysts on their performance. *Applied Catalysis A: General*, 186(1-2), 189-200.
- Leckel, D. (2009). Diesel production from fischer - Tropsch: The past, the present, and new concepts. *Energy and Fuels*, 23(Compendex), 2342-2358.
- Leibold, H., Hornung, A., & Seifert, H. (2008). HTHP syngas cleaning concept of two stage biomass gasification for FT synthesis. *Powder Technology*, 180(1-2), 265-270.

- Li, C., Ying, W., Cao, F., Zhang, H., & Fang, D. (2008). Effects of Impregnation Solvents on Catalytic Performance of Co-Ru-ZrO₂/γ-Al₂O₃ Catalyst for Fischer-Tropsch Synthesis. [doi: 10.1080/10916460701425900]. *Petroleum Science and Technology*, 26(6), 704-716.
- Li, J. (2007). Modelling of Energy Demand in a Sawmill - Personal Communication. Christchurch: University of Canterbury.
- Li, J., Jacobs, G., Das, T., Zhang, Y., & Davis, B. (2002). Fischer-Tropsch synthesis: effect of water on the catalytic properties of a Co/SiO₂ catalyst. [doi: 10.1016/S0926-860X(02)00276-4]. *Applied Catalysis A: General*, 236(1-2), 67-76.
- Liu, G., Larson, E. D., Williams, R. H., Kreutz, T. G., & Guo, X. (2011). Making Fischer-Tropsch fuels and electricity from coal and biomass: Performance and cost analysis. *Energy and Fuels*, 25(Compendex), 415-437.
- Liu, X., Hamasaki, A., Honma, T., & Tokunaga, M. (2011). Anti-ASF distribution in Fischer-Tropsch synthesis over unsupported cobalt catalysts in a batch slurry phase reactor. [doi: 10.1016/j.cattod.2011.03.030]. *Catalysis Today*, 175(1), 494-503.
- Logdberg, S. (2007). *Development of Fischer-Tropsch Catalysts for Gasified Biomass*. KTH School of Chemical Science and Engineering, Stockholm.
- Lögdberg, S., Boutonnet, M., Walmsley, J. C., Järås, S., Holmen, A., & Blekkan, E. A. (2011). Effect of water on the space-time yield of different supported cobalt catalysts during Fischer-Tropsch synthesis. [doi: 10.1016/j.apcata.2010.11.030]. *Applied Catalysis A: General*, 393(1-2), 109-121.
- Lualdi, M., Logdberg, S., Di Carlo, G., Jaras, S., Boutonnet, M., Venezia, A. M., et al. (2011). *Evidence for diffusion-controlled hydrocarbon selectivities in the fischer-tropsch synthesis over cobalt supported on ordered mesoporous silica*. Paper presented at the 14th Nordic Symposium on Catalysis : Editors: Anker Degn Jensen , Jeppe Vang Lauritsen, Anders Riisager, Thomas Bligaard, Van Godewijckstraat 30, Dordrecht, 3311 GZ, Netherlands.
- Lualdi, M., Logdberg, S., Regali, F., Boutonnet, M., & Jaras, S. (2011). Investigation of mixtures of a Co-based catalyst and a Cu-based catalyst for the fischer-tropsch synthesis with Bio-Syngas: The importance of indigenous water. *Topics in Catalysis*, 54(13-15), 977-985.
- Ma, W., Jacobs, G., Sparks, D. E., Gnanamani, M. K., Pendyala, V. R. R., Yen, C. H., et al. (2011). Fischer-Tropsch synthesis: Support and cobalt cluster size effects on kinetics over Co/Al₂O₃ and Co/SiO₂ catalysts. *Fuel*, 90(Compendex), 756-765.
- Madikizela-Mnqanqeni, N. N., & Coville, N. J. (2005). The effect of cobalt and zinc precursors on Co (10%)/Zn (x%)/TiO₂ (x=0, 5) Fischer-Tropsch catalysts. [doi: 10.1016/j.molcata.2004.09.004]. *Journal of Molecular Catalysis A: Chemical*, 225(2), 137-142.
- Mills, P. L., Quiram, D. J., & Ryley, J. F. (2007). Microreactor technology and process miniaturization for catalytic reactions - a perspective on recent developments and emerging technologies. *Chemical Engineering Science*, 62(Copyright 2007, The Institution of Engineering and Technology), 6992-7010.
- Ministry of Economic Development. (2007). New Zealand Energy Strategy to 2050 - Powering Our Future. Retrieved 14 December, 2007, from <http://www.med.govt.nz/upload/52164/nzes.pdf>
- Ministry of Economic Development. (2008a). New Zealand Energy Data File. Retrieved 26-Feb, 2009, from http://www.med.govt.nz/upload/59482/00_EDF-June2008.pdf
- Ministry of Economic Development. (2008b). New Zealand Energy Greenhouse Gas Emissions. Retrieved 26-Feb, 2009, from <http://www.med.govt.nz/upload/63349/GHG%20Report.pdf>

- Ministry of Economic Development. (2009). Oil price monitoring. Retrieved 26-Feb, 2009, from http://www.med.govt.nz/templates/Page_39566.aspx
- Ministry of Economic Development. (2010). New Zealand energy data file. Retrieved 30 March, 2011, from <http://www.med.govt.nz/upload/73585/EDF%202010.pdf>
- Ministry of Economic Development. (2011). Oil price monitoring. Retrieved 4 April, 2011, from http://www.med.govt.nz/templates/StandardSummary_353.aspx
- Moodley, D. J., van de Loosdrecht, J., Saib, A. M., Overett, M. J., Datye, A. K., & Niemantsverdriet, J. W. (2009). Carbon deposition as a deactivation mechanism of cobalt-based Fischer-Tropsch synthesis catalysts under realistic conditions. *Applied Catalysis A: General*, 354(1-2), 102-110.
- Morales, F., de Smit, E., de Groot, F. M. F., Visser, T., & Weckhuysen, B. M. (2007). Effects of manganese oxide promoter on the CO and H₂ adsorption properties of titania-supported cobalt Fischer-Tropsch catalysts. *Journal of Catalysis*, 246(1), 91-99.
- Myrstad, R., Eri, S., Pfeifer, P., Rytter, E., & Holmen, A. (2009). Fischer-Tropsch synthesis in a microstructured reactor. *Catalysis Today*, 147(SUPPL.), S301-S304.
- Nageswara Rao, P., & Kunzru, D. (2007). Fabrication of microchannels on stainless steel by wet chemical etching. *Journal of Micromechanics and Microengineering*, 17(12), N99-N106.
- Nagineeni, V. S., Zhao, S., Potluri, A., Liang, Y., Siriwardane, U., Seetala, N. V., et al. (2005). Microreactors for syngas conversion to higher alkanes: Characterization of sol-gel-encapsulated nanoscale Fe-Co catalysts in the microchannels. *Industrial and Engineering Chemistry Research*, 44(15), 5602-5607.
- Norske Skog. (2010). *Annual report 2010*.
- NZTIF. (2010). Domestic log supply 2011 & beyond. Retrieved 27-June, 2011, from <http://www.nztif.co.nz/news-item.php?id=83>
- O'Brien, R. J., & Davis, B. H. (2004). Impact of copper on an alkali promoted iron Fischer-Tropsch catalyst. *Catalysis Letters*, 94(1-2), 1-6.
- Oukaci, R., Singleton, A. H., & Goodwin, J. G. (1999). Comparison of patented Co F-T catalysts using fixed-bed and slurry bubble column reactors. [doi: 10.1016/S0926-860X(99)00169-6]. *Applied Catalysis A: General*, 186(1-2), 129-144.
- Penniall, C. L., & Williamson, C. J. (2009). Feasibility study into the potential for gasification plant in the New Zealand wood processing industry. *Energy Policy*, 37(Copyright 2010, The Institution of Engineering and Technology), 3377-3386.
- Pfeifer, P., Schubert, K., & Emig, G. (2005). Preparation of copper catalyst washcoats for methanol steam reforming in microchannels based on nanoparticles. [doi: DOI: 10.1016/j.apcata.2005.02.036]. *Applied Catalysis A: General*, 286(2), 175-185.
- Philippe, R., Lacroix, M., Dreibine, L., Pham-Huu, C., Edouard, D., Savin, S., et al. (2009). Effect of structure and thermal properties of a Fischer-Tropsch catalyst in a fixed bed. [doi: 10.1016/j.cattod.2009.07.058]. *Catalysis Today*, 147, Supplement(0), S305-S312.
- Photoetch Ltd. (2008). Communication about etching and bonding techniques. Christchurch.
- Poling, B. E., Prausnitz, J. M., & O'Connell, J. P. (2001). *The properties of gases and liquids* (5th ed.). New York: McGraw-Hill.
- Rapier, R. (2011). What happened at Choren? Retrieved from <http://www.energytrendsinsider.com/2011/07/08/what-happened-at-choren/>
- Rauch, R. (2011). Conversion of Biomass Over Steam Gasification to Biofuels and Chemicals - Actual Status of Work. Vienna University of Technology.
- Rutherford, J. (2006). *Heat and Power Applications of Advanced Biomass Gasifiers in New Zealand's Wood Processing Industry*. University of Canterbury, Christchurch.

- Rutherford, J. P., & Williamson, C. J. (2006). Integrating advanced biomass gasifiers into the New Zealand wood industry. *New Zealand Journal of Forestry*, 51(Compendex), 35-41.
- Rytter, E., Skagseth, T. H., Eri, S., & Sjøstad, A. O. (2010). Cobalt Fischer–Tropsch Catalysts Using Nickel Promoter as a Rhenium Substitute to Suppress Deactivation. [doi: 10.1021/ie100308f]. *Industrial & Engineering Chemistry Research*, 49(9), 4140-4148.
- Saeyns, M., Tan, K. F., Chang, J., & Borgna, A. (2010). Improving the Stability of Cobalt Fischer–Tropsch Catalysts by Boron Promotion. [doi: 10.1021/ie100523u]. *Industrial & Engineering Chemistry Research*, 49(21), 11098-11100.
- Saib, A. M., Moodley, D. J., Ciobîca, I. M., Hauman, M. M., Sigwebela, B. H., Weststrate, C. J., et al. (2010). Fundamental understanding of deactivation and regeneration of cobalt Fischer-Tropsch synthesis catalysts. [doi: DOI: 10.1016/j.cattod.2010.02.008]. *Catalysis Today*, 154(3-4), 271-282.
- Schulz, H. (1999). Short history and present trends of Fischer-Tropsch synthesis. *Applied Catalysis A: General*, 186(1-2), 3-12.
- SCION, Hall, P., & Gifford, J. (2007). Bioenergy Options for New Zealand - A situational analysis of biomass resources and conversion technologies. Retrieved 30 Mar, 2009, from <http://www.scionresearch.com/Portals/0/SCIONBioenergyOptionsReport.pdf>
- SCION, Hall, P., & Jack, M. (2008). Bioenergy Options for New Zealand - Pathways Analysis. Retrieved 30 Mar, 2009, from http://www.scionresearch.com/Portals/0/SCION%20Bioenergy%20Options_Pathways%20Analysis.pdf
- SCION, Hall, P., & Jack, M. (2009). Bioenergy Options for New Zealand: Transition Analysis. Retrieved from http://www.scionresearch.com/_data/assets/pdf_file/0014/6800/Bioenergy-Options-Transition-Report.pdf
- Searcy, E., & Flynn, P. (2009). *The impact of biomass availability and processing cost on optimum size and processing technology selection*, 999 Riverview Drive, Suite 208, Totowa, NJ 07512-1165, United States.
- Shree Krishna Engineering Works. (2012). Corrugated box making roller. Retrieved 29 Nov, 2012, from <http://shreekrishnaengineering.tradeindia.com/corrugated-box-making-roller--1186369.html>
- Smith, R. (2005). *Chemical process design and integration*. Hoboken, NJ: Wiley.
- Song, H.-S., Ramkrishna, D., Trinh, S., & Wright, H. (2003). Diagnostic nonlinear analysis of Fischer-Tropsch synthesis in stirred-tank slurry reactors. *AIChE Journal*, 49(Compendex), 1803-1820.
- Southall, D., Le Pierres, R., & Dewson, S. J. (2008, June 8-12). *Design Considerations for Compact Heat Exchangers*. Paper presented at the ICAPP '08, Anaheim, CA USA.
- Steynberg, A., & Dry, M. (2004). *Fischer-Tropsch technology*. Amsterdam ; Boston: Elsevier.
- Steynberg, A. P., Espinoza, R. L., Jager, B., & Vosloo, A. C. (1999). High temperature Fischer-Tropsch synthesis in commercial practice. [doi: 10.1016/S0926-860X(99)00163-5]. *Applied Catalysis A: General*, 186(1-2), 41-54.
- Storster, S., Ttdal, B., Walmsley, J. C., Tanem, B. S., & Holmen, A. (2005). Characterization of alumina-, silica-, and titania-supported cobalt Fischer-Tropsch catalysts. *Journal of Catalysis*, 236(1), 139-152.
- Sun, S., Tsubaki, N., & Fujimoto, K. (2000). The reaction performances and characterization of Fischer–Tropsch synthesis Co/SiO₂ catalysts prepared from mixed cobalt salts. [doi: 10.1016/S0926-860X(00)00455-5]. *Applied Catalysis A: General*, 202(1), 121-131.

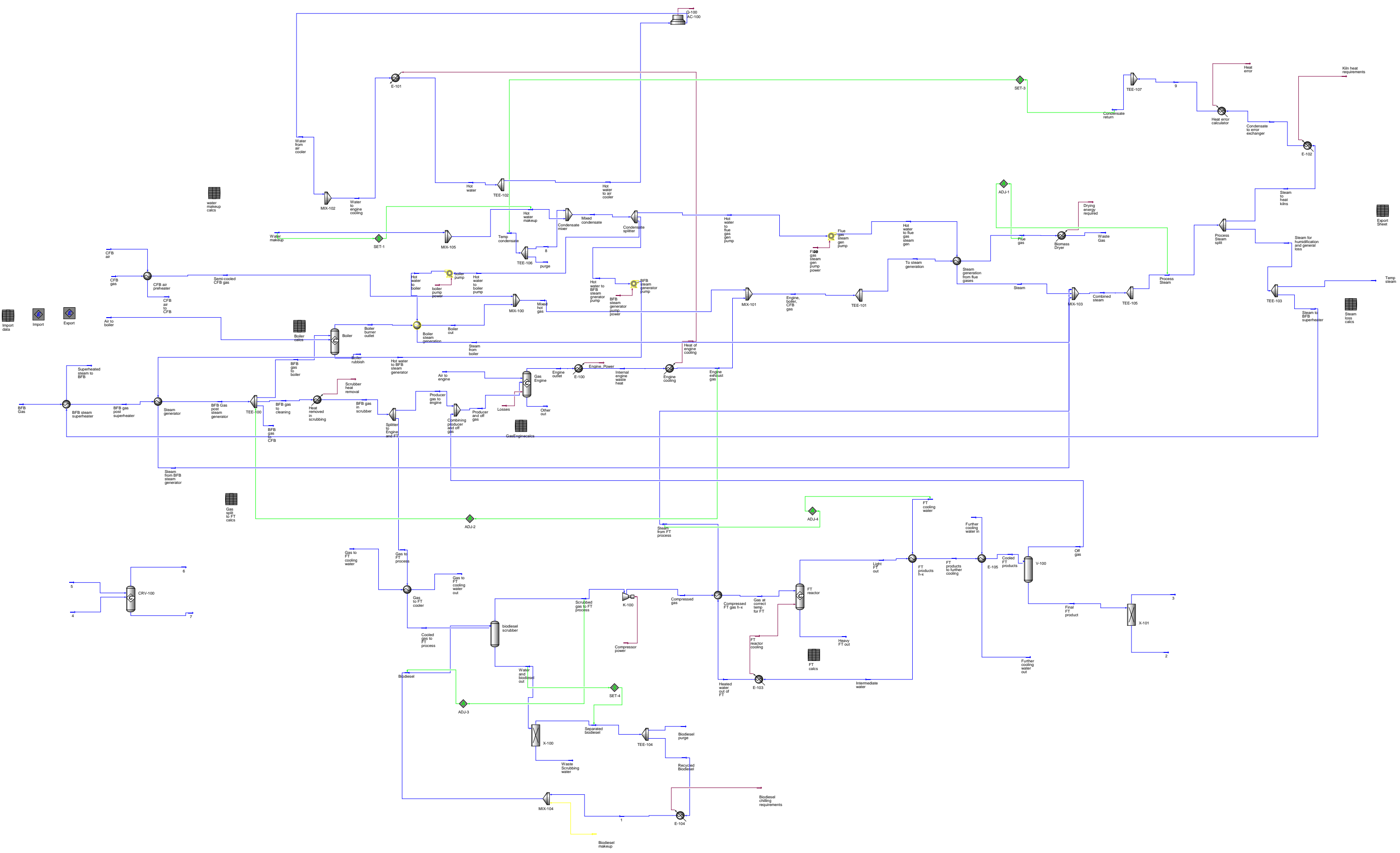
- Swanson, R. M., Platon, A., Satrio, J. A., & Brown, R. C. (2010). Techno-economic analysis of biomass-to-liquids production based on gasification. *Fuel*, 89(Compendex), S11-S19.
- Tavasoli, A., Malek Abbaslou, R. M., & Dalai, A. K. (2008). Deactivation behavior of ruthenium promoted Co/ γ -Al₂O₃ catalysts in Fischer-Tropsch synthesis. [doi: 10.1016/j.apcata.2008.05.001]. *Applied Catalysis A: General*, 346(1–2), 58-64.
- Tavasoli, A., Sadagiani, K., Khorashe, F., Seifkordi, A. A., Rohani, A. A., & Nakhaeipour, A. (2008). Cobalt supported on carbon nanotubes - A promising novel Fischer-Tropsch synthesis catalyst. *Fuel Processing Technology*, 89(5), 491-498.
- Teiseh, E. A., Capareda, S., & Rezenom, Y. H. (2012). Cobalt based hybrid Fischer-Tropsch synthesis catalyst for improved selectivity of hydrocarbons in the JP-8 carbon number range from a synthesis gas obtained from the pyrolysis of the MixAlco process derived sludge. [doi: 10.1016/j.apcata.2012.06.012]. *Applied Catalysis A: General*, 437–438(0), 63-71.
- Tijmensen, M. J. A., Faaij, A. P. C., Hamelinck, C. N., & Van Hardeveld, M. R. M. (2002). Exploration of the possibilities for production of Fischer Tropsch liquids and power via biomass gasification. *Biomass and Bioenergy*, 23(2), 129-152.
- Tonkovich, A., Kuhlmann, D., Rogers, A., McDaniel, J., Fitzgerald, S., Arora, R., et al. (2005). Microchannel technology scale-up to commercial capacity. *Chemical Engineering Research and Design*, 83(6 A), 634-639.
- Tonkovich, A., Mazanec, T., Jarosch, K., Fitzgerald, S., Yang, B., Taha, R., et al. (2008). Improved Fischer-Tropsch Economics Enabled by Microchannel Technology. Retrieved 3 June, 2009
- Tonkovich, A. L. Y., Yang, B., Perry, S. T., Fitzgerald, S. P., & Wang, Y. (2007). From seconds to milliseconds to microseconds through tailored microchannel reactor design of a steam methane reformer. *Catalysis Today*, 120(1), 21-29.
- Trepanier, M., Dalai, A. K., & Abatzoglou, N. (2010). Synthesis of CNT-supported cobalt nanoparticle catalysts using a microemulsion technique: Role of nanoparticle size on reducibility, activity and selectivity in Fischer-Tropsch reactions. *Applied Catalysis A: General*, 374(1-2), 79-86.
- Tsakoumis, N. E., Rønning, M., Borg, Ø., Rytter, E., & Holmen, A. (2010). Deactivation of cobalt based Fischer-Tropsch catalysts: A review. [doi: DOI: 10.1016/j.cattod.2010.02.077]. *Catalysis Today*, 154(3-4), 162-182.
- TUV. (2009). The FICFB gasification system. Retrieved 4 April, 2011, from <http://www.ficfb.at/>
- Ulrich, G. D., & Vasudevan, P. T. (2004). *Chemical Engineering Process Design and Economics* (Second Edition ed.). New Hampshire: Process Publishing.
- van de Loosdrecht, J., Balzhinimaev, B., Dalmon, J. A., Niemantsverdriet, J. W., Tsybulya, S. V., Saib, A. M., et al. (2007). Cobalt Fischer-Tropsch synthesis: Deactivation by oxidation? [doi: 10.1016/j.cattod.2007.02.032]. *Catalysis Today*, 123(1–4), 293-302.
- Van Der Laan, G. P., & Beenackers, A. A. C. M. (1999). Kinetics and Selectivity of the Fischer-Tropsch Synthesis: A Literature Review. *Catalysis Reviews - Science and Engineering*, 41(Compendex), 255-318.
- van Male, P., de Croon, M. H. J. M., Tiggelaar, R. M., van den Berg, A., & Schouten, J. C. (2004). Heat and mass transfer in a square microchannel with asymmetric heating. [doi: 10.1016/S0017-9310(03)00401-0]. *International Journal of Heat and Mass Transfer*, 47(1), 87-99.
- Van Steen, E., & Prinsloo, F. F. (2002). *Comparison of preparation methods for carbon nanotubes supported iron Fischer-Tropsch catalysts*.
- Velocys. (2012a). Microchannel Reactors. Retrieved from <http://www.velocys.com/ocge02.php>

- Velocys. (2012b). Velocys media web gallery. Retrieved from <http://www.velocys.com/ocgi02.php>
- Visconti, C. G., Tronconi, E., Groppi, G., Lietti, L., Iovane, M., Rossini, S., et al. (2011). Monolithic catalysts with high thermal conductivity for the Fischer–Tropsch synthesis in tubular reactors. [doi: 10.1016/j.cej.2011.05.014]. *Chemical Engineering Journal*, 171(3), 1294-1307.
- Visconti, C. G., Tronconi, E., Lietti, L., Groppi, G., Forzatti, P., Cristiani, C., et al. (2009). An experimental investigation of Fischer-Tropsch synthesis over washcoated metallic structured supports. *Applied Catalysis A: General*, 370(1-2), 93-101.
- Wei, D., Goodwin Jr, J. G., Oukaci, R., & Singleton, A. H. (2001). Attrition resistance of cobalt F–T catalysts for slurry bubble column reactor use. [doi: 10.1016/S0926-860X(00)00792-4]. *Applied Catalysis A: General*, 210(1–2), 137-150.
- Weir, P. (2012). Discussion of the application of the Emission Trading Scheme to Forestry. Christchurch.
- Williams, R. H., Larson, E. D., Liu, G., & Kreutz, T. G. (2009). *Fischer-Tropsch fuels from coal and biomass: Strategic advantages of once-through ("polygeneration") configurations*, Washington DC, United states.
- Wilson, J. (2008). Discussions with AAA technology about ability to wirecut small channels. Christchurch.
- Wright, J., & Bull, D. (2010). *Some biofuels are better than others: Thinking strategically about biofuels*. Retrieved from <http://www.pce.parliament.nz/assets/Uploads/Thinking-strategically-about-biofuels.pdf>.
- XACT. (2012). XACT Wire EDM Corporation. Retrieved 13 Aug, 2012, from <http://www.xactedm.com/>
- Yates, I. C., & Satterfield, C. N. (1991). Intrinsic kinetics of the Fischer-Tropsch synthesis on a cobalt catalyst. *Energy and Fuels*, 5(Compendex), 168-173.
- Zaman, M., Khodadi, A., & Mortazavi, Y. (2009). Fischer-Tropsch synthesis over cobalt dispersed on carbon nanotubes-based supports and activated carbon. *Fuel Processing Technology*, 90(10), 1214-1219.
- Zhang, Y., Liu, Y., Yang, G., Endo, Y., & Tsubaki, N. (2009). The solvent effects during preparation of Fischer–Tropsch synthesis catalysts: Improvement of reducibility, dispersion of supported cobalt and stability of catalyst. [doi: 10.1016/j.cattod.2009.01.014]. *Catalysis Today*, 142(1–2), 85-89.
- Zhang, Y., Liu, Y., Yang, G., Sun, S., & Tsubaki, N. (2007). Effects of impregnation solvent on Co/SiO₂ catalyst for Fischer-Tropsch synthesis: A highly active and stable catalyst with bimodal sized cobalt particles. [doi: 10.1016/j.apcata.2007.01.030]. *Applied Catalysis A: General*, 321(1), 79-85.
- Zwart, R., & van Ree, R. (2009). Bio-based Fischer–Tropsch Diesel Production Technologies *Biofuels* (pp. 95-116): John Wiley & Sons, Ltd.
- Zwart, R. W. R., & Boerrigter, H. (2005). High efficiency co-production of synthetic natural gas (SNG) and Fischer-Tropsch (FT) transportation fuels from biomass. *Energy and Fuels*, 19(2), 591-597.

Appendix A: UniSim Model

The intention of this Appendix is to give a fuller understanding of the process behind creating the UniSim plant flow sheet heat and material balance model. It is not a complete treatise as to how to replicate the model in detail, as this is impractical. If the reader wishes to obtain further information to enable them to perform their own modelling, it is suggested they contact the BTSL research group at the University of Canterbury, Chemical and Process Engineering Department where they can be provided with an electronic copy of the model.

The overall model can be seen on the fold out leaf on the following page. It should be noted that Peng-Robinson equation of state is used as the basis for the model. Post the main flow diagram pertinent aspects of the model will be explained.



In order for the overall techno-economic model to function cohesively it is necessary to pass data from Excel to Unisim and back again. This is performed using the functions shown in Figure A-1. The Import function obtains data from specified cells in Excel and deposits the data in specified cells in the Import data spreadsheet in UniSim. This data can then be utilised in the UniSim model. Exporting data is the reverse process where data is extracted from a spreadsheet in UniSim and exported to designated cells in Excel. This is a manual process which requires checking boxes at each time data is imported or exported. This means changes in the overall model have to be solved iteratively.



Figure A-1: Import and export functions allow data to be passed from and to Excel

Figure A-2 shows the lead up to the gas engine. This is shown due to the importance of the balance of flows at this point. The 'Splitter to Engine and FT' ratio is important as to optimise the fuel usage this ratio should be modified to be the maximum. However, there is a particular gas requirement for the gas engine and if too much gas is split to the FT reactor, the 'off gas' returning will exceed the requirement and cause a negative flow in the 'producer gas to engine' stream. Therefore the ratio is balanced to maintain a small positive buffer flow in 'producer gas to engine'. Not shown here is an added complication of balancing the boiler feed flow in a similar vein. This adds further complication to optimising the model but can be worked through iteratively, particularly as the user becomes more familiar with the reaction of the model to changes.

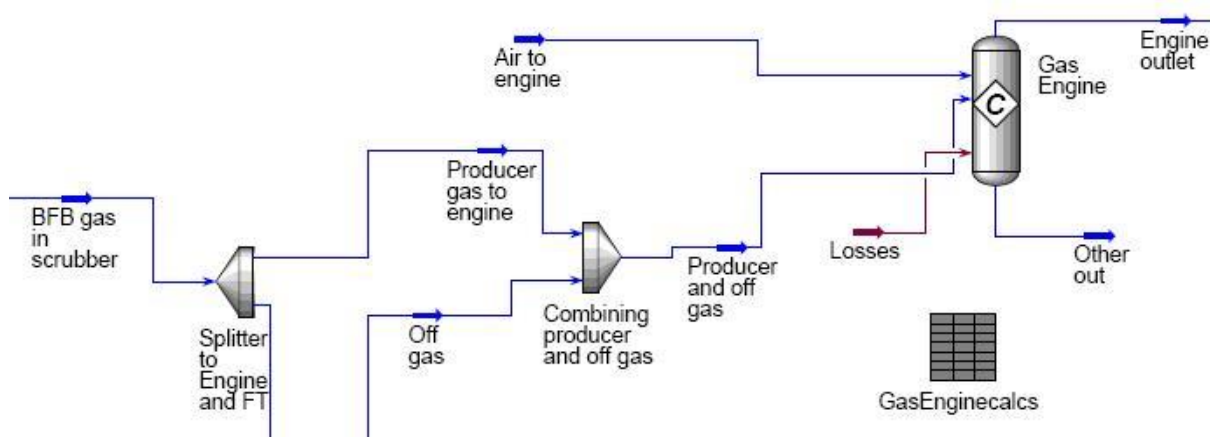


Figure A-2: Feed to the gas engine showing key balance points for gas flow

The gas engine has been modelled as a conversion reactor as shown in Figure A-3. The manufacturers specifications for the gas engine are used to establish the amount of heat and power

that will be generated from the engine. This is modelled using heat exchangers to extract energy from the heated gas stream from combustion. Energy losses are shown on the red stream entering the reactor (gas engine) and relate to the efficiency as provided from the manufacturer.

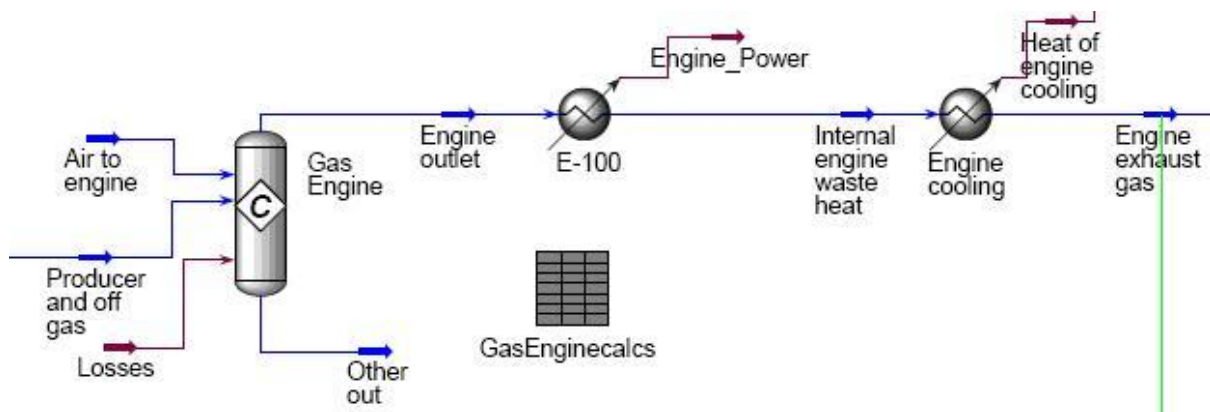


Figure A-3: Image showing the method for modelling the reactor

The FT reactor, like the gas engine and boiler, has been modelled using a conversion reactor. Figure A-4 shows the function window for the reactor. It can be seen the stoichiometry for each reaction is entered. Figure A-5 shows the reactions that were modelled, noting that C_{20+} is treated as generic waxy product. The amount of product produced from each reaction is calculated from a spreadsheet in the UniSim model based on a specified conversion and selectivity.

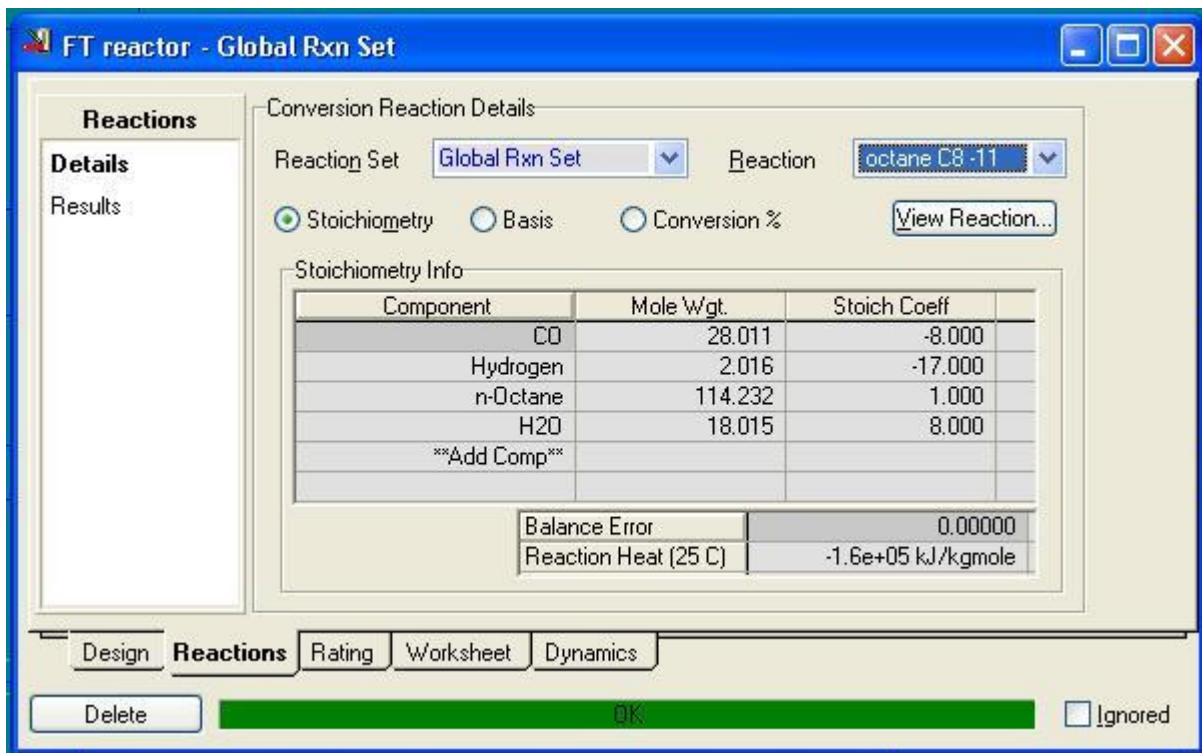


Figure A-4: Control window for FT reactor

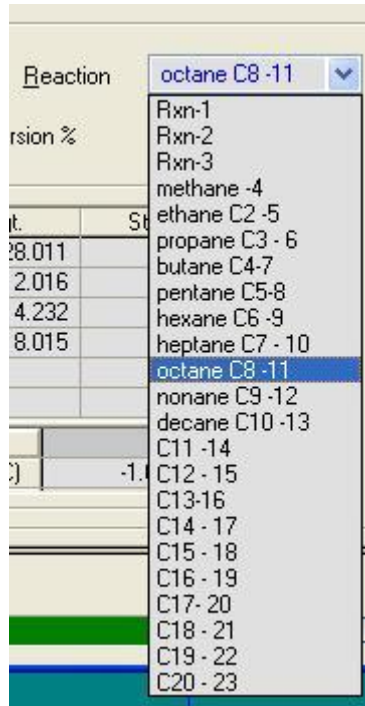


Figure A-5: Image showing reaction set used in the FT reactor

As mentioned previously the boiler is also modelled as a conversion reactor and has a heat exchanger post the reactor to model the heat transfer to steam. The control window is shown in Figure A-6. In this case it can be seen there are stoichiometric reactions based on combustion of syngas products with air. Methane combustion is the example shown.

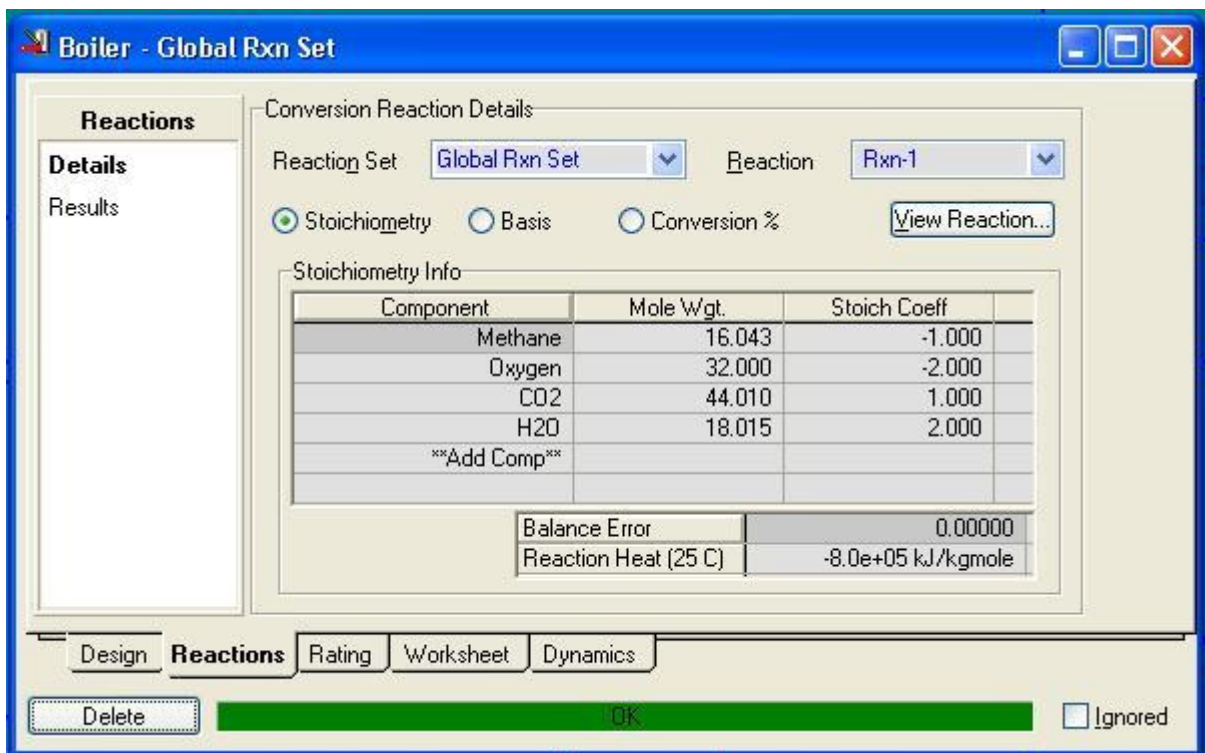


Figure A-6: Control window for the boiler

A constraint in the model is the temperature of the hot air available for drying as shown in Figure A-7. The adjust keeps the temperature of the flue gas at 300°C following a heat exchanger making process steam by adjusting the steam flowrate.

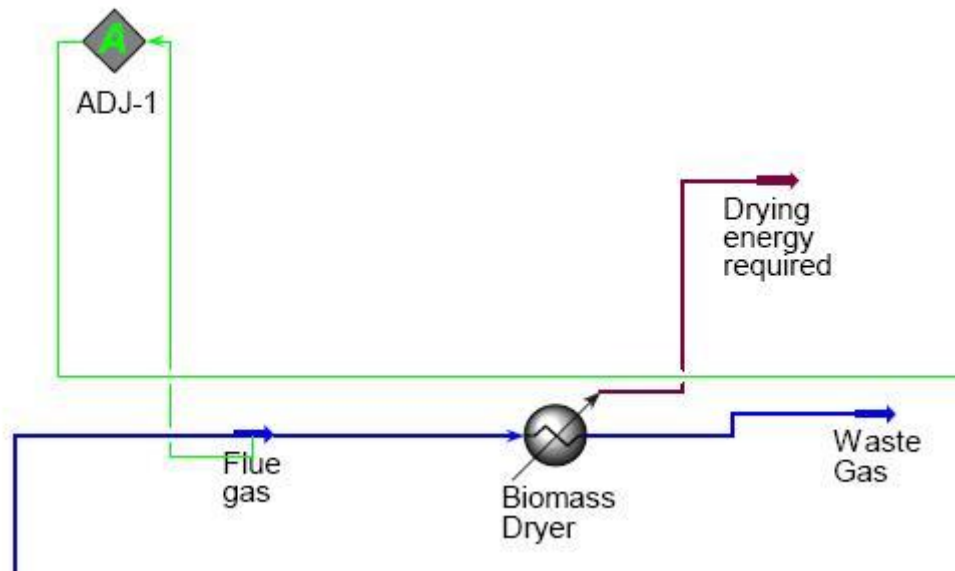


Figure A-7: Hot gas showing adjust to hold flue gas temperature constant

In Figure A-8 one can see the heat error energy stream. This is used as the balance between meeting the energy needs of the plant and the wood feed rate. Once everything else in the model is in balance, the wood feed rate is manipulated until the heat error is within $\pm 50\text{kW}$ which is approximately 0.1% of the total feedstock energy provided.

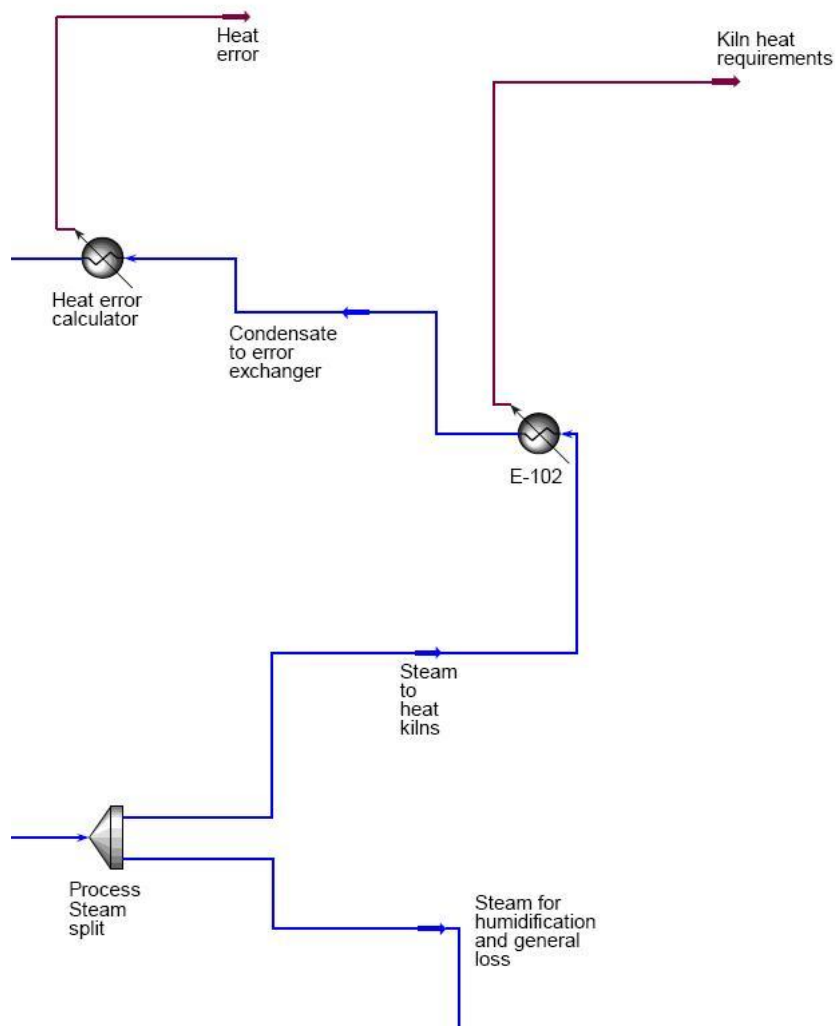


Figure A-8: Section of model that allows heat balance closure

Appendix B: Techno-economic study results

The purpose of this appendix is to provide complete capital and operating cost breakdowns, including the calculation of the revenue for electricity and heat for all the modelled techno-economic scenarios in this thesis. The results are divided into the initial study using the slurry reactor and the optimisation studies with the microchannel reactor and manipulated pressure.

Initial techno-economic results using slurry reactor technology

Scenario 1: All heat and power requirements of the sawmill are met, breakeven syncrude price \$US167 per barrel, production 74 barrels per day

Table B1: Capital Cost breakdown for scenario 1

Biomass Drying		3,055,220
Feed Handling		2,633,294
Gasifier		2,946,123
Gas Engine		7,257,896
Boiler		351,493
Misc.		160,486
Gas Scrubber		1,221,300
Gas filters and Guard Beds		185,812
Compressor		2,250,058
Heat exchange		638,015
FT slurry reactor		7,441,086
Contingency and Fee		4,221,118
Working Capital		3,236,190
Total		35,598,092

Table B2: Scenario 1 electricity and heat revenue calculations

Electricity Value Calculations			
On production power demand		1421 kW	
Off production power demand		362 kW	
Generation from energy plant going to mill		1429 kW	
		To buy	To sell
Price of electricity on peak	c/kWh	9.8	8.13
Price of electricity off peak	c/kWh	9.8	8.13
Operating hours per day		8 hrs	
FT power needs (compressor + chiller + 100kW)		2831 kW	
Gas engine generation		4260 kW	
Generation excess/shortfall during production		8 kW	
Generation excess/shortfall off production		1067 kW	
Electricity Profit/Expense during on production period assuming energy centre		5 \$/day	
Electricity Profit/Expense during off production period assuming energy centre		1388 \$/day	
Cost of electricity if no energy centre - on production period		1114 \$/day	
Cost of electricity if no energy centre - off production period		567 \$/day	
Final value from having energy centre during on production period		1119 \$/day	
Final value from having energy centre during off production period		1955 \$/day	
Total daily value of having energy centre		3074 \$/day	
		1066067 \$/year	
Steam Value Calculations			
Value of steam		8 \$/GJ	
Steam Usage (based on requirement from sawmill energy model)		620965 MJ/day	
		621 GJ/day	
		215320 GJ/year	
		1722558 \$/year	

Table B3: Operating cost breakdown for scenario 1

	Annual Use	\$/unit	\$/yr
Raw Materials			
Wood	67708 Dry T/yr	20	1,354,156
Utilities			
Diesel	544668.8 L	1 L	544,669
Labour			
Process Operation	13140 hrs	20 hr	262,800
Supervision	15 % of operating labour		39,420
Administrative and General Overh	60 % of labour + maintenance		611,912
Maintenance	2 % of capital cost		717,633
Local taxes	1 % of capital cost		358,816
Insurance	1.5 % of capital cost		538,224
Operating Supplies	15 % of maintenance cost		53,822
Total Operating Costs (\$NZ)			4,481,452
Revenue from sales			
		\$/unit	
Product sales	3328944	1.64982 kg	5,492,159
Heat revenue			1,722,558
Electricity revenue			1,066,067
Net Annual Profit			
Sales revenue			8,280,784
Less Operating Costs			4,481,452
Net Annual Profit after operating costs, before tax			3,799,332
Less depreciation on fixed capita	10 years straight line		3,229,347
Net annual profit after depreciation			569,985
Less tax	33 c/\$		188,095
Net Annual Profit after tax (\$NZ)			381,890
Add back depreciation			3,229,347
Total Net Annual Cashflow (\$NZ)			3,611,237

Scenario 2: Off peak electrical and all heat requirements of mill met, breakeven syncrude price \$US173 per barrel, production 75 barrels per day

Table B4: Scenario 2 capital cost breakdown

Biomass Drying		2,887,640
Feed Handling		2,534,333
Gasifier		2,829,906
Gas Engine		5,557,566
Boiler		333,479
Misc.		155,529
Gas Scrubber		1,227,698
Gas filters and Guard Beds		187,205
Compressor		2,267,172
Heat exchange		641,146
FT slurry reactor		7,497,381
Contingency and Fee		3,917,858
Working Capital		3,003,691
Total		33,040,603

Table B5: Scenario 2 electricity and heat revenue calculations

Electricity Value Calculations			
On production power demand		1421 kW	
Off production power demand		362 kW	
Generation from energy plant going to mill		398.1381 kW	
		To buy	To sell
Price of electricity on peak	c/kWh	9.8	8.13
Price of electricity off peak	c/kWh	9.8	8.13
Operating hours per day		8 hrs	
FT power needs (compressor + chiller + 100kW)		2851.862 kW	
Gas engine generation		3250 kW	
Generation excess/shortfall during production		-1023 kW	
Generation excess/shortfall off production		36 kW	
Electricity Profit/Expense during on production period assuming energy centre		-802.106 \$	
Electricity Profit/Expense during off production period assuming energy centre		47.28316 \$	
Cost of electricity if no energy centre - on production period		1114.246 \$	
Cost of electricity if no energy centre - off production period		567.2848 \$	
Final value from having energy centre during on production period		312.1403 \$/day	
Final value from having energy centre during off production period		614.568 \$/day	
Total daily value of having energy centre		926.7083 \$/day	
		321336.1 \$/year	
Steam Value Calculations			
Value of steam		8 \$/GJ	
Steam Usage (based on requirement from sawmill energy model)		620965 MJ/day	
		620.9653 GJ/day	
		215319.7 GJ/year	
		1722558 \$/year	

Table B6: Scenario 2 operating cost breakdown

	Annual Use	\$/unit	\$/yr
Raw Materials			
Wood	63514 Dry T/yr	20	1,270,270
Utilities			
Diesel	544668.7 L	1 L	544,669
Labour			
Process Operation	13140 hrs	20 hr	262,800
Supervision	15 % of operating labour		39,420
Administrative and General Overh	60 % of labour + maintenance		581,090
Maintenance	2 % of capital cost		666,263
Local taxes	1 % of capital cost		333,131
Insurance	1.5 % of capital cost		499,697
Operating Supplies	15 % of maintenance cost		49,970
Total Operating Costs (\$NZ)			4,247,309
Revenue from sales			
		\$/unit	
Product sales	3353959	1.709095 kg	5,732,235
Heat revenue			1,722,558
Electricity revenue			321,336
Net Annual Profit			
Sales revenue			7,776,129
Less Operating Costs			4,247,309
Net Annual Profit after operating costs, before tax			3,528,820
Less depreciation on fixed capita	10 years straight line		2,998,182
Net annual profit after depreciation			530,638
Less tax	33 c/\$		0
Net Annual Profit after tax (\$NZ)			530,638
Add back depreciation			2,998,182
Total Net Annual Cashflow (\$NZ)			3,528,820

Scenario 3: No power generation, all mill heat requirements met, breakeven syncrude price \$US219 per barrel, production 49 barrels per day

Table B7: Scenario 3 capital cost breakdown

Biomass Drying		2,085,650
Feed Handling		2,018,589
Gasifier		2,243,912
Gas Engine		-
Boiler		438,940
Misc.		111,594
Gas Scrubber		1,227,698
Gas filters and Guard Beds		187,205
Compressor		1,478,650
Heat exchange		469,338
FT slurry reactor		4,890,316
Contingency and Fee		2,272,784
Working Capital		1,742,468
Total		19,167,144

Table B8: Scenario 3 electricity and heat revenue calculations

Electricity Value Calculations			
On production power demand		1421 kW	
Off production power demand		362 kW	
Generation from energy plant going to mill		-1895 kW	
		To buy	To sell
Price of electricity on peak	c/kWh	9.8	8.13
Price of electricity off peak	c/kWh	9.8	8.13
Operating hours per day		8 hrs	
FT power needs (compressor + chiller + 100kW)		1895 kW	
Gas engine generation		0 kW	
Generation excess/shortfall during production		-3316 kW	
Generation excess/shortfall off production		-2257 kW	
Electricity Profit/Expense during on production period assuming energy centre		-2600 \$/day	
Electricity Profit/Expense during off production period assuming energy centre		-3539 \$/day	
Cost of electricity if no energy centre - on production period		1114 \$/day	
Cost of electricity if no energy centre - off production period		567 \$/day	
Final value from having energy centre during on production period		-1486 \$/day	
Final value from having energy centre during off production period		-2971 \$/day	
Total daily value of having energy centre		-4457 \$/day	
		-1545421 \$/year	
Steam Value Calculations			
Value of steam		8 \$/GJ	
Steam Usage (based on requirement from sawmill energy model)		620965 MJ/day	
		621 GJ/day	
		215320 GJ/year	
		1722558 \$/year	

Table B9: Scenario 3 operating cost breakdown

	Annual Use	\$/unit	\$/yr
Raw Materials			
Wood	43441 Dry T/yr	20	868,817
Utilities			
Diesel	362449 L	1 L	362,449
Labour			
Process Operation	13140 hrs	20 hr	262,800
Supervision	15 % of operating labour		39,420
Administrative and General Overh	60 % of labour + maintenance		413,648
Maintenance	2 % of capital cost		387,193
Local taxes	1 % of capital cost		193,597
Insurance	1.5 % of capital cost		290,395
Operating Supplies	15 % of maintenance cost		29,040
Total Operating Costs (\$NZ)			2,847,358
Revenue from sales			
		\$/unit	
Product sales	2187979	2.163537 kg	4,733,773
Heat revenue			1,722,558
Electricity revenue			-1,545,421
Net Annual Profit			
Sales revenue			4,910,910
Less Operating Costs			2,847,358
Net Annual Profit after operating costs, before tax			2,063,552
Less depreciation on fixed capita	10 years straight line		1,742,370
Net annual profit after depreciation			321,182
Less tax	33 c/\$		0
Net Annual Profit after tax (\$NZ)			321,182
Add back depreciation			1,742,370
Total Net Annual Cashflow (\$NZ)			2,063,552

Techno-economic results for the optimisation study using the microchannel reactor

2 bar pressure scenario, all heat and power requirements of the sawmill met, breakeven syncrude price \$US106 per barrel, production 63 barrels per day

Table B10: 2 bar pressure scenario capital cost breakdown

Biomass Drying		2,648,240
Feed Handling		2,388,283
Gasifier		2,660,544
Gas Engine		4,209,636
Boiler		458,282
Misc.		164,670
Gas Scrubber		1,083,014
Gas filters and Guard Beds		156,502
Compressor		276,033
Heat exchange		630,457
FT microchannel reactor		4,293,138
Contingency and Fee		2,845,320
Working Capital		2,181,412
Total		23,995,530

B11: 2 bar pressure scenario electricity and heat revenue calculations

Electricity Value Calculations			
On production power demand		1421	kW
Off production power demand		362	kW
Generation from energy plant going to mill		1961	kW
		To buy	To sell
Price of electricity on peak	c/kWh	9.8	8.13
Price of electricity off peak	c/kWh	9.8	8.13
Operating hours per day		8	hrs
FT power needs (compressor + chiller + 100kW)		489.0732	
Gas engine generation		2450	
Generation excess/shortfall during production		540	kW
Generation excess/shortfall off production		1599	kW
Electricity Profit/Expense during on production period assuming energy centre		351.017	\$/day
Electricity Profit/Expense during off production period assuming energy centre		2080.159	\$/day
Cost of electricity if no energy centre - on production period		1114.246	\$/day
Cost of electricity if no energy centre - off production period		567.2848	\$/day
Final value from having energy centre during on production period		1465.263	\$/day
Final value from having energy centre during off production period		2647.444	\$/day
Total daily value of having energy centre		4112.707	\$/day
		1426081	\$/year
Steam Value Calculations			
Value of steam		8	\$/GJ
Steam Usage (based on requirement from sawmill energy model)		620965	MJ/day
		620.9653	GJ/day
		215319.7	GJ/year
		1722558	\$/year

Table B12: 2 bar pressure scenario operating cost breakdown

	Annual Use	\$/unit	\$/yr
Raw Materials			
Wood	57522 Dry T/yr	20	1,150,433
Utilities			
Diesel	472171.8 L	1 L	472,172
Labour			
Process Operation	13140 hrs	20 hr	262,800
Supervision	15 % of operating labour		39,420
Administrative and General Overh	60 % of labour + maintenance		472,053
Maintenance	2 % of capital cost		484,535
Local taxes	1 % of capital cost		242,267
Insurance	1.5 % of capital cost		363,401
Operating Supplies	15 % of maintenance cost		36,340
Total Operating Costs (\$NZ)			3,523,422
Revenue from sales			
Product sales	2803592	1.047191 kg	2,935,897
Heat revenue			1,722,558
Electricity revenue			1,426,081
Net Annual Profit			
Sales revenue			6,084,536
Less Operating Costs			3,523,422
Net Annual Profit after operating costs, before tax			2,561,114
Less depreciation on fixed capita	10 years straight line		2,180,407
Net annual profit after depreciation			380,707
Less tax	33 c/\$		125,633
Net Annual Profit after tax (\$NZ)			255,073
Add back depreciation			2,180,407
Total Net Annual Cashflow (\$NZ)			2,435,481

5 bar pressure scenario, all heat and power requirements of the sawmill met, breakeven syncrude price \$US120 per barrel, production 88 barrels per day

Table B13: 5 bar pressure scenario capital cost breakdown

Biomass Drying		3,234,770
Feed Handling		2,736,634
Gasifier		3,068,707
Gas Engine		5,843,851
Boiler		356,703
Misc.		163,044
Gas Scrubber		1,371,771
Gas filters and Guard Beds		219,361
Compressor		1,531,230
Heat exchange		668,927
FT microchannel reactor		3,852,929
Contingency and Fee		3,457,189
Working Capital		2,650,512
Total		29,155,628

Table B14: 5 bar pressure scenario electricity and heat revenue calculations

Electricity Value Calculations			
On production power demand		1421 kW	
Off production power demand		362 kW	
Generation from energy plant going to mill		1430 kW	
		To buy	To sell
Price of electricity on peak	c/kWh	9.8	8.13
Price of electricity off peak	c/kWh	9.8	8.13
Operating hours per day		8 hrs	
FT power needs (compressor + chiller + 100kW)		1990	
Gas engine generation		3420	
Generation excess/shortfall during production		9 kW	
Generation excess/shortfall off production		1068 kW	
Electricity Profit/Expense during on production period assuming energy centre		6 \$	
Electricity Profit/Expense during off production period assuming energy centre		1390 \$	
Cost of electricity if no energy centre - on production period		1114 \$	
Cost of electricity if no energy centre - off production period		567 \$	
Final value from having energy centre during on production period		1120 \$/day	
Final value from having energy centre during off production period		1957 \$/day	
Total daily value of having energy centre		3077 \$/day	
		1066931 \$/year	
Steam Value Calculations			
Value of steam		8 \$/GJ	
Steam Usage (based on requirement from sawmill energy model)		620965 MJ/day	
		621 GJ/day	
		215320 GJ/year	
		1722558 \$/year	

Table B15: 5 bar pressure scenario operating cost breakdown

	Annual Use	\$/unit	\$/yr
Raw Materials			
Wood	72202 Dry T/yr	20	1,444,033
Utilities			
Diesel	646085.9 L	1 L	646,086
Labour			
Process Operation	13140 hrs	20 hr	262,800
Supervision	15 % of operating labour		39,420
Administrative and General Overh	60 % of labour + maintenance		534,767
Maintenance	2 % of capital cost		589,059
Local taxes	1 % of capital cost		294,529
Insurance	1.5 % of capital cost		441,794
Operating Supplies	15 % of maintenance cost		44,179
Total Operating Costs (\$NZ)			4,296,668
Revenue from sales			
		\$/unit	
Product sales	3930241	1.1855 kg	4,659,300
Heat revenue			1,722,558
Electricity revenue			1,066,931
Net Annual Profit			
Sales revenue			7,448,789
Less Operating Costs			4,296,668
Net Annual Profit after operating costs, before tax			3,152,120
Less depreciation on fixed capita	10 years straight line		2,650,765
Net annual profit after depreciation			501,356
Less tax	33 c/\$		165,447
Net Annual Profit after tax (\$NZ)			335,908
Add back depreciation			2,650,765
Total Net Annual Cashflow (\$NZ)			2,986,673

10 bar pressure scenario, all heat and power requirements of the sawmill met, breakeven syncrude price \$US118 per barrel, production 81 barrels per day

Table B16: 10 bar pressure scenario capital cost breakdown

Biomass Drying		3,079,160
Feed Handling		2,647,228
Gasifier		2,962,580
Gas Engine		5,827,012
Boiler		352,990
Misc.		160,490
Gas Scrubber		1,298,795
Gas filters and Guard Beds		202,882
Compressor		1,524,682
Heat exchange		666,423
FT microchannel reactor		3,118,119
Contingency and Fee		3,276,054
Working Capital		2,511,641
Total		27,628,056

Table B17: 10 bar pressure scenario electricity and heat revenue calculations

Electricity Value Calculations				
On production power demand			1421	kW
Off production power demand			362	kW
Generation from energy plant going to mill			1428	kW
			To buy	To sell
Price of electricity on peak	c/kWh		9.8	8.13
Price of electricity off peak	c/kWh		9.8	8.13
Operating hours per day			8	hrs
FT power needs (compressor + chiller + 100kW)			1982	
Gas engine generation			3410	
Generation excess/shortfall during production			7	kW
Generation excess/shortfall off production			1066	kW
Electricity Profit/Expense during on production period assuming energy centre			5	\$/day
Electricity Profit/Expense during off production period assuming energy centre			1387	\$/day
Cost of electricity if no energy centre - on production period			1114	\$/day
Cost of electricity if no energy centre - off production period			567	\$/day
Final value from having energy centre during on production period			1119	\$/day
Final value from having energy centre during off production period			1955	\$/day
Total daily value of having energy centre			3073	\$/day
			1065689	\$/year
Steam Value Calculations				
Value of steam			8	\$/GJ
Steam Usage (based on requirement from sawmill energy model)			620965	MJ/day
			621	GJ/day
			215320	GJ/year
			1722558	\$/year

Table B18: 10 bar pressure scenario operating cost breakdown

	Annual Use		\$/unit		\$/yr
Raw Materials					
Wood	68307	Dry T/yr	20		1,366,140
Utilities					
Diesel	599675.8	L	1 L		599,676
Labour					
Process Operation	13140	hrs	20 hr		262,800
Supervision	15	% of operating labour			39,420
Administrative and General Overh	60	% of labour + maintenance			516,293
Maintenance	2	% of capital cost			558,268
Local taxes	1	% of capital cost			279,134
Insurance	1.5	% of capital cost			418,701
Operating Supplies	15	% of maintenance cost			41,870
Total Operating Costs (\$NZ)					4,082,301
Revenue from sales					
			\$/unit		
Product sales	3634668		1.165741 kg		4,237,083
Heat revenue					1,722,558
Electricity revenue					1,065,689
Net Annual Profit					
Sales revenue					7,025,329
Less Operating Costs					4,082,301
Net Annual Profit after operating costs, before tax					2,943,029
Less depreciation on fixed capita	10	years straight line			2,512,205
Net annual profit after depreciation					430,823
Less tax	33	c/\$			142,172
Net Annual Profit after tax (\$NZ)					288,652
Add back depreciation					2,512,205
Total Net Annual Cashflow (\$NZ)					2,800,857

20 bar pressure scenario, all heat and power requirements of the sawmill met, breakeven syncrude price \$US131 per barrel, production 79 barrels per day

Table B19: 20 bar pressure scenario capital cost breakdown

Biomass Drying		3,085,145
Feed Handling		2,650,704
Gasifier		2,966,689
Gas Engine		6,988,613
Boiler		335,988
Misc.		158,767
Gas Scrubber		1,258,791
Gas filters and Guard Beds		194,014
Compressor		2,111,575
Heat exchange		654,481
FT microchannel reactor		2,751,053
Contingency and Fee		3,473,373
Working Capital		2,662,919
Total		29,292,113

Table B20: 20 bar pressure scenario electricity and heat revenue calculations

Electricity Value Calculations			
On production power demand		1421	kW
Off production power demand		362	kW
Generation from energy plant going to mill		1429	kW
		To buy	To sell
Price of electricity on peak	c/kWh	9.8	8.13
Price of electricity off peak	c/kWh	9.8	8.13
Operating hours per day		8	hrs
FT power needs (compressor + chiller + 100kW)		2671	
Generation from gas engine		4100	
Generation excess/shortfall during production		8	kW
Generation excess/shortfall off production		1067	kW
Electricity Profit/Expense during on production period assuming energy centre		5	\$
Electricity Profit/Expense during off production period assuming energy centre		1388	\$
Cost of electricity if no energy centre - on production period		1114	\$
Cost of electricity if no energy centre - off production period		567	\$
Final value from having energy centre during on production period		1119	\$/day
Final value from having energy centre during off production period		1955	\$/day
Total daily value of having energy centre		3075	\$/day
		1066159	\$/year
Steam Value Calculations			
Value of steam		8	\$/GJ
Steam Usage (based on requirement from sawmill energy model)		620965	MJ/day
		621	GJ/day
		215320	GJ/year
		1722558	\$/year

Table B21: 20 bar pressure scenario operating cost breakdown

	Annual Use	\$/unit		\$/yr
Raw Materials				
Wood	68457 Dry T/yr	20		1,369,135
Utilities				
Diesel	571776.5 L	1 L		571,776
Labour				
Process Operation	13140 hrs	20 hr		262,800
Supervision	15 % of operating labour			39,420
Administrative and General Overhead	60 % of labour + maintenance			536,297
Maintenance	2 % of capital cost			591,609
Local taxes	1 % of capital cost			295,805
Insurance	1.5 % of capital cost			443,707
Operating Supplies	15 % of maintenance cost			44,371
Total Operating Costs (\$NZ)				4,154,920
Revenue from sales				
		\$/unit		
Product sales	3475830	1.29417 kg		4,498,317
Heat revenue				1,722,558
Electricity revenue				1,066,159
Net Annual Profit				
Sales revenue				7,287,034
Less Operating Costs				4,154,920
Net Annual Profit after operating costs, before tax				3,132,114
Less depreciation on fixed capital	10 years straight line			2,662,241
Net annual profit after depreciation				469,873
Less tax	33 c/\$			155,058
Net Annual Profit after tax (\$NZ)				314,815
Add back depreciation				2,662,241
Total Net Annual Cashflow (\$NZ)				2,977,056

225°C, 10 bar pressure and α of 0.89 scenario, all heat and power requirements of the sawmill met, breakeven syncrude price \$US107 per barrel, production 108 barrels per day

Table B22: 225°C, 10 bar pressure and α of 0.89 scenario capital cost breakdown

Biomass Drying		3,174,920
Feed Handling		2,702,481
Gasifier		3,028,059
Gas Engine		5,827,012
Boiler		345,288
Misc.		161,035
Gas Scrubber		1,323,412
Gas filters and Guard Beds		208,398
Compressor		1,565,912
Heat exchange		686,677
FT microchannel reactor		6,357,039
Contingency and Fee		3,807,035
Working Capital		2,918,727
Total		32,105,993

Table B23: 225°C, 10 bar pressure and α of 0.89 scenario electricity and heat revenue calculation

Electricity Value Calculations		
On production power demand		1421 kW
Off production power demand		362 kW
Generation from energy plant going to mill		1377 kW
		To buy To sell
Price of electricity on peak	c/kWh	9.8 8.13
Price of electricity off peak	c/kWh	9.8 8.13
Operating hours per day		8 hrs
FT power needs (compressor + chiller + 100kW)		2033 kW
Generation from gas engine		3410 kW
Generation excess/shortfall during production		-44 kW
Generation excess/shortfall off production		1015 kW
Electricity Profit/Expense during on production period assuming energy centre		-34 \$/day
Electricity Profit/Expense during off production period assuming energy centre		1321 \$/day
Cost of electricity if no energy centre - on production period		1114 \$/day
Cost of electricity if no energy centre - off production period		567 \$/day
Final value from having energy centre during on production period		1080 \$/day
Final value from having energy centre during off production period		1888 \$/day
Total daily value of having energy centre		2968 \$/day
		1029135 \$/year
Steam Value Calculations		
Value of steam		8 \$/GJ
Steam Usage (based on requirement from sawmill energy model)		620965 MJ/day
		621 GJ/day
		215320 GJ/year
		1722558 \$/year

Table B24: 225°C, 10 bar pressure and α of 0.89 scenario operating cost breakdown

	Annual Use	\$/unit		\$/yr
Raw Materials				
Wood	70704 Dry T/yr	20		1,414,074
Utilities				
Diesel	621629.3 L	1 L		621,629
Labour				
Process Operation	13140 hrs	20 hr		262,800
Supervision	15 % of operating labour			39,420
Administrative and General Overh	60 % of labour + maintenance			570,135
Maintenance	2 % of capital cost			648,005
Local taxes	1 % of capital cost			324,003
Insurance	1.5 % of capital cost			486,004
Operating Supplies	15 % of maintenance cost			48,600
Total Operating Costs (\$NZ)				4,414,671
Revenue from sales				
		\$/unit		
Product sales	4844387	1.057 kg		5,120,859
Heat revenue				1,722,558
Electricity revenue				1,029,135
Net Annual Profit				
Sales revenue				7,872,552
Less Operating Costs				4,414,671
Net Annual Profit after operating costs, before tax				3,457,880
Less depreciation on fixed capita	10 years straight line			2,916,024
Net annual profit after depreciation				541,856
Less tax	33 c/\$			178,812
Net Annual Profit after tax (\$NZ)				363,043
Add back depreciation				2,916,024
Total Net Annual Cashflow (\$NZ)				3,279,068

Appendix C: Laboratory Rig Safety and Risk Considerations with the Fischer-Tropsch system

The following document was submitted to the safety committee for approval of the process and gives a fuller description of the precautions taken with the use of CO in the laboratory.

Submitted document:

Ultimately the greatest risk is the release of CO into the room. There is an explosion hazard associated with the release of the hydrogen and CO mix, however, poisoning is far more likely to be the greatest risk.

Likely modes of failure

- Minor leak from around reactor fittings
- Failure of extraction system

Due to small flows (around 20cc/min process flow of 2:1 H₂:CO gas with any fitting leaks expected to be much less) under normal operation it is unlikely to leak significant quantities and therefore create a high level of CO in the lab. It is estimated if there were no extraction it would take 5 hours to reach 50ppm (50ppm STEL (short term exposure limit) 60min, 25ppm TWA (time weighted average – for an 8 hour day)) in the lab assuming a 40m³ lab, 20cc/min total gas flow and perfect mixing.

Hopefully unlikely modes of failure

-Earthquake or similar causing line failure that will cause entire contents of gas bottle to vent into room – and then into the greater Denham building.

-Regulator failure that will pressurise system too high resulting in a failure that will leak significant quantities

The consequences of these types of failures are potentially very significant

The toxicity would likely be the first concern with the 2:1 H₂:CO mix but there is also the flammability concern. The LEL for hydrogen is 4.1% and for carbon monoxide 12.5%.

The ambient pressure volume of the cylinder is approximately 6m³

Safety measures implemented to minimise risk

- CO sensor to give a readout of CO levels within lab.
- Automatic shutdown system that will cut power to fail-closed shutoff valve and heating system if CO sensor alarms, or power is lost to fan (or general power loss). The system has to be manually reset before power will restore to the valve or heaters. The system will be proof tested before the series of long runs. The CO sensor will be calibrated upon commissioning and should be checked every 6 months after that at which point a full safety systems check should be performed. If extraction stops without loss of power then the CO sensor will eventually shut down the system if the concentration reaches the alarm point
- Webcam to allow viewing of gas flow and temperature every 30 seconds which can be accessed anywhere with internet. Will also have a light to show if CO sensor is alarming
- Routine operator checks, and general attempt to be last person out of Denham at night and first person in the morning, or at very least returning to university to check in the evening.
- Portable CO sensor on operator when in lab which has a ppm readout and a visual and audible alarm
- When not in the lab leave the portable CO sensor hanging just outside the lab. This will therefore indicate if there is any CO outside the lab
- There is a pressure relief valve installed on the rig that will (should) break at 500psi. This relief valve vents into the extraction system. This will be checked before the series of long runs commence, and should be part of the orange card reapplication procedure so that it will be checked annually.

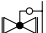

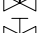
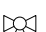

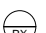



With these measures in place, there would have to be either a failure of the line before the automatic shutoff valve while the bottle is open to cause considerable venting, or a failure of the automatic shutoff valve, caused by for example the regulator failing or set far too high.

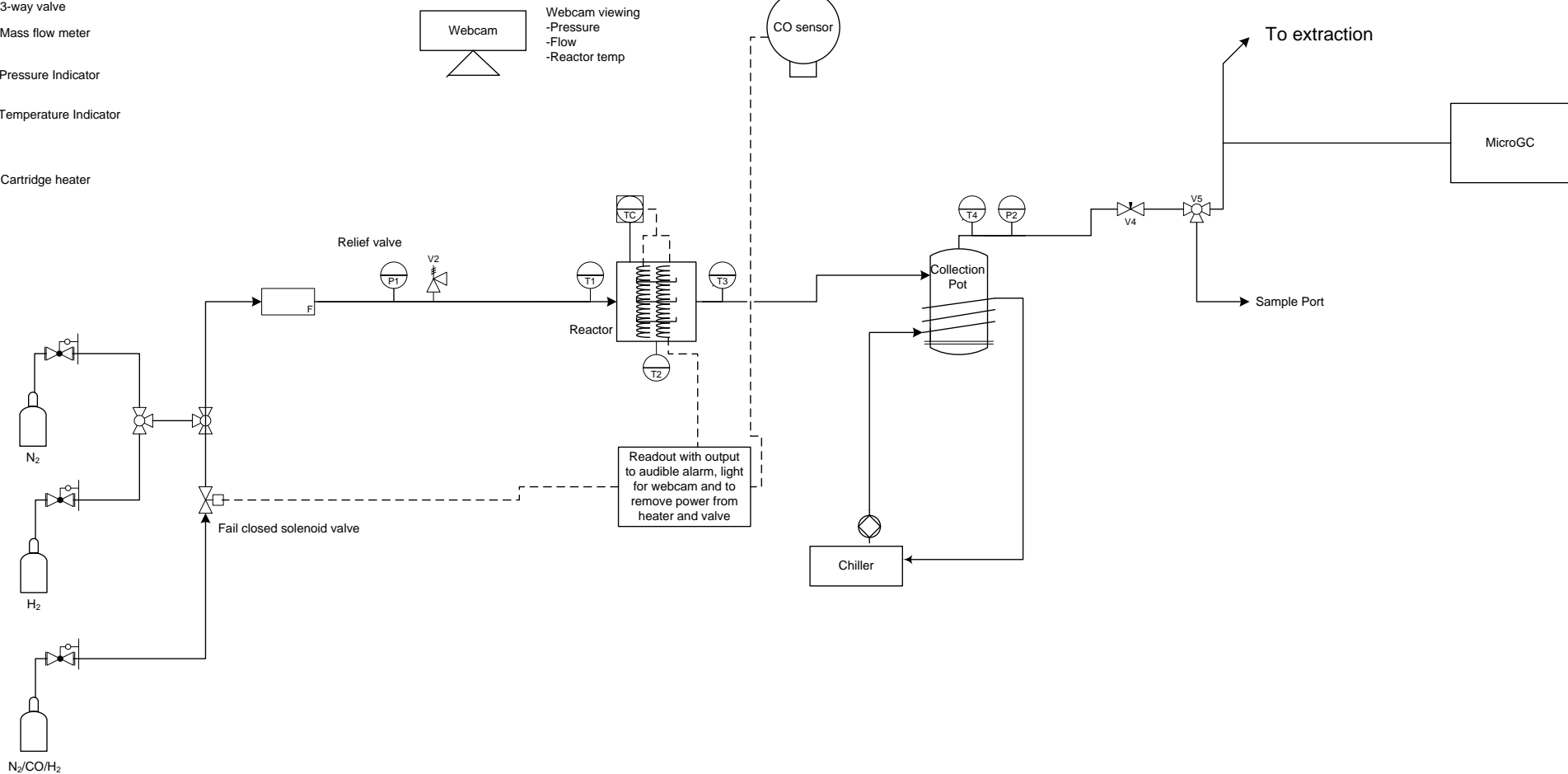
The rig is all hard stainless steel lined, with Swagelok fittings in most places, with screw in fittings at the automatic shutoff valve, and at the collection pot.

The rig is bolted to the bench, and has survived all the current earthquakes unscathed.

I was concerned about the potential for regulator creep with no flow if the automatic shutoff valve closed while the rig was unattended for a few hours so I replicated this with a test. The regulator was wound up to normal operating pressure with a manual valve shut to the rig. There was no noticeable creep after around 3.5 hours.

Also note that the recommended non powered storage life of the CO sensor is 3 months otherwise life of the sensor may be shortened. Because it has been longer than this the 6 monthly checks of calibration are critical. Normal sensor life is 2-3 years. – Update 7-2-11 – sensor has been checked and is fine, has new calibration sticker.

-  Regulator
-  Ball valve
-  Needle valve
-  Screw down valve
-  3-way valve
-  Mass flow meter
-  Pressure Indicator
-  Temperature Indicator
-  Cartridge heater



Notes:

- Electronic mass flow meters max pressure 500 psi (34 bar)
- All line 1/4" s/s tube with swagelok fittings
- Collection pot has an external water jacket (or a water bath) to cool gas and condense liquids/waxes

REV.	DESCRIPTION	DATE	BY
V7	Auto shutoff valve, and control strategy for CO sensor alarm included	14-7-11	CLP
V6	CO sensor, webcam, microGC and collection pot cooling added	28-04-11	CLP
V5	PRV moved further back in system and a needle valve used for pressure control, sample port after flowmeter removed, P1 moved	9-6-09	CLP
V4	Valve removed from bottom of collection pot, notes made about burner system, temp probes removed, notes about water jacket	27-4-09	CLP
V3	Collection pot 1 removed and pressure gauge and relief valve after water-jacketed collection pot to avoid overheating components	6-1-09	CLP
V3	Filter and needle valve added to cooling water to reactor stream	6-1-09	CLP

C-4

Lab Scale FT Process				
P&ID for Fischer-Tropsch process incorporating a microchannel reactor				
14-7-11	SIZE	FSCM NO	DWG NO	REV
C Penniall	SCALE	N/A	1	V7
			SHEET	1 OF 1

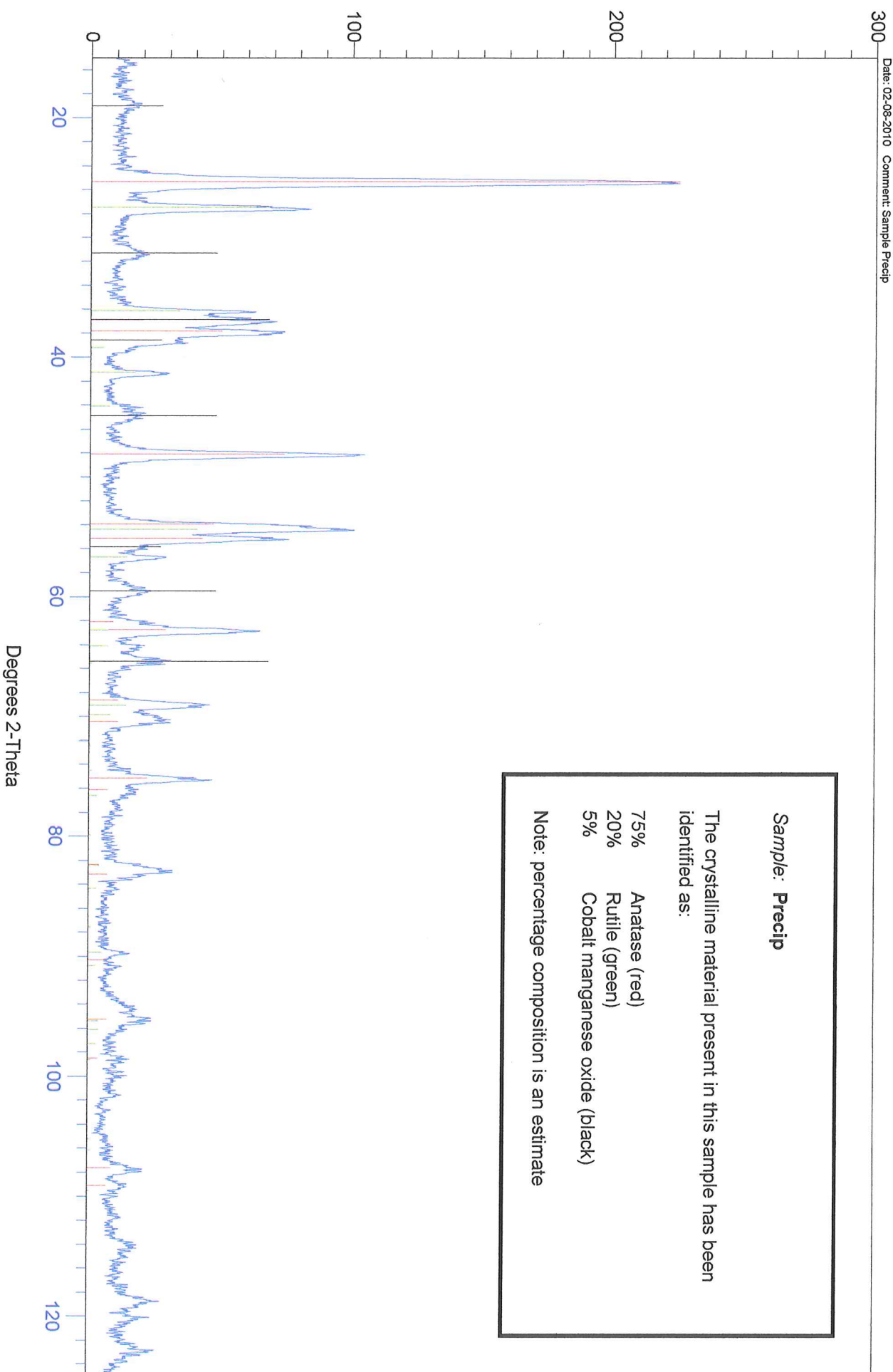
Appendix D: XRD results for powdered catalysts

The following pages are the produced graphs from performing XRD analysis on the powdered catalysts for use in the fixed bed reactor

XRD Analysis

Date: 02-08-2010 Comment: Sample Precip

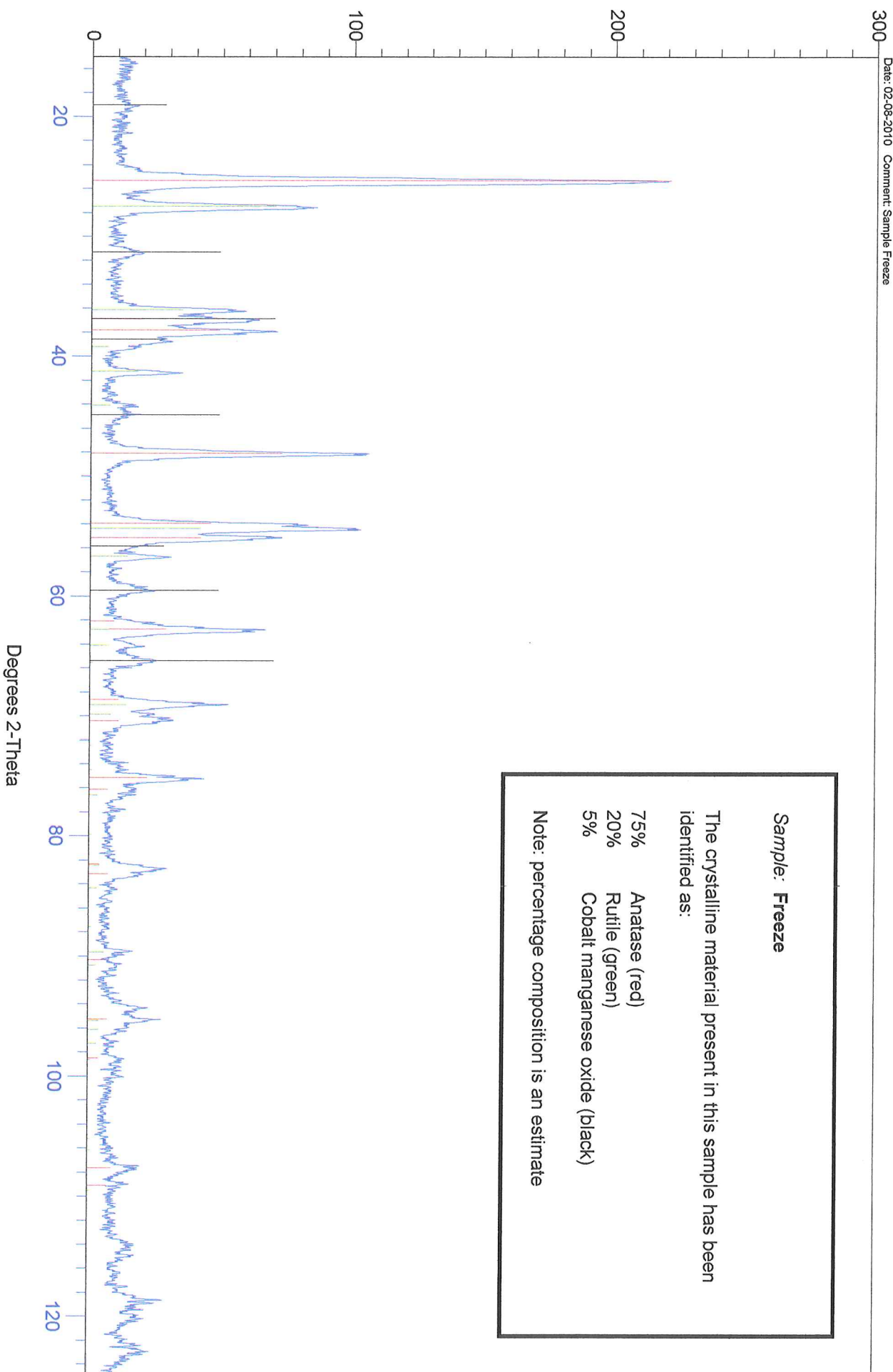
C
o
u
n
t
s



XRD Analysis

Date: 02-08-2010 Comment: Sample Freeze

C
o
u
n
t
s




~~~~~  
 Card Number: 21-1276  
 PDF Index Name: RUTILE, SYN  
 Mineral Name: RUTILE, SYN  
 Chemical Name: TITANIUM OXIDE  
 Chemical Formula: Ti O2

CAS Number:

References

~~~~~

Unit Cell	H	K	L	d-Space	Int	H	K	L	d-Space	Int	H	K	L	d-Space	Int
~~~~~	-----														
Space Group:				3.2469	100										
Quality Code:				2.4871	50										
Molecular Weight:				2.2970	8										
Cell Volume:				2.1880	25										
Measured Density:				2.0540	10										
Calc. Density:				1.6874	60										
				1.6237	20										
a: Alpha:				1.4797	10										
b: Beta:				1.4528	10										
c: Gamma:				1.4243	2										
				1.3598	20										
				1.3465	12										
				1.3041	2										
				1.2739	1										
Data Collection				1.2441	4										
~~~~~	-----														
Instrument:				1.2006	2										
SS/FOM:				1.1702	6										
Filter:				1.1483	4										
Ref. Int. Ratio:				1.1143	2										
Radiation:				1.0936	8										
Wavelength:				1.0827	4										
				1.0425	6										
				1.0364	6										
				1.0271	4										
				1.0167	1										
				0.9703	2										
				0.9644	2										
				0.9438	2										
				0.9072	4										
				0.9009	4										
				0.8892	8										
				0.8774	8										
				0.8738	8										
				0.8437	6										
				0.8292	8										
				0.8196	12										
				0.8120	2										
				0.7877	2										


~~~~~  
 Card Number: 32-0297 CAS Number:  
 PDF Index Name: Cobalt Manganese Oxide  
 Mineral Name:  
 Chemical Name:  
 Chemical Formula: Mn Co2 O4.5Mn Co2 Ox

References

~~~~~  
 CHDBAN Vol.283, p71 1976 Koenig, J., Brenet.

Unit Cell	H	K	L	d-Space	Int	H	K	L	d-Space	Int	H	K	L	d-Spac
Space Group: ()	1	1	1	4.6700	40									
Quality Code: I	2	2	0	2.8590	70									
Molecular Weight: 244.80	3	1	1	2.4390	100									
Cell Volume: 527.51	2	2	2	2.3360	40									
Measured Density:	4	0	0	2.0200	70									
Calc. Density: 6.160	4	2	2	1.6470	40									
	5	1	1	1.5530	70									
a: 8.08 Alpha:	4	4	0	1.4270	100									
b: Beta:														
c: Gamma:														

Data Collection

~~~~~  
 Instrument:  
 SS/FOM:  
 Filter:  
 Ref. Int. Ratio:  
 Radiation:  
 Wavelength: 1.5405

## Appendix E: Fitting Kinetic Equations to Experimental Data

The following graphs represent the fitting of experimental data to kinetic equations based on Yates & Satterfield (1991) and is discussed in Chapter 5.

### Neat cobalt washcoat

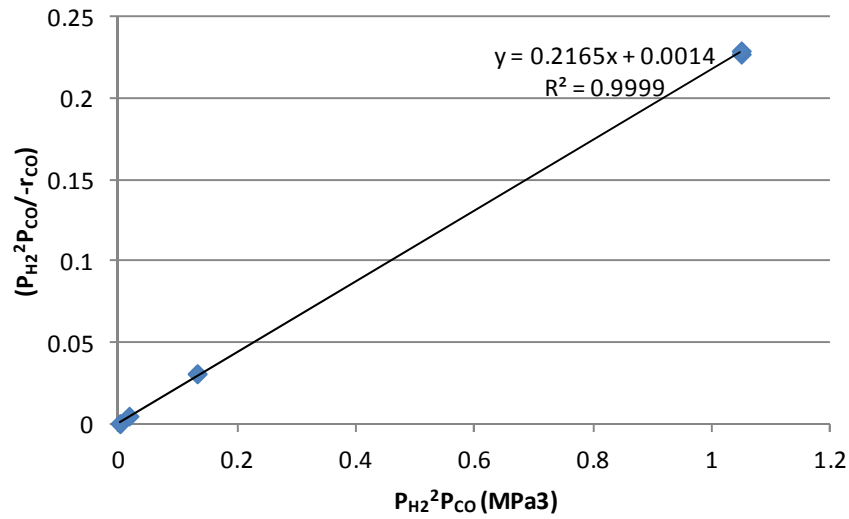


Figure E1: Plot of linearised equation 19

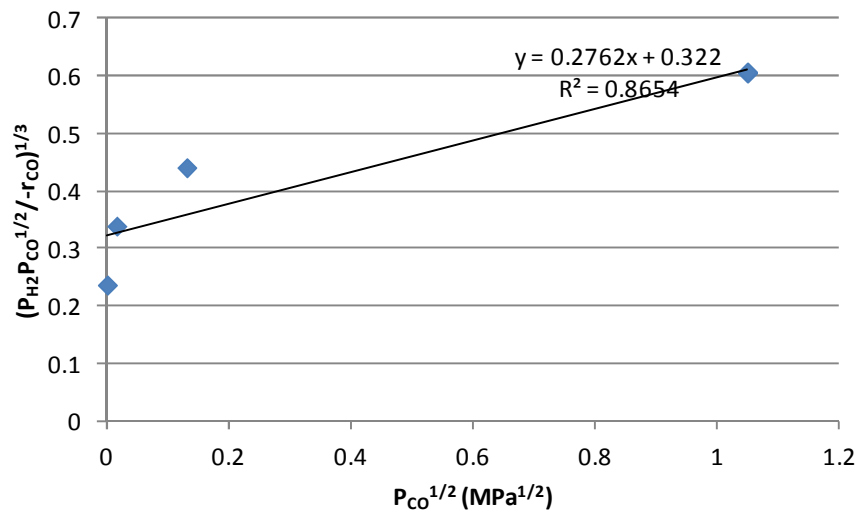


Figure E2: Plot of linearised equation 20

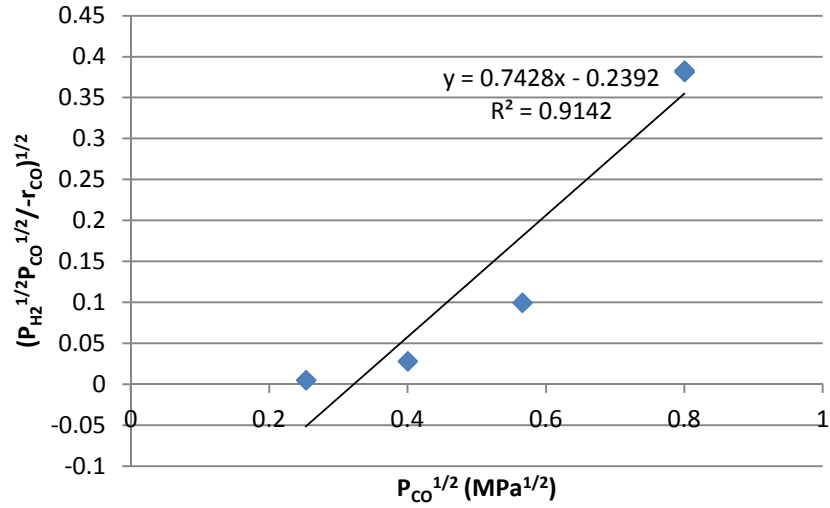


Figure E3: Plot of linearised equation 21

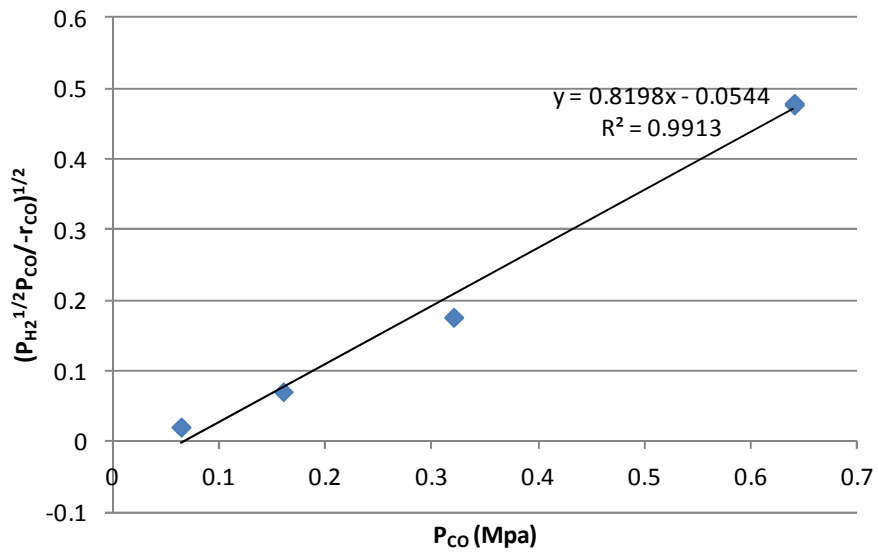


Figure E4: Plot of linearised equation 22

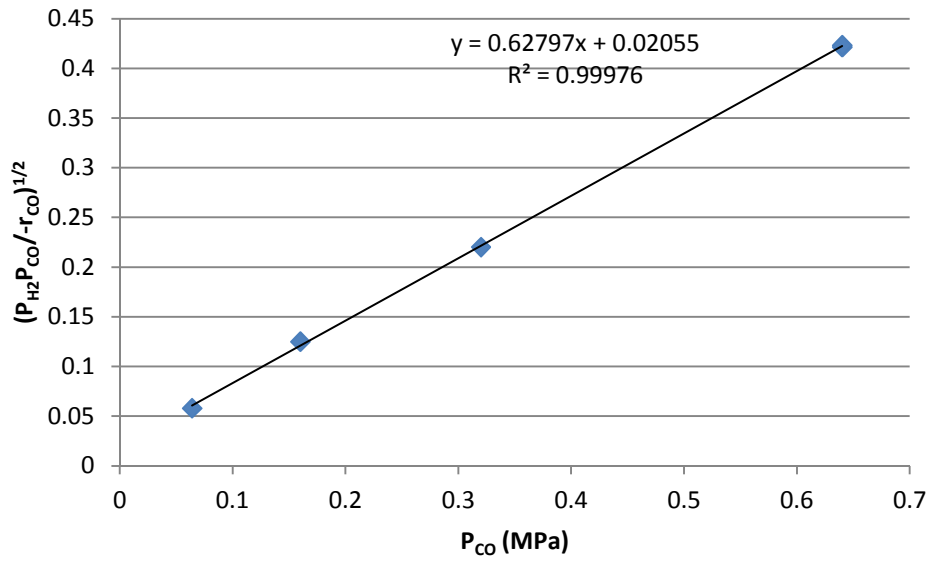


Figure E5: Plot of linearised equation 23

**Cobalt on titania washcoat**

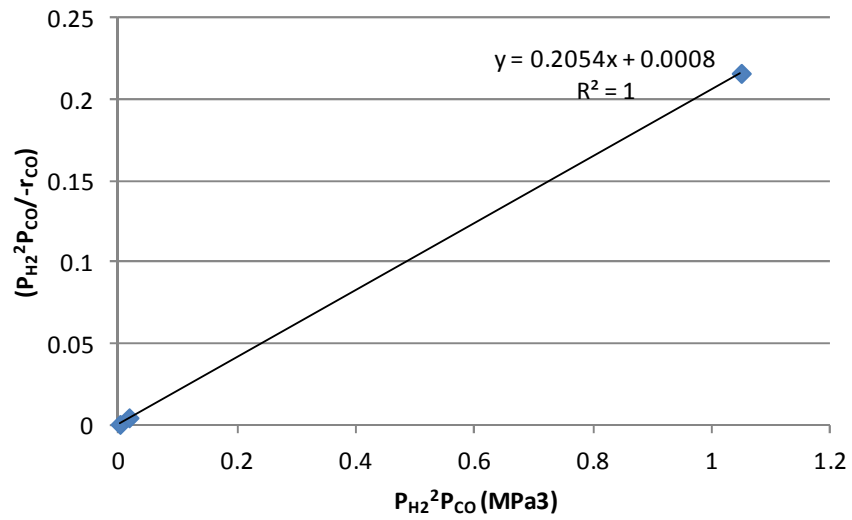


Figure E6: Plot of linearised equation 19

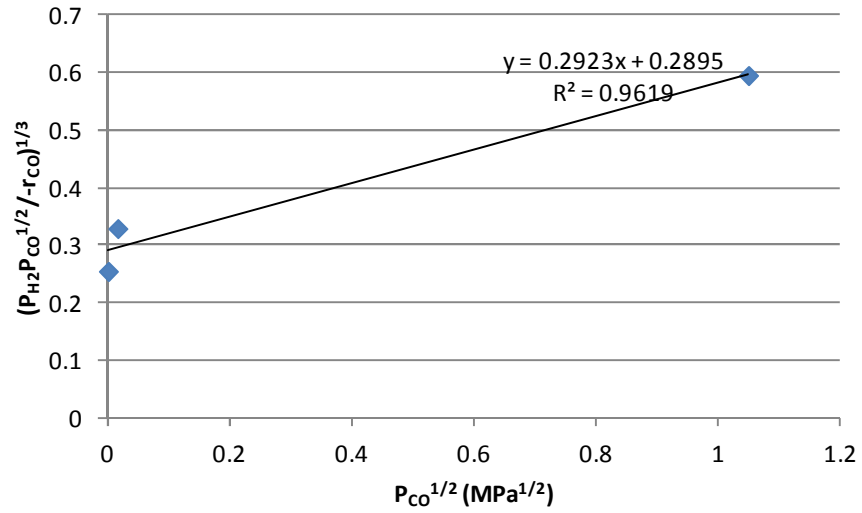


Figure E7: Plot of linearised equation 20

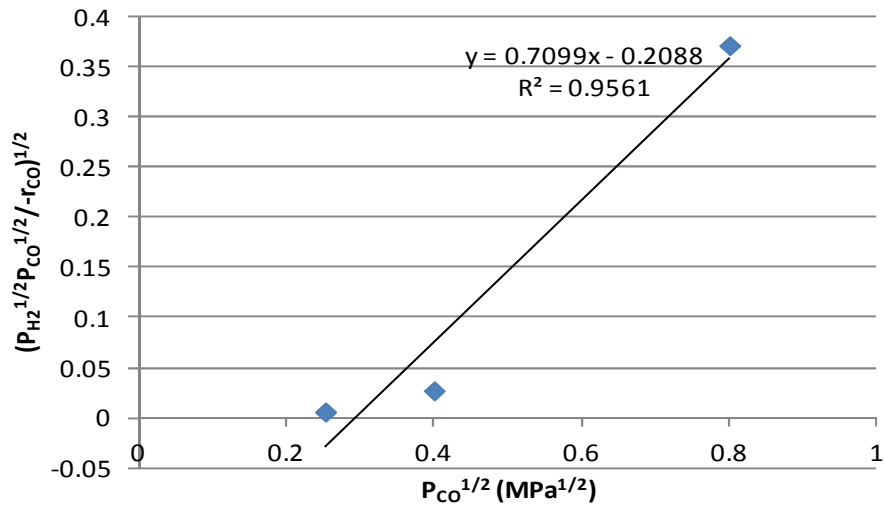


Figure E8: Plot of linearised equation 21

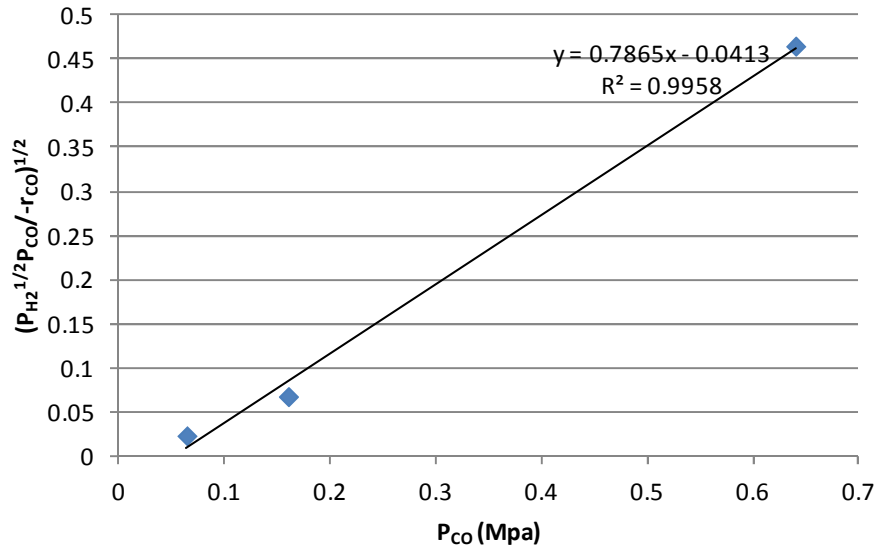


Figure E9: Plot of linearised equation 22

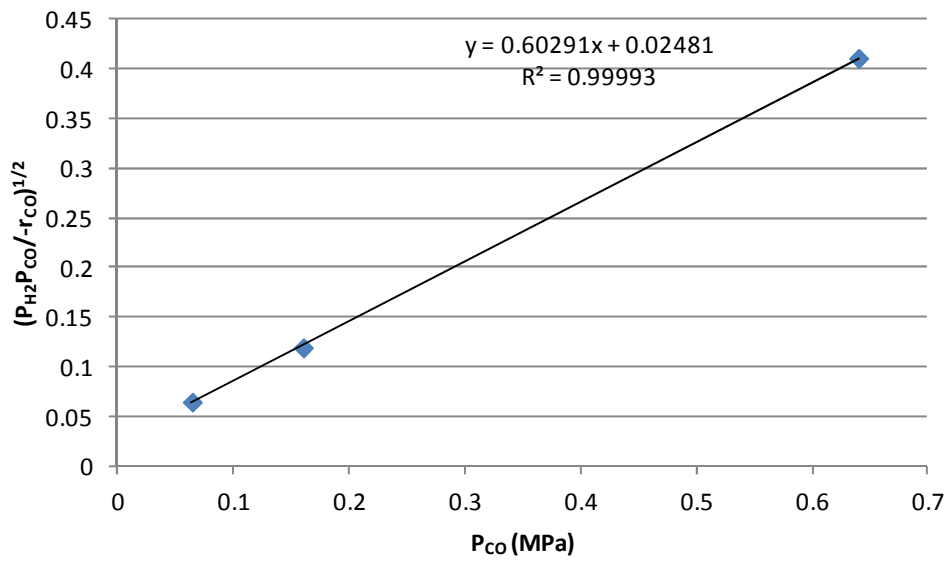


Figure E10: Plot of linearised equation 23

## **Appendix F - Batch Slurry Reactor Fischer Tropsch Catalyst Development**

### **1.1. Introduction**

Batch Slurry Fischer Tropsch experiments were performed at the Centre for Environmentally Beneficial Catalysis (CEBC) at the University of Kansas. The purpose of performing the work was twofold, firstly as a comparison and verification of the microchannel and fixed bed reactors in use at the University of Canterbury and secondly as investigation of the batch slurry reactor as a development tool for Fischer-Tropsch catalysts. The advantage seen with the batch slurry reactor is the speed at which tests on the catalyst can be performed. It is not unreasonable to be able to examine 2 different catalysts or variables per day. This therefore provides an opportunity for fast screening of catalysts, which after narrowing down, can be applied to longer term runs in a microchannel reactor. The obvious limitation of this quick analysis, however, is the brevity of the run does not allow for settling in of the catalyst. This and other limitations will be discussed in greater depth later in the chapter. Because of the main motivation for this work this chapter pulls significantly on the data obtained in Chapter 5 for comparison.

The type of reactor available at the CEBC for use was a batch stirred reactor with a volume of 100mL supplied by Parr Instruments. This system required a reconsideration of the standard way of performing a FT synthesis reaction and analysis as it is typically performed in a continuous manner. There is very little in the literature about batch slurry FT. Only one full paper reference was found (X. Liu, Hamasaki, Honma, & Tokunaga, 2011a) and therefore this is relatively new research.

It was decided that trialling two different catalysts over a range of pressures and temperatures with all other variables held constant would be the best use of the short timeframe available for experimentation. In regards to catalyst preparation the first and most simple option was to make a Co on TiO<sub>2</sub> catalyst using a simple impregnation or incipient wetness method similar to what had already been done at the University of Canterbury (UC). Another option was to investigate literature for a suitable catalyst that utilises materials already available at the CEBC, such as a catalyst with an alumina support. This follows below

Oukaci et al. (1999) compared patented FT catalysts using fixed bed and slurry bubble column reactors. They made 8 different catalysts in the experiment based on patented catalyst recipes. The catalyst supports were  $\gamma$ -alumina (vista), silica (Davison 952) and titania (Degussa P25). All catalysts had a loading of 20 wt% cobalt except the titania which only had 12 wt% due to low surface area and pore volume. As a benchmark they made unpromoted catalysts for each support, and then made recipes based on the patented catalysts using promoters.

From the results in the fixed bed the promoted catalysts seemed to work significantly better than the unpromoted ones, however, in the slurry bed there was not such a difference and the unpromoted  $\gamma$ -alumina supported catalyst performed very well. It was concluded that the unpromoted alumina catalyst may, therefore, be very suitable for this research as it performed well in the slurry reactor, and the microchannel reactor would be loaded with a similar particle size (and should achieve equivalent mass and heat transfer) as used in the slurry reactor.

It was also decided that it would be quite simple to prepare a 12 wt% Co on titania catalyst and use it for comparison as this is what was used in the fixed bed reactor at UC. The two catalysts chosen in the study were therefore a 12% cobalt on titania catalyst, and a 20% cobalt on  $\gamma$ -alumina catalyst. Both catalysts were prepared by incipient wetness impregnation. The titania supported catalyst was produced as a catalyst similar to that used in the fixed bed at UC, while the alumina was made as a comparison. The catalysts were also based on the work by Oukaci et al. (1999) as discussed earlier. Therefore, this should show a comparison both to the UC work, as well as that of patented Fischer-Tropsch catalysts.

The basis for the calculation of rates of conversion are the ideal gas laws applied to the pressure changes observed in the batch reactor. This is deemed adequate as the pressure based errors are likely to be small relative to other inherent uncertainties in the experimentation. Of note is that when performing the calculations based on partial pressures the vapour pressure of the decane solvent had to be taken into consideration in the analysis. Also the amount of CO and H<sub>2</sub> dissolved in the decane was considered using solubility constants.



## 1.2. Experimental

### 1.2.1. Catalyst production

The important steps for the catalyst production are described as follows:

#### 1.2.1.1. 12% Co on titania catalyst

Hombikat titania from Sigma Aldrich was impregnated with cobalt nitrate using an incipient wetness technique. Only a single impregnation step was required to achieve the 12% cobalt loading. The catalyst was then dried for several hours at 120°C. Calcination was performed in flowing air with a ramp rate of 1°C/min to 300°C then held for 2 hours. Reduction was performed in flowing ultra high purity hydrogen, with a temperature ramp of 1°C/min to 350°C then held at 1.5 hours. Passivation of the catalyst followed, by flowing a 1%O<sub>2</sub> in He mix over the catalyst at room temperature for an hour, followed by flowing air at room temperature for an hour.

#### 1.2.1.2. 20% Co on alumina catalyst

The alumina catalyst required a two step incipient wetness impregnation to achieve the required loading, drying the catalyst at 120°C after each impregnation. The methods for calcination, reduction and passivation were the same as for the Co on titania catalyst.

### 1.2.2. Reactor operation

A brief description of the pertinent points of the operation have been included below. Figure 1 shows the rig setup while Figure 2 to Figure 4 show the physical reactor system.

- The reactor was loaded with the appropriate amounts of catalyst and decane (approximately 85 mg and 32.5 mL respectively).
- The reactor was purged several times with nitrogen then hydrogen while stirring at low rpm
- The reactor was heated to the required temperature (240°C, 225°C and 210°C), then pressurised with hydrogen to the required pressure to achieve a 2:1 H<sub>2</sub>:CO ratio when the other gas was added. The stirrer was increased to 1000rpm and held for 1 hour to reduce
- Pressure was made up to either 900, 600 or 300 psig with the 1:1 H<sub>2</sub>:CO syngas and left to react until 10% of the pressure had degraded. Such high pressures were used to give a larger amount of reactant for the 10% pressure degradation
- The reactor was left to cool (usually took over an hour) before analysing the gas on the GC.

- The liquid product was filtered to remove the catalyst and then a sample was stored for later GC analysis

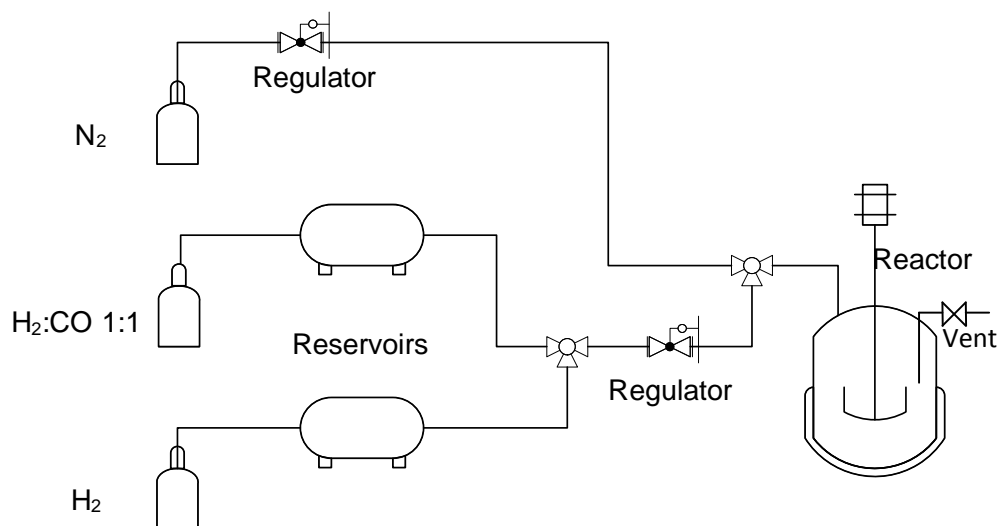


Figure 1: Flow diagram of reactor experimental setup



Figure 2: Reactor installed in rig showing electrical and plumbing connections and heating element in place



**Figure 3: Reactor pressure, temperature and rpm readout/control. Note in the foreground are the syngas and the H<sub>2</sub> reservoirs running to the regulator**



**Figure 4: Inside view of the reactor showing the gas inlet, the thermocouple well and the stirrer**

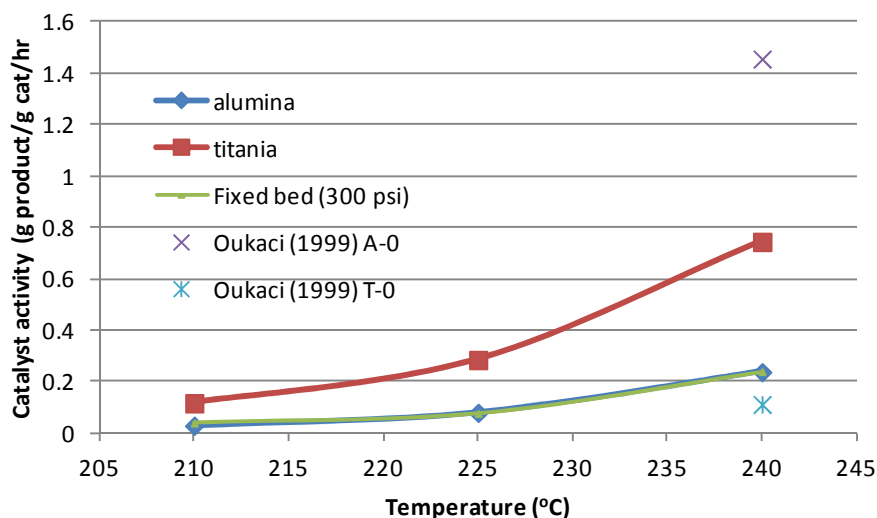
### *1.2.3. GC analysis*

Gas analysis was performed using a Shimadzu 2014 GC using previously developed methods at the CEBC. Liquid analysis was performed on an Agilent 7890A using a HP-5 column. Standards were developed using a mix of hydrocarbons in hexane from C<sub>9</sub>-C<sub>34</sub> (Restek). As a starting point the GC method applied was similar to that used at UC for FT liquids analysis. Split ratios and injection volumes were modified until sufficient peaks were obtained for analysis.

### 1.3. Results and Discussion

It was elected to trial the two catalysts over three temperatures (240, 225 and 210°C) as well as three starting pressures (900, 600 and 300 psi). Unfortunately the method of charging gas into the reactors particularly at the 300psi runs did not yield the H<sub>2</sub>:CO ratio anticipated. While for most of the tests the ratio was consistent around 4:1 (where 2:1 was the aim), the 300psi runs ended up with a very high H<sub>2</sub>:CO ratio rendering the results unusable, at least as a comparison to the other runs. The cause of the discrepancy was the result of the line to the reactor not being purged between charging the reactor with hydrogen, and then switching to syngas for the second charge. There was obviously still sufficient volume of hydrogen in the regulator and line to offset the H<sub>2</sub>:CO ratio further towards H<sub>2</sub> than intended.

Another interesting observation was a significant temperature spike upon charging with H<sub>2</sub> at temperature and increased stirring rate. There was commonly a 25°C temperature jump which would indicate the catalyst was being reduced. However, given the small volume of catalyst such a significant jump was unexpected, particularly given that with the passivation step only the outside surface of the catalyst is supposedly oxidised. It may have been the case that the passivation of 1%O<sub>2</sub> in He followed by exposure to air could have in fact oxidised a significant amount of the catalyst. One difference between the experimental work at the CEBC and that at UC is that the UC catalysts were reduced in situ and brought straight online. It was possible that this would make a significant difference to activity and therefore comparability of the data. However, literature shows (Hammache, Goodwin, & Oukaci, 2002) that if a re-reduction is performed the catalyst reaction rate returns to near the same performance of one that has been reduced and run online immediately.



**Figure 5: Catalyst production rate vs. temperature for the two catalysts tested at the CEBC at 600psi and the catalyst tested in the fixed bed reactor at the University of Canterbury at 300psi as well as comparison to that of literature (Oukaci, et al., 1999) at 470 psi.**

Comparison of the kinetics to Yates and Satterfield (1991) was attempted as this is considered somewhat of a benchmark. However, the pressures used in the CEBC experiments were far higher than those used in the fore mentioned study and their kinetic equation yields results far higher than anticipated. It is likely their equation cannot be extrapolated that far. Based on the appearance of the data collected, general observations can be made in comparison to other catalysts and typical FT performance. However, it is not considered appropriate to attempt any kinetic or other modelling on the data collected due to inconsistencies.

Of great interest is the comparability of catalyst run in the fixed bed reactor at UC to that of the Co on alumina catalyst. Whilst the tests were performed at different pressures with different types of catalyst, they have almost identical activity as shown in Figure 5. The particular reaction rate being identical could be considered somewhat coincidental but the similarity in the temperature dependence is not. This result is very encouraging as it shows great comparability between the temperature control and analysis of the two systems, leading to the conclusion that both are likely accurate. Also included in Figure 5 is slurry reactor data from Oukaci et al. (Oukaci, et al., 1999) with a simple 20% Co on alumina (A-0) and 12% Co on titania (T-0). It should be noted the production rate is approximated from their data using given or assumed methane selectivity. The comparison shows the CEBC and UC data sits

between the literature data. However, in the literature, the titania supported catalyst performed very poorly with the alumina catalyst having the higher performance. The reverse was found in the CEBC research. While it is unknown as to why the alumina supported catalyst at the CEBC performed so poorly, it is possible to suggest an explanation as to why the titania catalyst performed better than expected. In the literature (Oukaci, et al., 1999) comment was made that the titania support is predominantly in its rutile form which has a high density and a low surface area leading to settling in the reactor and poor cobalt dispersion. In the CEBC experiments the Hombikat titania was not first calcined to convert to the rutile form so it is possible this exhibited better catalyst support properties. While the anatase form of titania is less attrition resistant than the rutile form, and therefore not suitable for long term operation in a slurry reactor, it was decided it was suitable for this situation as the slurry reactor runs were short, and the intended application is in a fixed bed arrangement (i.e. the microchannel reactor). The BET area for the titania supported catalyst was  $45 \text{ m}^2/\text{g}$ . Rutile titania can have surface area as low as  $10\text{-}15 \text{ m}^2/\text{g}$  (Oukaci, et al., 1999) showing that the increased performance of the catalyst at the CEBC was possibly in part due to this. The alumina supported catalyst had a BET surface area of  $74 \text{ m}^2/\text{g}$  which was lower than expected and may have contributed to the poor performance.

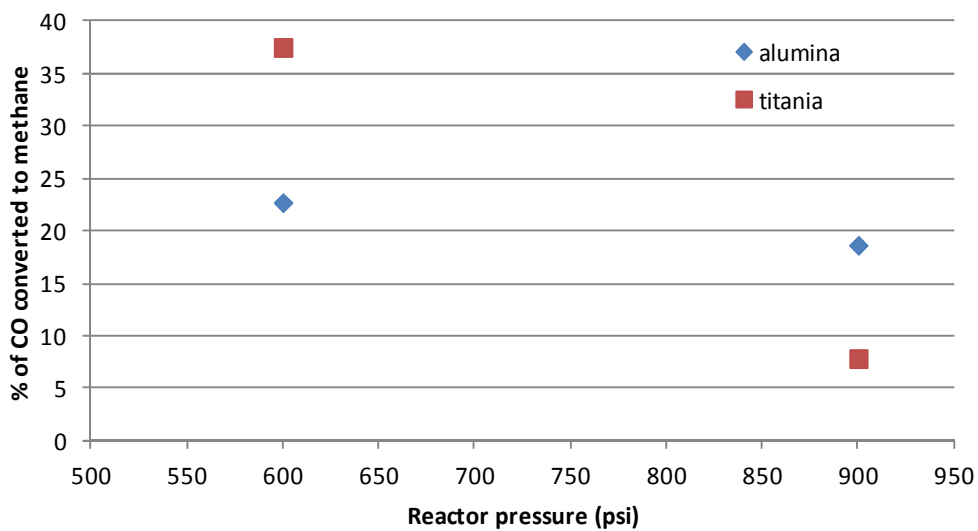
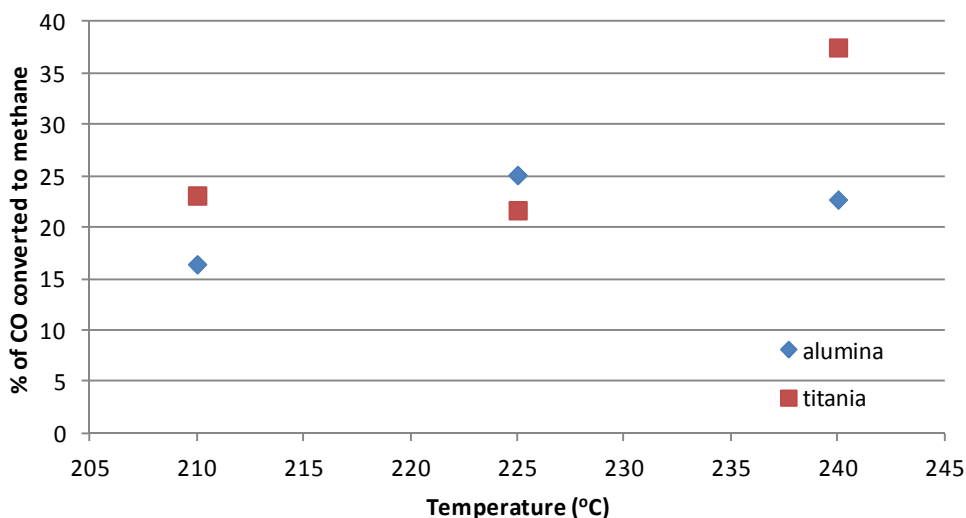


Figure 6: Fraction of CO that is converted to methane vs. reactor pressure at 240°C



**Figure 7: Fraction of CO that is converted to methane vs. reactor temperature at 600psi**

As expected, methane selectivity decreased with increased pressure as shown in Figure 6. It appears that the pressure had a much more significant effect on the methane selectivity of the titania supported catalyst. It is unfortunate that the 300psi runs were unsuitable as the third pressure point would have made a very interesting comparison. The methane selectivity of the titania catalyst is very high, which is unsuitable for an industrial application. Oukaci et al. (1999) also tended to show the titania supported catalyst forming significant fractions of methane.

The temperature dependence of methane selectivity was not as pronounced as expected. Although there were only 3 data points for comparison, in both the alumina and titania supported catalysts there was an unexpected inflection as seen in Figure 7.

The titania supported catalyst followed the expectations of selectivity in regards to temperature and pressure, however, the alumina supported catalyst did not (see Figure 8 and Figure 9). However, there is the potential for significant error in the  $\alpha$  values as there was only a small range of standards to base the  $\alpha$  value on, and the concentration of the products in the decane solvent was very low. Song et al. (2003) gave an approximation of  $\alpha$  to temperature which is also shown on Figure 9. There does seem to be a considerable discrepancy, however, it is positive that the values of  $\alpha$  were higher for the CEBC results.

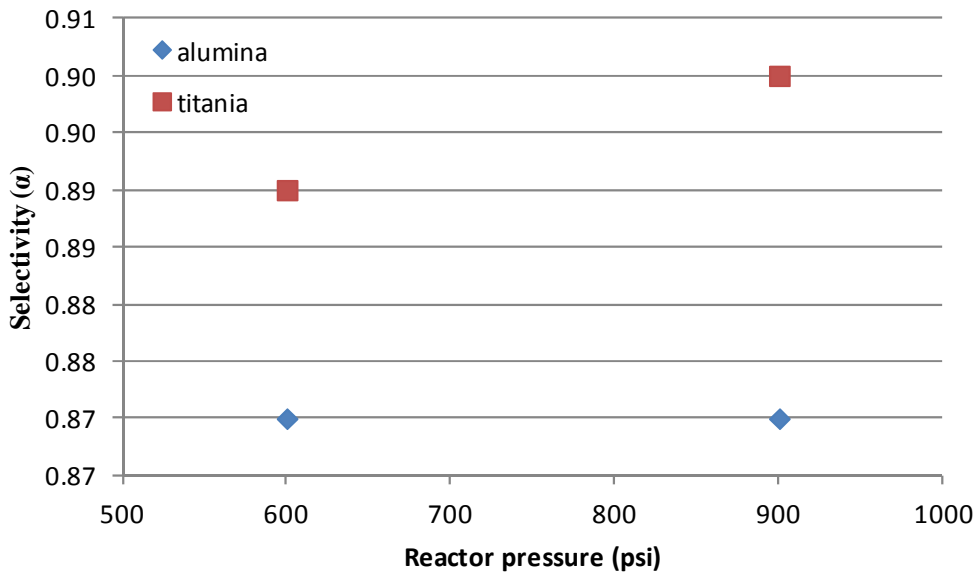


Figure 8: Selectivity of the catalyst vs. reactor pressure at 240°C

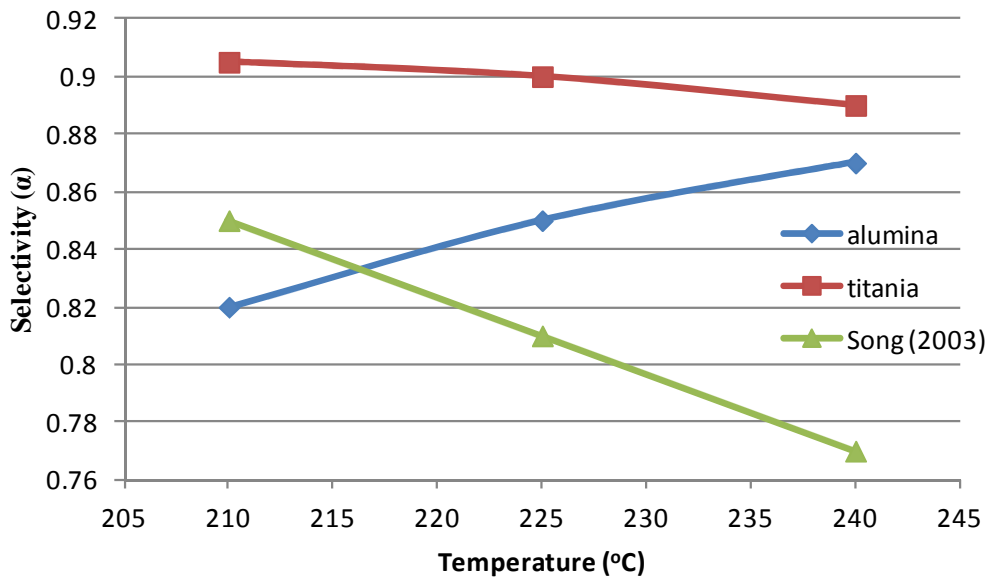


Figure 9: Selectivity of the catalyst vs. reactor temperature (600psi for CEBC work, Song unknown pressure)



#### 1.4. Conclusion

The short timeframe for experimentation removed the opportunity for analysis and repetition of runs in order to increase reliability of the data. However, there were still beneficial results particularly in respect to the production rate per unit catalyst. The change in activity of the catalyst with increasing temperature was as expected. Very encouraging was the close match of activity of the alumina supported catalyst at the CEBC and the titania supported catalyst at UC. While it is not possible to make a definitive conclusion, it does allow it to be reasoned that for both to trend the same required accurate temperature control and analysis in both experiments. This helps to benchmark the UC system against a proven Parr Instruments system.

The rates of reaction were also comparable to within an order of magnitude with literature. Of interest is that the rates were similar to that of the fixed bed system at UC, with the production per unit mass of catalyst in the microchannel reactor remaining much higher.

The batch slurry reactor system did prove to be a useful tool for fast characterisation of the performance of a catalyst for the Fischer-Tropsch process. Depending on the conditions and therefore reaction rate, two experiments could be performed in a day, allowing many conditions to be tested in a relatively short space of time.

If the experiments were to be repeated, a dedicated supply of 2:1 H<sub>2</sub>:CO is deemed necessary, as well as more particular attention to charging the reactor. Additionally if the correct ratio of gas were available it would also be possible to use a reservoir, therefore providing more reactants and a greater accuracy of experimentation overall.